SEQUENCE SPECIFIC RECOGNITION AND PHOTOCLEAVAGE OF DNA BY PHENANTHRENEQUINONE DIIMINE COMPLEXES OF RHODIUM(III)

Thesis by

Ayesha Sitlani

In Partial Fulfillment of the Requirements

for the Degree of

Doctor of Philosophy

California Institute of Technology

Pasadena, California

(Submitted May 18, 1993)

ACKNOWLEDGEMENTS

I wish to express my most sincere regards and appreciation for my advisor, Jacqueline K. Barton, who has influenced my life in many positive ways. Jackie has been supportive and encouraging to me throughout my years in graduate school, both at Columbia and Caltech. I am very grateful to her for her trust in me, and for her very thoughtful advice and direction. Jackie has taught me that in scientific research, it is important to trust one's intuitions and perceptions to ask important but not so obvious questions. She has taught me to maintain an optimistic spirit about research and her philosophies and advice will continue to guide me. I also wish to thank her for all the opportunities she has given me, and for her friendship.

I am also very grateful to a number of coworkers, who have contributed to much of the work presented here. I wish to thank Anna Marie Pyle, who got me started in the lab; her work provided me with a sound platform on which a major portion of my work is based. I would also like to thank Takashi Morii, who advised and taught me a lot. I wish to thank both Takashi Morii and Eric Long, both of whom helped me immensely in the mechanistic aspect of my project. I am very grateful to Achim Krotz, who taught me very important synthetic skills. I wish to thank him for his constant assistance in the synthesis of my complexes and for his useful and critical suggestions. I am also very grateful to Cindy Dupureur, for her assistance in making enantiomers and for her advice and encouragement. I would also wish to thank the rest of the Barton group for their generous advice and support and for all the many fun times I have shared with them. I would like to thank Dan Hall, Brian Hudson, Tom Shields, Bob Terbrueggen, Tim Johann, Susanne Lin, Inho Lee, Ai Ching Lim, Scott Klakamp, Yonchu Jenkins, Kaspar Zimmermann, Michael Pustilnik, Donna Campisi, Niranjan Sardesai, Cathy Murphy, Michelle Arkin, Marilena Fitzsimons and Kim Waldron for all their advice and help. I

also wish to express my sincere thanks to Maureen Renta, who has been wonderful to me and helped me a lot.

On a more personal level, I wish to thank my friends and family, without whose support this work would not be completed. I wish to express a very special thanks to Donna, Niranjan, Michael, and Inho, who have always been good friends to me. I also wish to thank my friend Shoba Mathew, who was very supportive to me at Columbia and encouraged me to move to Caltech. I am extremely grateful to my parents who have made many tough sacrifices in allowing me to leave India to continue my education in the United States. I wish to thank them for their love and support. I am also very grateful to my brother, Sanjay, who has always been there for me. I wish to thank him for his constant and invaluable advice, encouragement, and sense of humor. Finally, I wish to thank Adrian Looney who deserves a lot of credit for the completion of this program. I wish to thank him for adding a sense of balance and perspective in my life, and for his constant love, patience, and understanding.

ABSTRACT

Sequence-specific recognition and photocleavage of DNA by a series of 9,10-phenanthrenequinone diimine (phi) complexes of rhodium(III) was studied. $[Rh(phi)]^{3+}$ complexes bind to DNA via intercalation of their phi ligand and upon photoactivation promote strand scission. The DNA degradation products formed are consistent with photoreaction of $[Rh(phi)]^{3+}$ intercalated in the major groove of DNA, via abstraction of the C3'-H atom of the deoxyribose. For the complex $[Rh(phen)_2phi]^{3+}$ and its derivatives $[Rh(X)_2phi]^{3+}$, the primary products are 5' and 3' phosphate termini and nucleic acid bases. For the complex $[Rh(phi)_2bpy]^{3+}$ and its derivatives $[Rh(phi)_2X]^{3+}$, additional products, dependent on dioxygen concentrations, are characterized as base propenoic acids and 3'-phosphoglycaldehyde termini. The partitioning between the oxygen dependent and oxygen independent pathways correlates best with how the shapes of these complexes limit access of dioxygen to the C3' deoxyribose position. The shapes of $[Rh(phi)]^{3+}$ complexes also govern their sequence-specific DNA recognition. The more sterically bulky complexes with methyl or phenyl groups on their ancillary ligands cleave at a subset of sequences recognized by their parent molecules. The Δ and Λ isomers of $[Rh(5,5'\text{-dimethylbpy})_2phi]^{3+}$ cleave specifically at sites that are defined by the consensus sequences 5'-C-T-pu/py-G-3' and 5'-A-C/G-T-C/G-3', respectively. This sequence-specificity may be understood on the basis of negative steric clashes and positive van der Waals interactions between methyl groups on the metal complex and thymine methyl groups in the DNA major groove. The complex $[Rh(4,4'\text{-diphenylbpy})_2phi]^{3+}$ recognizes the self-complementary eight base-pair sequence 5'-CTCTAGAG-3', both due to its bulky shape and its ability to cooperatively associate through non-covalent dimerization on the DNA helix. $[Rh(4,4'\text{-diphenylbpy})_2phi]^{3+}$ is shown to inhibit sequence-specific cleavage by the restriction enzyme Xba1. It is likely that, like $[Rh(phi)]^{3+}$ complexes, DNA binding proteins exploit shape selection to achieve high levels of sequence-specificity.

TABLE OF CONTENTS

LIST OF FIGURES

Chapter 3:

Chapter 4:

Chapter 5:

LIST OF SCHEMES

LIST OF TABLES

Chapter 4:

Chapter 6:

Chapter 1:

Introduction: The Interaction of Metal Complexes with Nucleic Acids†

1.1. Introduction

The recognition of a nucleic acid site through a myriad of specific non-covalent interactions is a process that is central to a living cell. Proteins recognize DNA and RNA in a sequence-specific fashion to regulate selectively the expression of genetic material. During the last decade several structural studies have been directed towards understanding protein-nucleic acid recognition. X-ray and NMR structural studies have shown us that the conformations of nucleic acids are varied and complex, and that a simple code comprising specific interactions between individual amino acid residues and nucleic acid bases cannot generally account for the sequence specificity observed. We have also learned that nature has evolved a range of structural motifs for nucleic acid binding proteins[1,2]. These include helix turn helix proteins, homeodomains, zinc finger proteins, steroid receptors, leucine-zipper proteins, helix loop helix proteins, and β-sheet proteins. In comparison, less rapid progress has been made on determining the structures of protein complexes with folded RNA molecules and on the significance of RNA-binding motifs[2].

In addition to providing a distinct DNA-binding motif, zinc fingers have recently also been implicated in the recognition of RNA by retroviral proteins and synthetases[3]. However, unlike other nucleic acid binding motifs, zinc fingers are unique in that they contain a central metal ion which, due to predisposed coordination geometry requirements, serves to organize structurally the folding of protein around it. Several

---

† Adapted from Sitlani, A. and Barton, J. K. "The Interaction of Metal Complexes with Nucleic Acids," chapter submitted for book titled "Handbook of Metal-Ligand Interactions of Biological Fluids," published by Marcel Dekker, Inc., NY, NY.

types of zinc-containing motifs have been discovered which have different shapes depending on the length of folded peptide around the metal ion, the stoichiometry of zinc ions, and the nature of the amino acids involved in ligation to the zinc ion. Zinc finger proteins therefore exemplify how nature has very judiciously used the properties of metal ion-ligand interactions to design structures which recognize specific nucleic acid sites. Perhaps analogously, transition metal complexes, which like zinc fingers have well-defined shapes owing to their distinct and rigid coordination geometries, have been designed in our laboratory to probe the basic principles of nucleic acid recognition.

Unlike most small molecules and natural products which bind nucleic acids, the rigid coordination geometries of transition metal complexes provide us with a well-defined scaffold on which to append moieties that may contribute to site-selective recognition. In this way, we may build complexes to match the shape and symmetry of specific nucleic acid sites. This strategy lends itself potentially to the general design of transition metal complexes as site-specific chemotherapeutic agents that would discriminate among specific nucleic acid sites in a predictable manner. The design of metal complexes with shapes that match the local structure of nucleic acid sites has taught us some of the features which are important to nucleic-acid recognition.

The first section of this chapter describes how various characteristic features of transition metal complexes may be exploited to probe nucleic acids. For example, the inherent reactivities and electronic properties of transition metal complexes provide sensitive spectroscopic assays to detect their binding to nucleic acids. Importantly, the well-defined shapes of transition metal complexes, as determined by their distinct and rigid coordination geometries, make them sensitive probes of nucleic acid conformation. These features have allowed us to study the nucleic-acid binding and recognition properties of a wide range of transition metal complexes, as described in the second section of this chapter. Interestingly, a correlation between site-specific discrimination

by metal complexes and by proteins has been observed. This correlation supports the notion that transition metal-nucleic acid interactions may be viewed as a model to delineate some basic principles of protein-nucleic acid recognition. We have learned that the overall shape-complementarity between metal complex and its cognate nucleic acid site is a crucial element of site-specificity, and it is likely that similar steric factors are significant in protein-nucleic acid interactions as well. Recognition of nucleic acids, however, is far from being completely understood, and important issues involving the predictability of nucleic acid recognition and the rational design of drugs still remain. We are currently addressing these issues by exploring the use of transition metal complexes as recognition building blocks in the development of site-specific chemotherapeutic agents.

1.2. Methods to Probe Nucleic Acid-Metal Complex Interactions.

This section describe the methods used to study nucleic acid binding and recognition by transition metal complexes. The rich spectroscopic properties and chemical reactivities of transition metals offer several methods to probe metal complex-nucleic acid interactions. Spectroscopic perturbations in the metal complex on binding to its target provide sensitive assays to study nucleic acid binding. For example, simple absorption and luminescence measurements have been useful in elucidating the overall nucleic acid binding modes of metal complexes, while NMR spectroscopy has provided more detailed structural information on site-specific binding characteristics. Furthermore, the redox and photochemical reactivities of transition metal complexes have also been exploited to examine nucleic acid binding interactions. Chemical reactions of the metal complexes bound to nucleic acids have provided sensitive chemical reporters that mark the specific nucleic acid binding site.

1.2.1. Spectroscopic Assays Used to Measure Binding.

Simple UV-visible and luminescence measurements on a family of Ru(II) and Rh(III) mixed ligand complexes (Figure 1.1) have provided a description of the general characteristics of how these metal complexes interact with double helical DNA[4]. Except for the complex $[Ru(bpy)_3]^{2+}$, binding of simple polypyridyl complexes of Ru(II) complexes to DNA is associated with hypochromism and red shifting of the metal-to-ligand charge transfer bands in the visible absorption spectra of the bound forms. In the case of Ru(II) and Rh(III) complexes containing the 9,10-phenanthrenequinone diimine (phi) ligand, substantial hypochromism and shifts to longer wavelengths of the phi centered π-π^* transition is observed upon binding to DNA. The magnitude of red shifts is greatest for phi complexes (> 16 nm), followed by DIP complexes (> 6 nm), phen complexes (> 2 nm), and bpy complexes (no red shift). If red shifts upon binding are taken as a measure of the stacking interaction, a trend is observed in which the optimal shape for metal complex intercalation into DNA is phi > DIP > phen > bpy.

Paralleling the measurements of absorbance hypochromism, for the Ru(II) complexes that luminesce, emission enhancements are apparent with DNA binding[4]. Depending on the mixed-ligand complex examined (Figure 1.1), red shifts or blue shifts in the emission spectra are observed. Complexes such as $[Ru(bpy)_3]^{2+}$ that bind through weak electrostatic modes do not exhibit appreciable changes in luminescence or absorption intensity. The most dramatic change in luminescence upon binding to nucleic acids is observed for Ru(II) polypyridyl complexes containing a dipyrido[3,2-a:2',3'-c]phenazine (dppz) ligand (Figure 1.2)[5]. The dppz complexes show no photoluminescence in aqueous solutions; however, in the presence of double-stranded DNA they luminesce intensely. The luminescence enhancement observed upon nucleic acid binding is attributed to the sensitivity of the excited state of dppz complexes to quenching by water. Upon intercalation into the helix, the dppz ligand is protected from

Figure 1.1. Illustration of several mixed-ligand Ru(II) and Rh(III) complexes: $[Ru(bpy)_3]^{2+}$ (top left); $[Ru(phen)_3]^{2+}$ (top right); $[Ru(DIP)_2(phen)]^{2+}$ (middle left); $[Ru(bpy)_2(phen)]^{2+}$ (middle right); $[Rh(phen)_2(phi)]^{3+}$ (bottom left); $[Rh(phi)_2(bpy)]^{3+}$ (bottom right). Bpy = 2,2'-bipyridine, phen = 1,10-phenanthroline, DIP = 4,7-diphenylphenanthroline, phi = 9,10-phenanthrenequinone diimine.

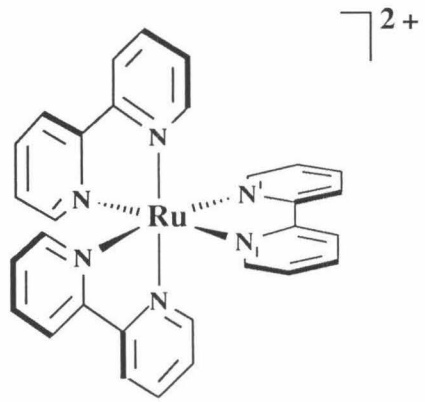
2+
Ru
N
N'

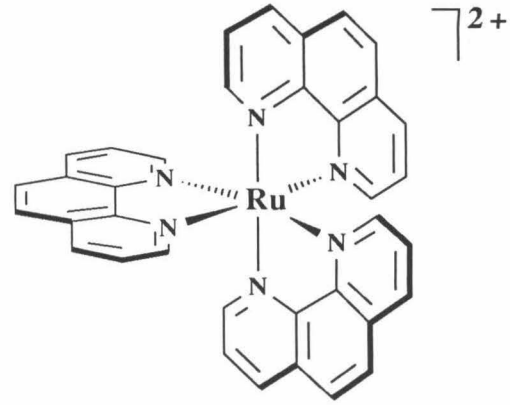
2+
Ru
N

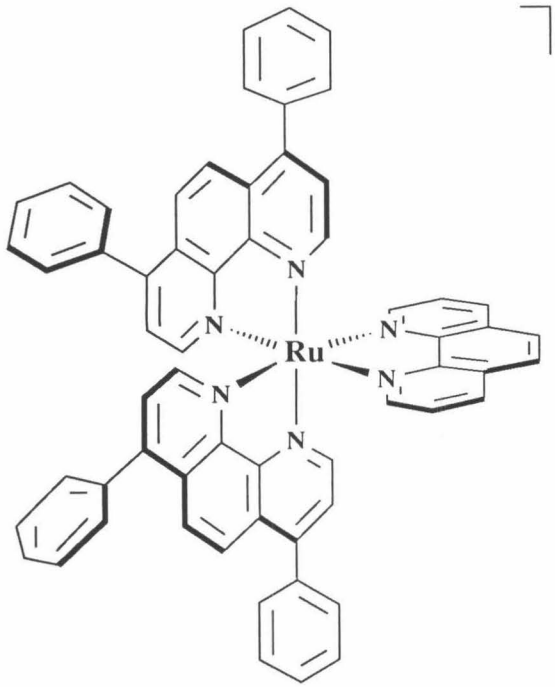
2+
Ru
N
N'

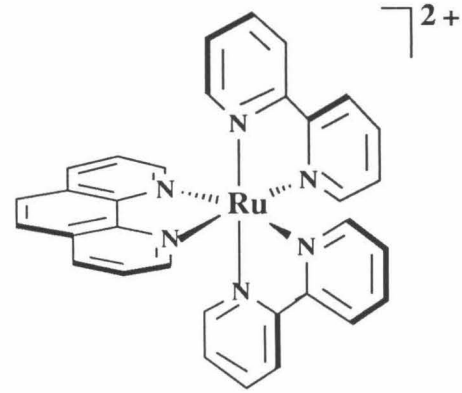
2+
Ru
N

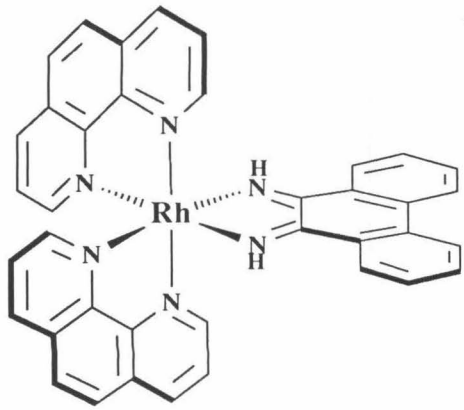
3+
Rh
N
H

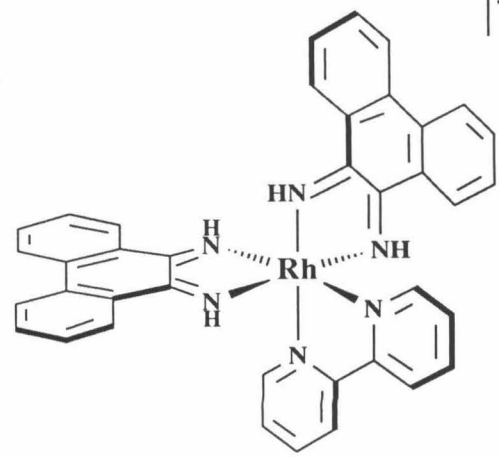
3+
Rh
HN
NH
N
H

Figure 1.2. Luminescence enhancement of $[Ru(bpy)_2(dppz)]^{2+}$ upon binding to DNA (adapted from ref. 5a). **A.** Structure of $[Ru(bpy)_2(dppz)]^{2+}$, (bpy = 2,2'-bipyridine, dppz = dipyrido [3,2-a: 2',3'-c] phenazine). **B.** Steady-state emission spectrum of $[Ru(bpy)_2(dppz)]^{2+}$ in the presence and absence of B-form poly d(GC).d(GC). In the absence of polynucleotide, there is no detectable luminescence; however, intense emission centered at 628 nm is observed in the presence of polynucleotide.

A.

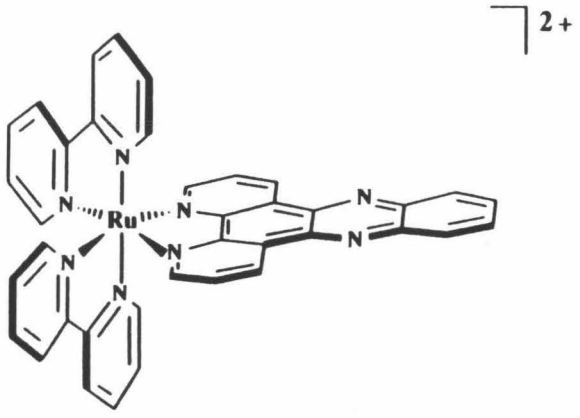

B.

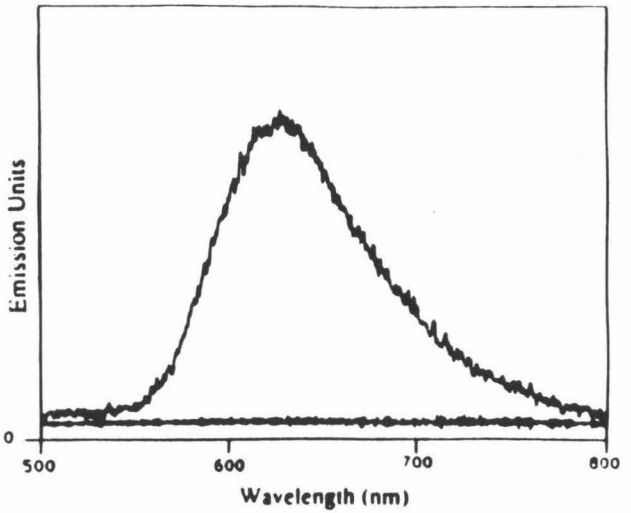

the aqueous solvent, thereby preserving the luminescence. Furthermore, the luminescent parameters of $[Ru(phen)_2dppz]^{2+}$ and $[Ru(bpy)_2dppz]^{2+}$ are remarkably sensitive to the DNA structure at the intercalation site and, more specifically, to how the structure protects the dppz ligand from interactions with the solvent[5b]. In particular, the highest level of emission is observed upon binding to triple-helical DNA, where substantial overlap and stacking between the dppz ligand and base triple may occur.

The extent of luminescence enhancement, absorption hypochromism, and red shifts associated with spectra of the bound forms all seem to reflect the extent of overlap of the ligand with the base pairs of the helix. The phi ligand is particularly well-suited for intercalation, likely because the ligand most closely mimics the spacial arrangement of the aromatic regions of a base pair, thereby allowing greater helical overlap; in comparison, the phenanthroline ligand permits a substantially smaller surface area for intercalative stacking. Consistent with this observation, the binding affinity of phi complexes are three orders of magnitude greater than other simple polypyridyl complexes of Ru(II) and Rh(III)[6]. Therefore, to achieve high affinity in DNA binding and to favor the intercalative mode, large planar aromatic heterocyclic ligands such as dppz or phi are preferred.

More detailed structural characterizations of binding modes and site-selective recognition are derived from the one-dimensional ^{1}H-NMR studies[7] of tris(phenanthroline) complexes of Rh(III), Ru(II), Ni(II) and Cr(III) and the two-dimensional ^{1}H-NMR studies[7c] of $[Rh(phen)_2phi]^{3+}$ bound to DNA. The NMR spectral titrations of $[Ru(phen)_3]^{2+}$ and $[Rh(phen)_3]^{3+}$ indicate that the complexes bind to the oligomer $d(GTGCAC)_2$ through two binding modes: the intercalative mode favoring the Δ isomer and the surface bound mode favoring the Λ isomer. However, NMR chemical shift variations appear particularly sensitive to the surface-bound interaction, with the adenine H2 proton showing the largest upfield shifts upon DNA-binding by the Λ isomers

of the metal complexes. The major groove thymine methyl protons (TMe) shift downfield to a lesser extent, and more so for the Δ isomers. Selective paramagnetic relaxation of oligonucleotide protons of $d(GTGCAC)_2$ by Δ- and Λ-$[Ni(phen)_3]^{3+}$ and by Δ- and Λ-$[Cr(phen)_3]^{3+}$ support these observations. Two binding modes are necessary to account for the binding of each isomer to the oligonucleotide. Direct evidence for major groove intercalation by metal complexes is apparent in the two-dimensional NOESY experiments performed on $[Rh(phen)_2phi]^{3+}$-$[d(GTCGAC)_2]$. Dramatic upfield shifts are observed only for the phi ligand, while the ancillary phenanthroline protons are now only slightly shifted, which points to preferential intercalation of the phi ligand. Furthermore, evidence for specific intercalation comes from an observed disruption in the sequential NOE connectivities at the 5'-CG-3' step (Figure 1.3A). Parallel to this observation, site-specific cleavage at the 5'-CG-3' step is observed upon irradiation of the oligonucleotide substrate in the presence of Δ-$[Rh(phen)_2phi]^{3+}$ (Figure 1.3B). Clearly, these studies indicate that replacing a phenanthroline with a phi ligand not only favors the intercalative mode of binding, but also enhances the overall site-specific recognition of the metal complexes.

1.2.2. DNA Cleavage Assays to Measure Site-Specific Binding and Recognition.

The redox and chemical reactivities of transition metal complexes also provide a sensitive means to examine nucleic acid binding interactions. Reactions which promote DNA strand scission are powerful in marking sites of binding along the DNA polymer. Coupling the variety of reactivities of transition metal complexes to differing modes of binding leads to an array of site-specific reactions on DNA. Agents such as Fe(II)-bleomycin[8a], MPE-Fe(II) and $Fe(EDTA)^{2-}$ [8b,c], $Cu(phen)_2$[8a], and metalloporphyrins[8d] bind to most sites in the minor groove of DNA and react primarily with the DNA sugars through either a metal bound or diffusing radical. Our laboratory has taken advantage of

inorganic photochemistry to couple reactions which promote DNA strand scission to recognition in the major groove of DNA.

Rhodium polypyridyl complexes are known to be powerful photooxidants; it has been proposed that irradiation into ligand transitions leads to a ligand-to-metal charge transfer producing a redox active excited state species[9]. This species may be responsible for the oxidative cleavage of nucleic acids by tris(polypyridyl) complexes of rhodium(III) and cobalt(III), with the target being the backbone sugars[10]. Cleavage by these tris(polypyridyl) complexes produces sharp cleavage bands which have been assigned as 5'-phosphates and 3'-phosphates based on their gel electrophoretic mobilities. The concomitant release of free nucleic acid bases supports the proposal that the site of oxidative damage is the sugar moiety and not the nucleic acid bases[10]. It is likely that photocleavage of nucleic acids by phi complexes of Rh(III) occurs through an analogous mechanism involving an excited state redox active species. The production of sharp cleavage bands (Figure 1.3B) by phi complexes of Rh(III) suggests that cleavage is mediated by a non-diffusible oxidant, likely a phi cation radical. The reactive radical species could form through irradiation of the ligand to metal charge transfer (LMCT) transition.

The DNA photocleavage products identified[11] are consistent with photoreaction of $Rh(phi)^{3+}$ intercalated in the major groove of DNA, via abstraction of a deoxyribose C3'-H atom (Figure 1.4). A single base 5'-asymmetry in cleavage is observed at specific sites on the helix, consistent with reaction from the major groove upon photoactivation of the intercalated ligand radical. As summarized in Figure 1.4, following abstraction of the C3'-H, subsequent oxidation of the C3'-radical species, possibly by the transiently formed Rh(II), and solvation of the resultant cation would lead, through a series of β-elimination steps, to the 5'-phosphate, 3'-phosphate, and nucleic acid base products observed. Alternatively, addition of dioxygen to the C3'-radical, followed by oxygen

Figure 1.3. Site-specific intercalation of Δ $[Rh(phen)_2phi]^{3+}$ into $d(GTGCAC)_2$, (adapted from ref. 7c). **A.** Expanded NOESY contour plot of Δ $[Rh(phen)_2phi]^{3+}$-$[d(GTCGAC)_2]$. The labeled cross peaks correspond to the internucleotide NOEs between the base protons and the H2'2" protons of the sugar residue of the 5' nucleotide. The numbering scheme for the bases is given from the 5' end of the nucleotide. A loss in intensity at the 5'-CG-3' step indicates site-specific binding of the complex.

B. Structure of Δ $[Rh(phen)_2phi]^{3+}$, (phen = 1,10-phenanthroline, phi = 9,10-phenanthrenequinone diimine), with each unique proton labeled.

C. Site-specific photocleavage by Δ $[Rh(phen)_2phi]^{3+}$ on a 5'-^{32}P-end labeled hexamer, 5'-GTCGAC-3'. Cleavage is seen at the 5'-CG-3' step, which is consistent with the site of intercalation shown by the NOESY plot.

A

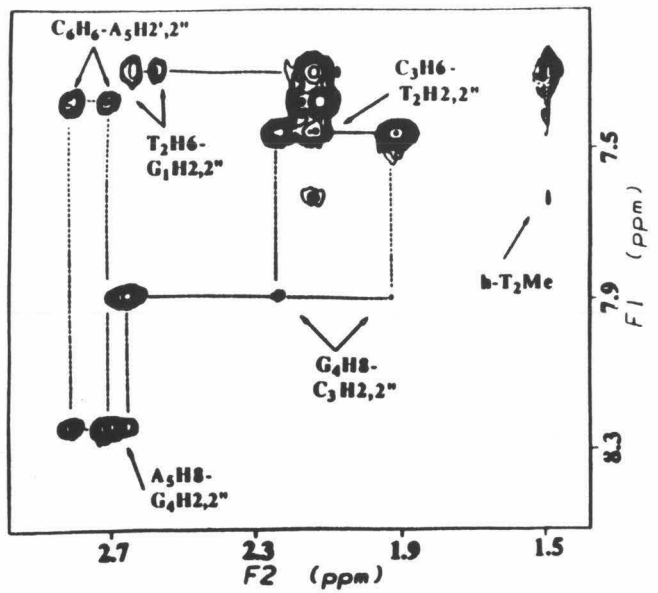
C6H6-A5H2',2"
C3H6-
T2H2,2"
T2H6-
G1H2,2"
h-T2Me
G4H8-
C3H2,2"
A5H8-
G4H2,2"
7.5
7.9
8.3
F1 (ppm)
2.7
2.3
1.9
1.5
F2 (ppm)

B

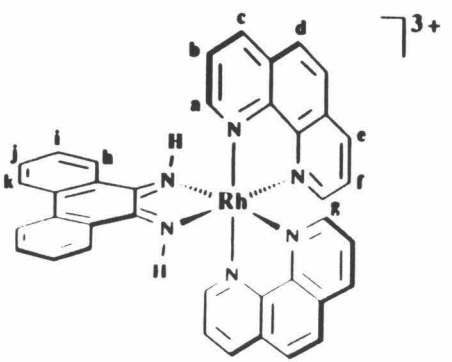
3+
Rh
N
H

C

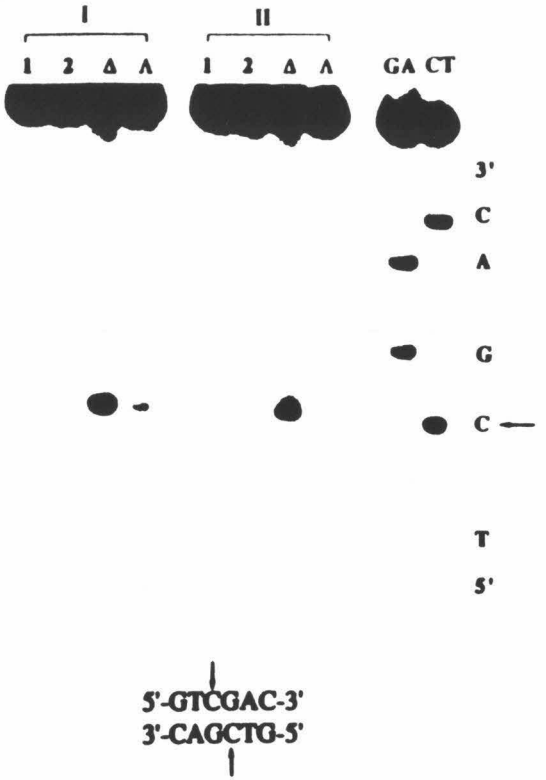
I
II
1 2 Δ Λ
1 2 Δ Λ
GA CT
3'
C
A
G
C
T
5'
5'-GTCGAC-3'
3'-CAGCTG-5'

Figure 1.4. Proposed mechanism of DNA cleavage by $[Rh(phi)]^{3+}$ complexes, (adapted from ref. 10). Photolysis of $[Rh(phi)]^{3+}$ complexes intercalated into the major groove of DNA leads to selective abstraction of the C3'-H atom, with formation of the C3'-radical. This can lead to degradation through oxygen-independent and oxygen-dependent pathways to form the identified products (boxed).

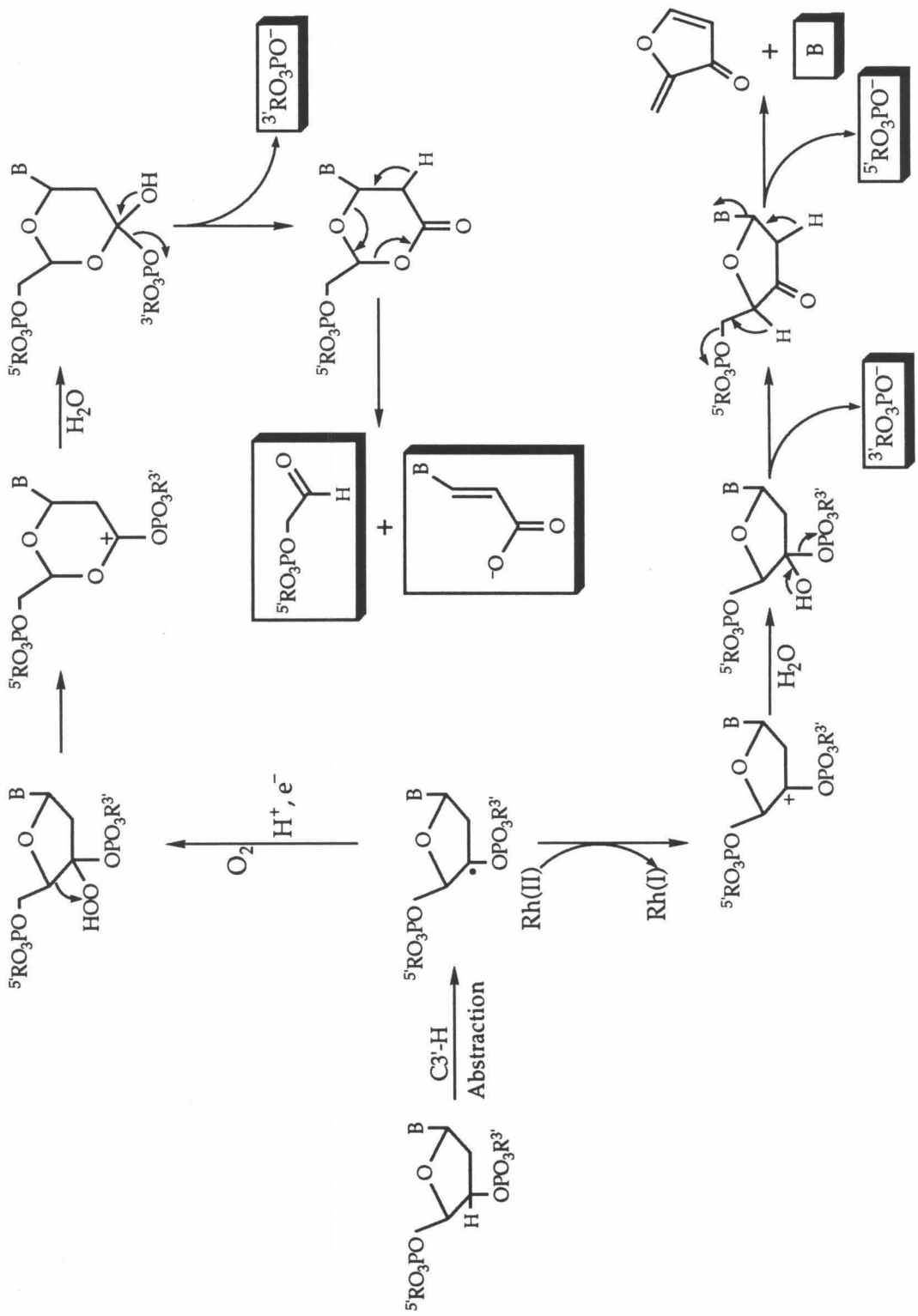
C3'-H
Abstraction
Rh(II)
Rh(I)
O_2
H^+, e^-
H_2O
H_2O
B
$5'RO_3PO$
$3'RO_3PO$
OPO_3R3'
HOO
HO
OH
H
$3'RO_3PO^-$
$5'RO_3PO^-$

insertion into the C3'-C4' bond and decomposition would yield the identified 5'-phosphate, 3'-phosphoglycaldehyde terminus and base propenoic acid. The quantitation of these products as well as the absence of detectable degradation products formed by modification at the C1'-, 4'-, or 5'- positions of the deoxyribose ring are therefore consistent with the model where phi complexes of rhodium bind and, with photolysis, react in the major groove of DNA. Unlike other small molecules and natural products which bind to and recognize the DNA minor groove, these metal complexes therefore appear to be unique in that they bind in the DNA major groove. Furthermore, since most proteins bind in the major groove of DNA, the study of site- and sequence-specific recognition by these metal complexes may be viewed as a model to understand some aspects of protein-DNA interactions.

While the mechanistic studies have been carried out on phi complexes containing polypyridyl ancillary ligands, the cleavage products obtained by Rh(polyamine)phi^{3+} complexes are consistent with a parallel mechanism of DNA strand scission. In general, then, the exploration of the mechanism of DNA photocleavage by these complexes has allowed us to use photocleavage as an assay to probe site-specific recognition. Since cleavage is mediated by a non-diffusible species, the point of strand scission represents the site of bound metal complex.

This mechanism contrasts with the photocleavage reactions found with [Ru(phen)$_3$]$^{2+}$. Here photolysis in the MLCT band sensitizes the formation of a diffusible singlet oxygen species that oxidatively adds to the DNA bases; addition of piperidine to the modified DNA strand leads to DNA strand scission. However, singlet oxygen reacts with different efficiencies with different bases (G >> T > A,C). Therefore in this case, normalization of the differing cleavage efficiencies must first be made before photocleavage is directly correlated with site-specific binding[10]. In the case of the rhodium(III) and cobalt(III) complexes, since the site of oxidative damage is the sugar, to

a first approximation, the sugars at each site should be equally reactive and thus photocleavage can provide a direct, unweighted marker for sites of binding.

1.3. Factors Important in Metal Complex-Nucleic Acid Recognition.

1.3.1. Steric Factors.

A simple understanding of the surface and intercalative binding modes of metal complexes to nucleic acids has allowed us to design metal complexes that can preferentially bind to and recognize specific nucleic acid structures. The nucleic acid photocleavage reactions of metal complexes has served as an important assay to examine nucleic acid recognition. In this section we illustrate, with examples, that nucleic acid recognition by metal complexes is dominated by steric and symmetry factors. Shape-selection, where the three-dimensional structure of the metal complex is matched in shape and symmetry to a nucleic acid site, may serve as a primary recognition element in distinguishing not only global features of nucleic acid tertiary structure, but also subtle variations in the local structure associated with single base pair steps.

Recognition of Global Features of Nucleic Acids.

The studies of $[Ru(phen)_3]^{2+}$ binding to B-DNA illustrates that the overall shape and chirality of octahedral, coordinatively saturated metal complexes determines the nature of nucleic acid-metal complex binding interactions. The complementarity between B-form DNA and $[Ru(phen)_3]^{2+}$ is such that surface binding in the minor groove is favored by the Λ isomer, and intercalative binding in the major groove is favored by the Δ isomer (Figure 1.5). Replacing the phenanthroline ligands with 3,4,7,8 -tetramethylphenanthroline ligands (TMP) precludes both intercalation and surface binding to B-form DNA; instead, $[Ru(TMP)_3]^{2+}$ binds preferentially to A-form helices[12]. Figure 1.6 illustrates that the bulky, sterically hindered shape of $[Ru(TMP)_3]^{2+}$

Figure 1.5. Binding modes of the Δ and Λ isomers of $[Ru(phen)_3]^{2+}$ to B-form DNA. Bottom panel shows that intercalation in the major groove of DNA is sterically favored by the Δ isomer since the disposition of the non-intercalated ligands follows the right-handed groove. The top panel illustrates the basis for preferential surface binding by the Λ isomer in the minor groove of DNA, since here the disposition of its ligands follows the right-handed groove.

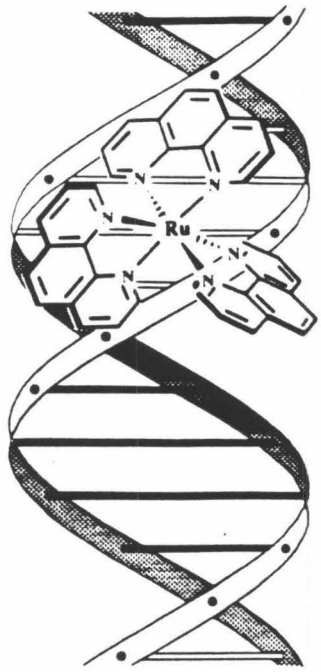

Λ

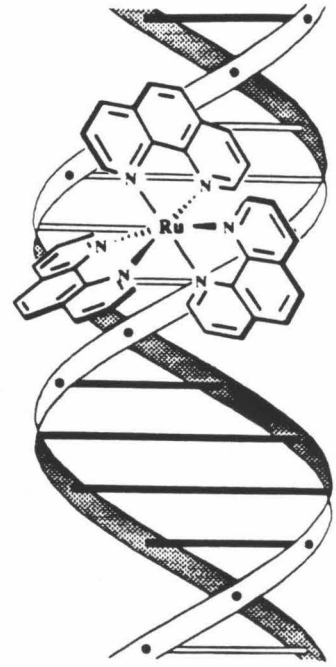

Δ

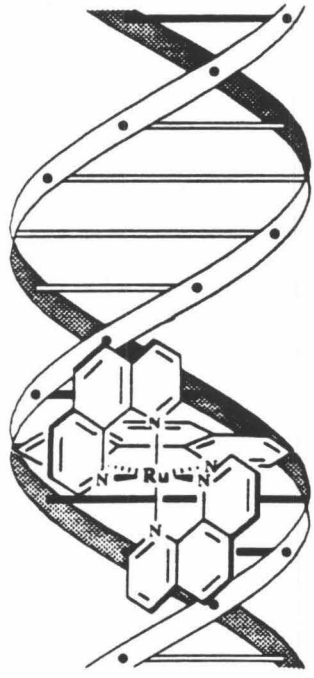

Λ

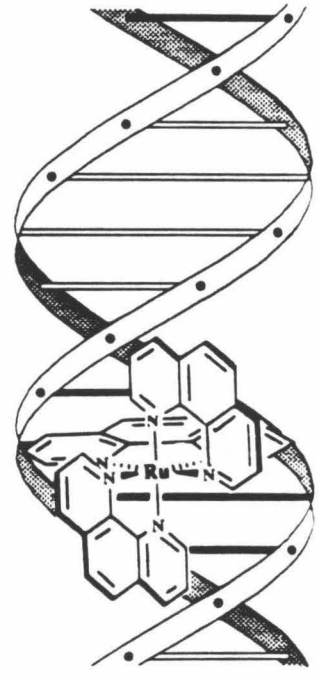

Δ

Figure 1.6. An illustration of preferential binding by $[Ru(TMP)_3]^{2+}$ in A-form over B-form helices. The shape of the complex is well-matched to bind against the shallow and wide minor groove surface of A-form helices (left), but is too large to surface bind in the deep and narrow minor groove of B-form DNA (right).

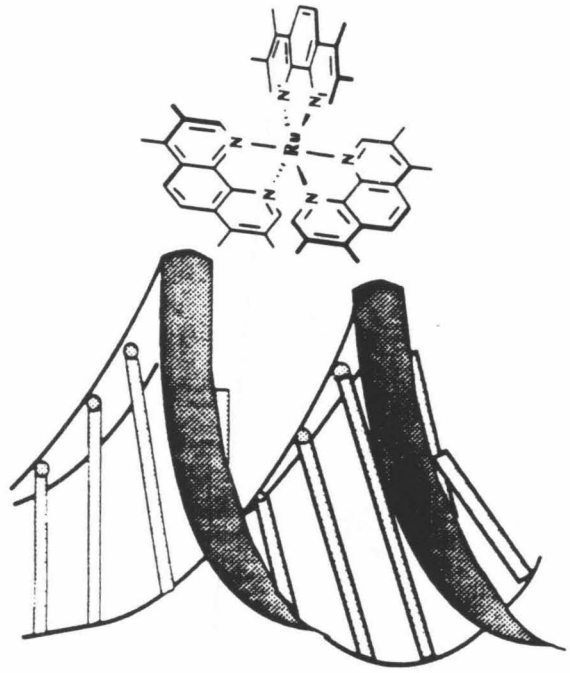

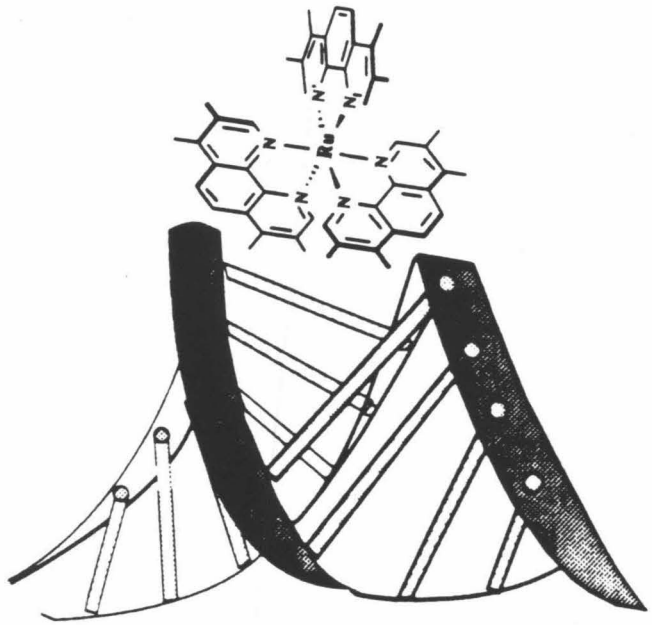

prevents it from binding in the deep and narrow minor groove of B-form DNA, but allows a hydrophobic association with the shallow and wide minor groove of A-form helices. Furthermore, owing to the right-handedness of A-form helices, preferential surface binding by the Λ isomer of $[Ru(TMP)_3]^{2+}$, with complementary symmetry, is observed.

Recognition of Sequence-Specific Secondary Structures and Tertiary Interactions.

On a more detailed level, shape-complementarity also appears to govern sequence-specific structural recognition by metal complexes. The complexes $[Rh(phen)_2phi]^{3+}$ and $[Rh(phi)_2bpy]^{3+}$ are highly shape-selective in their DNA sequence recognition characteristics[13]. Both complexes contain the phenanthrenequinone diimine (phi) ligand, which promotes tight intercalation and which allows them to associate intimately with the helix and to sense the local structure at the site of intercalation. Consistent with their DNA photocleavage chemistry[11], both complexes bind in the major groove of DNA. However, $[Rh(phen)_2phi]^{3+}$ and $[Rh(phi)_2bpy]^{3+}$ display remarkably different DNA recognition characteristics. With $[Rh(phen)_2phi]^{3+}$, upon intercalation of the phi ligand, the steric constraints imposed by the ancillary phenanthroline ligands leads to selective binding at sites which are more open in the major groove (Figure 1.7). For $[Rh(phi)_2bpy]^{3+}$, no similar steric constraints arise, because the steric bulk associated with the ancillary ligands is pulled back from the axial direction; therefore, this complex binds to most sites with equal affinity (Figure 1.7). Thus, despite the possibility of hydrogen bonding between the imine protons of the ancillary phi ligand in $[Rh(phi)_2bpy]^{3+}$ and the DNA bases, the complex is largely sequence-neutral in its recognition characteristics. In this instance, the simple comparison between $[Rh(phen)_2phi]^{3+}$ and $[Rh(phi)_2bpy]^{3+}$ underscores the importance of shape rather than hydrogen bonding in site-specific recognition of DNA.

$[Rh(phen)_2phi]^{3+}$ also displays chiral recognition within 5'-pyrimidine-purine-3' base-pair steps on the basis of its shape and symmetry[14]. Strong cleavage by the Δ isomer is observed at 5'-py-py-pu-3' steps where the shape of Δ-$[Rh(phen)_2phi]^{3+}$ matches the chiral pocket created by differential propeller twisting at these steps. The Λ isomer, with the opposite disposition of ancillary ligands upon intercalation, clashes with the pyrimidines at these steps; hence little or no cleavage is observed for this isomer. $[Rh(phen)_2phi]^{3+}$ also recognizes 5'-py-py-py-3' steps, but since this step has no C_2 axis along the intercalative dyad axis, little or no enantiomeric discrimination is observed (Figure 1.8); likely these sites are recognized owing to an opening in the major groove which results from base tilting. Thus, based on steric and symmetry considerations, $[Rh(phen)_2phi]^{3+}$ shows selectivity in the recognition of sites within B-DNA.

$[Rh(phen)_2phi]^{3+}$ also displays shape-selectivity in its recognition of crystallographically well-characterized t-RNA molecules[15]. While double helical regions of RNA adopt primarily the A-conformation, RNA molecules also contain complex tertiary interactions which establish the three-dimensional folding of the nucleic acid. Consistent with its DNA recognition characteristics, $[Rh(phen)_2phi]^{3+}$ does not intercalate into the deepened major groove of A-like conformations. Instead the complex, which binds avidly by intercalation from the major groove, specifically targets sites in tRNA in which three bases are hydrogen bonded to another. As is evident in crystal structures of t-RNAs, the third base in triply hydrogen bonded array interacts in the major groove through Hoogsteen base hydrogen bonding with a purine of a normal Watson Crick base pair. This stabilized base position then creates a filled major groove site which may serve as a platform for intercalative stacking by the metal complex. Mutations which preserve the structures of the triply bonded region of the tRNA are still cleaved by $[Rh(phen)_2phi]^{3+}$ indicating that the molecule recognizes the structure generated by the triply bonded array rather than individual nucleotides (Figure 1.9).

Figure 1.7. Shape-selective recognition of local DNA structure by $[Rh(phen)_2phi]^{3+}$ and $[Rh(phi)_2bpy]^{3+}$ (adapted from ref. 13). The schematic illustrates intercalation of $[Rh(phen)_2phi]^{3+}$ and $[Rh(phi)_2bpy]^{3+}$ into either an opened or canonical major groove DNA site, respectively. For $[Rh(phen)_2phi]^{3+}$, the steric constraints imposed by its ancillary phenanthroline ligands promotes selective intercalation of this complex at such opened sites. In $[Rh(phi)_2bpy]^{3+}$, the lack of similar steric requirements by its ancillary phi ligand, which is pulled back from the metal center, allows the complex to bind to most sites.

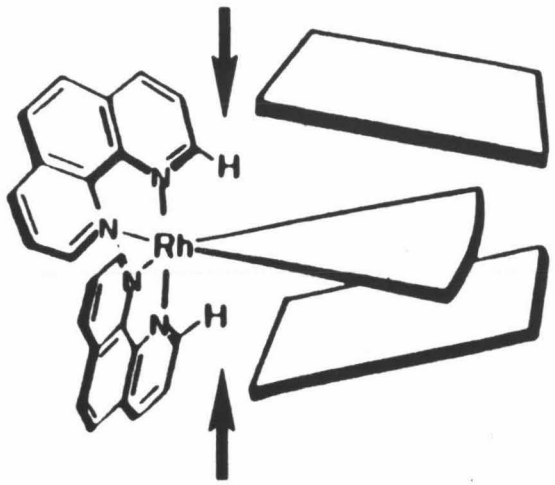

$[Rh(phen)_2(phi)]^{3+}$

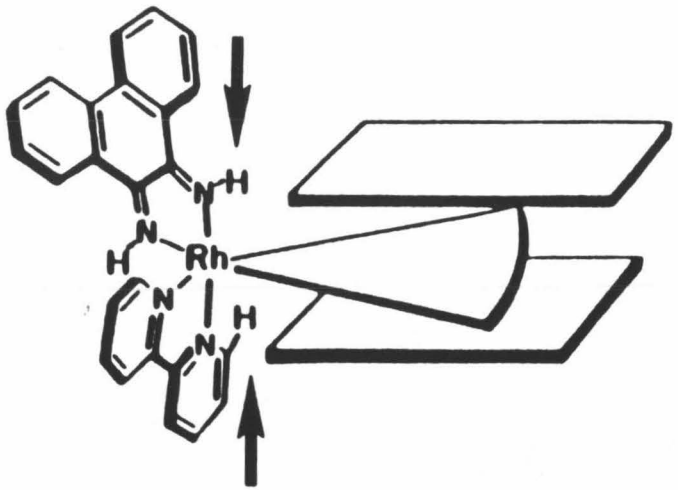

$[Rh(phi)_2(bpy)]^{3+}$

Figure 1.8. Chiral discrimination in binding to propeller-twisted sites on DNA by the Δ and Λ isomers of $[Rh(phen)_2phi]^{3+}$ (adapted from ref. 14a). As shown in the top panel, a highly differentially propeller-twisted 5'-py-pu-3' step creates a chiral pocket which matches the shape of the Δ isomer, but clashes with the orientation of the ancillary ligands of the Λ isomer. Thus this C_2 symmetric step (with an intercalative dyad axis marked by the ·) promotes enantiospecific recognition by the isomers of $[Rh(phen)_2phi]^{3+}$. As shown in the bottom panel, a 5'-py-py-3' step lacks a C_2 dyad axis and thus enantiomeric discrimination of this step does not occur.

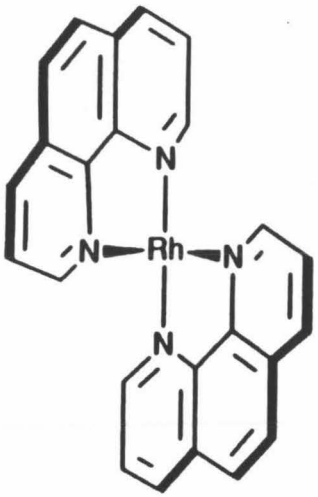

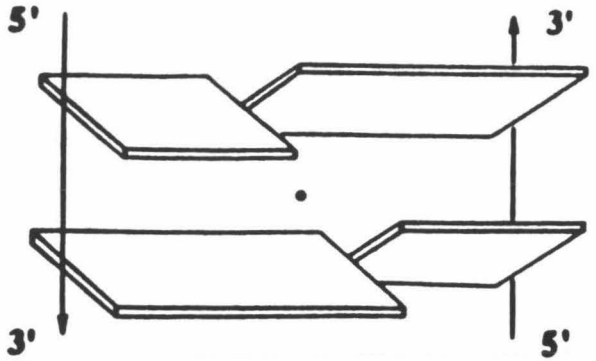

5' Py-Pu 3'

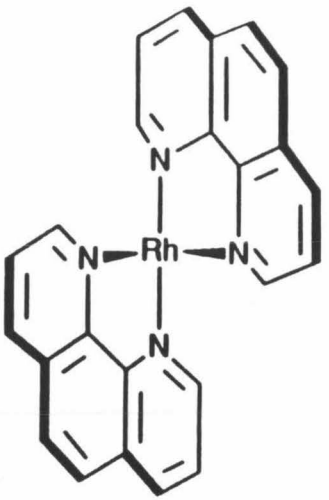

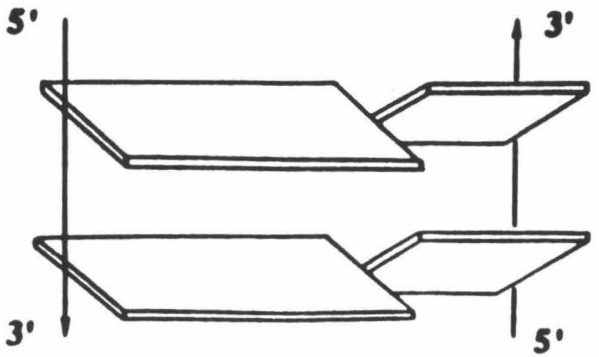

5' Pu-Pu 3'

Figure 1.9. $[Rh(phen)_2phi]^{3+}$ cleavage at triple-base sites on native and mutant t-RNA^{phe} substrates (adapted from ref. 15b).

A. Schematic showing cleavage sites on native yeast t-RNAphe. The arrow points to cleavage at the G45-[G10-C25] tertiary interaction.

B. Cleavage on t-RNA^{phe} substrates containing a single G45U mutation (left) and a double G10C, C25G mutation (right). The arrows point to cleavage at the mutated triple base sites. Both these mutations should preserve the triple-base interaction at this site by forming the base triplets **U45**-[G10-C25] and G45-[**C10-G25**], respectively. Cleavage at this site in both mutants is comparable to cleavage on the native t-RNA^{phe} substrate.

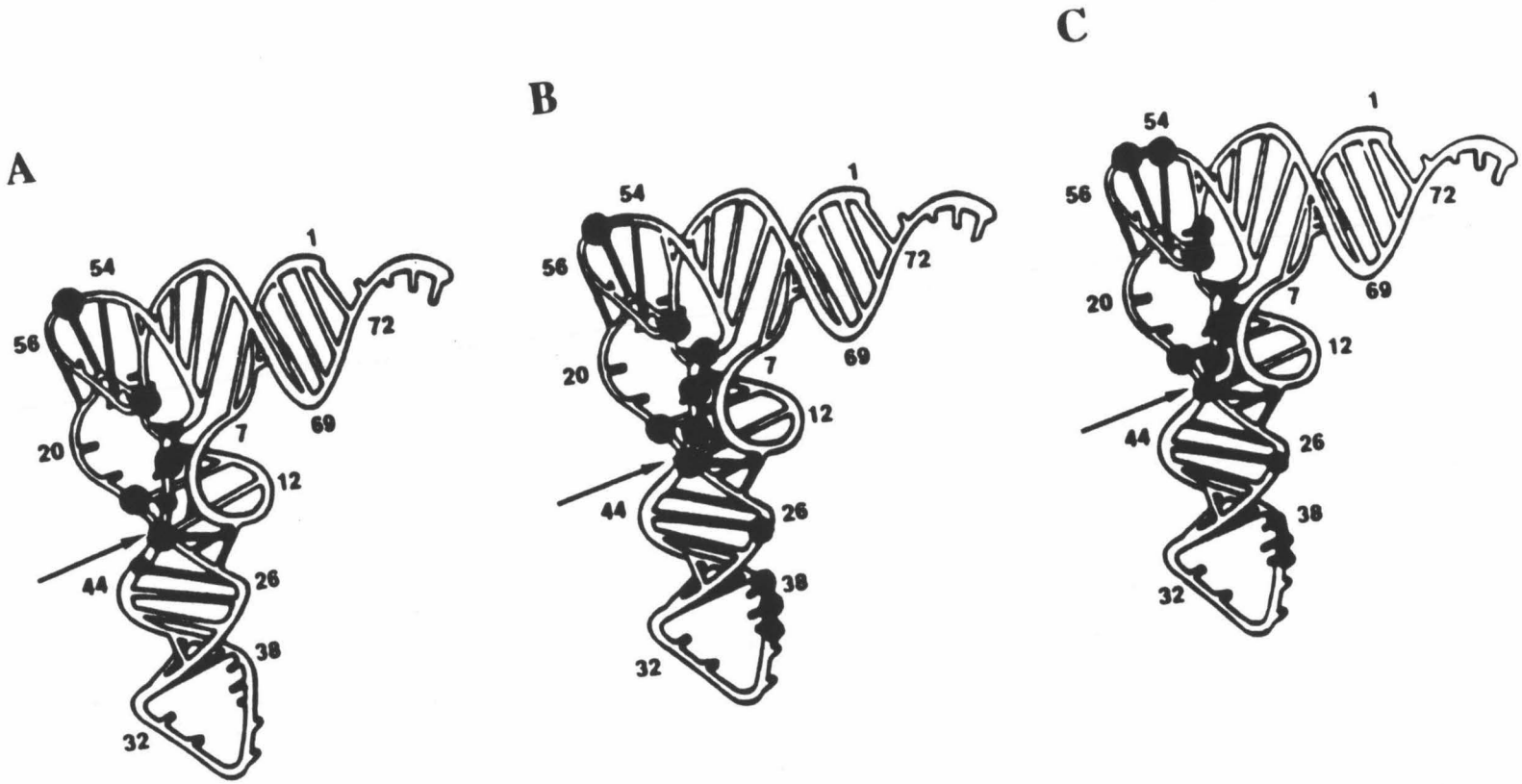
A
54
1
56
72
20
7
69
12
44
26
38
32
B
54
1
56
72
20
7
69
12
44
26
38
32
C
54
1
56
72
20
7
69
12
44
26
38
32

Selective depurination of this third base position furthermore decreases selective targeting by $[Rh(phen)_2phi]^{3+}$. Interestingly, competition experiments[5b] have shown that the complex $[Ru(bpy)_2dppz]^{2+}$, owing to its avidly intercalating dppz ligand, also binds to some of the t-RNA triple sites targeted by $[Rh(phen)_2phi]^{3+}$.

Recognition of Folded RNA and DNA Molecules of Unknown Structure.

Based upon the cleavage characteristics observed on the crystallographically well-characterized tRNAs, $[Rh(phen)_2phi]^{3+}$ appears to target sites of tertiary interactions and hence may be a valuable chemical probe in structurally characterizing the folding of RNA molecules. In that context $[Rh(phen)_2phi]^{3+}$ has been useful in probing the tertiary structure of *Xenopus oocyte* 5S rRNA[16]. A map of the photocleavage patterns of $[Rh(phen)_2phi]^{3+}$ on the proposed secondary structure of 5S rRNA (Figure 1.10) shows that the rhodium complex recognizes several families of localized tertiary interactions, including stem-loops, structured loops, and sites with mismatched bases. Consistent with its recognition of crystallographically characterized tRNAs, $[Rh(phen)_2phi]^{3+}$ does not bind to double-helical or single stranded regions of 5S RNA. Instead, the complex targets regions containing complex tertiary structure in which the major groove has become more accessible. Stem-loop junctions, multiple bulged nucleotides and base-pair mismatches in helical regions all appear to cause a widening of the major groove. These sites of localized tertiary interactions are thus likely to facilitate intercalation via the phi ligand and to accommodate the steric bulk offered by the ancillary phenanthroline ligands. Furthermore, as shown in Figure 1.10, strong cleavage by $[Rh(phen)_2phi]^{3+}$ is seen in the loop regions of C and E, indicating that the two loops are intimately and intrinsically structured by noncanonical base-pairing or base stacking interactions. This conclusion is consistent with the results that both loops are not only resistant to single- and double- strand-specific nucleases but also inaccessible to chemical probing.

Cleavage on a truncated *Xenopus* oocyte 5S rRNA, comprising of stems IV and V and loops E and D, is almost identical to that obtained for wild-type 5S rRNA. This observation is consistent with a model for the RNA which adopts an opened T-structure and where the rhodium complex recognizes independent tertiary structures in which the major groove has become accessible to intercalative stacking, as in helix IV and loop E. Interestingly, in support of these observations, recent NMR studies by Wimberly et al.[17] have suggested that the two strands of loop E are involved in base-pairing or stacking interactions.

Shape-selective recognition has also been useful in probing folded DNA structures which are held together by tertiary interactions. The complex $[Rh(DIP)_3]^{3+}$ yields specific double-stranded cleavage at the base of cruciforms extruded by supercoiled plasmids[18a]. No specific cleavage is observed in the corresponding linearized plasmids, which illustrates that the complex is recognizing a folded structure and not local structures associated with particular sequences. Clearly, the complex has no hydrogen bond donors or acceptors; instead the well-defined hydrophobic structure may recognize a small pocket created by cruciform helices that interact with each other. $[Rh(DIP)_3]^{3+}$ also cleaves specifically at the junction point of Holliday junctions[18b], which are believed to be structural intermediates in genetic recombination and bear some resemblance to the folding of cruciforms.

The complex has also been a powerful shape-selective tool in probing completely unknown tertiary DNA structures. Site-specific targeting by $[Rh(DIP)_3]^{3+}$ has provided evidence for a distinct structure delineating introns on the DNA level[18c]. The complex cleaves specifically adjacent to the branch points of introns of Simian Virus 40 T-antigen and Adenovirus 2 E1A genes inserted in supercoiled double-stranded plasmids (Figure 1.11). Also cleavage at the donor and acceptor sites of the intron of the SV40 -T antigen gene is observed. Importantly, while the cleavage sites in the coding strand of the two

Figure 1.10. Recognition of stem-loop junctions and base-pair mismatches in *Xenopus* 5S rRNA by $[Rh(phen)_2phi]^{3+}$ (adapted from ref. 16). The arrows indicate the positions of $[Rh(phen)_2phi]^{3+}$ promoted strand scission with length corresponding to relative cleavage intensity.

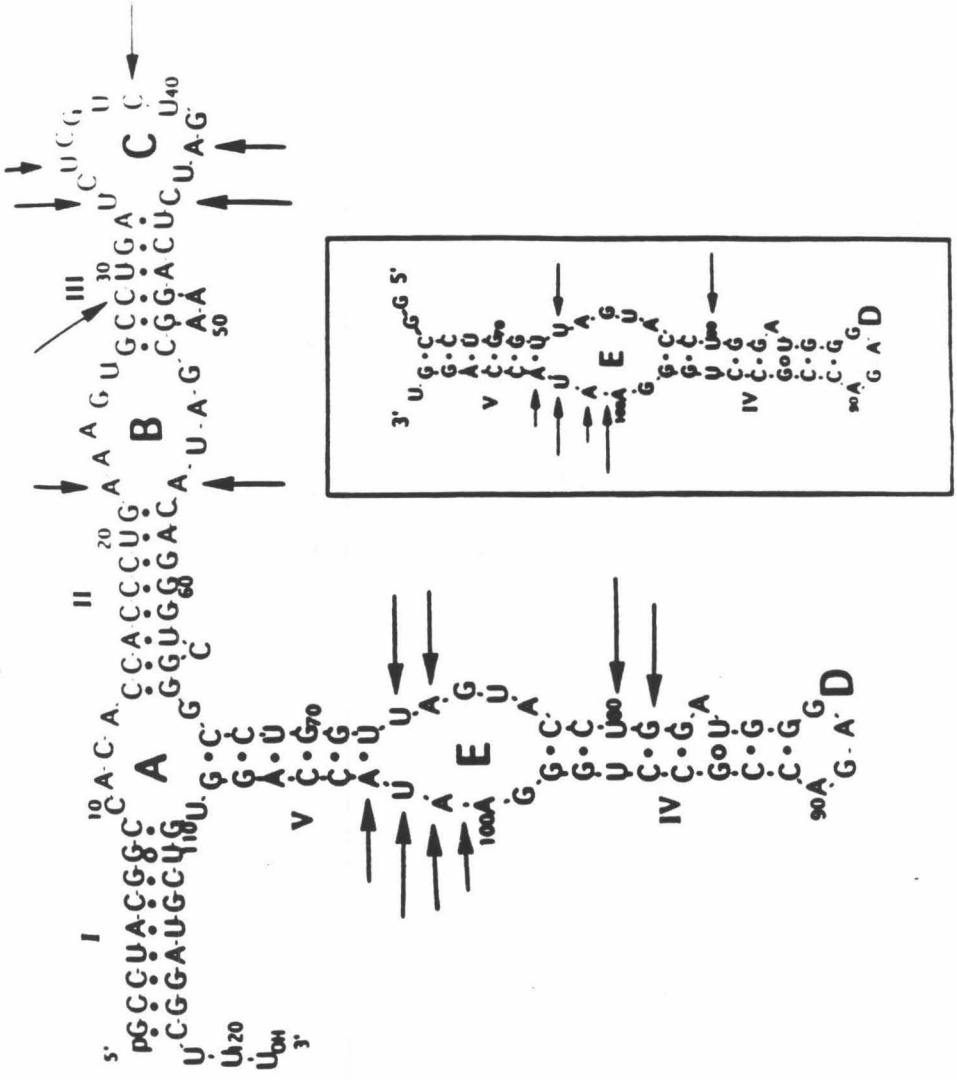

Figure 1.11. Schematic illustration of cleavage by $[Rh(DIP)_3]^{3+}$ at functionally important sites in the introns of Simian Virus 40 T-antigen and Adenovirus 2E1A genes (adapted from ref. 18c). The two genes are represented, roughly to scale, by bars. Solid shaded elements represent exons and the unshaded elements, the introns of interest. The arrows point to the sites of $[Rh(DIP)_3]^{3+}$ cleavage. On the 2E1A gene, substantial cleavage is observed near the branch point of the intron; however, on the SV40 gene cleavage is seen most strongly at the donor site and less strongly at the acceptor site and near the branch site.

Simian Virus 40 T Antigen Transcription Unit

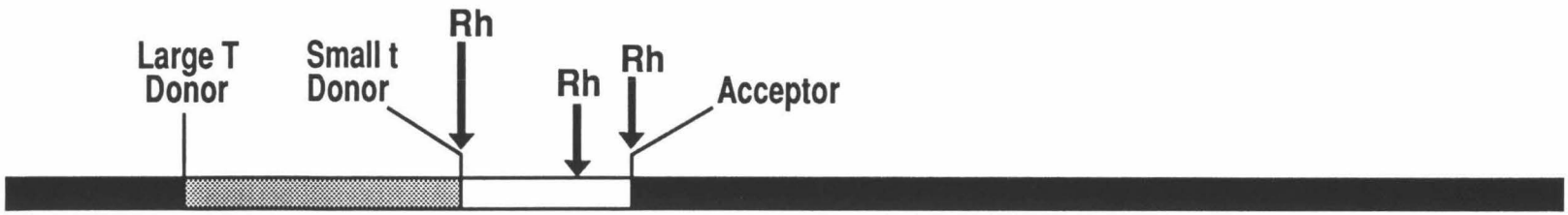

Adenovirus 2 E1A Transcription Unit

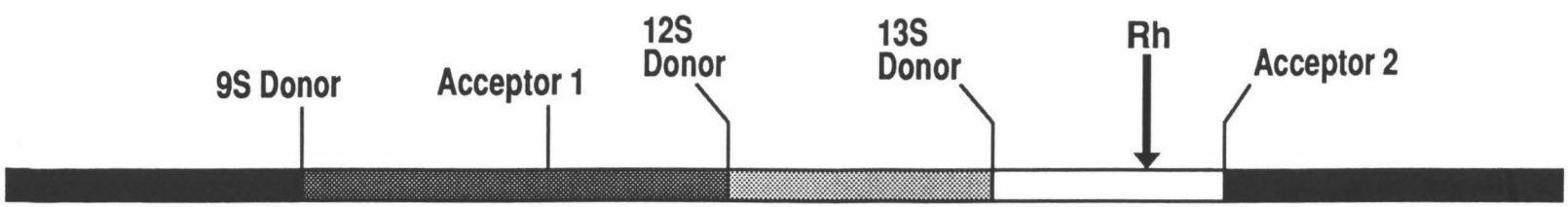

mammalian viral genes lack sequence homology, they are similar in that they demarcate functionally important sites. Targeting by the metal complex may suggest a similar targeting by proteins within the cell. In conclusion, shape-selective metal complexes have the potential to recognize novel and unknown sites of tertiary structures, which are prone to structural characterization by chemical probes.

1.3.2. Other Factors Important in Recognition.

While the importance of shape-selection in recognition of nucleic acids by metal complexes cannot be overstated, this section will present examples that illustrate the importance of other factors in site-selective recognition. Positive contributions to site-selectivity may emanate not only through specific hydrogen bonding interactions to base positions, but also as the result of site-specific stacking interactions or even through the cooperative non-covalent associations of two metal complexes bound at adjacent sites along the polymer.

The study of phi complexes of rhodium(III) containing saturated amines and macrocyclic thioethers as ancillary ligands (Figure 1.12) has pointed to the importance of hydrogen bonding and van der Waals interactions to DNA site specificity[19]. Phi complexes of rhodium containing saturated amine ligands also bind avidly to DNA by intercalation and with photoactivation promote efficient strand cleavage. A 5'-GC-3' selectivity in cleavage is observed with the complexes $[Rh(en)_2phi]^{3+}$, $[Rh(NH_3)_4phi]^{3+}$, and $[Rh([12]aneN_4)phi]^{3+}$ and this site-selectivity is likely to arise from hydrogen bonding between the axial amines in their ancillary ligands and the O6 of guanines (Figure 1.13). The cyclic thioether complex $[Rh([12]aneS_4)phi]^{3+}$, which lacks hydrogen bonding functionalities, shows no preference for 5'-GC-3' steps. Instead, the complex has a remarkably high level of specificity for 5'-ATG, 5'-ACG and 5'-ACT steps, with cleavage occurring at the highlighted residues, presumably again based upon

Figure 1.12. Structures of some $[Rh(phi)]^{3+}$ complexes with saturated amines and thioethers as ancillary ligands (adapted from ref. 19). The top panel shows the Δ and Λ isomers of $[Rh(en)_2phi]^{3+}$ (en = ethylenediamine, phi = 9,10-phenanthrenequinone diimine). The bottom panel shows the structures of $[Rh([12]andN_4)phi]^{3+}$ (left) and $[Rh([12]aneS_4)phi]^{3+}$ (right).

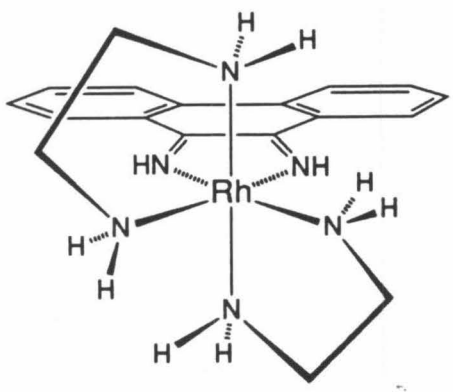
H
H
N
HN
NH
Rh
H
H
N
H
H
N
H
H
N
H
H

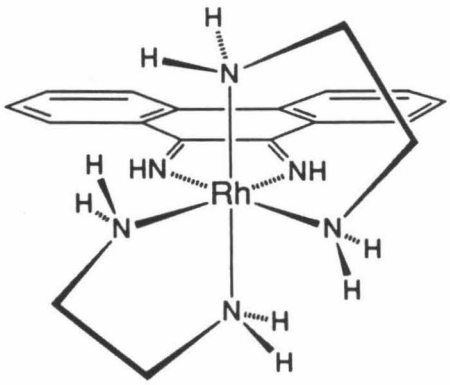
H
H
N
H
HN
NH
Rh
H
N
N
H
H
N
H
H

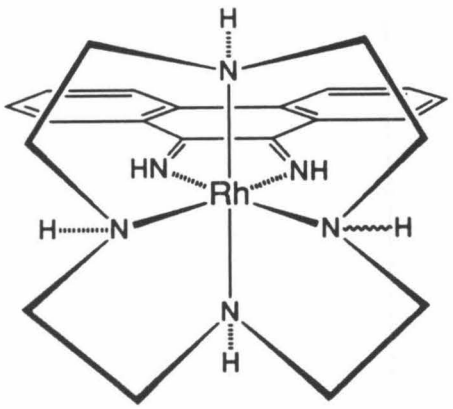
H
N
HN
NH
Rh
H
N
N
H
N
H

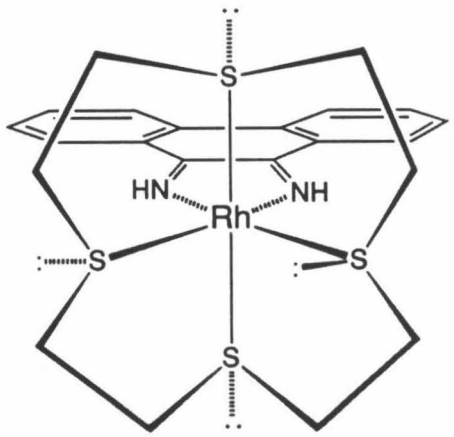
S
HN
NH
Rh
S
S
S

Figure 1.13. Recognition of 5'-GC-3' and 5'-TA-3' steps by the Δ and Λ isomers of $[Rh(en)_2phi]^{3+}$: importance of hydrogen bonding and methyl-methylene Van der Waals interactions. The top panel illustrates the basis for GC specificity by both isomers. The O6 of guanines in the GC base step is well-positioned to make H-bonding contacts with the axial amines of the ethylendiamine ligands. The bottom panel illustrates the basis for enantiospecific recognition of the TA step by the isomers. While the Λ isomer is well-positioned to afford positive Van der Waals interactions, between its methylene groups and the thymine methyl groups, the symmetry of the intercalated Δ isomer does not afford similar interactions.

Λ-[Rh(en)$_2$ phi]$^{3+}$

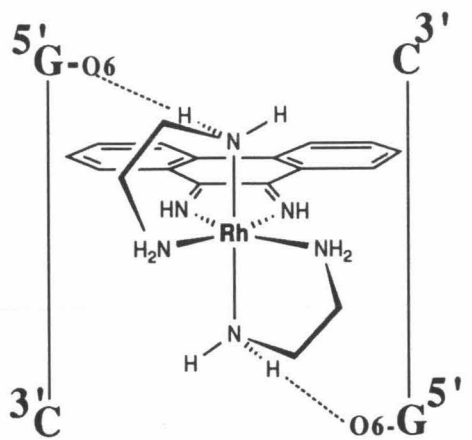

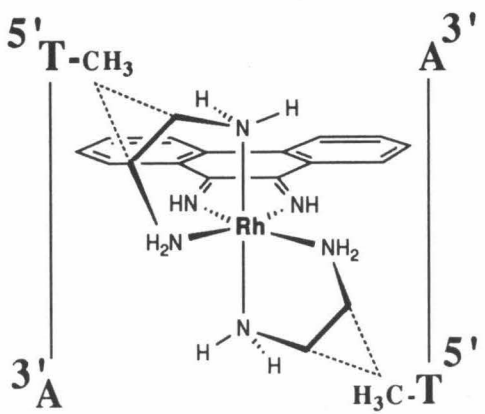

Δ-[Rh(en)$_2$ phi]$^{3+}$

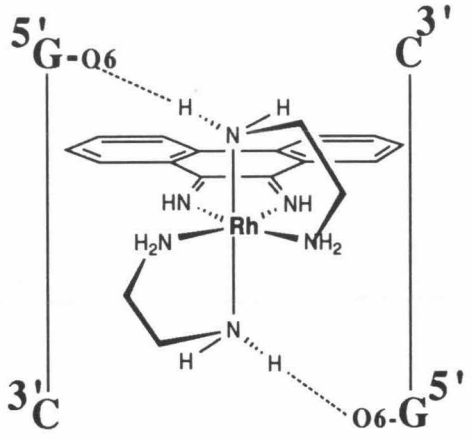

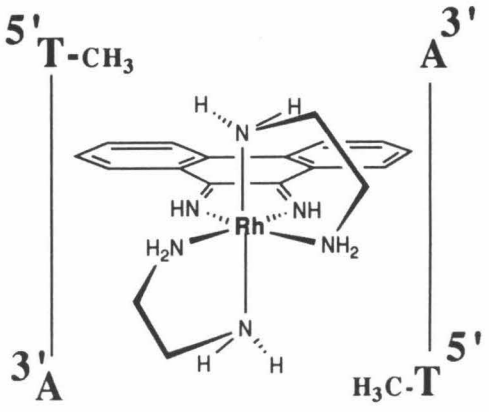

shape-selection. It is interesting that besides targeting 5'-GC-3' steps, Λ-$[Rh(en)_2phi]^{3+}$ also enantioselectively targets 5'-TX-3' sites. The preference of the Λ isomer of $[Rh(en)_2phi]^{3+}$ for 5'-TA-3' steps suggests the possibility of stabilizing van der Waals contacts between the methylene groups of the ancillary ethylene diamine ligand and the thymine methyl group, located in the major groove (Figure 1.13). Moreover, replacement of a thymine by uracil, which lacks the methyl group, abolishes the enantioselectivity in cleavage at the 5'-UA-3' site on an oligonucleotide. Modeling studies have shown that analogous interactions between the Δ isomer and a 5'-AT-3' step are not available owing to the right handed helicity of DNA.

It is noteworthy in this discussion that $[Rh([12]aneS_4)phi]^{3+}$ shows a strong preference for 5'-AXY sites with the complex intercalated between the XY base step, even though molecular modeling has shown that the complex is small enough to span only a single base step in an intercalated DNA site. This observation points to the role that sequences flanking the binding site may play in stabilizing the post-intercalative binding state. Intercalation and unwinding of the helix via the phi ligand may promote significant structural changes in the binding site which must be accommodated through stacking interactions with the neighboring base-pairs. It is likely that the structural change induced by this complex is stabilized by the neighboring 5'-AT base pair. However, the importance of flanking sequences in recognition by metallointercalators is likely to be a more general phenomenon. As is typical for classical intercalating agents, intercalation by the octahedral metal complexes causes the DNA helix to unwind by 15-25 degrees; the contribution of neighboring base-pairs is likely to depend on the structural changes induced at the binding site[20]. The ability of flanking base-pairs to accommodate structural perturbations at the binding site may be closely related to their level of deformability in the context of a particular sequence. While recognition by metallointercalators of the pre-intercalation state may be more directly related to the local

structural variations, stabilization of the post-intercalation state may be more directly related to the extent of sequence-deformability.

The energy gained through base-pair stacking interactions is the driving force for intercalation by metal complexes. This intercalative stacking may also play an important role in site-specific recognition. Preferential intercalative binding at unstacked or weakly stacked regions of nucleic acids may occur; conversely, destacked regions may form a distinct structure that is preferentially stabilized by the metal complex. For example, the complex $[Rh(DIP)_3]^{3+}$ shows a remarkable level of specificity for guanine-uracil (G-U) mismatches in double helical regions of folded RNAs[21]. In particular, specific cleavage is observed by the complex at the residue which lies to the 3'-side of the wobble-paired U. Changing the orientation of the G-U wobble pair changes the position of cleavage. Interestingly, crystal structures[22] have revealed that the geometry of the G-U wobble base-pair results in an unusual stacking of its bases with the neighboring bases. The stacking interactions on either side of the G-U mismatch differ greatly, with the base-pair on the 3'-side of the U exhibiting highly destacked structures with the U extended into the major groove of the RNA (Figure 1.14.). It appears that the highly hydrophobic complex $[Rh(DIP)_3]^{3+}$ is able to detect these differences in base-stacking with the flanking base-pairs without specific hydrogen bonding interactions. Shape-selective targeting of the 3'-side of the G-U mismatch is favored.

Finally, there is reason to believe that like DNA binding proteins, metal complexes have the potential to associate or non-covalently dimerize in order to afford high levels of specificity. The complex $[Rh(4,4'\text{-diphenylbipyridyl})_2phi]^{3+}$ has a level of specificity for the eight base-pair palindromic site 5'-CTCTAGAG-3' that rivals restriction enzymes[23]. This complex, which is highly hydrophobic and lacks hydrogen-bonding functionalities, is able to shape-selectively recognize the specific sequence-dependent structure associated with the eight base-pair 5'-CTCTAGAG-3' site.

Competitive thermodynamic experiments have suggested that two molecules of the complex [Rh(4,4'-diphenylbipyridyl)$_2$phi]$^{3+}$ bind simultaneously and cooperatively through non-covalent associations one with another on an eight base-pair site on linear DNA. As shown in Figure 1.15, at low concentrations of the metal complex, cleavage is observed at the eight base-pair dimeric 5'-CTCTAGAG-3' site preferentially over the monomeric six base-pair 5'-CTCTAG-3' site. This added stabilization, derived through dimerization on the DNA polymer, therefore provides a valuable strategy to increase sequence-specificity of the small transition metal complexes on DNA.

1.4. Parallels Between Metal Complex- and Protein-Nucleic acid Recognition: Biological Implications.

Correlations between the sites specifically targeted by metal complexes and important protein-binding sites on DNA were initially observed in studies of cleavage by the chiral complex Λ-Co(DIP)$_3^{3+}$ on the Simian Virus-40 genome[24]. The sites of Λ-Co(DIP)$_3^{3+}$ cleavage include the origin of replication, transcriptional promoter and enhancer regions, and the ends of coding regions for early and late genes. Interestingly, all these sites flank protein coding regions and perhaps the specific structures associated with these cleavage sites may play a role in protein recognition and gene expression. Similarly, several rhodium intercalators appear to target specific sites in RNA and DNA that correspond to important protein-binding sites. Perhaps, then, these metal complexes may serve as models to understand basic principles governing the recognition of nucleic acids by proteins.

In particular, the complex [Rh(4,4'-diphenylbpy)$_2$phi]$^{3+}$ is specific for the palindromic eight base-pair 5'-CTCTAGAG-3' site, with the central six base-pair sequence 5'-TCTAGA-3' forming the central core for the overlapping recognition boxes of the *E.coli met* repressor protein[25]. While there is evidence to suggest that two

molecules of this complex dimerize across the central CTAG sequence, the *E.coli met*-DNA crystal structure shows that the *met* dimerization domain contains β-sheets which lie across a CTAG site, central to the operator sequence. The CTAG sequence appears to be a recognition motif for other DNA binding proteins such as the *E.coli trp* repressor and S1 and micrococcal nucleases. Crystal structures have shown that this sequence is characterized by an unusually distorted phosphate backbone, which may be an important recognition signal for both the metal complex $[Rh(4,4'\text{-diphenylbpy})_2phi]^{3+}$ and DNA-binding proteins. Importantly, the co-crystal structures of the *met*-DNA and *trp*-DNA complexes[25,26] show no direct amino acid-base specific contacts in this region, thereby implicating the importance of indirect-readout or shape-selection in DNA recognition at these sites.

Similarly, the study of the interactions between rhodium complexes and RNA have shown that shape selection may also be an important criterion in determining protein-RNA recognition. Interestingly, the sites generally recognized by $[Rh(phen)_2phi]^{3+}$ and $[Rh(DIP)_3]^{3+}$ appear to correspond to critical elements for RNA recognition by proteins: triple-base sites, stem-loop junctions, base-pair mismatches, and bulged residues. The rhodium complexes we have studied appear to bind at sites where the normally deep and narrow major groove of RNA has become more accessible and open, due to tertiary interactions. Similarly, recent studies have suggested a model for RNA-protein recognition which involves the distortion of the A-form double helix in RNA by bulged nucleotides, thereby permitting protein binding in the open major groove[27]. Additionally, the importance of stem-loop junctions and G-U base mismatches have been implicated as recognition motifs for t-RNA binding yeast aspartyl-tRNA synthetase and E.coli alanyl-tRNA synthetase respectively[3a,28]. Hence sites of unique structural distortion may not only punctuate sites for the specific binding by transition metal complexes but also mark structural elements that are recognized by proteins.

Figure 1.14. The stacking configuration at the 3'-end (top) and 5'-end (bottom) of the G4-U69 wobble pair in the middle of the acceptor stem of yeast $tRNA^{phe}$ (adapted from ref. 22). Compared to the 5'-end of the mismatch, the 3'-side of the U exhibits a highly destacked structure which may be recognized by the shape-selective $[Rh(DIP)_3]^{3+}$ metal complex.

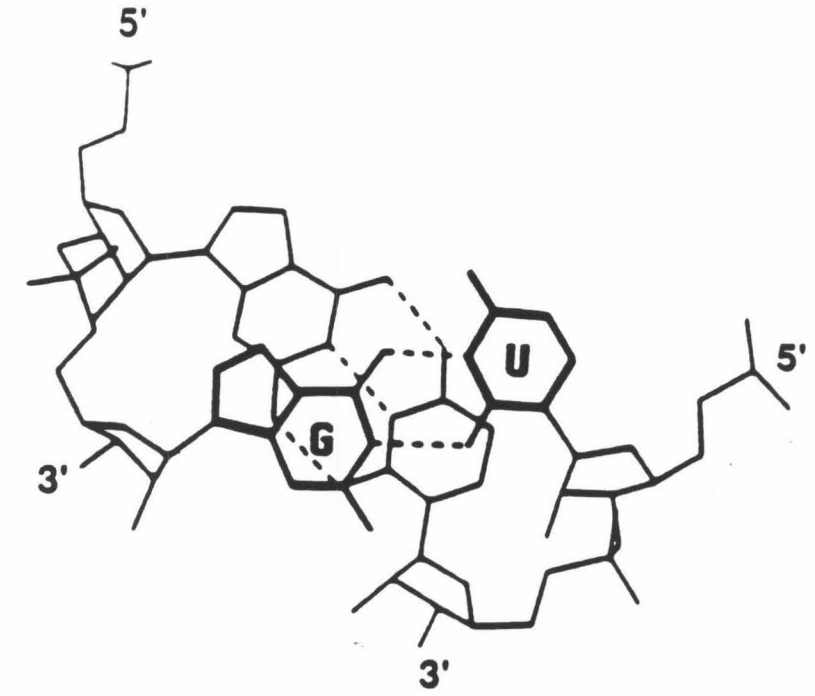
5'
U
5'
G
3'
3'

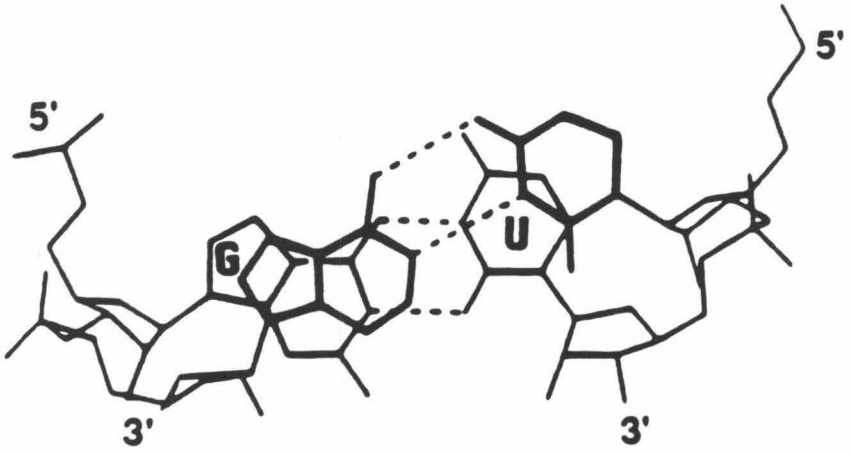
5'
5'
U
G
3'
3'

Figure 1.15. Evidence for non-covalent dimerization of $[Rh(DPB)_2phi]^{3+}$ at the eight base-pair palindromic 5'-CTCTAGAG-3' site.

A. Structure of $[Rh(DPB)_2phi]^{3+}$, where DPB = 4,4'-diphenylbipyridyl and phi = 9,10-phenanthrenequinone diimine.

B. The top panel shows a schematic of a 28 mer double-stranded oligomer containing the indicated eight base-pair, six base-pair, and four base-pair sites. Note that the eight base-pair site is a composite of two overlapping 6 mer 5'-CTCTAG-3' sites located on opposite strands. Arrows refer to cleavage by $[Rh(DPB)_2phi]^{3+}$ on both strands of the oligomer and the short lines between the two strands of the oligonucleotide, represent the site of intercalation by the metal complex. A table summarizing the cleavage at each site as a function of DNA/Rh concentration (where the DNA/Rh ratio is kept constant at 2 duplexes/ 1 Rh-complex) is shown in the bottom panel. At low concentrations, the cleavage per strand at the eight-mer site is greater than that observed for the six-mer and four-mer sites. This suggests that the two complexes bind *simultaneously and cooperatively* at the two overlapping six-mer 5'-CTCTAG-3' sites contained in the composite eight-mer site.

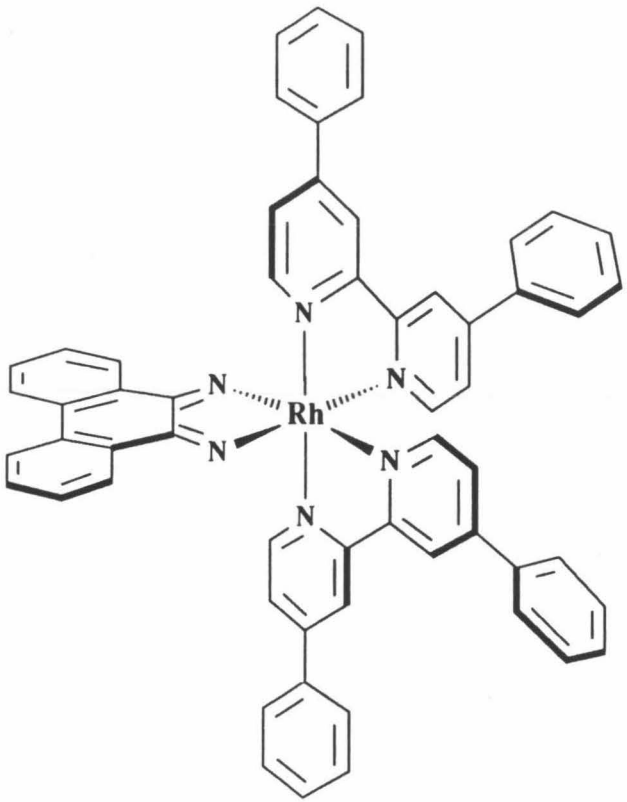

$[Rh(4,4'\text{-diphenylbpy})_2(phi)]^{3+}$

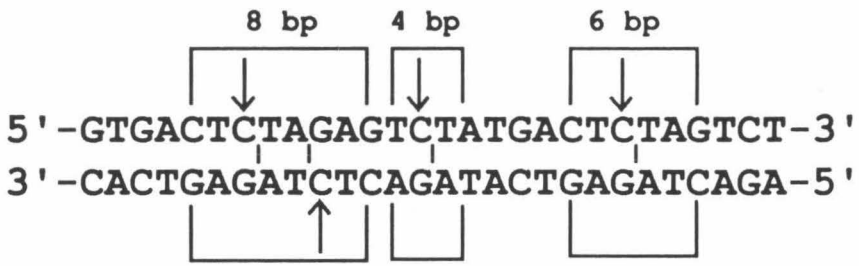

	Cleavage		
Conc. (nM)	8 bp	4 bp	6 bp
1000 - 500	+++++	+	+++++
500 - 300	++++	-	+++
300 - 100	+++	-	++
100 - 50	+	-	-

1.5. Prospects for the Future.

The examples we have described illustrate how novel metal complexes may be constructed to achieve site-specific targeting. The primary lesson we have learned thus far has been the critical importance of a shape-selective matching of the structure of the metal complex to its nucleic acid binding site. Indeed the correlations between nucleic acid sites recognized by rhodium complexes and sites specifically bound by proteins highlight the value of shape-selective recognition.

Could this shape-selective design be useful in the construction of novel therapeutics? Inorganic pharmaceuticals such as cis-platin and metallobleomycin have proven to be remarkably successful as anticancer agents, but for a truly new generation of inorganic compounds the goal is clearly a new level of selective targeting and specificity. Certainly the first step in this rational design depends upon a chemical understanding of what hierarchy of factors govern the ensemble of non-covalent interactions which together lead to site-specific recognition. Transition metal chemistry has already been proven to be valuable in elucidating these factors. Shape-selection is surely one important element. It has now been demonstrated that shape-selection may be exploited in the construction of metal complexes which bind DNA with both affinities and specificities that rival DNA-binding proteins. New designs based upon shape-selection, however, require a better three-dimensional understanding of the local sequence-dependent structure of DNA. Here the transition metal complexes already prepared may be useful in probing local variations in structure, but much work needs still to be done.

What strategies provide solutions with a greater level of predictability? Considerations of hydrogen bonding and positive stabilizing van der Waals interactions surely offer a route to more predictive approaches to site-specific design, with the metal center providing a coordinate system upon which to append site-selecting functionalities in three-dimensional space. Furthermore, the strategy of DNA-promoted dimerization,

again mimicking a tool well-used in site-specific DNA recognition by proteins, provides a general approach to enhancing specificity in binding by small metal complexes. Therefore, schemes to exploit general strategies for metal based dimerization need to be developed.

What is apparent thus far is the utility of transition metal chemistry to this endeavor, not only in the construction of new molecules of defined structure and stereochemistry, but in the sensitive detection and characterization of sites and modes of binding. Transition metal chemistry therefore provides the arena not only in which to learn subtle lessons regarding site-selective recognition, but also in which, with versatility, to create new, rationally designed molecules which may serve as the next generation of bioinorganic pharmaceutical agents. Metal-nucleic acid chemistry offers promise and challenge for new site-selective recognition.

References

1. Pabo, C. O. *Annu. Rev. Biochem.*, **1992**, 61, 1053.
2. Steitz, T. *Q. Rev. Bioph.*, **1990**, 23, 205.
3. (a) Miller, W. T.; Hill, K. A. W.; Schimmel, P. *Biochemistry*, **1991**, 30, 6970. (b) Fitzgerald, D. W. and Coleman, J. E. *Biochemistry*, **1990**, 30, 5195. (c) Delahunty, M. D.; South, T. L.; Summers, M. F.; Karpel, R. L. *Biochemistry*, **1992**, 31, 6461.
4. Pyle, A. M.; Rehmann, J. P.; Meshoyrer, R.; Kumar, C. V.; Turro, N. J.; Barton, J. K. *J. Am. Chem. Soc.*, **1989**, 111, 3051.
5. (a) Friedman, A. E.; Chambron, J.-C.; Sauvage, J.-P.; Turro, N. J.; Barton, J. K. *J. Am. Chem. Soc.*, **1990**, 112, 4960. (b) Jenkins, Y.; Friedman, A. E.; Turro, N. J.; Barton, J. K. *Biochemistry*, **1992,** 31, 10809.
6. Pyle, A. M.; Chiang, M. Y.; Barton, J. K. *Inorg. Chem.*, **1990**, 29, 4487.
7. (a) Rehmann, J. P. and Barton, J. K. *Biochemistry*, **1990**, 29, 1701. (b) Rehmann, J. P. and Barton, J. K. *Biochemistry*, **1990**, 29, 1710. (c) David, S. S. and Barton, J. K. *J. Am. Chem. Soc.*, **1993**, 115, 2984.
8. (a) Stubbe, J. and Kozarich, J. W. *Chem. Rev.*, **1987**, 87, 1107. (b) Dervan, P. B. *Science,* **1986**, 232, 464. (c) Moser, H. E. and Dervan, P. B. Science, **1987**, 238, 645. (d) Pasternack, R. F.; Gibbs, E. J.; and Villafranca, J. J. *Biochemistry,* **1983**, 22, 2406.
9. (a) Indelli, M. T.; Carioli, A.; Scandola, F. *J. Phys. Chem.*, **1984**, 88, 2685. (b) Ballardini, R.; Varani, G.; Balzani, V. *J. Am. Chem. Soc.*, **1980**, 102, 1719.
10. (a) Fleisher, M. B.; Waterman, K. C.; Turro, N. J.; Barton, J. K. *Inorg. Chem.*, **1986**, 25, 3549. (b) Fleisher, M. B.; Mei, H.-Y.; Barton, J. K. *Nucl. Acids Mol. Biol.*, **1988**, 2, 65.
11. Sitlani, A.; Long, E. C.; Pyle, A. M.; Barton, J. K. *J. Am. Chem. Soc.*, **1992**,

114, 2303.

12. Mei, H.-Y. and Barton, J. K. *J. Am. Chem. Soc.*, **1986,** 108, 7414.

13. Pyle, A. M.; Long, E. C.; Barton, J. K. *J. Am. Chem. Soc.*, **1989**, 111, 4520.

14. (a) Pyle, A. M.; Morii, T.; Barton, J. K. *J. Am. Chem. Soc.*, **1990**, 112, 9432. (b) Campisi, D. M.; Morii, T.; Barton, J. K. *J. Am. Chem. Soc.*, **1993**, manuscript in preparation.

15. (a) Chow, C. S. and Barton, J. K. *J. Am. Chem. Soc.*, **1990**, 112, 2839. (b) Chow, C. S.; Behlen, L. S.; Uhlenbeck, O. C.; Barton, J. K. *Biochemistry*, **1992**, 31, 972.

16. Chow, C. S.; Hartmann, K. M.; Rawlings, S. L.; Huber, P. W.; Barton, J. K. *Biochemistry*, **1992**, 31, 3534.

17. Wimberly, B.; Varani, G.; Tinoco, I. *Biochemistry*, **1993**, 32, 1078.

18. (a) Kirshenbaum, M. R.; Tribolet, R.; Barton, J. K. *Nucleic Acids Res.*, **1988**, 16, 7943. (b) Waldron, K.; Voulgaris, T., Barton, J. K. unpublished results. (c) Lee, I. and Barton, J. K. *Biochemistry*, **1993**, in press.

19. Krotz, A.; Kuo, L.; Sheilds, T. P.; Barton, J. K. *J. Am. Chem. Soc.*, **1993**, in press.

20. Pyle, A. M., PhD thesis, Columbia University, New York, 1989.

21. Chow, C. S. and Barton, J. K. *Biochemistry*, **1992**, 31, 5423.

22. Mizuno, H. and Sudaralingam, M. *Nucleic Acids Res.*, **1978**, 5, 4451.

23. Sitlani, A. and Barton, J. K. manuscript in preparation.

24. Muller, B.; Raphael, A. L.; Barton, J. K. *Proc. Natl. Acad. Sci.*, **1987**, 84, 1764.

25. Somers, W. E. and Philips, S. E. V. *Nature*, **1992**, 359, 387.

26. Otwinowski, Z.; Schevitz, R. W.; Zhang, R.-G.; Lawson, C. L.; Joachimiak, A; Marmorstein, R. Q.; Luisi, B. F.; Siglar, P. B. *Nature*, **1988**, 355, 321.

27. Weeks, K. and Crothers, D. M. *Cell*, **1991**, 66, 577.

28. Ruff, M.; Krishnaswamy, S.; Boeglin, M.; Poterszman, A.; Mitschler, A.; Podjarny, A.; Rees, B.; Thierry, J. C.; Moras, D. *Science*, **1991**, 252, 1682.

Chapter 2:

DNA Photocleavage by $[Rh(phen)_2phi]^{3+}$ and $[Rh(phi)_2bpy]^{3+}$: Shape-Selective Recognition and Reaction¥

2.1. Introduction

During the past decade there has been increasing attention paid to the study and development of novel molecules which recognize DNA sites and induce strand scission.[1-4] While most small molecular weight natural products bind to DNA in the minor groove of the helix,[2-4] the Barton laboratory has been interested in the design of transition metal complexes which target DNA sites in the major groove.[1] The development of such agents may ultimately result in the discovery of novel chemotherapeutics, tools for biotechnology, and probes of DNA structure and may also lead to an increased understanding of the forces governing binding and recognition of DNA by both small molecules and proteins. This chapter involves the study of photocleavage and recognition of DNA by the complexes bis(phenanthroline) 9,10-phenanthrenequinone diimine rhodium(III) $[Rh(phen)_2(phi)]^{3+}$ and bis(9,10-phenanthrenequinone diimine) (bipyridyl) rhodium(III) $[Rh(phi)_2(bpy)]^{3+}$ (Figure 2.1).

Previous work has shown that the complexes $[Rh(phen)_2(phi)]^{3+}$ and $[Rh(phi)_2(bpy)]^{3+}$ intercalate into DNA via their phi ligand and induce efficient nucleic acid strand scission in the presence of long wavelength UV light.[5] While both complexes exhibit similar DNA cleavage properties, they display vastly different DNA recognition characteristics, as indicated by their photocleavage patterns. Specifically, $[Rh(phen)_2phi]^{3+}$ displays a marked sequence selectivity with a general preference for 5'-pyrimidine(py)- *pyrimidine*-purine(pu)-3' steps. In comparison $[Rh(phi)_2bpy]^{3+}$ prefers

¥ Adapted from Sitlani, A.; Long, E. C.; Pyle, A. M.; Barton, J. K. *J. Am. Chem. Soc.* 1992, **114**, 2303-2312.

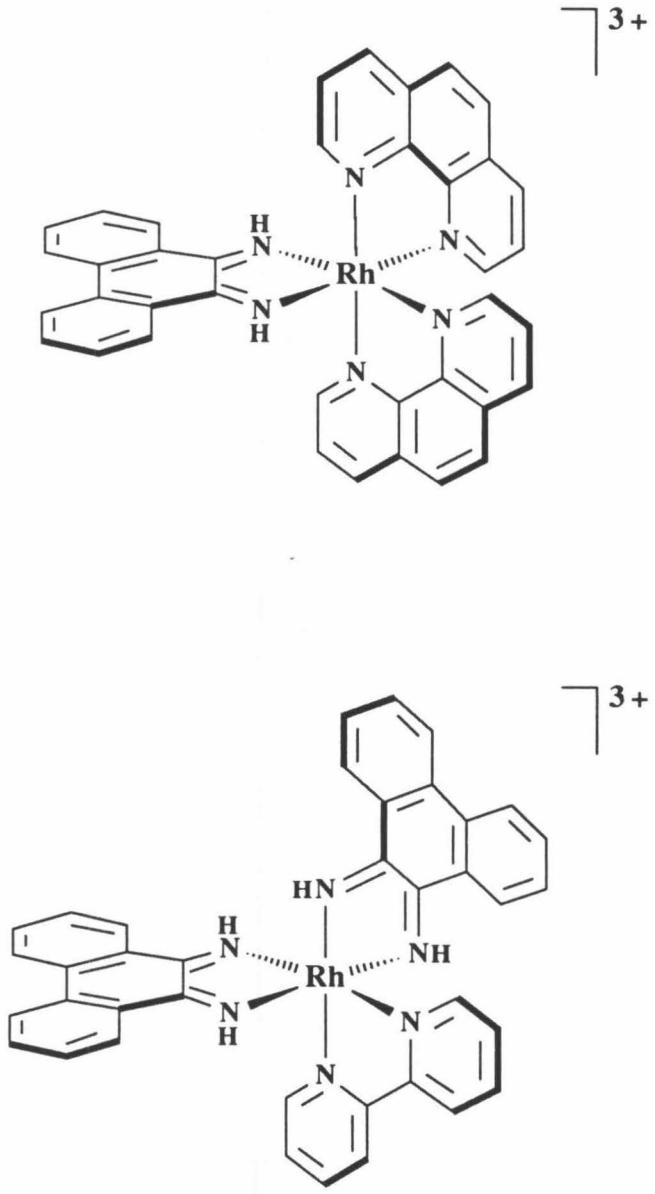

Figure 2.1. Structures of $[Rh(phen)_2(phi)]^{3+}$ (top) and $[Rh(phi)_2bpy]^{3+}$ (bottom).

5′-pu-*py*-pu-3′ steps and induces DNA strand scission in a predominantly sequence-neutral fashion.

This chapter describes in detail the DNA site recognition and cleavage products exhibited by the above complexes and shows how the differences in the individual shapes of these molecules affect both their DNA recognition characteristics and chemistry of strand scission. These findings illustrate a unique relationship between shape-selective recognition and the mechanism of DNA cleavage. Such an intimate relationship between recognition and reaction of molecules bound selectively to DNA requires consideration in understanding the reactions of DNA-binding proteins and small molecules.

2.2. Experimental

Materials: Calf Thymus DNA was purchased from Sigma. Topoisomerase I was purchased from BRL and plasmid pUC18 was from Boeringer-Mannheim. Phosphoramidites and solid supports for oligonucleotide synthesis were obtained from Pharmacia. $[Rh(phen)_2(phi)]Cl_3$ and $[Rh(phi)_2(bpy)]Cl_3$ were synthesized as described previously[5,6]. All enzymes utilized were from commercial sources. [α-^{32}P]dideoxy-ATP and [γ-^{32}P]ATP were obtained from Amersham and NEN-Dupont, respectively.

Instrumentation: The light source utilized in all cleavage experiments was an Oriel Model 6140 1000 W Hg/Xe lamp fitted with a monochromator and a 300 nm cut-off filter to avoid extraneous light damage to the DNA. Absorption spectra were recorded on a Cary 219 spectrophotometer. High Performance Liquid Chromatography (HPLC) was performed on a Waters 600E system equipped with a 484 tunable detector. Autoradiograms were scanned with a LKB 2202 Ultrascan Laser Densitometer.

Photocleavage of a DNA Restriction Fragment: Supercoiled pUC18 plasmid was digested with HindIII restriction endonuclease followed by treatment with calf intestinal alkaline phosphatase. Separate batches of digested plasmid were either 3′-end labeled by

treatment with terminal deoxynucleotidyl transferase and [α-^{32}P]-dideoxy-ATP or 5'-end labeled with T4 polynucleotide kinase and [γ-^{32}P]-ATP. After labeling, the DNA was digested with PvuII to yield a 90 and 230 base pair fragment. The 90 base pair fragment was purified by 6% preparative non-denaturing gel electrophoresis and isolated by electroelution.

Cleavage reactions were carried out in 20 µl volumes contained in 0.65 ml siliconized eppendorf tubes. The reaction mixtures were prepared with 50 µM (nucleotide) calf thymus DNA containing labeled restriction fragment and 5µM rhodium in 50 mM sodium cacodylate buffer, pH 7.0. Reaction mixtures containing $[Rh(phen)_2phi]^{3+}$ were irradiated for 1 min at 356 nm while those containing $[Rh(phi)_2bpy]^{3+}$ were irradiated for 4 min at 313 nm. Controls without metal complex were also irradiated in parallel to test for light damage.

After irradiation, all reaction mixtures were ethanol precipitated with the addition of 10 µl of 7.5 M NH_4OAc and 90 µl EtOH. The precipitated DNA was dried and resuspended in 3 µl of 80% formamide loading buffer. All rhodium reactions along with Maxam-Gilbert G+A sequencing reactions were heat denatured at 90 °C and quick-chilled on ice. The samples were loaded onto a 12% (19:1) polyacrylamide/7.5 M urea sequencing gel. Gels were electrophoresed at 1700 V for approximately 4 hrs and transferred to a cassette and stored at -70 °C with Kodak X-Omat film.

Photocleavage of Oligonucleotides: All oligonucleotides utilized during the course of study were synthesized on a Pharmacia Gene Assembler using the phosophoramidite method and purified by reverse-phase HPLC. Oligonucleotides were 5'- or [3'-^{32}P]-end-labeled using T4 polynucleotide kinase and [γ-^{32}P]ATP or terminal deoxytransferase and [α-^{32}P]dideoxy -ATP, respectively. The end-labeled oligonucleotides were subjected to photocleavage in a 40 µl total volume containing 0.5 mM (nucleotide) of the oligonucleotide substrate, 50 mM Na-cacodylate buffer, pH 7.0, and 25 µM metal

complex. Samples were irradiated with a 1000 W Hg/Xe lamp at 310 nm for 7.5 minutes. Samples containing typically 25000 cpm ^{32}P were resuspended in loading dye, loaded onto a 20% denaturing polyacrylamide sequencing gel and electrophoresed at 1700 Volts for approximately 4 hours. Autoradiography was performed using Kodak X-Omat film followed by densitometric analysis.

In order to determine the effects of neutral, alkaline and reductive conditions on photocleavage products, a single photocleavage reaction in a 40 μL reaction volume was divided into 3 aliquots and treated as follows: i. neutral: 10 μL photocleavage reaction was lyophilized, resuspended in loading buffer (80% v/v deionized formamide, 50 mM tris-borate, pH 8.3, 1 mM EDTA, 0.1 w/v xylene cyanol, 0.1% w/v bromphenol blue); ii. alkaline: 10 μL reaction mixture was brought to a final NaOH concentration of 0.1 M and incubated at 60°C for 2 minutes. The reaction was quenched with HCl, lyophilized to dryness, then resuspended in loading buffer; iii. $NaBH_4$ treatment: 10 μL reaction was brought to a final $NaBH_4$ concentration of 0.3 M and incubated at 0°C for 90 minutes. The sample was then quenched with HCl, lyophilized to dryness, and resuspended in loading buffer. All the samples resuspended in loading dye were then heat denatured at 90 °C for 2 min and loaded onto a 20% polyacrylamide gel. Alternatively, to detect the presence of metastable intermediates, the heat treatment was avoided and the samples were directly loaded onto a 20% polyacrylamide gel.

Cleavage of Oligonucleotides under Conditions of Varying Oxygen Concentration: Cleavage reactions contained 500 μM (nucleotide) 5'-CTGGCATGCCAG-3' with 5'-^{32}P end labeled material and 25 μM final concentration metal complex in 50 mM Na-cacodylate, pH 7.0, 40μL total volume. Reaction mixtures were contained in a quartz tube with a septum; they were either purged with dioxygen or argon through a narrow gauge needle or maintained under ambient conditions during the course of sample irradiation (7.5 min at 310 nm). After irradiation the reaction mixtures were dried and resuspended in

loading buffer. Reaction aliquots were then heat denatured at 90°C for 2 min and examined by 20% polyacrylamide gel electrophoresis, as described above.

Densitometry and Data Analysis: Densitometry was performed directly on negatives from polaroid photographs of agarose gels or autoradiograms produced from polyacrylamide gels. Methods for densitometry and data collection have all been described previously.[8]

Quantitative Cleavage of Oligonucleotide Substrates and Determination of Base Products Released: Typically, nucleic acid base release from oligonucleotide substrates was examined after irradiation (310 nm light for 7.5 min) of a reaction volume of 40 μL containing 0.5 mM (nucleotide) of the oligonucleotide and 25 μM metal complex in 50 mM Na-cacodylate buffer, pH 7.0 (differences from this standard procedure are noted in Table III). Quantitation of nucleic acid base release was performed on a Cosmosil 5 μ, 15 cm C-18 column washed with 0.05 M NH_4-formate at a flow rate of 1.5 $mLmin^{1-}$. Products were detected by UV absorbance at 260 nm and quantitated by comparison of peak areas generated with commercial standards. Quantitation of the extent of oligonucleotide digested for comparison to nucleic acid base release was made on a Cosmosil 5 μ, 15 cm C-18 column washed with 0.1 M NH_4-formate using a 0-20% linear CH_3CN gradient. Nucleic acid base products were detected at 260 nm. Adenine, thymine, guanine and cytosine were eluted with retention times of 13 , 5.7 , 4.4 , and 2.0 min, respectively, while the base propenoic acids had a retention time of 1.4 min.

2.3. Results

2.3.1. Site-Selectivities on DNA Restriction Fragments and Oligonucleotides.

Both $[Rh(phen)_2phi]^{3+}$ and $[Rh(phi)_2bpy]^{3+}$ have been shown[6] previously to have similar photochemical properties and overall binding affinities; however, their cleavage

patterns observed on ^{32}P-end-labeled DNA restriction fragments and oligonucleotide substrates indicate substantially different recognition characteristics. As shown in Figure 2.2, $[Rh(phen)_2phi]^{3+}$ promotes DNA cleavage with site-selectivity, while $[Rh(phi)_2bpy]^{3+}$ appears more sequence-neutral in terms of its recognition properties. Cleavage is seen with $[Rh(phi)_2bpy]^{3+}$ at all sites on the ^{32}P-end-labeled restriction fragment whereas a few preferred sites of cleavage are apparent with $[Rh(phen)_2phi]^{3+}$. In this experiment comparable concentrations and irradiation times have been employed; therefore, the differences in cleavage may be seen to reflect differences in the recognition properties of the complexes.

The sequence-selective nature of $[Rh(phen)_2phi]^{3+}$ can be examined in the histogram shown in Figure 2.3 (top panel). Inspection of this figure indicates that the preferred sites of cleavage for this complex are contained within a 5'- py-*py*-pu-pu -3' site with cleavage occurring directly at the highlighted residue. Although the sequence 5'-CCAG-3' shows the highest levels of cleavage, there is a marked level of cleavage at similar sequences such as 5'-CCAA-3'. Significant levels of induced strand scission also occur at sequences such as 5'-TTGG-3', 5'-TTAA-3' and to a lesser extent at other sites containing a central 5'-py-pu-3' site. Figure 2.3 also illustrates that cleavage of these sequences are usually associated with an additional cleavage site located at the pyrimidine residue of the complementary strand resulting in a 5'-asymmetric cleavage pattern. This observed 5'-asymmetry is usually separated by one nucleotide, although two nucleotide shifts and occasionally no shift (cleavage directly across from the pyrimidine residue) is observed. Figure 2.3 also illustrates that along with a preference for 5'-py-*py*-pu-3' sites, $[Rh(phen)_2phi]^{3+}$ shows some preference for homopyrimidine stretches.

In contrast to $[Rh(phen)_2phi]^{3+}$, $[Rh(phi)_2bpy]^{3+}$ is less selective for particular DNA sites. The histogram (Figure 2.3, bottom panel) reveals a comparable extent of cleavage at all sites. However, the photocleavage patterns do show some preference for

Figure 2.2. Comparison of $[Rh(phen)_2phi]^{3+}$ and $[Rh(phi)_2phi]^{3+}$ photocleavage of the [3'-^{32}P]-end labelled Hind III ---> Pvu II restriction fragment of pUC18. Cleavage was performed on reaction mixtures containing 50 μM (in nucleotides) of calf thymus DNA, labeled restriction fragment, 5 μM rhodium, and 50 mM sodium cacodylate buffer, pH 7.0. The reaction mixture containing $[Rh(phen)_2phi]^{3+}$ was irradiated for 1 min at 356 nm, while that containing $[Rh(phi)_2bpy]^{3+}$ was irradiated for 4 min at 313 nm. Lane 1: Maxam-Gilbert G + A reaction; Lane 2: Light control in the absence of metal complex; Lane 3: $[Rh(phi)_2bpy]^{3+}$ cleavage lane; Lane 4: $[Rh(phen)_2phi]^{3+}$ cleavage lane.

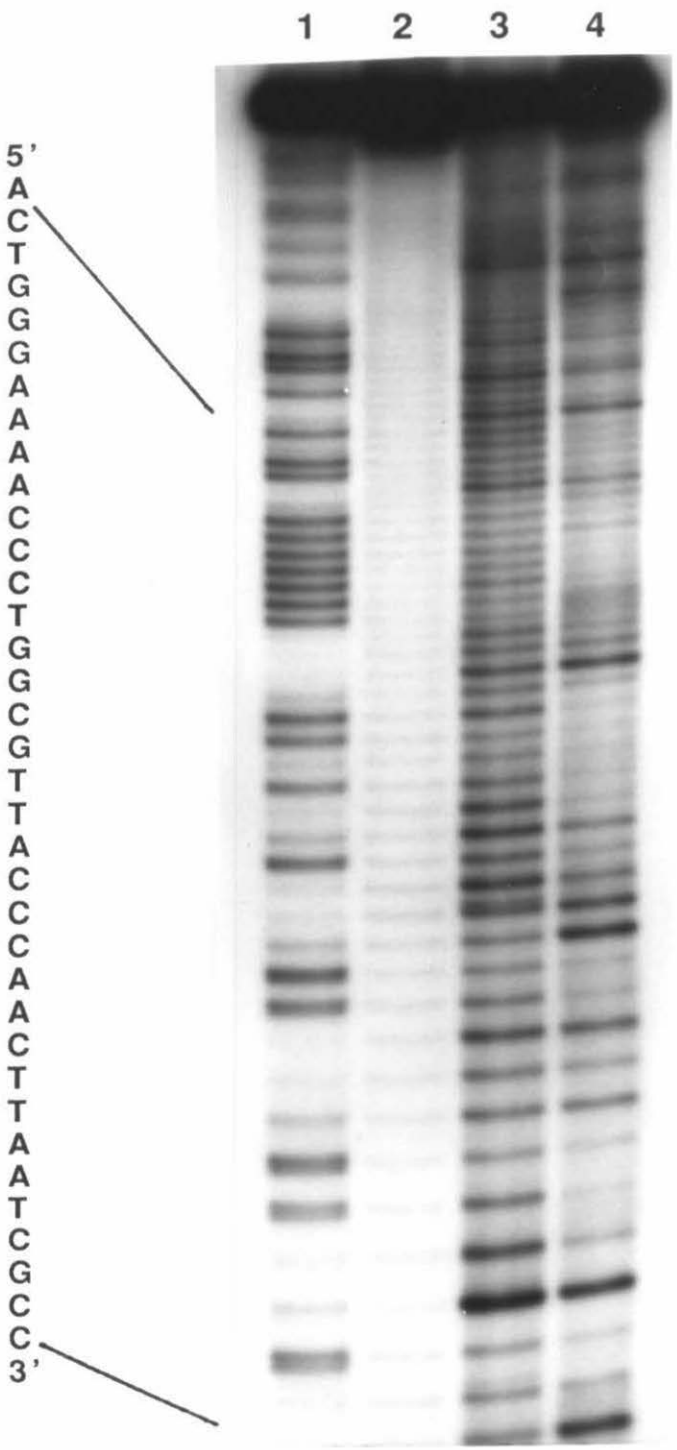
1
2
3
4
5'
A
C
T
G
G
G
A
A
A
A
C
C
C
C
T
G
G
C
G
T
T
A
C
C
C
A
A
C
T
T
A
A
T
C
G
C
C
3'

Figure 2.3. Histogram illustrating the quantitation and position of $[Rh(phen)_2phi]^{3+}$ cleavage (upper panel) and $[Rh(phi)_2bpy]^{3+}$ cleavage (lower panel) of the 5'- and [3'-^{32}P]-end labelled Hind III ---> Pvu II restriction fragment of pUC18. $[Rh(phen)_2phi]^{3+}$ cleaves sequence-specifically at 5'-py-*py*-pu-3' stretches in a 5'-asymmetric manner, as indicated by the boxed regions. $[Rh(phi)_2bpy]^{3+}$ cleaves equally at most sites with some preference for 5'-py-py-3' base steps.

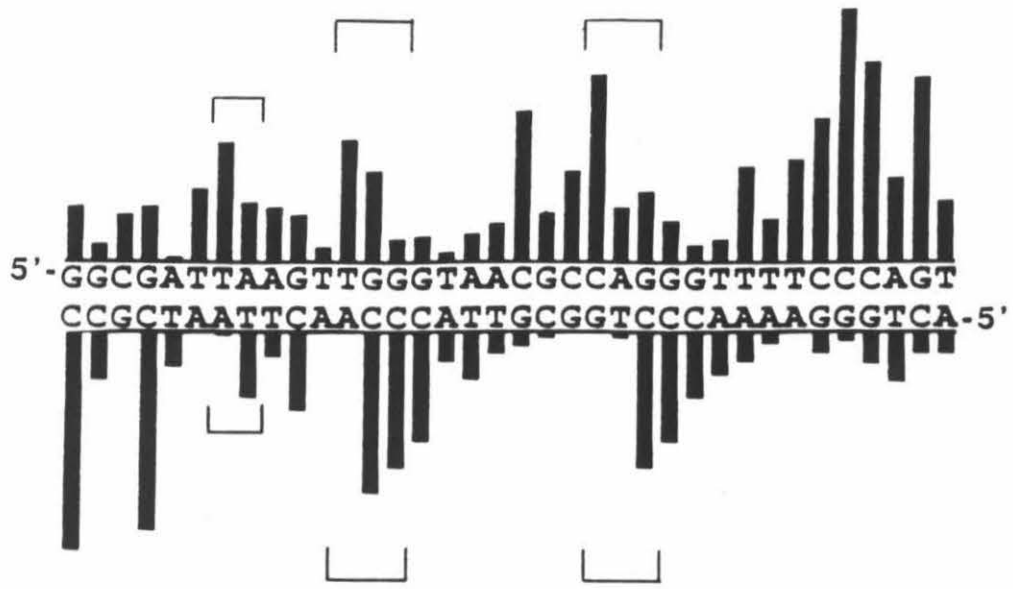
5'-GGCGATTAAGTTGGGTAACGCCAGGGTTTTCCCAGT
CCGCTAATTCAACCCATTGCGGTCCCAAAAGGGTCA-5'


5'-GGCGATTAAGTTGGGTAACGCCAGGGTTTTCCCAGT
CCGCTAATTCAACCCATTGCGGTCCCAAAAGGGTCA-5'

sites 5'-ATCG-3', 5'-ACCA-3' and 5'-CCCA-3', all of which contain a central 5'-*py*-py-3'. In comparison, cleavage experiments on other restriction fragments[5,8] have demonstrated that $[Rh(phi)_2bpy]^{3+}$ shows an overall preference for 5'-pu-*py*-pu-py-3' stretches, in particular the 5'-A*T*GC-3' site, with cleavage occurring at the highlighted pyrimidine.

As illustrated in Figure 2.4, similar recognition patterns for the complexes are also observed when the oligonucleotide 5'-CTGGCATGCCAG-3' is utilized as a substrate. As expected, $[Rh(phi)_2bpy]^{3+}$ cleaves strongly at the T_7 of the 5'-$A_6T_7G_8C_9$-3' (5'-pu-*py*-pu-py-3') site, and moderately at the C_9 of the 5'-$G_8C_9C_{10}A_{11}$-3' (5'-pu-*py*-py-3') site. $[Rh(phen)_2phi]^{3+}$ cleaves most strongly at the C_{10} of the 5'-$C_9C_{10}A_{11}G_{12}$-3' site and targets the alternating 5'-pu-*py*-pu-py-3' (5'-ATGC-3') site to a lesser extent.

2.3.2. Identification of the Oligonucleotide Termini Formed at the Site of Strand Scission.

Gel electrophoretic analysis may be used to distinguish the termini obtained after strand cleavage by these complexes. Figure 2.4 (A and B) illustrates the results of experiments in which $[Rh(phen)_2phi]^{3+}$ and $[Rh(phi)_2bpy]^{3+}$ were employed in reaction mixtures utilizing 3'- and [5'-^{32}P]-end labeled oligonucleotide substrates. These reactions were examined by 20% polyacrylamide gel electrophoresis subsequent to treatment under neutral (control), alkaline or reductive ($NaBH_4$) conditions. Figure 2.4(A) illustrates the products resulting from cleavage of the [3'-^{32}P]-end labeled oligonucleotide indicating the exclusive formation of 5'-phosphate termini at the site of photocleavage, as evidenced by co-migration with the products of Maxam-Gilbert sequencing reactions.[9] In comparison, an analysis of the products of the 5'-^{32}P-end-labeled substrate, as shown in figure 2.4(B), indicates the formation of both 3'-phosphate termini and an additional product **1** which moves at a significantly slower rate relative to the 3'-phosphate terminus at each nucleotide

Figure 2.4. Polyacrylamide gel electrophoretic analysis of the termini produced in the $[Rh(phi)_2bpy]^{3+}$ and $[Rh(phen)_2phi]^{3+}$ induced photocleavage reactions of [3′-^{32}P]-end labeled (**A**) and [5'-^{32}P]-end labeled (**B**) 5'-CTGGCATGCCAG-3'. Conditions for cleavage reactions: 42 μM oligonucleotide, 25 μM Rh^{3+}, 50 mM Na-cacodylate, 7.5 min, 310 nm UV light. Lanes A and B: Maxam-Gilbert A+G and C+T reactions respectively. Lanes C and D: dark and light controls respectively. Lanes E and F: $[Rh(phi)_2bpy]^{3+}$ and $[Rh(phen)_2phi]^{3+}$ cleavage, respectively under ambient conditions. Lanes G-I: reactions corresponding to lanes D-F treated with alkali (0.1 M NaOH, 60° C, 2 min) prior to loading on gel. Lanes J-L: reactions corresponding to lanes D-F treated with reducing agent (0.1 M $NaBH_4$, 0° C, 15 min) prior to loading on gel. In **B**, ends marked b and b' (lanes K and L) are assigned as the 3'-phosphoglycaldehyde terminus and the corresponding 3′-phosphoglycol terminus respectively.

A

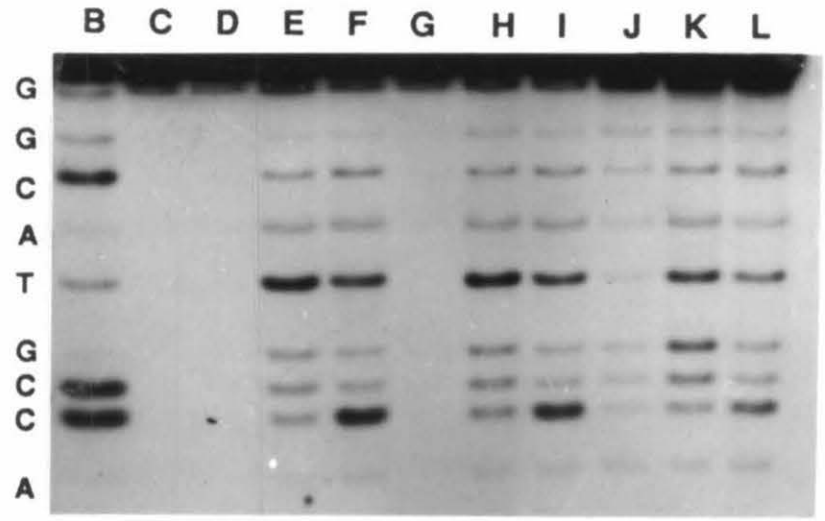

B

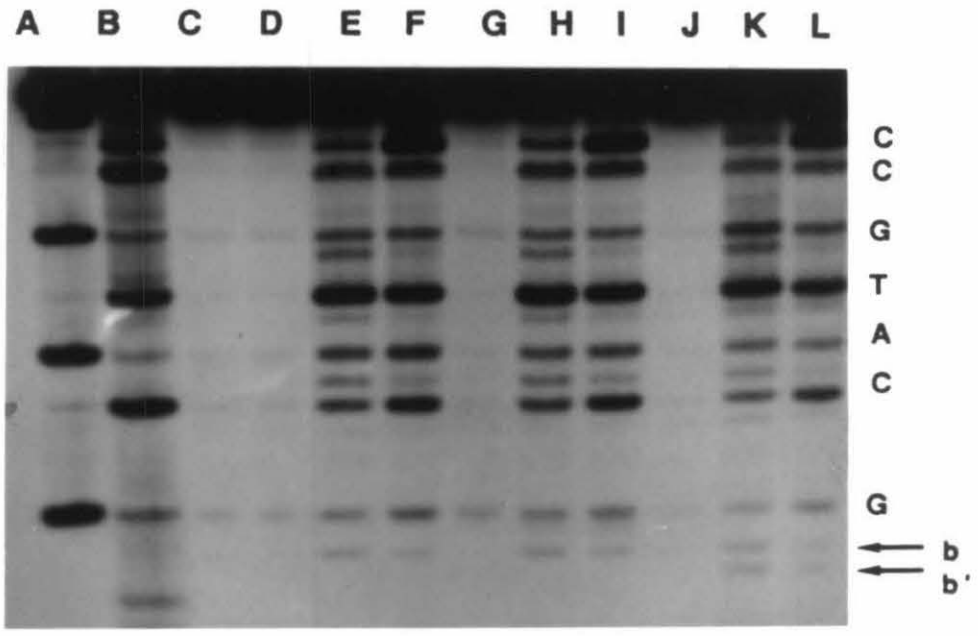

step. While the formation of this slower moving product is apparent at each cleavage site after reaction with $[Rh(phi)_2bpy]^{3+}$, the secondary terminus is seen to a much smaller extent after reaction with $Rh(phen)_2phi^{3+}$. Figure 2.4(B) also shows the absence of 3'-phosphoglycolate termini, which migrates at a faster rate than the 3'-phosphate termini. Additional experiments, where the samples were loaded directly onto the gels without heat denaturation, were carried out to search for the presence of any metastable intermediates[2c] as have been seen after cleavage with $Cu(phen)_2^{1+}$; no evidence of such intermediates was found.

Following oligonucleotide cleavage, additional chemical modifications were carried out to characterize **1**. To evaluate the extent of alkaline lability of the lesions formed, 5'- and [3'-^{32}P]-end labeled reactions were treated with alkali (0.1M NaOH, 60 °C, 2 min) prior to gel analysis (Figure 2.4). This treatment yielded no additional strand scission. More stringent alkaline treatment (1M piperidine, 90 °C, 30 min) of the reaction mixtures also had no effect on the extent of 5'- and 3'-phosphate termini produced, nor did such reaction alter the mobility or intensity of the unassigned slower moving end **1**. Figure 2.4 shows that reduction (0.1M $NaBH_4$, 0 °C, 15 min) of the [5'-^{32}P]-end labeled reaction mixtures prior to gel electrophoresis results in a slight increase in mobility of **1**; this is most readily apparent at the highly resolved 5'-G site (Fig 2.5). Similarly, harsher reduction (0.28M $NaBH_4$, 25 °C, 90 min) of the 5'-^{32}P-end labeled reaction mixtures produced the faster migrating band, which was observed at each base site, and a concomitant diminution in the intensity of **1**. In comparison, $NaBH_4$ reduction of the [3'-^{32}P]-end labeled substrate reaction mixtures (Fig 2.4B) had no effect on the mobility of the 5'-phosphate termini.

2.3.3. Effect of Oxygen Concentration on Oligonucleotide Product Formation.

The effect of dioxygen concentration on the formation of the oligonucleotide products was examined in order to evaluate whether they were derived from aerobic or anaerobic pathways of degradation. $[Rh(phi)_2bpy]^{3+}$ induced photocleavage of [5'-^{32}P]-end-labeled oligonucleotide substrate was carried out under conditions of ambient, dioxygen purge, or argon saturation. This experiment demonstrated, as shown in Figure 2.5, that DNA cleavage which leads to the 3'-phosphate terminus is independent of oxygen. However, the production of the secondary 3'-terminus **1** is clearly dependent upon the concentration of dioxygen. These results are quantitated in Table 2.1.

2.3.4. Identification and Quantitation of Monomeric Oligonucleotide Cleavage Products.

Previous work[5] had indicated the formation of nucleic acid bases in DNA photoreactions mediated by the rhodium complexes. Cleavage products formed upon interaction of $[Rh(phen)_2(phi)]^{3+}$ or $[Rh(phi)_2(bpy)]^{3+}$ with the substrate 5'-CTGGCATGCCAG-3' were studied by HPLC in order to correlate quantitatively the extent of nucleic acid base release with the total amount of oligonucleotide strand scission. As shown in Table 2.2, a nearly 1:1 ratio of total nucleic acid base released to oligonucleotide digested is found in the $[Rh(phen)_2phi]^{3+}$ induced photocleavage reactions. In comparison, $[Rh(phi)_2bpy]^{3+}$-induced photoreactions produced a 0.7:1 ratio of total nucleic acid base released to oligonucleotide digested. This finding suggests that approximately 30% of $Rh(phi)_2bpy^{3+}$-photocleavage may produce another monomeric product. Moreover, densitometric quantitation (Table 2.1) of the products observed by gel electrophoresis indicates that approximately 25% of the photocleavage mediated by $[Rh(phi)_2bpy]^{3+}$ under ambient conditions produces the secondary 3'-terminus. These

Figure 2.5. The effect of dioxygen on the production of 3'-phosphoglycaldehyde and 3'-phosphate termini. Trace marked- - - - -: Densitometric analysis of the 3'-termini detected through polyacrylamide gel electrophoresis of the photoreaction (310 nm, 7.5 min) of 42 μM oligonucleotide 5'-CTGGCATGCCAG-3', 25 μM $[Rh(phi)_2bpy]^{3+}$, 50 mM Na-cacodylate, under ambient dioxygen conditions. Trace marked ———: Densitometric scan of 3'-termini produced in the photoreaction above, under conditions of argon saturation. The presence of dissolved dioxygen was minimized by saturating the reaction mixture with argon for 30 min prior to irradiation. The 3'- phosphate terminus at each labeled base site is associated with a slower moving 3'- phosphoglycaldehyde terminus, which is formed only in the presence of dioxygen.

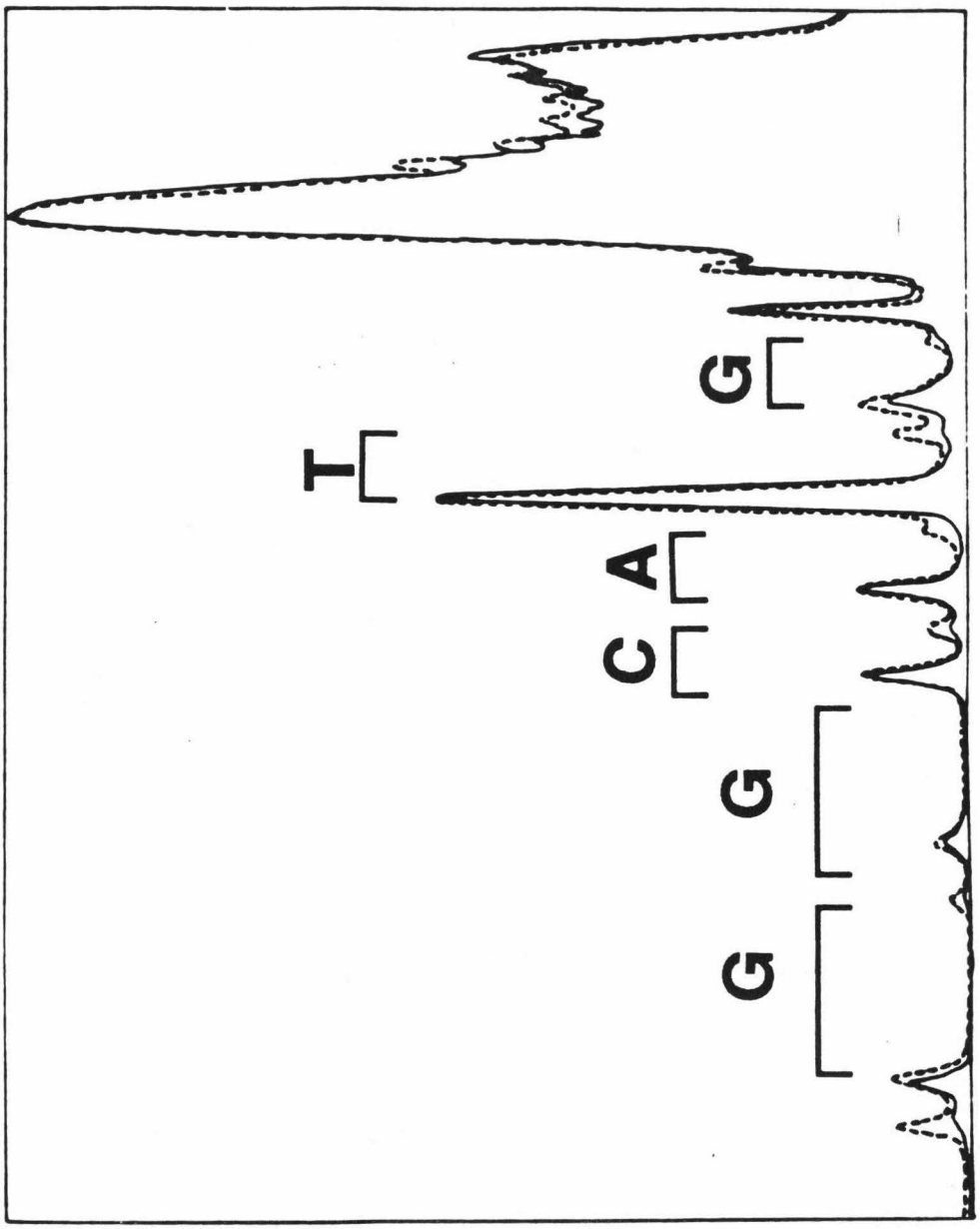
G
T
C
A
G
G

Table 2.1. Effect[a] of Oxygen Concentration on the production of 3'-Termini Produced in $Rh(phi)_2bpy^{3+}$ Induced Photocleavage Reaction of 5'-$C_1T_2G_3G_4C_5A_6T_7G_8C_9C_{10}A_{11}G_{12}$-3'.

	Experimental Conditions					
	OXYGEN		AMBIENT		ARGON	
	3'-P[b]	1[c]	3'-P	1	3'-P	1
G_3	1.6	0.6	1.7	0.4	1.6	0.1
G_4	0.6	0.2	0.9	0.2	0.8	0.2
C_5	2.3	1.4	2.8	1.3	2.2	0.6
A_6	2.2	1.2	2.5	1.0	2.2	0.0
T_7	11.8	2.3	13.0	1.5	13.0	0.6
G_8	3.7	1.1	3.4	0.9	2.3	0.4
Total	**22.2**	**6.8**	**24.3**	**5.3**	**22.1**	**1.9**

[a] % yield of cleaved oligonucleotide. All numbers represent averages with ± 5% of the densitometric quantification of three cleavage experiments and are normalized to the amount of undigested oligonucleotide.

[b] Refers to the production of the 3'-phosphate terminus.

[c] Refers to the production of the slower migrating 3'-phosphoglycaldehyde terminus.

Table 2.2. Quantitation of Products Formed by $[Rh(phen)_2phi]^{3+}$ and $[Rh(phi)_2bpy]^{3+}$ Induced Photocleavage[a] of 5'-CTGGCATGCCAG-3'.

Complex	Base (μM)	Oligonucleotide digested (μM)	Nucleic acid base yield[b] (%)
$[Rh(phen)_2phi]^{3+}$	4.9	4.8	100
$[Rh(phi)_2bpy]^{3+}$	3.8	5.5	70

a: Photocleavage reaction conditions for both complexes: 25 μM Rh, 42 μM oligonucleotide, 50mM Na-cacodylate, 310 nm irradiation, 7.5 mins.
b: These values are based on oligonucleotide digested. The values represent averages of three experiments with deviations of < 5%.

observations suggested a 1:1 correlation between the production of the slower moving 3'-end, the formation of which is dependent on the dioxygen concentration of the reaction mixture, and of an alternate base lesion.

Examination of oligonucleotide reaction mixtures after photocleavage by $[Rh(phi)_2bpy]^{3+}$ using HPLC reveals a product in addition to nucleic acid bases. Identification of this degradation product was facilitated by HPLC analyses of product mixtures, as shown in Figure 2.6. HPLC traces of the $[Rh(phi)_2bpy]^{3+}$ and $[Rh(phen)_2phi]^{3+}$ photoreactions show the release of nucleic acid base and a second product, **2**, (labeled P in Figure 2.6). Clearly, **2** is produced to a greater extent in the $[Rh(phi)_2bpy]^{3+}$ photoreaction than with $[Rh(phen)_2phi]^{3+}$. The product **2** shows a retention time substantially different from nucleic acid bases or authentic base propenals, which are formed in the Fe-bleomycin mediated degradation of DNA.[3,4] Furthermore, as shown in Figure 2.7, the wavelength of maximum absorbance is greater for P than for the free nucleic acid bases. The formation of **2** was also examined as a function of dioxygen concentration. As shown in Figure 2.8 (left), this product diminishes in the absence of oxygen suggesting a correlation with the oxygen dependent production of the 3'-terminus, **1**.

The product **2** was collected and subjected to further photolytic degradation and re-examined by HPLC (Fig 2.9, A). This analysis revealed degradation to free nucleic acid base. Mass spectral analysis of the collected peak (before photolytic degradation) indicates the presence of the ammonium salts of nucleic acid base propenoic acids of adenine, guanine and cytosine (molecular ions 223, 234, and 199). Reduction of **2** was carried out with $NaBH_4/AlCl_3$, which was expected to reduce the acid to the corresponding alcohol [10] and was found to yield products which coelute with propenols formed through the $NaBH_4$ reduction of the authentic propenals (generated through Fe-bleomycin-mediated degradation

Figure 2.6. HPLC analysis of free nucleic acid bases and base-propenoic acids produced during the $[Rh(phen)_2phi]^{3+}$ and $[Rh(phi)_2bpy]^{3+}$ degradation of DNA. **(A)**: Trace 1 is the analysis of products obtained from the irradiation at 310 nm for 10 min of the reaction mixture containing 1mM (in nucleotide) 5'-CTGGCATGCCAG-3', 50 μM $[Rh(phen)_2phi]^{3+}$ in 50 mM NH_4-formate (elution buffer). The putative propenoic acids are marked P; C,G and T refer to free nucleic acid bases cytosine, guanine and thymine respectively. Trace 2 is the control reaction identical to the above in the absence of oligonucleotide substrate. **(B)**: Trace 1 and Trace 2 are the corresponding analyses of products obtained in the $[Rh(phi)_2bpy]^{3+}$ induced photocleavage of oligonucleotide. The reaction conditions are identical to those above.

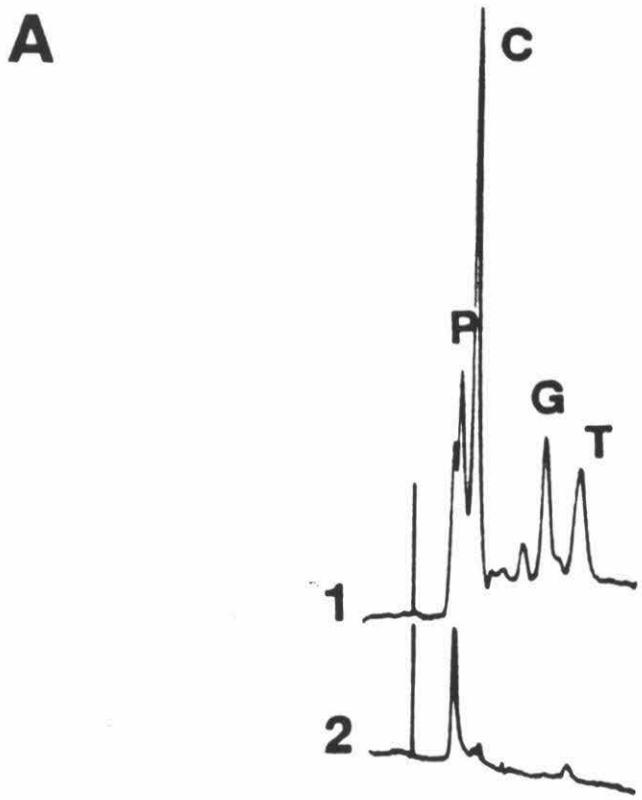
A
C
P
G
T
1
2

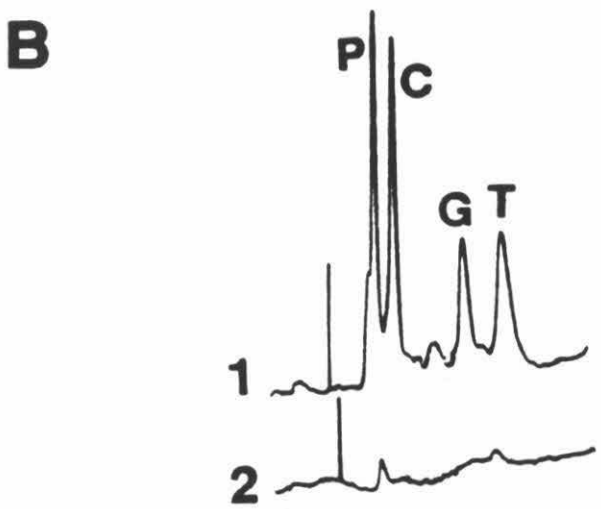
B
P
C
G
T
1
2

Figure 2.7. HPLC analysis of the absorbances of free nucleic acid bases and base-propenoic acids as function of detection wavelength. Traces **A**, **B**, and **C** are the analyses of products obtained from irradiation at 310 nm for 10 min of reaction mixtures containing 500 μM (in nucleotide) calf-thymus DNA, 25 μM $[Rh(phi)_2bpy]^{3+}$ in 50 mM NH_4-formate (elution buffer). The propenoic acids are marked P; C, G and T refer to free nucleic acid bases cytosine, guanine, and thymine, respectively. Note that increasing the detection wavelength from 260 nm (**A**) to 280 nm (**B**) to 300 nm (**C**) increases the height of the propenoic acid peaks with respect to the nucleic acid base peaks.

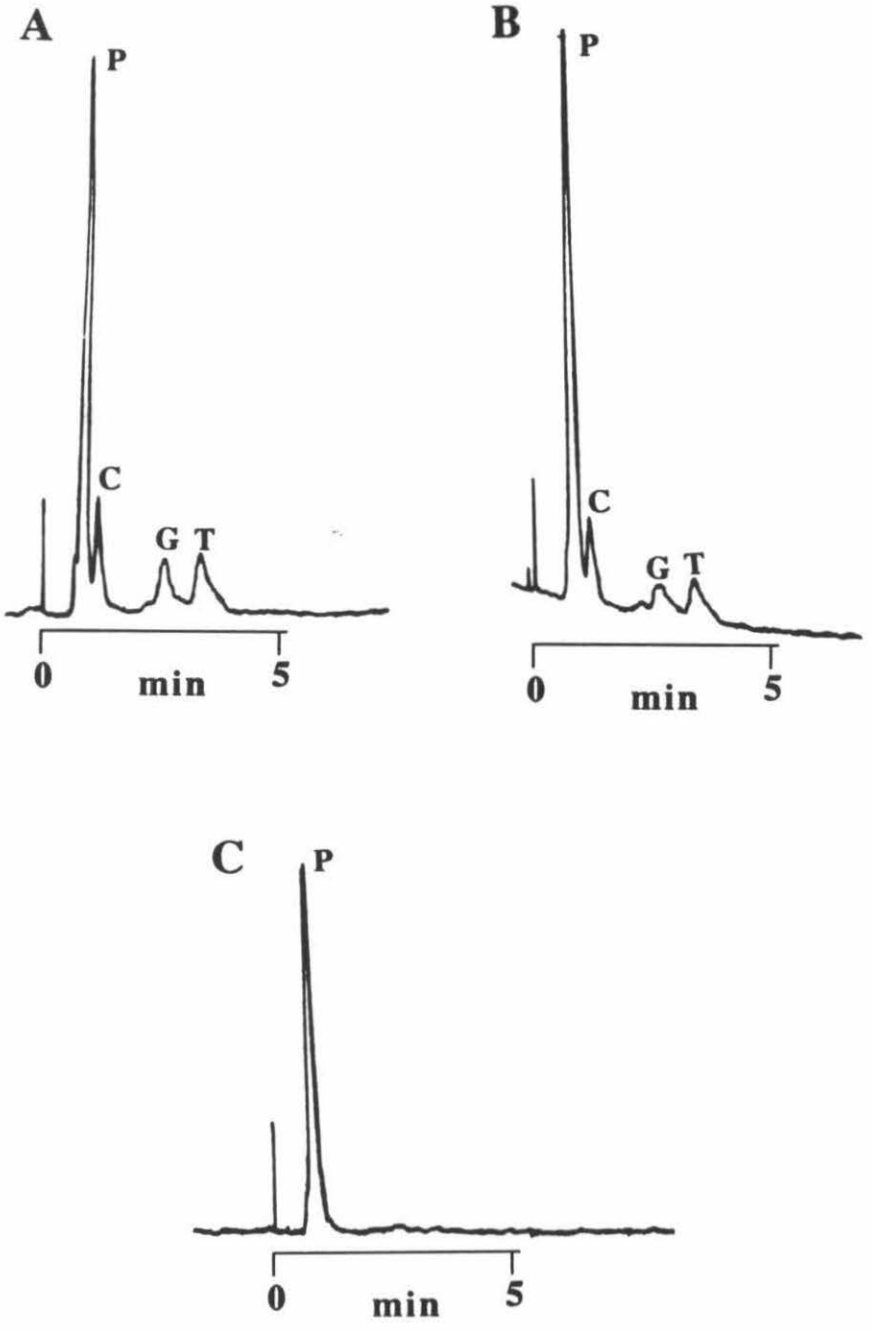
A
P
C
G T
0
min
5
B
P
C
G T
0
min
5
C
P
0
min
5

Figure 2.8. HPLC analyses of the effect of oxygen concentration on the production of base-propenoic acids (P). Traces **(A)** and **(B)** are the analyses of products obtained in the absence and presence of dioxygen, respectively, from irradiation at 310 nm for 10 min of reaction mixtures containing 500 μM (in nucleotide) calf-thymus DNA, 25 μM $[Rh(phi)_2bpy]^{3+}$ in 50 mM NH_4-formate (elution buffer). The putative propenoic acids are marked P; C, G, and T refer to free nucleic acid bases cytosine, guanine, and thymine respectively. Note that the presence of dioxygen **(B)** promotes the formation of propenoic acids and depresses the production of free nucleic acid bases.

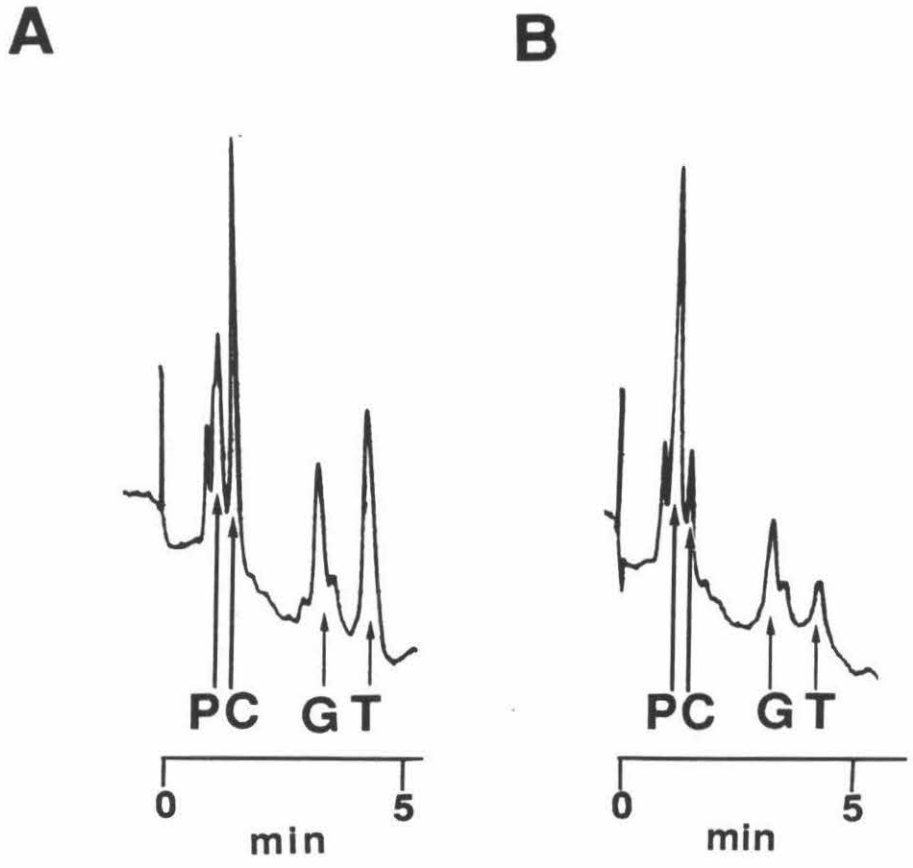
A
B
PC
G
T
0
5
min
PC
G
T
0
5
min

Figure 2.9. HPLC analyses of the photolysis (**A**) and reduction (**B**) of base-propenoic acids. Propenoic acids are isolated by HPLC purification of products obtained from the irradiation at 310 nm for 10 min of the reaction mixture containing 1mM (in nucleotides) 5'-CTGGCATGCCAG-3', 50 μM $[Rh(phi)_2bpy]^{3+}$ in 50 mM NH_4-formate (elution buffer). **A** shows the analysis of the photoproducts obtained from the irradiation of putative base propenoic acids (peak marked P). Nucleic acid base cytosine (C) and guanine (G) are the identifiable photoproducts. In **B,** trace 1 is the analysis of cytosine-, thymine- and adenine- base propenals (marked C-al, T-al and A-al), formed in a Fe(II)-bleomycin mediated DNA cleavage reaction. Traces 2 and 3 in **B** show the analyses of the reduction products of P and base-propenals, respectively. The arrows point to a base-propenol, which is formed by the $NaBH_4$ reduction of authentic base-propenals (Trace 2) and the $NaBH_4/AlCl_3$ reduction of putative propenoic acids (Trace 3), respectively. In all three traces, a gradient from 100% water to 25% acetonitrile over 25 min, is used.

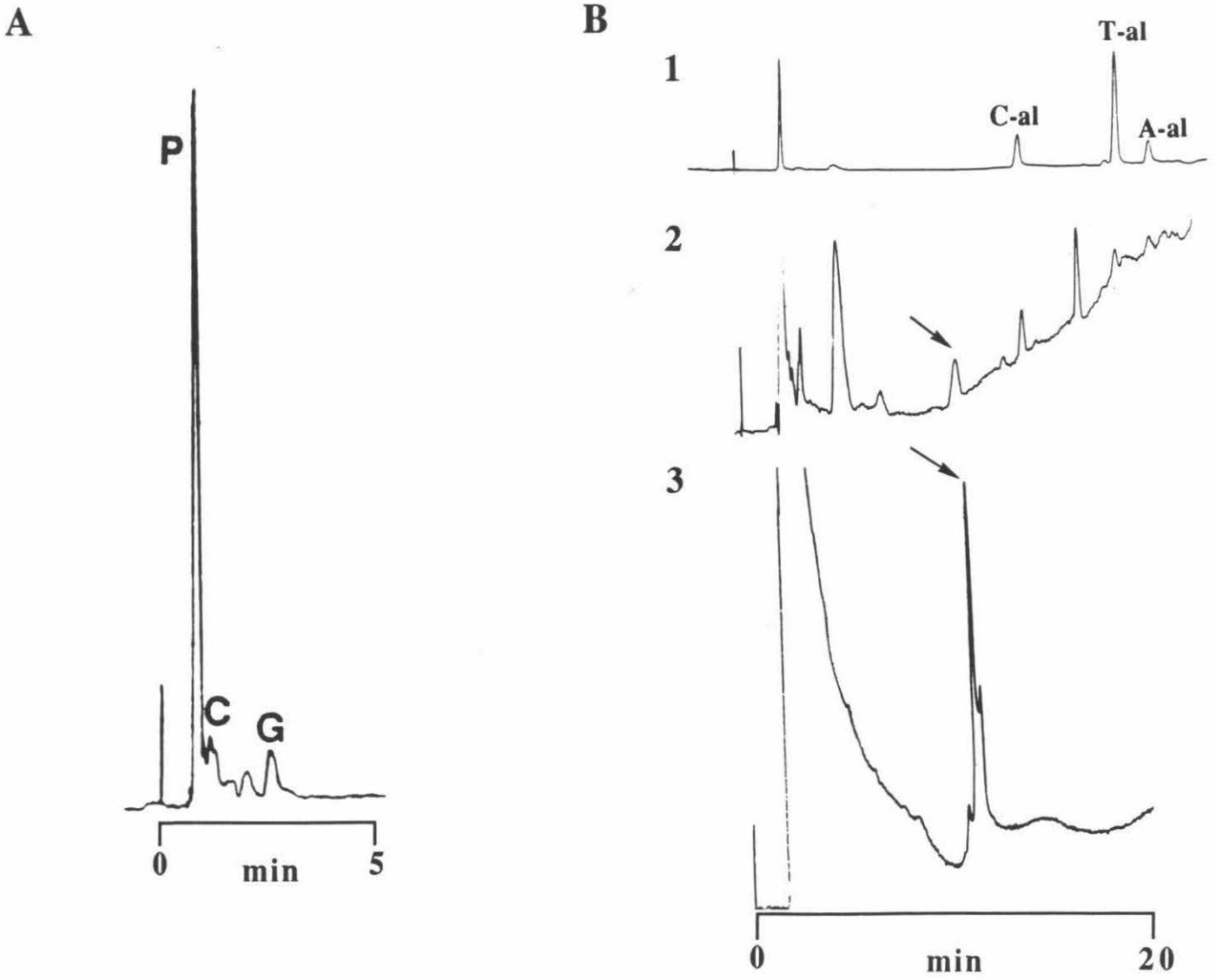
A
P
C
G
0
min
5
B
1
T-al
C-al
A-al
2
3
0
min
20

of DNA) (Fig 2.9, B). This result indicates the formation of a common product upon reduction of base propenals and **2**.

HPLC analysis of $[Rh(phi)]^{3+}$ reaction mixtures showed no evidence of nucleic acid base propenals in comparison to those formed in Fe-bleomycin induced DNA degradation reactions. However, it was important to assess whether photolysis had led to photodegradation of base propenals, which may have been formed in the course of the cleavage reaction. Nucleic acid base propenals produced by Fe-bleomycin induced degradation of DNA were found to be relatively stable under the conditions of UV-irradiation used for the $[Rh(phi)_2bpy]^{3+}$ and $[Rh(phen)_2phi]^{3+}$ photoreactions. This observation verifies the lack of base propenal formation with DNA cleavage by $Rh(phi)^{3+}$ complexes. A summary of products obtained following photocleavage by the two rhodium complexes is given in Table 2.3.

2.3.5. Identification of Rhodium-Containing Photoproducts.

Photolysis in the presence of the rhodium complexes also results in the formation of a distinct band of radiolabeled material which migrates at a decreased rate relative to the unmodified oligonucleotide. This material was isolated by gel electrophoresis and then treated with concentrated nitric acid, to extract all the rhodium containing species from the gel. Isolation of this material followed by atomic absorption analysis indicated the presence of high levels of rhodium, suggesting that photolysis also promotes covalent binding. Specifically, following irradiation of a sample containing 5×10^{-11} moles of rhodium, 0.8×10^{-11} moles of rhodium (16%) was detected in the putative covalent adduct. These observations are consistent with work done by others where the photolysis of $[Rh(phen)_2Cl_2]^+$ has been shown to yield $[Rh(phen)_2(H_2O)_2]^{3+}$, which in a secondary reaction photobinds DNA[11].

Table 2.3. Summary of Products Formed by $[Rh(phi)_2bpy]^{3+}$ and $[Rh(phen)_2phi]^{3+}$ Induced Photocleavage of 5'-CTGGCATGCCAG-3'.

$[Rh(phi)_2bpy]^{3+}$	$[Rh(phen)_2phi]^{3+}$	Oxygen dependence
5' and 3'-phosphate termini	5' and 3'-phosphate termini	-
3'-phosphoglycaldehyde termini		+
Nucleic acid base and base propenoic acid	Nucleic acid base	- +

2.4. Discussion

2.4.1. Recognition of DNA by Phi Complexes of Rhodium.

Both $[Rh(phen)_2(phi)]^{3+}$ and $[Rh(phi)_2(bpy)]^{3+}$ intercalate into DNA and, with photoactivation, promote strand scission. However, their sites of reaction differ substantially. The complexes, extremely similar to each other with respect to their electronic structure, show comparable quantum efficiencies for photoanation in the absence of DNA[5] and comparable quantum efficiencies for DNA strand scission[5b]. Therefore, the differences in DNA sites cleaved between the two complexes must represent a difference in their recognition characteristics.

$[Rh(phi)_2(bpy)]^{3+}$ induces DNA strand scission in a predominantly sequence-neutral fashion, while $[Rh(phen)_2(phi)]^{3+}$ is observed to cleave only a subset of available sites. The strongest cleavage sites observed for $[Rh(phen)_2(phi)]^{3+}$ are those containing the consensus sequence 5'-py-*py*-pu-3' such as 5'-C*C*AG-3'. Results indicate that 5'-CCAG-3' sites are cleaved to an even greater extent at the 5'-*py*-pu-3' step if the sequence is preceded by additional pyrimidines to the 5'-side. $[Rh(phen)_2(phi)]^{3+}$ also consistently recognizes homopyrimidine stretches of four or more base-pairs. The recognition characteristics of $[Rh(phen)_2phi]^{3+}$ have been explained[5] based upon a consideration of structural features of the sequences targeted. X-ray crystallographic studies of oligonucleotides containing 5'-py-py-pu-3' sites and homopyrimidine stretches all show openings at such sites in the major groove.[12,13] Owing to steric clashes between the overhanging phenanthrolines and the base-pair column upon intercalation of the phi ligand into the helix, some opening of the major groove would facilitate complex binding. For 5'-py-py-pu-3' sites such openings arise because of DNA propeller twisting. Previous studies indicate a correlation between enantioselective cleavage by $[Rh(phen)_2phi]^{3+}$ and the extent of differential propeller twisting at these sites.[7]

For $[Rh(phi)_2bpy]^{3+}$, however, no similar steric constraints appear to apply. The ancillary phi ligand is remarkably free of appendages which would normally clash with the base pair planes above and below the intercalation site; since the coordinated nitrogens on the ancillary phi ligand are primary imines, the only substituent on the nitrogen is a hydrogen atom. The shape of the complex therefore allows binding of $[Rh(phi)_2bpy]^{3+}$ at many sites along the DNA strand. Indeed $[Rh(phi)_2bpy]^{3+}$ cleaves at most sites along the DNA helix exhibiting a small preference for alternating 5'-py-pu-3' sequences such as 5'-ATGC-3'.

The structural basis for this difference in the site recognition characteristics of $[Rh(phen)_2phi]^{3+}$ and $[Rh(phi)_2bpy]^{3+}$ is illustrated in Figure 2.10. Here is shown a model for intercalation of each of the complexes into a base-pair step. Intercalation is shown in this model from the major groove of DNA. The results described here and elsewhere[5,7] all seem to support intercalation by metal complexes from the major groove. Remarkably, the differences in recognition characteristics of the two rhodium complexes may be understood based on the subtle differences in the shapes of these intercalators. These results underscore the importance of *shape-selection* in governing the recognition of a DNA site.

2.4.2. Phi Complexes of Rhodium Exhibit a 5'-Asymmetric Cleavage Pattern.

Another prominent and novel characteristic of cleavage by $[Rh(phen)_2phi]^{3+}$ is the consistent 5' shift in strand scission at a base-pair site on one strand compared to the other. For $[Rh(phi)_2bpy]^{3+}$, this 5'-asymmetry is less evident owing to the greater sequence neutrality in cleavage of this rhodium complex. However, this asymmetry can be observed at the preferred cleavage site 5'-A*T*GC-3' on the oligonucleotide. According to a model derived by Dervan and co-workers,[14] an asymmetry in the cleavage pattern by a *diffusible*

Figure 2.10. Models illustrating the intercalation of $[Rh(phi)_2bpy]^{3+}$ (dark blue) and $[Rh(phen)_2phi]^{3+}$ (aqua) through the phi into an unwound base-pair step (green). The figure illustrates a model of how the shapes of $[Rh(phi)_2bpy]^{3+}$ (left) and $[Rh(phen)_2phi]^{3+}$ (right) may affect both their binding and cleavage chemistry. Above is a view showing intercalation into the major groove and below, the same model after 90° rotation, giving the side view of the complexes. The unhindered ancillary phi ligand of $[Rh(phi)_2bpy]^{3+}$, possibly owing to its hydrophobicity, allows the complex to slide to one side of the helix making the C-3' hydrogen atom (marked in red) on the opposite strand more accessible to dioxygen. The side view emphasizes how the unhindered shape of $[Rh(phi)_2bpy]^{3+}$ permits access into many local conformations along the DNA helix, while the steric interactions of the ancillary phenanthrolines of $[Rh(phen)_2phi]^{3+}$ are evident with base-pairs above and below.

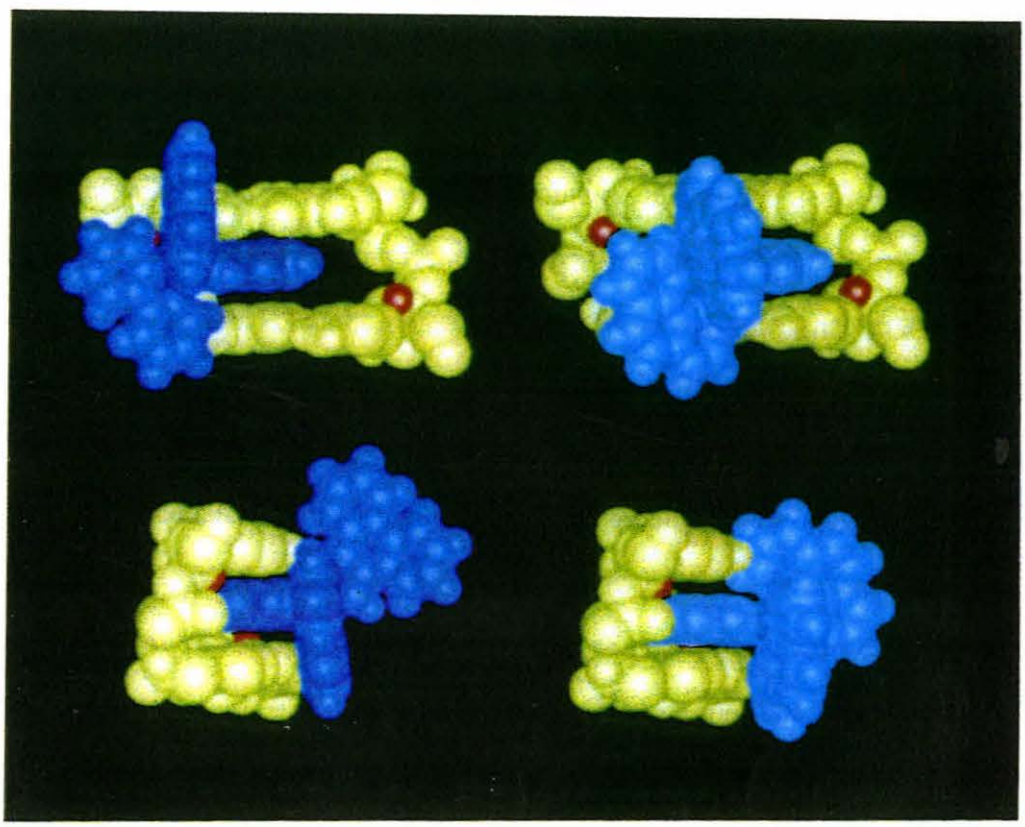

species will indicate whether the DNA cleavage agent is bound in the major or minor groove of the helix. A shift to the 3'-side was suggested as evidence for binding in the minor groove, while a shift to the 5'-side would indicate binding in the major groove. While this notion has been applied most to cleavage agents which produce a diffusible DNA oxidant,[12] it has also been invoked as evidence for minor groove binding by calicheamicin,[4b] an antitumor agent which cleaves DNA in a reaction yielding sharp bands, not unlike those seen with $[Rh(phen)_2(phi)]^{3+}$ and $[Rh(phi)_2bpy]^{3+}$. For both species the shift is 1-2 nucleotides, in contrast to the 5-nucleotide shift seen with a diffusible oxidant. Since the $[Rh(phi)]^{3+}$ complexes show a 5'-asymmetry, this finding lends further support to the hypothesis that binding occurs from the major groove. Such a 5' shift in the observed cleavage pattern is unprecedented and clearly provides information with regards to the orientation of the phi cleaving moiety relative to the DNA helix.

In addition to the 5'- shift in cleavage patterns, the extent to which cleavage occurs on the 5'- side of the intercalation site is not identical in both strands, and this difference also provides information regarding the structures of the bound complexes. The differences in extent of cleavage on each strand is more clearly seen in the cleavage patterns of the dodecanucleotide 5'-$C_1T_2G_3G_4C_5A_6T_7G_8C_9C_{10}A_{11}G_{12}$-3'. Here $[Rh(phen)_2phi]^{3+}$ and $[Rh(phi)_2bpy]^{3+}$ cleave most strongly at the 5'-C*C*AG-3' and 5'-A*T*GC-3' sites respectively. The 5'-asymmetry indicates intercalation by $[Rh(phen)_2phi]^{3+}$ at the CA step and by $[Rh(phi)_2bpy]^{3+}$ at the TG step. Cleavage by $[Rh(phi)_2bpy]^{3+}$ appears highly skewed towards one strand of the site as suggested by the 5-fold decrease in cleavage at the 5'-C_5 of the complementary strand. This observation suggests that the complex may be slid or canted to one side of the helix in the bound complex; steric clashes of the ancillary bipyridyl ligand with the helical column are not present with the ancillary phi ligand. To minimize such clashes, then, the complex may be oriented asymmetrically (towards one strand) in the site. In comparison, $[Rh(phen)_2phi]^{3+}$ appears to cleave

strongly at both the 5'-T_7 and the 5'-C_5 (5'-G*C*AT-3'; on the other strand) of the 5'-A*T*GC-3' site, with only a slight preference for the 5'-T_7 (see Figure 2.4). This implies that, unlike $[Rh(phi)_2bpy]^{3+}$, $[Rh(phen)_2phi]^{3+}$ is not significantly canted to one side of the helix; both the ancillary ligands in this complex are phenanthrolines. This asymmetry is also illustrated in the model shown in Figure 2.10.

2.4.3. Cleavage Products and Pathways of DNA Strand Scission.

The characterization of photocleavage products has proved to be valuable in delineating aspects of the mechanism of strand scission by the $[Rh(phi)]^{3+}$ complexes. The results described in this chapter are consistent with a DNA cleavage mechanism that involves modification of the C-3' position of the deoxyribose ring. While the DNA photodegradation products have been successfully characterized by gel electrophoresis and HPLC analyses, the precise nature of the reactive rhodium species and the rhodium-containing photoproducts has not been elucidated. The production of sharp cleavage bands after the cleavage of restriction fragments or oligonucleotides suggests that the strand scission of DNA by rhodium complexes is not mediated by a diffusible oxidant. Rather, the cleavage appears to involve a species which is generated and induces strand scission of the DNA backbone at precisely the position of binding. Rhodium polypyridyl complexes are known to be potent photo-oxidants; irradiation of the ligand transitions leads to ligand-to-metal-charge transfer (LMCT)[6,15]. Previous work has shown the quantum efficiencies for photoreaction by the phi complexes of rhodium to be comparable to those of $[Rh(phen)_3]^{3+}$ and that photolysis into a phi transition promotes preferential reaction of the phi ligand.[6] Therefore, the active radical species responsible for DNA cleavage is likely to be the phi cation radical formed as a result of LMCT and intimately bound to DNA. The positioning of the phi cation radical in the site can lead to the ready abstraction of a hydrogen atom from the deoxyribose ring to form an intermediate C-3' radical species. As

summarized in Scheme 2.1, irradiation of $[Rh(phen)_2phi]^{3+}$ in the presence of DNA may lead to the formation of the $[Rh(phen)_2]^{2+}$ intermediate. This species can then readily oxidize the C3'-radical to form the C3'-cation, which may be subsequently hydrolyzed to DNA degradation products. The resulting $[Rh(phen)_2]^{+}$ intermediate may then be readily oxidized to form $[Rh(phen)_2(H_2O)_2]^{3+}$, previously identified as the end product of the photocleavage reaction[6]. Furthermore, it is likely that $[Rh(phen)_2(H_2O)_2]^{3+}$ forms a covalent adduct with DNA, which is identified by gel electrophoresis as a slower moving band with respect to the unmodified DNA substrate.

Analysis of DNA degradation products resulting from photoreactions involving $[Rh(phen)_2phi]^{3+}$ and $[Rh(phi)_2bpy]^{3+}$ is consistent with a primary lesion at the C3'-position of the deoxyribose. Recently, the chemical products formed through oxygen independent and dependent pathways of strand scission involving the initial abstraction of the hydrogen from the C3' position have been proposed.[3] It was predicted that in an oxygen *independent* pathway, abstraction of the C3'-H would result in the formation of nucleic acid bases and oligonucleotide termini containing 3'- and 5'-phosphates. Alternatively, an oxygen *dependent* pathway would result in the formation of nucleotide base propenoic acids, 5'-phosphate termini, and 3'-phosphoglycaldehyde termini. Table 2.3 summarizes the products obtained after reaction with $[Rh(phen)_2phi]^{3+}$ and $[Rh(phi)_2bpy]^{3+}$. As summarized in Scheme 2.2, the products found correspond to those predicted for radical formation at the C3'-position. However, there is no evidence for reaction at the C1'-, C4'- and C5'- positions, which would yield products that have been previously observed and characterized in detail.[2,4] Upon photocleavage with the rhodium complexes in the absence of oxygen, product analysis reveals the formation of 5'- and 3'-phosphate termini and the release of nucleic acid bases. Either with or without oxygen, no nucleic acid base propenals or phosphoglycolate termini associated with C-4' modification were detected under conditions in which, given the extents of reaction, such products

Scheme 2.1. Proposed mechanism of the photodecomposition of $[Rh(phen)_2(phi)]^{3+}$ in the presence of DNA. The scheme shows that irradiation into the LMCT band (310 nm) of $[Rh(phen)_2(phi)]^{3+}$ may yield an excited state phi-cation radical, which is capable of abstracting the C3'-H atom from the deoxyribose. Oxidation of the intermediete C3'-radical may occur with concomitant formation of $[Rh(phen)_2]^{+}$, which readily oxidizes in the presence of aerated solutions to form the identified $[Rh(phen)_2(H_2O)_2]^{3+}$ complex.

Scheme 2.1.

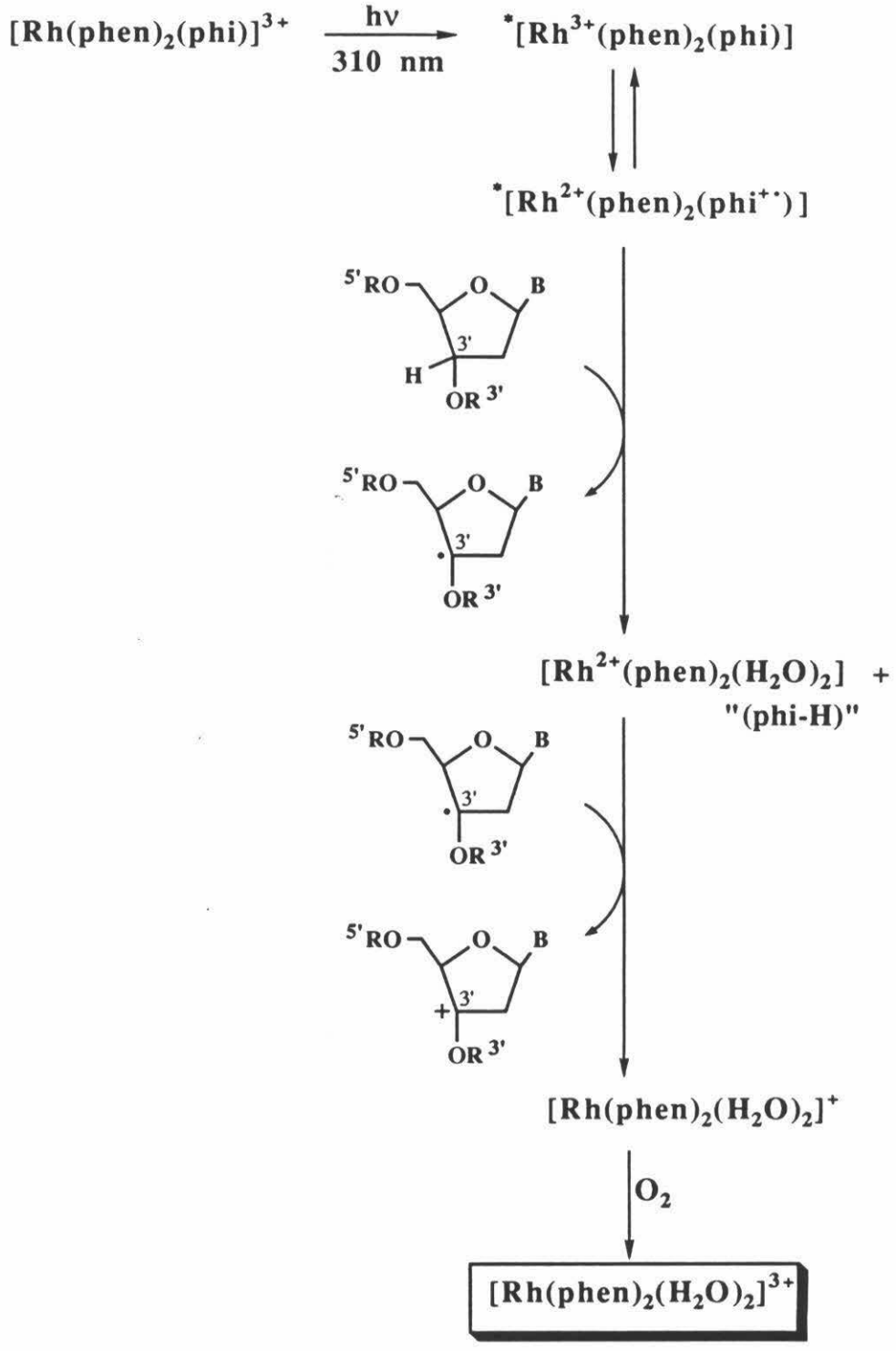
[Rh(phen)2(phi)]3+
hν
310 nm
*[Rh3+(phen)2(phi)]
*[Rh2+(phen)2(phi+·)]
5'RO
O
B
3'
H
OR 3'
[Rh2+(phen)2(H2O)2] +
"(phi-H)"
+
[Rh(phen)2(H2O)2]+
O2
[Rh(phen)2(H2O)2]3+

Scheme 2.2. The proposed mechanism (adapted from reference 3) of DNA photocleavage by $[Rh(phen)_2phi]^{3+}$ and $[Rh(phi)_2bpy]^{3+}$. The cleavage is mediated by abstraction of a C3'- hydrogen atom from the deoxyribose, followed by degradation via oxygen dependent and oxygen independent pathways to form the identified products (boxed).

Scheme 2.2.

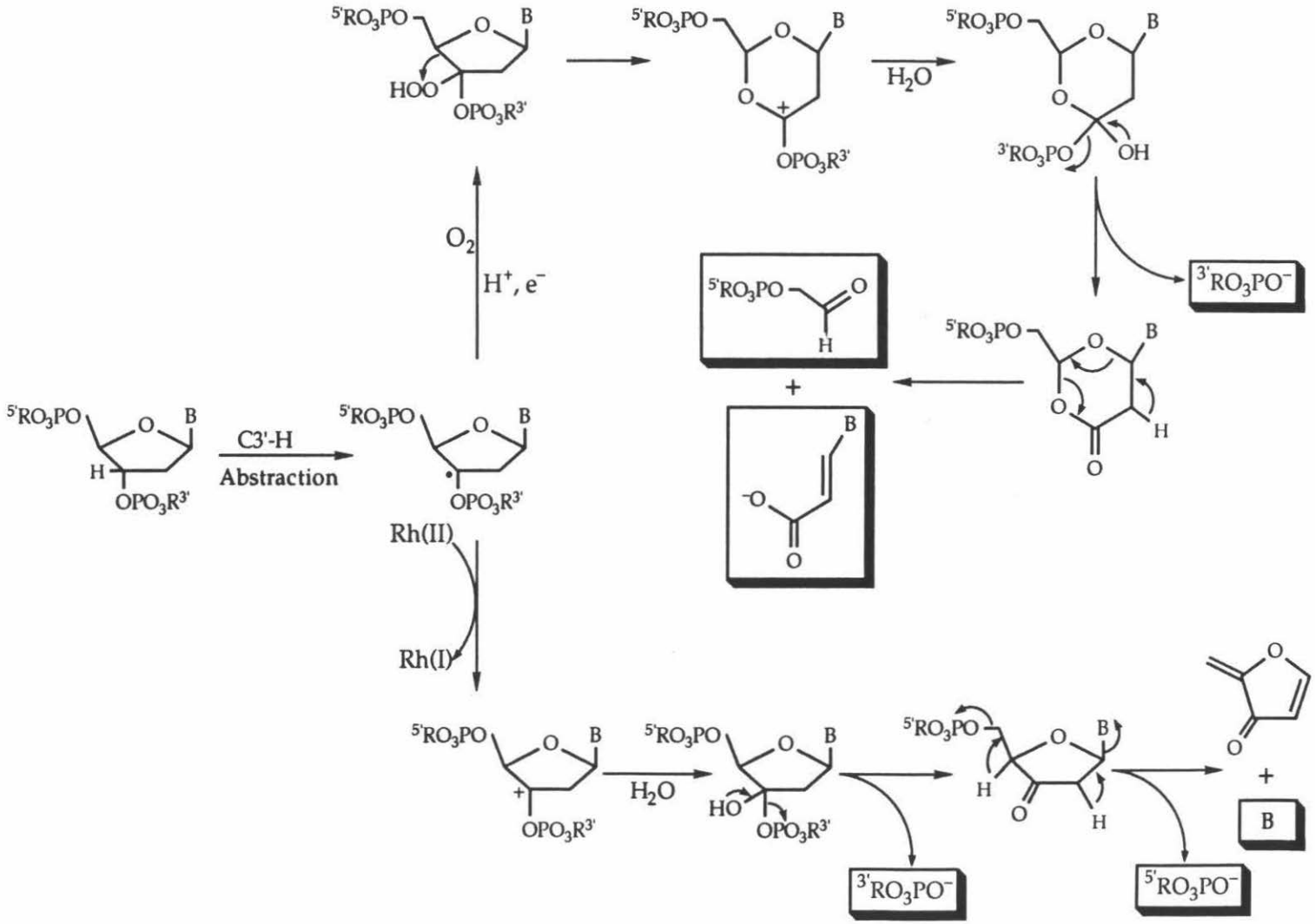
5'RO3PO
B
HOO
OPO3R3'
H2O
3'RO3PO
OH
3'RO3PO−
O2
H+, e−
C3'-H
Abstraction
H
Rh(II)
Rh(I)
HO
5'RO3PO−
B

would have been readily apparent. However, in the presence of oxygen, an additional 3'-terminus which migrates significantly slower than the corresponding 3'-phosphate product is apparent. This terminus is produced to a greater extent in the DNA photocleavage reaction with $[Rh(phi)_2bpy]^{3+}$ than $[Rh(phen)_2phi]^{3+}$. The effects of alkali and of treatment with $NaBH_4$ confirm that the terminus is not a metastable species which decays ultimately to a 3'-phosphate. Neither the production of this 3'-terminus nor of the 3'- or 5'-phosphate termini are increased upon alkaline treatment. Alkaline lability in cleavage is commonly associated with lesions derived from C-1' or C-4' modification.[2-4,16] The lack of 3'-phosphoglycolate termini, the absence of an observable metastable intermediate, and the clear production of only a 5'-phosphate terminus are clearly inconsistent with modification at the C4', C1', and C5'-deoxyribose positions, respectively.

The secondary 3'-terminus **1** is assigned as a 3'-phosphoglycaldehyde, which may be formed due to modification at the C3'- position (Scheme 2.2). Treatment with $NaBH_4$ causes an increase in the mobility of the terminus. A 3'-phosphoglycaldehyde, under these conditions, would be reduced to the corresponding, faster migrating alcohol. The DNA minor groove binding calicheamicin produces a modified deoxyribose fragment containing 5'-aldehyde ends which become reduced by $NaBH_4$ to produce faster moving 5'-alcohol ends.[4b] The possibility of an acidic functionality is ruled out because the addition of a negatively charged moiety would migrate faster, not slower, as observed, than the corresponding phosphate end. It is noteworthy that in peroxide damaged Escherichia coli a stable 3'-phosphoglycaldehyde lesion has been characterized and found to migrate more slowly than the corresponding 3'-phosphate terminus using paper chromatography[17]. Importantly, the formation of this phosphoglycaldehyde terminus is correlated with the production of a base-propenoic acid. The comparison of the HPLC quantitation of nucleic acid base versus base-propenoic acid formation with the densitometric quantitation of 3'-phosphate and 3'-phosphoglycaldehyde termini shows excellent agreement between the

extent of base-propenoic acid and the extent of 3'-phosphoglycaldehyde termini formed. Additionally, the 3'-phosphoglycaldehyde and base-propenoic acid are dependent upon the presence of dioxygen while the production of phosphate termini and nucleic acid bases are not. $[Rh(phen)_2phi]^{3+}$ appears to promote degradation primarily through the oxygen independent pathway, leading to the production of 3'- and 5'-phosphate termini and nucleic acid bases. For $[Rh(phi)_2bpy]^{3+}$ instead there is a partitioning between the oxygen independent pathway and the oxygen dependent pathway which leads to production of 3'phosphoglycaldehyde termini, 5'-phosphates, and base-propenoic acids. Photolysis of either phi complex intercalated into DNA leads to abstraction of the C3'-H atom, with formation of the C3'-radical. Oxidation of a radical species with the intermediate Rh^{2+} species and solvation of the resultant cation would lead, through a series of β-elimination steps, to the 5'-phosphate, 3'-phosphate and free nucleic acid base products observed. Alternatively, addition of dioxygen to the C3'-radical, followed by oxygen insertion into the C3'-C4' bond and decomposition, yields a 5'-phosphate and the correlated 3'-phosphoglycaldehyde terminus and base-propenoic acid.

The above analyses clearly indicates that the C3'- position on the deoxyribose is the primary site of photoreaction by $[Rh(phi)]^{3+}$ complexes. The lack of modification at the C1'-, 4'-and 5'- positions of the deoxyribose ring is quite reasonable given the proposed structure shown in Figure 2.10 of the DNA-bound $[Rh(phi)]^{3+}$ complexes. A phi complex intercalated in the major groove of the DNA helix does not have access to these minor groove positions. However, the bound complex has ready access to the C3'-H of the deoxyribose ring. Indeed dinucleotide crystal structures of intercalation complexes[18,19,20] show alternating sugar puckering at an intercalation site, in which the C3'-H to the 5'-side of the intercalation site is pointed directly towards the intercalating moiety. This observation suggests one potential reason for the observed 5'-asymmetry in cleavage pattern.

2.4.4. The Shape-Selectivity in Reaction.

The partitioning of the C3'-radical between oxygen dependent and oxygen independent pathways of decomposition clearly differs for $[Rh(phen)_2(phi)]^{3+}$ and $[Rh(phi)_2bpy]^{3+}$. $[Rh(phi)_2bpy]^{3+}$ photocleavage shows a greater level of reaction through the oxygen-dependent pathway than does $[Rh(phen)_2phi]^{3+}$. This difference may also be understood based upon our models for their binding to the helix and also explained through the differences in the *shapes* of these complexes. The binding by $[Rh(phi)_2bpy]^{3+}$ occurs at all sites since the ancillary phi ligand is pulled back from the intercalating phi ligand; this disposition of the ancillary phi also permits access of dioxygen to the C3'- position. In the case of $[Rh(phen)_2phi]^{3+}$, the bulky ancillary phenanthroline ligands not only preclude binding at closed sites but also shelter the C3'-position from addition of dioxygen. Furthermore, canting of $[Rh(phi)_2bpy]^{3+}$ towards one strand of the helix appears to increase the accessibility for dioxygen to the complementary strand at the site of intercalation. Consistent with this notion, we observe that oligonucleotide cleavage with $[Rh(phi)_2bpy]^{3+}$ at the T_7 of the strong 5'-$A_6T_7G_8C_9$-3' site is associated with a large extent of 3'-phosphoglycaldehyde formed at the C_5 of the complementary strand. It appears therefore that $[Rh(phi)_2bpy]^{3+}$ promotes both pathways of strand degradation from the C-3' radical intermediate while $[Rh(phen)_2phi]^{3+}$ disfavors the utilization of dioxygen in DNA strand scission.

These observations suggest that the overall shape of the $[Rh(phi)]^{3+}$ complexes not only dictates DNA recognition but also determines the outcome of DNA cleavage. The reaction *and* the site-recognition is shape-selective. These results illustrate the intimate relationship between recognition and reactive characteristics of molecules bound selectively to DNA[21]. In designing mimics of DNA-binding proteins and natural products, and in constructing wholly original designs for sequence-specific cleaving agents, there has been

much focus on the separation of binding and cleaving domains. In the case of the transition metal complexes designed in the Barton laboratory, a clear separation between binding and cleaving functionalities is inappropriate. Such an intimate relationship between recognition and reaction of DNA-binding molecules may be more general and important to consider in understanding the reactions of DNA-binding proteins and small molecules.

In conclusion, these studies have shown that $[Rh(phen)_2(phi)]^{3+}$ and $[Rh(phi)_2(bpy)]^{3+}$ mediate the efficient photo-induced strand scission of the DNA backbone through a mechanism consistent with initial C3'-H abstraction. Further, the structure of these molecules indicate binding and DNA recognition properties dominated by a complementation of the shape of the individual complex and the structure of the DNA binding site.

References and Footnotes

1. (a) Barton, J. K. *Science* **1986**, 233, 727. (b) Fleisher, M. B.; Mei, H.-Y.; Barton, J. K. *Nucleic Acids Mol. Biol.* **1988**, 2, 65. (c) Kirshenbaum, M. R.; Tribolet, R.; Barton, J. K. *Nucl. Acids Res.* **1988**, 16, 7983. (d) Mei, H.-Y.; Barton, J. K. *Proc. Natl. Acad. Sci. U.S.A.* **1988**, 85, 1339. (e) Barton, J. K.; Pyle, A. M. Prog. *Inorg. Chem.* **1990**, 38, 413.
2. (a) Dervan, P. B. *Science* **1986**, 232, 464. (b) Moser, H. E.; Dervan, P. B. *Science* **1987**, 238, 645. (c) Sigman, D. S. *Acc. Chem. Res.* **1986**, 19, 180. (d) Tullius, T. D., Ed. "Metal-DNA Chemistry" ACS Symposium Series 402; American Chemical Society: Washington, D. C., 1989.
3. Stubbe, J.; Kozarich, J. W. *Chem. Rev.* **1987**, 87, 1107.
4. (a) Hecht, S. M. *Acc. Chem. Res.* **1986**, 19, 383. (b) Zein, N.; Sinha, A. M.; McGarhren, W. J.; Ellestad, G. A. *Science* **1988**, 240, 1198. (c) Kappen, L. S.; Goldberg, I. H.; Wu, S. H.; Stubbe, J.; Worth, L. Jr.; Kozarich, J. W. *J. Am. Chem. Soc.* **1990**, 112, 2797. (d) Gale, E. F.; Cundliffe, E.; Reynolds, P. E.; Richmond, M. H.; Waring, M. J. "The Molecular Basis of Antibiotic Action" Wiley: London 1981.
5. (a) Pyle, A. M.; Long, E. C.; Barton, J. K. *J. Am. Chem. Soc.* **1989**, 111, 4520. (b) Pyle, A. M., PhD thesis, Columbia University, 1989. (c) David, S. S.; Barton, J. K. *J. Am. Chem. Soc.*, 115, 294.
6. Pyle, A. M.; Chiang, M.; Barton, J. K. *Inorg. Chem.* **1990**, 29, 4487.
7. (a) Pyle, A. M.; Morii, T.; Barton, J. K. *J. Am. Chem. Soc.*, **1990**, 112, 9432. (b) Campisi, D.; Morii, T.; Barton, J. K., manuscript in preparation.
8. Uchida, K.; Pyle, A. M.; Morii, T.; Barton, J. K. *Nucl. Acids Res.* **1989**, 17, 10259.

9. Maniatis, T.; Fritsch, E. F.; Sambrook, J. "Molecular Cloning" 1982, Cold Spring Harbor Laboratory.

10. Brown and Krishnamurthy, *Tetrahedron* **1967**, 35, 567.

11 (a) Mahnken, R. E.; Bina, M.; Diebel, R. M.; Luebke, K.; Morrison, H. *Photochem. Photobiol.* **1989**, 49, 519. (b) Mahnken, R. E.; Billadeau, M. A.; Nikonowicz, E. P.; Morrison, H.; *J. Am. Chem. Soc.* **1992**, 114, 9253-9265.

12. (a) Heinemann, U.; Lauble, H.; Frank, R.; Blocker, H. *Nucl. Acids Res.* **1987**, 15, 9531. (b) Dickerson, R.; Drew, H. R. *J. Mol. Biol.* **1981**, 149, 761. (c) Hunter, W. N.; D'Estaintoto, D. L.; Kennard, O. *Biochemistry* **1989**, 28, 2444. (d) Nelson, H. C. M.; Finch, J. T.; Luisi, B. F.; Klug, A. *Nature* **1987**, 330, 221. (e) Coll, M.; Frederic, A.; Wang, A. H. J.; Rich, A. *Proc. Natl. Acad. Sci. U.S.A.* **1987**, 84, 8385. (f) Timsit, Y.; Westhof, E.; Fuchs, R. P. P.; Moras, D. *Nature* **1989**, 341, 459. (g) Wing, R.; Drew, H.; Takano, T.; Broka, C.; Tanaka, S.; Itakura, K.; Dickerson, R. E. *Nature* **1980**, 287, 755. (h) Wang, A. H.-J.; Fujii, S.; van Boom, J. H.; Rich, A. *Proc. Natl. Acad. Sci. U.S.A.* **1982**, 79, 3968. (i) Shakked, Z.; Rabinovich, D.; Cruse, W. T. B.; Egert, E.; Kennard, O.; Sala, G.; Salisbury, S. A.; Viswamitra, M. A. *Proc. R. Soc. London, B.* **1981**, 231, 479.

13. Dickerson, R. E. *J. Molec. Struct. Dyn.* **1989**, 6, 627.

14. Sluka, J. P.; Horvath, S. J.; Bruist, M. F.; Simon, M. I.; Dervan, P. B. *Science* **1987**, 238, 1129.

15. (a) Chan, S.-F.; Chou, M.; Creutz, C.; Matsubara, T.; Sutin, N. *J. Am. Chem. Soc.* **1981**, 103, 369. (b) Brown, G. M.; Chan, S.-F.; Creutz, C.; Schwartz, H. A.; Sutin, N.; *J. Am. Chem. Soc.* **1979**, 101, 7639. (c) Indelli, M. T.; Carioli, A.; Scandola, F. *J. Phys. Chem.* **1984**, 88, 2685. (d) Ballardini, R.; Varani, G.; Balzani, V. *J. Am. Chem. Soc.* **1980**, 102, 1719. (e) Frink, M. E.;

Sprouse, S. D.; Goodwin, H. A.; Watts, R. J.; Ford. P. C. *Inorg. Chem.* **1988**, 27, 1283.

16. (a) Goldberg, I. H.; *Free Radical Biol. Med.* **1987**, 3, 41. (b) Kappen, L. S.; Chen, I.-H.; Goldberg, I. H. *Biochemistry* **1988**, 27, 4331. (c) Kappen, L. S.; Goldberg, I. H. *Biochemistry* **1989**, 28, 1027.

17 Mulazzani, Q. G.; Emmi, S.; Hoffman, M. Z.; Venturi, M. *J. Am. Chem. Soc.* **1981**, 103, 3362.

18. (a) Trifonov, E. N.; Sussman, J. L.; *Proc. Natl. Acad. Sci. U.S.A.* **1980**, 77, 3816. (b) Marini, J. C.; Levene, S. D.; Crothers, D. M.; Englund, P. T. *Proc. Natl. Acad. Sci. U.S.A.* **1982**, 79, 7664. (c) Koo, H.-S.; Wu, H.-M.; Crothers, D. M. *Nature* **1986**, 320, 501.

19. (a) Burkhoff, A. M. and Tullius, T. D. *Cell* **1987**, 48, 935. (b) Burkhoff, A. M. and Tullius, T. D. *Nature* **1988**, 331, 455. (c) Wu, H.-M. and Crothers, D. M. *Nature* **1984**, 308, 509.

20. Wang, A. H. J.; Nathans, J.; van der Marel, G.; van Boom, J. H.; Rich, A. *Nature* **1978**, 276, 471.

21. Two examples illustrating this relationship have been seen with bleomycin. See, for example: Long, E. C.; Hecht, S. M.; van der Marl, G. A.; van Boom, J. H. *J. Am. Chem. Soc.* **1990**, 112, 5272. Carter, B. C.; Murty, V. S.; Reddy, K. S; Wang, S. N.; Hecht, S. M. *J. Biol. Chem.* **1990**, 256, 4193.

Chapter 3:

Synthesis and Characterization of a Series of Rh(9,10-phenanthrenequinone diimine)$^{3+}$ Complexes

3.1. Introduction

Octahedral polypyridyl complexes of rhodium(III) which contain a phi (9,10-phenanthrenequinone diimine) ligand are attractive frameworks for the design and preparation of metal complexes that bind sequence-selectively to nucleic acids. Biophysical (UV-visible spectroscopy)[1] and structural (2D-NMR)[2] studies have indicated that $[Rh(phi)]^{3+}$ complexes bind to DNA by selective intercalation of the phi ligand. Moreover, these studies have shown that intercalation is favored over other modes of DNA binding (surface and ionic interactions) by three to four orders of magnitude. Unlike simple polypyridyl ligands such as bipyridyl and phenanthroline, the phi ligand is well-suited for intercalation, probably because it mimics the spacial arrangement of the aromatic regions of a base-pair. Preferential intercalation of the phi ligand, therefore, fixes the approximate orientation of the octahedral metal complex with respect to the DNA helix. This allows for the systematic variation of the non-intercalating (ancillary) ligands, which make sequence-specific contacts with the DNA base-pairs above and below the intercalation site.

For example, previous studies have shown that while the complexes $[Rh(phen)_2phi]^{3+}$ and $[Rh(phi)_2bpy]^{3+}$ intercalate into DNA via their phi ligand, their ancillary ligands determine their vastly different DNA recognition properties[3]. In $[Rh(phen)_2phi]^{3+}$, the ancillary phenanthroline ligands introduce steric constraints which are accomodated by highly differentially propellar twisted 5'-py-pu-3' steps. However, in $[Rh(phi)_2bpy]^{3+}$, the ancillary phi ligand is pulled back from the metal center which allows the complex to bind at most sites on the DNA helix. These studies have illustrated

that the shapes of these complexes determine their overall DNA recognition properties. Based on these observations, we decided to alter systematically the shapes of these complexes to understand further their recognition properties and to explore the potential of shape-selection in the development of sequence-specific metal complexes.

In this chapter, the synthesis and characterization of derivatives of the complexes $[Rh(phen)_2phi]^{3+}$ and $[Rh(phi)_2bpy]^{3+}$ are reported. Families of complexes (Figures 3.1 and 3.2) of the type $[Rh(X)_2phi]^{3+}$ (where X = bpy, 4,4'-diphenylbpy, 5,5'-dimethylbpy, 4,4'-diamidobpy) and $[Rh(Y)(phi)_2]^{3+}$ (where Y= 4,7-dihydroxymethylphen, 4-hydroxymethylphen, 4,7-dimethylphen) have been prepared. These complexes contain functional groups, which are hydrophobic or hydrophillic in nature and are attached to varying positions of their ancillary phenanthroline or bipyridyl ligands. Different schemes and methods of preparation of the $[Rh(X)_2phi]^{3+}$ and $[Rh(Y)(phi)_2]^{3+}$ complexes and their respective functionalized ligands are reported. One-dimensional NMR spectroscopy, in conjuction with mass-spectrometry and UV-Vis spectrophotometry, has been successful in determining the identity and purity of the $[Rh(phi)]^{3+}$ complexes.

3.2. Experimental and Results

3.2.1. Instrumentation and Materials:

The reagents used in this study were obtained from the following suppliers: $RhCl_3$ (42.5% Rh, Aesar Johnson Matthey, Seabrook, NH); 4,7-dimethylphenanthroline, phenanthroline (phen), 2,2'-bipyridyl (bpy), 9,10-phenanthrenequinone, N_2H_4.HCl, (Aldrich, Milwaukee, WI); 4,4'-diphenylbipyridyl (GFS, Columbus, OH). Absorption spectra were recorded on a Cary 219 spectrophotometer, and NMR spectra were recorded on GE-300 MHz and JEOL-400 MHz spectrophotometers.

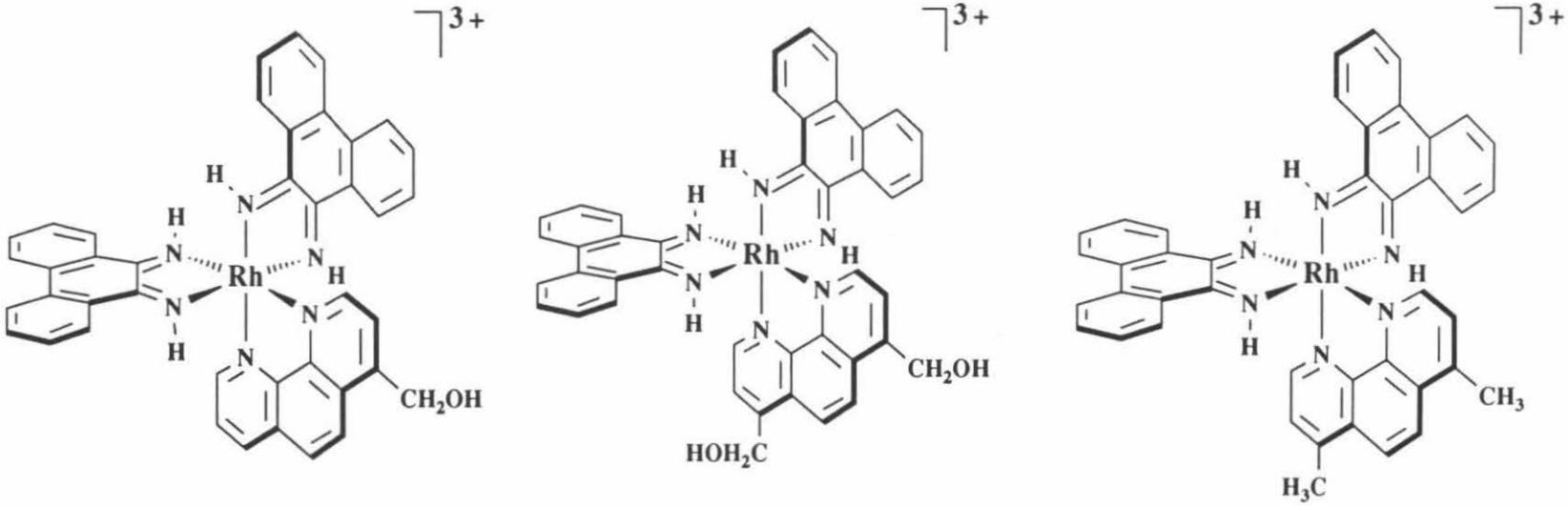

Figure 3.1. Structures of $[Rh(phi)_2Y]^{3+}$ complexes.
From left to right: $[Rh(phi)_2(4\text{-dydroxymethylphen})]^{3+}$, $[Rh(phi)_2(4,7\text{-dihydroxymethylphen})]^{3+}$, $[Rh(phi)_2(4,7\text{-dimethylphen})]^{3+}$.

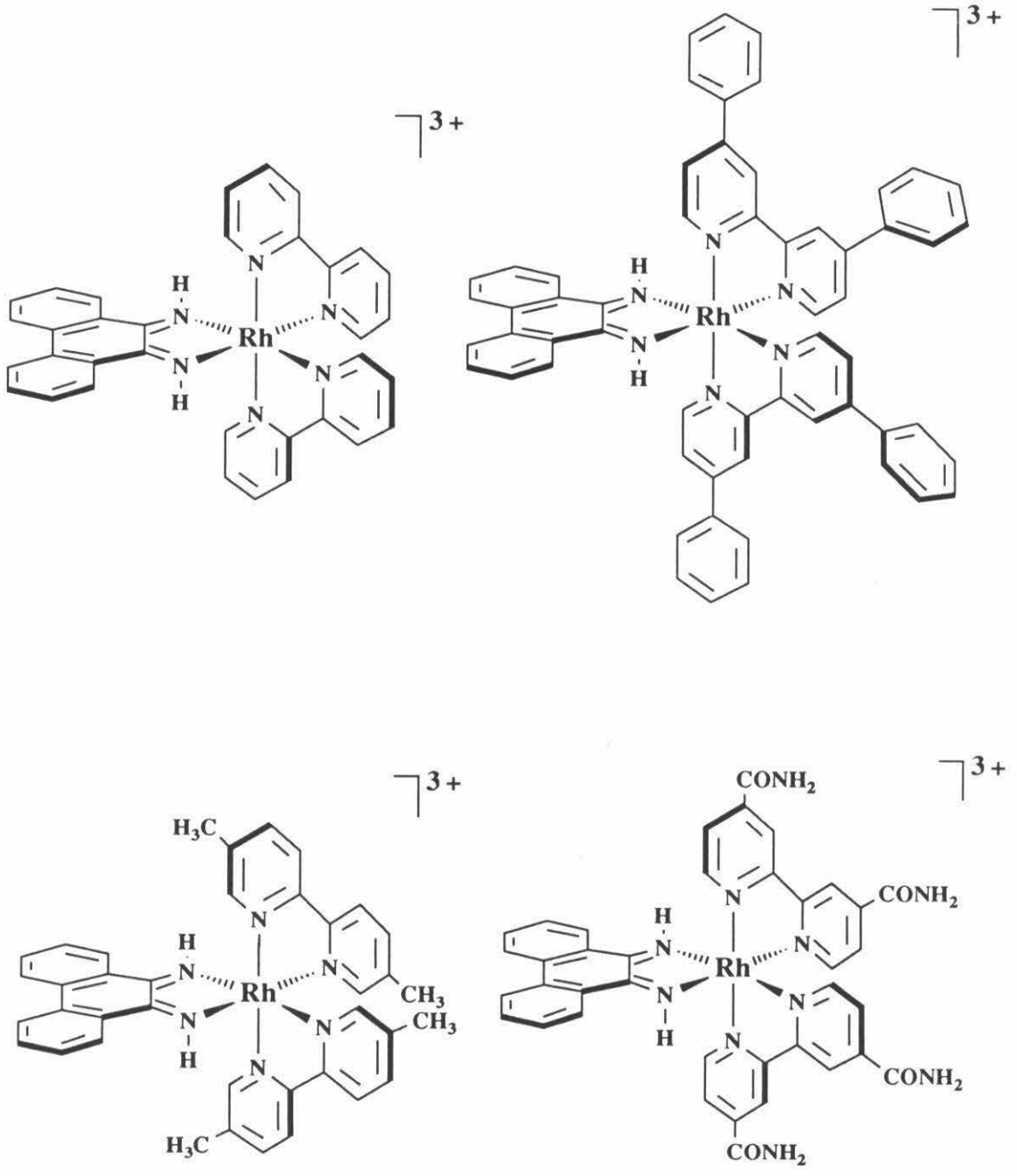

Figure 3.2. Structures of $[Rh(phi)X_2]^{3+}$ complexes.
Clockwise from top: $[Rh(phi)(bpy)_2]^{3+}$, $[Rh(phi)(4,4'\text{-diphenylbpy})_2]^{3+}$, $[Rh(phi)(5,5'\text{-dimethylbpy})_2]^{3+}$, $[Rh(phi)(4,4'\text{-diamidobpy})_2]^{3+}$.

3.2.2. Synthesis of $[Rh(Y)(phi)_2]^{3+}$ Complexes:

The complexes of the type $[Rh(Y)(phi)_2]^{3+}$, where Y= phen, 4,7-dihydroxymethylphen, 4-hydroxymethylphen, 4,7-dimethylphen, 4,4'-diphenylbpy, 5,5'-dimethylbpy, and 4,4'-diamidobpy, were prepared according to a modified version of the synthetic procedure reported[2] for $Rh(phi)_2bpy^{3+}$. This procedure involves the addition of 9,10-diaminophenanthrene to $RhCl_3.6H_2O$, followed by subsequent air-oxidation to prepare the $[Rh(phi)_2Cl_2]^+$. The inner-sphere chloride ligands are then replaced by more labile water ligands to form $[Rh(phi)_2(H_2O)_2]^{3+}$ using standard methods.[4] This intermediate complex is then readily converted to the desired $[Rh(phi)_2Y]^{3+}$ upon the addition of stoichiometric amounts of Y. A summary of the three-step synthesis is presented in Scheme 3.1.

Step 1. Preparation of $[Rh(phi)_2Cl_2]Cl$:

The complex was made as described in the literature[2]. The NMR of the product shows formation of both the cis and trans isomers of the complex. Yield: 70%. NMR (DMSO) trans: 14.73 (s, 2 imine protons); 8.73 (d, 4H); 8.53, (d, 4H); 7.91 (t, 4H); 7.81 (t, 4H). Cis isomer: 14.6 (s, 1 imine proton); 13.2 (s, 1 imine proton); 9.23 (d, 4H); 8.48 (t, 4H); 8.36 (d, 2H); 7.95 (d, 2H); 7.8 (d, 2H); 7.75 (t, 2H); 7.58 (t, 2H).

Step 2. Preparation of $[Rh(phi)_2(H_2O)_2](CF_3SO_2O)_3$:

$[Rh(phi)_2Cl_2]Cl$ and $Ag(CF_3SO_2O)$ in a ratio of about 1:3.5 are dissolved in a DMF/H_2O mixture (5/1) and reacted in the dark for about 12 hours. The solution turns cloudy with time indicating the formation of insoluble AgCl. The mixture is then filtered to remove AgCl and the filtrate is rotovaped to dryness. The product is then washed with water to remove unreacted $Ag(CF_3SO_2O)$. The product $[Rh(phi)_2(H_2O)_2](CF_3SO_2O)_3$ is insoluble in water and the NMR of this complex is taken in d-DMSO. The NMR shows the formation of the symmetric trans isomer, with resonances that are shifted with respect to that of trans $[Rh(phi)_2Cl_2]Cl$. NMR shifts of the trans isomer in d-DMSO: 14.28 (s, 2

Scheme 3.1.: Synthesis of $[Rh(phi)_2Y]Cl_3$ Complexes.

Step 1.

$RhCl_3$ + 9,10-diaminophenanthrene (DAP) $\xrightarrow{DMF,\ 65\ ^\circ,\ N_2}$ $[Rh(DAP)_2Cl_2]Cl$

$\downarrow$ O_2, 24 h

$[Rh(phi)_2Cl_2]Cl$

(phi = 9,10-phenanthrene-quinone diimine)

Step 2.

$[Rh(phi)_2Cl_2]Cl$ + $Ag(CF_3SO_2O)$ $\xrightarrow[DMF/H_2O\ (5:1)]{24\ h,\ dark}$ $[Rh(phi)_2(H_2O)_2](CF_3SO_2O)_3$

Step 3.

$[Rh(phi)_2(CF_3SO_2O)_2](CF_3SO_2O)$ + Y* $\xrightarrow{DMF,\ 65\ ^\circ}$ $[Rh(phi)_2Y](CF_3SO_2O)_3$

* (Y = 4,7-dimethylphenanthroline, 4,7-dihydroxymethylphenanthroline, 4-hydroxymethylphenanthroline)

$\downarrow$ Anion-exchange chromatography

$[Rh(phi)_2Y]Cl_3$

imine protons), 8.65 (d, 4H); 8.50 (dd, 4H); 7.92 (t, 4H); 7.80 (t, 4H). The UV-Vis spectrum of the product shows the phi π-π^* transition (at 340 nm) blue-shifted by 8 nm with respect to the corresponding transition at 348 nm in $[Rh(phi)_2Cl_2]Cl$. FAB Mass Spec ion: 552, $[Rh(phi)_2(H_2O)_2]^+$; 515, $[Rh(phi)_2]^+$; 306, $[Rh(phi)]^+$.

Step 3. Preparation of $[Rh(phi)_2Y]Cl_3$.

An equimolar mixture of $[Rh(phi)_2(H_2O)_2](CF_3SO_2O)_3$ and Y are reacted in DMF at 50 degrees celcius for 5 hrs. The reaction mixture is then rotovaped to dryness and the product extracted into water. The product is then precipitated by the addition of KCl and then passed through a C-18 sep pak to remove excess KCl. The purified product is then characterized by NMR, UV-Vis, Mass-ion spectrometry and Elemental analysis.

3.2.3. Characterization of $[Rh(Y)(phi)_2]^{3+}$ Complexes:

A description of the characterization data for the complexes $[Rh(phi)_2(HMP)]^{3+}$, $[Rh(phi)_2(DHMP)]^{3+}$, $[Rh(phi)_2(DMP)]^{3+}$ (Figure 3.1), where HMP = 4-hydroxymethylphen, DHMP = 4,7-dihydroxymethylphen, and DMP = 4,7-dimethylphen, is presented below. Since the complexes $[Rh(phi)_2Y]Cl_3$ (where Y = 4,4'-diamidobpy, 5,5'-dimethylbpy, 4,4'-diphenylbpy, phen) have previously been made and characterized,[5] the characterization of these complexes, synthesized via the modified synthetic scheme 3.1, is not reported here. In most of the $[Rh(phi)_2X]^{3+}$ complexes, the 1D-NMR spectral data is not sufficient to completely and unambiguously assign the spectra; however, the degree of multiplicity of each resonance and its relative integral value can in some cases give strong evidence for its assignment. However, in all cases, the NMR spectral data adequately define the nature and purity of the complexes, which is further confirmed by mass-spectral data and elemental analyses. Each listed resonance is followed by information describing its degree of multiplicity (where m = multiplet, t = triplet, d = doublet, dd = doublet of doublets, and s = singlet), the # of protons its integral represents,

and when known, the alphabet letter which refers to its structural assignment. Extinction coefficients are obtained at their isosbestic points (λ = 350 nm) using atomic absorption spectroscopy. UV-visible and NMR spectral data are presented in Appendix I and II, respectively, of this chapter.

$[Rh(phi)_2(HMP)]Cl_3$: HMP is the abbreviation for 4,-hydroxymethylphenanthroline, which was synthesized from 4-methyl phenanthroline according to a literature procedure[6]. NMR shifts in ppm (d-MeOH): *4 phi triplets (8 H)*: 7.42 (t, 2H), 7.55 (t, 2H), 7.68 (t, 2H), 7.75 (t, 2H); *Other phi and HMP resonances*: 7.95 (dd, 1H), 8.15 (d, 1H), 8.6 (d, 2H), 11 protons for multiplets centered at 8.9 and 8.3; 2 benzyl protons at 5.3. UV-visible spectrum shows maxima at 367 nm and 271 nm. FAB Mass Spec ion mass: 725, $[Rh(phi)_2(HMP)]^+$; 519, $[Rh(phi)_2]^+$ or $[Rh(phi)(HMP)]^+$. Elemental analysis calculated for $[Rh(phi)_2HMP]Cl_3.6H_2O$ C: 48.2 (found: 47.86), H: 3.56 (3.33), N: 8.23 (8.25). Extinction coefficient (ε) at (λ = 350 nm) is 24300 $M^{-1}cm^{-1}$.

$[Rh(phi)_2(DHMP)]Cl_3$: DHMP is the abbreviation for 4,7-dihydroxymethylphenanthroline, which was synthesized according to literature reported procedures[6]. NMR shifts in ppm (d-MeOH): *phi resonances (8 H)*: 7.40 (t, 2H), 7.52 (t, 2H), 7.7 (t, 2H), 7.75 (t, 2H), 8.10 (d, 2H), 8.52 (dd , 4H), 8.25 (d, 2H), *DHMP resonances*: 8.8 (d, 4H), 8.3 (s, 2H), 4 benzyl protons at 5.3; the observed ratio of the integrals for the aromatic to benzyl protons is 5.52, with a corresponding expected value of 5.75. NMR shifts in ppm (D_2O): *phi resonances (8 H)*: 7.32 (t, 2H), 7.45 (t, 2H), 7.62 (t, 2H), 7.7 (t, 2H); 7.95 (t, 4H-e, f), 8.15 (t, 4H, k, j), *DHMP resonances* : 8.25 (s, 2H-c), 8.26 (d, 2H-b), 8.78 (d, 2H-a), 4 benzyl protons at 5.3. UV-visible spectrum shows maxima at 369 nm and 272 nm. FAB Mass Spec ion mass: 755, $[Rh(phi)_2(DHMP)]^+$;

549, $[Rh(phi)(DHMP)]^+$; 515, $[Rh(phi)_2]^+$. Extinction coefficient (ε) at (λ = 350 nm) is 24100 $M^{-1}cm^{-1}$.

$[Rh(phi)_2(DMP)]Cl_3$: DMP refers to 4,7-dimethylphenanthroline. NMR shifts in ppm (d-MeOH): *phi resonances (16 H)*: 7.42 (t, 2H), 7.55 (t, 2H), 7.7 (t, 2H), 7.75 (t, 2H), 7.85 (t, 2H-j), 8.25 (m, 6H-k,e,f); *DMP resonances*: 8.45 (s, 2H-c), 8.58 (d, 2H-b), 8.72 (d, 2H-a), 6 CH_3 protons at 4.78. UV-visible spectrum shows maxima at 367 nm and 271 nm. FAB Mass Spec ion mass: 722, $[Rh(phi)_2DMP]^+$; 517, $[Rh(phi)_2]^+$ or $[Rh(phi)(DMP)]^+$. Elemental analysis calculated for $[Rh(phi)_2(DMP)]Cl_3.12H_2O$ C: 49.7 (found: 51.76), H: 3.77 (4.14), N: 8.24 (8.10). Extinction coefficient (ε) at (λ = 350 nm) is 30400 $M^{-1}cm^{-1}$.

3.2.4. Synthesis of $[Rh(X)_2(phi)]^{3+}$ Complexes:

The synthesis of $[Rh(X)_2(phi)]^{3+}$ type of complexes (where X = bpy, 4,4'-diphenylbpy, 5,5'-dimethylbpy, 4,4'-diamidobpy) is summarized in scheme 3.2. This is based on a previously described procedure[1] for the preparation of $[Rh(phen)_2phi]^{3+}$. The synthesis involves preparation of the bis-bipyridyl rhodium complexes $[Rh(X)_2Cl_2]Cl$, followed by displacement of the inner sphere chloride ligands with more labile water ligands to form the $[Rh(X)_2(H_2O)_2]Cl_3$ intermediates. Both the chloride and aquo bis-bipyridyl-like rhodium complexes have been isolated and characterized and, in all cases, NMR provides evidence for exclusive formation of the cis and not the trans isomers. Similarly, formation of the trans isomers of $[Rh(bpy)_2Cl_2]Cl$ or $[Rh(phen)_2Cl_2]Cl$ has not been observed in the literature[7]. Aquation of the $[Rh(X)_2Cl_2]Cl$ complexes has been carried out by two methods, the first involving the use of Ag_2O which promotes displacement of the chloride ligands by formation of insoluble AgCl. The second method involves using NaOH to provide strong hydroxide ligands[8], which displace the

Scheme 3.2.: Synthesis of $[Rh(phi)X_2]Cl_3$ Complexes

Step 1.

$$1RhCl_3 \quad + \quad 2X^* \xrightarrow{0.2\ eq.\ N_2H_4.HCl} [RhX_2Cl_2]Cl$$

*(X = bpy, 4,4'-diamidobpy, 5,5'-diphenylbpy, 4,4'-diphenylbpy)

Step 2.

$$[RhX_2Cl_2]Cl \xrightarrow[NaOH,\ H_2O\ pH\ 9.0]{Ag_2O,\ DMF,\ or} [RhX_2(H_2O)_2]Cl_3$$

Step 3.

$$[RhX_2(H_2O)_2]Cl_3 \quad + \quad \underset{(DAP)}{9,10\text{-diaminophenanthrene}} \xrightarrow[2.\ O_2,\ 12\ hr]{1.\ N_2,\ 65^\circ C,\ 24\ hr} [Rh(phi)X_2]Cl_3$$

(phi = 9,10-phenanthrenequinone diimine)

coordinated chlorides. The bis-aquo complex is then added to 9,10-diaminophenanthrene (DAP) in an inert atmosphere, followed by oxidation to form the desired $[Rh(X)_2phi]Cl_3$, complex. Preparation of $[Rh(DPB)_2phi]Cl_3$ (DPB = 4,4'-diphenylbipyridyl) and its precursor complexes $[Rh(DPB)_2(H_2O)_2]Cl$ and $[Rh(DPB)_2Cl_2]Cl$ required modifications in the synthetic procedures due to the solubility properties of DPB. These alterations in the procedure are included in the description of the general synthesis reported below.

Step 1.: Preparation of $[Rh(X)_2Cl_2]Cl$ complexes:

The bipyridyl-derivative ligand X (2.2 mmoles) is dissolved in 7.5 ml of ethanol and added to a solution of $RhCl_3.6H_2O$ (1 mmole) and hydrazine sulfate catalyst (0.2 mmoles) dissolved in 5 ml of H_2O. (In the specific preparation of $[Rh(DPB)_2Cl_2]Cl$, a solution of 2.2 mmoles of DPB dissolved in 700 ml of ethanol, is added to the rhodium chloride and hydrazine mixture.) The reaction mixture is then refluxed overnight. Upon addition of the ligand, the solution first turns cloudy, but then clears up after overnight refluxation. The reaction mixture is then cooled on ice to promote precipitation of the $[Rh(X)_2Cl_2]Cl$ complex. The product is then washed with cold water to remove unreacted $RhCl_3.6H_2O$.

Step 2.: Preparation of $[Rh(X)_2(H_2O)]Cl_3$ complexes:

Method 1. (Ag_2O method):

The complex $[Rh(X)_2Cl_2]Cl_3$ (0.3 mmoles) is dissolved in 11 ml of H_2O, to which is added a suspension of Ag_2O (1.5 mmoles) in 20 ml of H_2O. The mixture is warmed to 50° C and reacted in the dark for 24 hrs. The brown precipitate and insoluble AgCl formed in the reaction is removed by filtration through a fine-fritted funnel. Concentrated HNO_3 (3-5 drops) is added to the filtrate to promote crystallization of the bis-aquo complex. The white fluffy product formed is then filtered and washed with cold H_2O. In the specific preparation of $[Rh(DPB)_2(H_2O)_2]Cl_3$, 0.3 mmoles of $[Rh(DPB)_2Cl_2]Cl$ is dissolved in 10 ml of DMF, to which is added 1.5 mmoles of Ag_2O suspended in 20 ml

of H_2O. After 24 hrs of reaction in the dark, the mixture is rotovapped to dryness and the product extracted by the addition of 10 ml of isopropanol. Addition of a few drops of concentrated nitric acid promotes the formation of the white fluffy $[Rh(DPB)_2(H_2O)_2](NO_3)_3$ complex.

Method 2. (NaOH method):

This method has been exclusively used for the preparation of $[Rh(DPB)_2Cl_2]Cl$. A small amount of hydrazine hydrochloride catalyst (8 mg) is added to a solution of $[Rh(DPB)_2Cl_2]Cl$ (0.1 mmoles) suspended in 20 ml of H_2O. A concentrated 2 M solution of NaOH (0.5 mmoles) is added very slowly to the suspension and the reaction mixture boiled at 90° C for about 1 hr. The alkaline solution is then cooled and neutralized with concentrated nitric acid, which promotes precipitation of a milky yellow precipitate. This precipitate has not been isolated and characterized; however, it is used *in situ* to prepare the final product $[Rh(DPB)_2(phi)]Cl_3$. This is done by dissolving the bis-aquo complex in 10 ml of DMF and 5 ml of isopropanol, thoroughly degassing the mixture, and then using this for the next step of the reaction.

Step 3.: Preparation of $[Rh(X)_2(phi)]Cl_3$ complexes:

Solutions of the $[Rh(X)_2(H_2O)_2](NO_3)_3$ (0.1 mmole) and 9,10-diaminophenanthrene or DAP (0.12 mmoles) in 5 ml of H_2O and 5 ml of ethanol, respectively, are thoroughly purged to remove dissolved dioxgyen. Using syringe techniques, the rhodium solution is carefully transferred to the DAP solution and the reaction mixture refluxed at 65° C for 24 hrs, in an inert atmosphere. The solution initially looks milky, but upon reaction acquires a dark orange coloration. The reaction mixture is then air-oxidized for 12 hrs, rotovapped to dryness, and the product extracted into H_2O. Using a separatory funnel, impurities in the water solution are removed by extraction into chloroform and ether. The crude product contained in the water solution is then purified by cation-exchange chromotography, using CM-C25 or SP-C25 resin,

using solutions containing NaCl as the eluent. Thus the chloride salt of the product is obtained.

Synthesis and purification of [Rh(DPB)$_2$(phi)]Cl$_3$.

In the preparation of [Rh(DPB)$_2$(phi)]Cl$_3$, 0.1 mmoles of [Rh(DPB)$_2$(H$_2$O)$_2$]Cl$_3$ is dissolved in a 50/50 mixture of 4 ml of ethanol/water. This solution is thoroughly degassed and transferred to a 5 ml degassed ethanolic solution containing 0.12 mmoles of DAP. The reaction mixture is then heated at 65^o C for 24 hrs, after which the deep red solution is opened to air. Oxidation causes the solution to slowly turn milky orange, with precipitation of a brown orange solid. The milky suspension was then redissolved by the addition of ethanol, and the solution oxidized for 24 hrs. The reaction mixture was then purified by silica column chromatography. A mixture of 60% ethyl acetate/40% ethanol worked best to elute pure product off the silica column.

3.2.5. Characterization of [Rh(X)$_2$(phi)]Cl$_3$ complexes:

The NMR and Mass-spectral data and elemental analyses of [Rh(bpy)$_2$(phi)]Cl$_3$, [Rh(4,4'-diphenylbpy)$_2$(phi)]Cl$_3$, [Rh(5,5'-dimethylbpy)$_2$(phi)]Cl$_3$ and [Rh(4,4'-diamidobpy)$_2$(phi)]Cl$_3$ (Figure 3.2) and their precursors is presented below. Since the syntheses of the precursor complexes [Rh(bpy)$_2$Cl$_2$]Cl and [Rh(bpy)$_2$(H$_2$O)$_2$]Cl$_3$ have been reported in the literature[8], their characterization data is not presented here. In each case, while the NMR data cannot provide unambiguous assignments of the resonances, it sufficiently provides evidence for the identity and purity of the [Rh(phi)]$^{3+}$ complexes. The identity of the complexes is further supported by mass-spectral and elemental analyses. The extinction coefficients for each [Rh(phi)X$_2$]$^{3+}$ complex are obtained at their isosbestic point (λ = 362 nm) using atomic absorption spectroscopy. UV-visible and NMR spectral data are presented in Appendix I and II, respectively, of this chapter.

[Rh(phi)(bpy)$_2$]Cl$_3$: NMR shifts are in ppm (D_2O): 7.55 (t, 2H), 7.6 (t, 2H), 7.7 (d, 2H), 7.75 (2 overlapping triplets, 4H), 8.25 (2 overlapping triplets, 4H), 8.35 (t, 2H), 8.5 (t, 2H), 8.55 (d, 2H), 8.65 (d, 2H), 8.72 (d, 2H). As expected, the NMR spectrum shows four triplets and four doublets corresponding to the bipyridyl ligands and two triplets and two doublets for the phi ligand. UV-visible spectra show maxima at 358 nm, 313 nm, and 301 nm. FAB Mass spec ion mass: 609, [Rh(bpy)$_2$phi - 2H]$^+$; 465, [Rh(bpy)(phi)]$^+$; 415, [Rh(bpy)$_2$]$^+$; 259, [Rh(bpy)]$^+$. Elemental analysis calculated for [Rh(bpy)$_2$phi]Cl$_3$.12H$_2$O C: 46.3 (found:45.81), H: 3.70 (3.71), N: 9.7 (9.20). Extinction coefficient (ε) at λ = 362 nm is 19400 $M^{-1}cm^{-1}$.

[Rh(5,5'-dimethylbpy)$_2$Cl$_2$]Cl : The 5,5'-dimethylbpy ligand was a gift from T. Morii and was prepared according to a literature procedure[9]. NMR shifts in ppm (D_2O): 7.40 (s, 2H), 7.9 (d, 2H), 8.2 (d, 2H), 8.38 (d, 2H), 8.48 (d, 2H), 9.52 (s, 2H), 2 methyl resonances at 2.10 (s, 6H), 2.55 (s, 6H). The NMR spectrum shows well separated resonances corresponding to four doublets and two singlets from the aromatic protons of the 5,5'-dimethylbpy ligands and two aliphatic singlets corresponding to the two methyl resonances.

[Rh(5,5'-dimethylbpy)$_2$(H$_2$O)$_2$]Cl$_3$: NMR shifts in ppm (D_2O): 7.37 (s, 2H), 7.95 (d, 2H), 8.12 (d, 2H), 8.40 (d, 2H), 8.47 (d, 2H), 9.38 (s, 2H), 2 methyl resonances at 2.10 (s, 6H) and 2.30 (s, 6H). The NMR spectrum has the same resonance splitting pattern as compared to the chloride complex; however, all the peaks are relatively shifted. The observed ratio of integrals for the aromatic to methyl protons is 1.08:1, as compared to an expected value of 1:1.

[Rh(5,5'-dimethylbpy)$_2$(phi)]Cl$_3$: NMR shifts in ppm (D_2O): The spectrum is sensitive to pH; addition of fumes of triflouroacetic acid sharpens the spectrum and improves the peak resolution. The splitting pattern in a TFA treated NMR sample is: 2.0 (s, 2H), 2.15 (s, 2H), 7.15 (s, 2H) , 7.32 (t, 2H), 7.62 (t, 2H), 7.95 (d, 2H), 8.05 (t, 6H= 3 overlapping doublets), 8.29 (d, 2H), 8.31 (d, 2H). UV-visible spectra show maxima at 360 nm, 320 nm, 314 nm. FAB Mass Spec ion mass: 675, [Rh(DMB)$_2$phi - 2H]$^+$; 493, [Rh(DMB)(phi)]$^+$; 287, [Rh(DMB)]$^+$; 471, [Rh(DMB)$_2$]$^+$. Elemental analysis calculated for [Rh(5,5'-dimethylbpy)$_2$phi]Cl$_3$.12H$_2$O C: 48.98 (48.5), H: 4.64 (4.22), N: 9.78 (8.89). Extinction coefficient (ε) at λ = 362 nm is 21000 $M^{-1}cm^{-1}$.

[Rh(4,4'-diamidobpy)$_2$Cl$_2$]Cl : NMR shifts in ppm (D_2O): 7.65 (d, 2H), 7.75 (d, 2H), 8.25 (d, 2H), 8.85 (s, 2H), 8.95 (d, 2H), 9.80 (d, 2H). The NMR spectrum clearly shows two singlets and four doublets corresponding to the 4,4'-diamidobpy ligands.

[Rh(4,4'-diamidobpy)$_2$(H$_2$O)$_2$]Cl$_3$: NMR shifts in ppm (D_2O): 7.76 (m, 2H); 7.80 (d, 2H); 8.41 (dd, 2H); 8.93 (s, 2H); 9.1 (s, 2H); 9.34 (d, 2H). The NMR spectrum shows two singlets, three doublets and one multiplet which are shifted with respect to the precursor bis-chloride complex.

[Rh(4,4'-diamidobpy)$_2$(phi)]Cl$_3$: NMR shifts in ppm (D_2O): 7.38 (t, 2H), 7.7 (t, 2H), 7.8 (d, 2H), 7.85 (d, 2H), 8.1 (3 overlapping doublets, 6H), 8.65 (d, 2H), 9.00 (s, 2H), 9.05 (s, 2H). As expected, the spectrum shows two singlets and four doublets corresponding to the DAB ligand and two triplets and two doublets corresponding to the phi ligand. UV-visible spectrum shows maxima at 354 nm, 325 nm, 316 nm. FAB Mass Spec ion mass: 792, [Rh(DAB)$_2$phi - H]$^+$; 552, [Rh(DAB)phi]; 345, [Rh(DAB)]$^+$; 588, [Rh(DAB)$_2$]$^+$. Elemental analysis calculated for [Rh(DAB)$_2$phi](NO$_3$)$_3$.6H$_2$O C:43.2

(found: 45.4), H: 3.4 (3.8), N: 13.2 (14.1). Extinction coefficient (ε) at λ = 362 nm is 18000 $M^{-1}cm^{-1}$.

[Rh(4,4'-diphenylbpy)$_2$Cl$_2$]Cl : NMR shifts in ppm (d-MeOH): 7.48 (m), 7.58 (m), 7.72 (two doublets), 7.80 (d), 7.85 (m), 8.10 (dd), 8.32 (dd), 9.12 (d), 9.22 (d), 9.82(d).

[Rh(4,4'-diphenylbpy)$_2$(H$_2$O)$_2$]Cl$_3$: NMR shifts in ppm (d-MeOH): 7.50 (m), 7.62 (m), 7.82 (m), 7.9 (m), 8.18 (dd), 8.52 (dd), 9.28 (m), 9.42 (d).

Rh(4,4'-diphenylbpy)$_2$(phi)]Cl$_3$: NMR shifts in ppm (d-MeOH): 7.65 (m), 7.88 (t), 7.95 (d), 8.05 (m), 8.15 (m), 8.25 (dd), 8.45 (d), 8.62 (dd), 8.75 (dd), 9.4 (d), 9.45 (d). The NMR spectral resonances in D_2O are relatively more spread out, which makes the spectrum more assignable. The resonances observed in D_2O are: 7.43 (t, 2H), 7.5 (m, 12 H), 7.7 (t, 2H), 7.72 (d, 2H), 7.8 (m, 6H), 7.85 (m, 4H), 8.02 (d, 2H), 8.16 (d, 4H), 8.45 (d, 2H), 8.92 (s, 2H), 8.98 (s, 2H), and the integrations correspond well with the expected values. UV-visible spectrum shows maximum at 272 nm. FAB Mass Spec ion mass: 925, [Rh(DPB)$_2$phi]$^+$; 717, [Rh(DPB)$_2$]$^+$; 617, [Rh(DPB)(phi)]$^+$. Elemental analysis calculated for [Rh(4,4'-diphenylbpy)$_2$phi]Cl$_3$ C: 59.7 (58.7), H: 4.0 (3.28), N: 7.20 (6.98). Extinction coefficient (ε) at λ= 362 nm is 47000 $M^{-1}cm^{-1}$.

3.3. Discussion

Synthetic Methodology:

The preparation of derivatives of [Rh(phen)$_2$phi]$^{3+}$ and [Rh(phi)$_2$bpy]$^{3+}$ required alterations in previously reported syntheses. The previously reported procedure[2] involved using catalytic amounts of hydrazine to promote direct addition of bipyridyl to [Rh(phi)$_2$Cl$_2$]$^+$ to form [Rh(phi)$_2$bpy]$^{3+}$. However, this route was avoided due to low

product yields (~ 10%) and major side product formation. Instead, standard Ag(triflate) methodology[4] was used to displace the chloride ligands with more labile water ligands to form the bis-aquo complex $[Rh(phi)_2(H_2O)_2]^{3+}$. Subsequent addition of the functionalized phenanthroline ligand to the bis-aquo intermediate yielded the desired $[Rh(phi)_2Y]^{3+}$ complex in 70% yield. Thus, this method provides a more general route for the preparation of $[Rh(phi)_2Y]^{3+}$ complexes.

Several studies[10] have suggested the use of two electron reducing agents such as hydrazine, sodium borohydride, and ethanol in substitution reactions involving bis polypyridyl complexes of Rh(III). This is based on the theory that inert Rh(III) must be reduced to the more labile Rh(II) or Rh(I) center for ligand exchange to occur. However, other studies have shown that replacement of Rh-Cl bonds with Rh-OH_2 bonds makes Rh labile to substitution[11]. Similarly, the synthetic studies reported here show that $[Rh(phi)_2Cl_2]^+$ may be readily converted to the $[Rh(phi)_2(H_2O)_2]^{3+}$ complex, which is labile towards ligand substitution. Moreover, the previously reported synthesis[2] of $[Rh(phen)_2(phi)]^{3+}$ and the syntheses of $[Rh(X_2)phi]^{3+}$ (X= bpy derivative) type of complexes reported here also require formation of the labile $[Rh(X)_2(H_2O)_2]^{3+}$ precursor complex. Therefore, it is likely that much of the inertness associated with $[Rh(phi)_2Cl_2]^+$, $[Rh(phen)_2Cl_2]^+$, and $[Rh(bpy)_2Cl_2]^+$ may not be due to the nature of the Rh(III) oxidation state, but rather the strength of the Rh-Cl bonds.

In most of the syntheses described in this chapter, Ag_2O and $Ag(CF_3SO_2O)$ are used in the preparation of the more labile $[Rh(X)_2(H_2O)_2]^{3+}$ (X = phi, phen, bpy) from the inert $[Rh(X)_2Cl_2]^+$ complexes. This aquation reaction is driven by the formation of insoluble and stable AgCl, by displacement of the inner sphere chloride ligands from $[Rh(X)_2Cl_2]^+$. However, this strategy does not work well reproducibly in the synthesis of $[Rh(4,4'\text{-diphenylbpy})_2(phi)]^{3+}$. The preparation of $[Rh(4,4'\text{-diphenylbpy})_2(H_2O)_2]^{3+}$ from $[Rh(4,4'\text{-diphenylbpy})_2Cl_2]^+$ was more readily accomplished by base hydrolysis[8].

Boiling $[Rh(4,4'\text{-diphenylbpy})_2Cl_2]^+$ with sodium hydroxide for 30 min, followed by the in situ addition of 9,10-diaminophenanthrene and subsequent oxidation, resulted in the formation of $[Rh(4,4'\text{-diphenylbpy})_2phi]^{3+}$ in 30% yield. It is likely that the sterically hindered $[Rh(4,4'\text{-diphenylbpy})_2Cl_2]^+$ complex is more inert to substitution as compared to the other derivatives.

Spectroscopic characterization of the rhodium(III) complexes:

UV-visible, NMR, and Mass spectroscopy has been successful in unambiguously determining the identity and purity of the rhodium(III)-phi complexes reported. The UV-visible spectra (Appendix I) of the $[Rh(phi)_2Y]^{3+}$ series of complexes were affected only slightly by functionalization of the Y ligand. However, the band centered at 307 nm in $[Rh(bpy)_2phi]^{3+}$ red-shifted to approximately 318 nm in the spectra of the $[Rh(X)_2phi]^{3+}$ derivatives (where X = functionalized bipyridyl).

Both the UV-visible and NMR spectra of all the rhodium(III)-phi complexes are sensitive to the state of protonation of the imines in the phi ligand, and therefore to the pH of the solutions. However, all the derivatives behaved similarly to $[Rh(phen)_2phi]^{3+}$ and $[Rh(phi)_2bpy]^{3+}$ with respect to their pH dependencies and pK_a values. UV-visible pH titrations of the derivatives indicated pK_a values of approximately 6.5, as previously reported[5]. The extinction coefficients (ε) for each $[Rh(phi)_2Y]^{3+}$ complex were obtained for their phi-centered isosbestic points at λ = 350 nm, and for each $[Rh(phi)X_2]^{3+}$ complex for their phi-centered isosbestic points at λ = 362 nm. The ε values obtained for the $[Rh(phi)]^{3+}$ complexes (except for the complexes with 4,4'-diphenylbpy ligands), are similar to those obtained for the previously studied $[Rh(phen)_2phi]^{3+}$ (ε_{362} = 19400) and $[Rh(phi)_2bpy]^{3+}$ (ε_{350} = 23600) complexes. The complexes $[Rh(4,4'\text{-diphenylbpy})_2phi]^{3+}$ and $[Rh(phi)_2(4,4'\text{-diphenylbpy})]^{3+}$ have extinction coefficients of 47000 at λ = 362 nm and λ= 350 nm, respectively, values which are approximately twice that obtained for the other phi complexes. This is consistent with their UV-visible spectra

(Appendix I), which show overlap of the 4,4'-diphenylbpy and phi absorbances in the 350 - 360 nm region. Interestingly, the resolution of the NMR spectra of the complexes (Appendix II) was greatly enhanced upon acidification with trifluoroacetic acid; this ensured that most of the molecules in the NMR sample were in the same state of complete protonation,with respect to their imine nitrogens. While complete NMR resonance assignments of the complexes was not possible from 1D-NMR data, the position, multiplicity and integral value of the resonances provided strong evidence for their identity. Furthermore, FAB Mass spectral and elemental analyses provided further evidence for the identity and purity, respectively, of the $[Rh(phi)]^{3+}$ complexes.

References

1. (a) Pyle, A. M.; Rehmann, J. P.; Meshoyrer, R.; Kumar, C. V.; Turro, N. J.; Barton, J. K. *J. Am. Chem. Soc.*, **1989**, 111, 3051. (b) Pyle, A. M.; Chiang, M. Y.; Barton, J. K. *Biochemistry*, **1992**, 29, 4487.
2. David, S. S. and Barton, J. K. *J. Am. Chem. Soc.*, **1993**, 115, 2984.
3. (a) Pyle, A. M.; Long, E. C.; Barton, J. K. *J. Am. Chem. Soc.*, **1989**, 111, 4520. (b) Pyle, A. M.; Morii, T.; Barton, J. K. *J. Am. Chem. Soc.*, **1990**, 112, 9432.
4. Howells, R. D. and McCown, J. D. *Chem. Rev.*, **1977**, 77, 69.
5. Pyle, A. M., PhD thesis, Columbia University, New York, **1989**.
6. Chandler et al. *J. Het. Chem.*, **1981**, 18, 599.
7. (a) McKenzie, E. D.; Plowman, R. A. *J. Inorg. Nucl. Chem.*, **1970**, 32, 199. (b) Kulasingman, G. C.; McWhinnie, W. R.; Miller, J. D. *Inorg. Phys. Theor.* **1969**, 521.
8. Gideney, P. M.; Gillard, R. D.; Heaton, B. T. *J. C. S. Dalton*, **1972**, 2621.
9. Badger, G. H. and Sasse, W. H. F. *J. Chem. Soc.* **1956**, 616.
10. Gillard, R. D. and Heaton, B. T. *Coord. Chem. Rev.* **1971**, 149.
11. (a) Saliby, M. J.; Kaplan, E. B.; Sheridan, P. S.; Madan, S. K. *Inorg. Chem.*, **1981**, 20, 728. (b) Lay, P. A. and Sargeson, A. M. *Inorg. Synthesis* **1986**, 24, 283.

Appendices

I. UV-visible spectra of $[Rh(phi)_2Y]^{3+}$ and $[Rh(phi)X_2]^{3+}$ complexes.

II. NMR spectra of $[Rh(phi)_2Y]^{3+}$ and $[Rh(phi)X_2]^{3+}$ complexes and their synthetic intermediates.

Appendix I. UV-visible Spectra

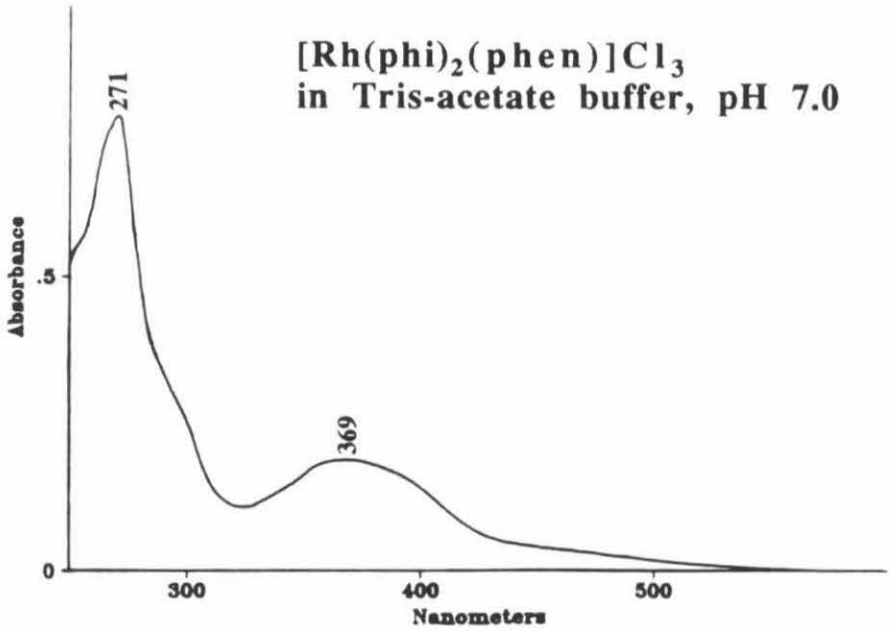

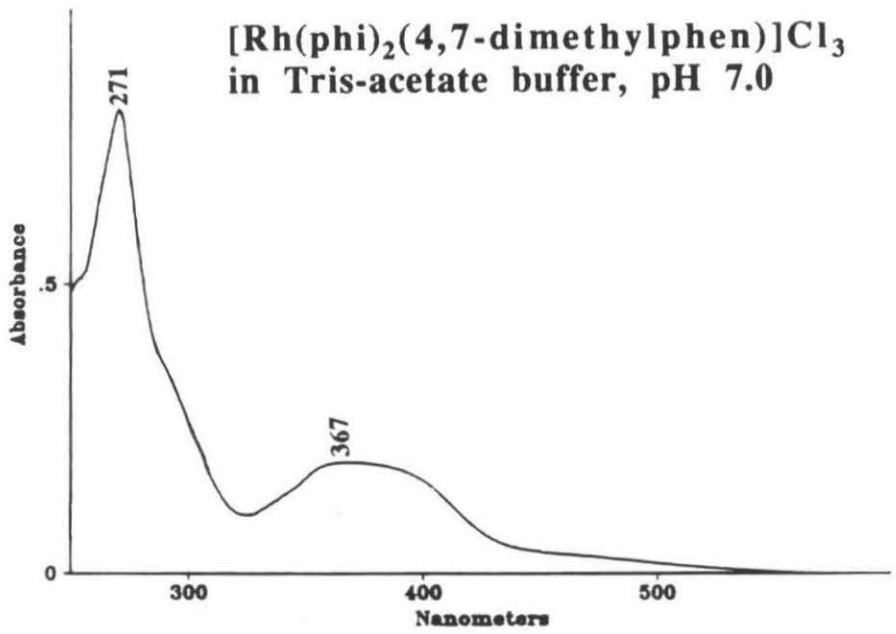

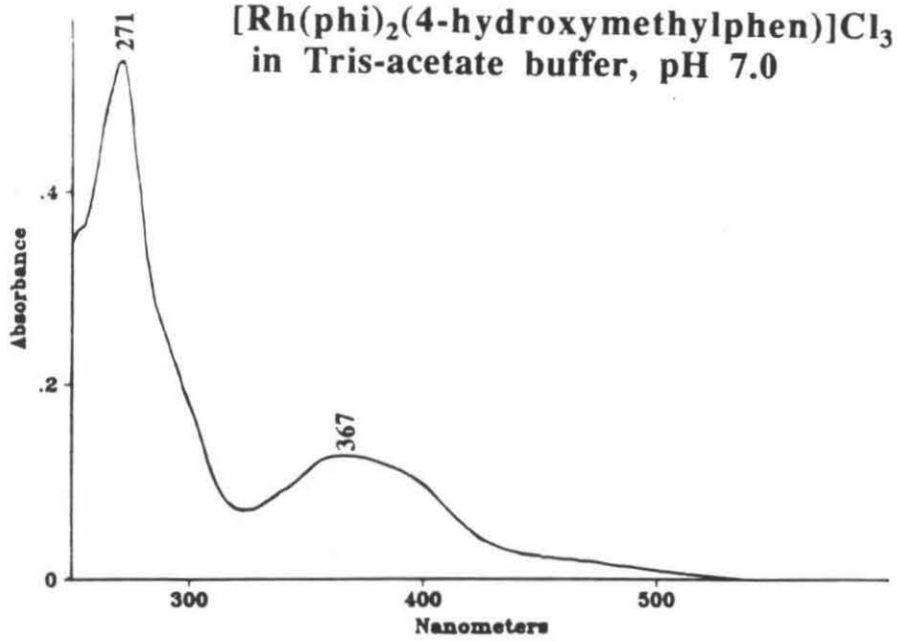
[Rh(phi)2(4-hydroxymethylphen)]Cl3
in Tris-acetate buffer, pH 7.0
271
367
.4
.2
0
Absorbance
300
400
500
Nanometers

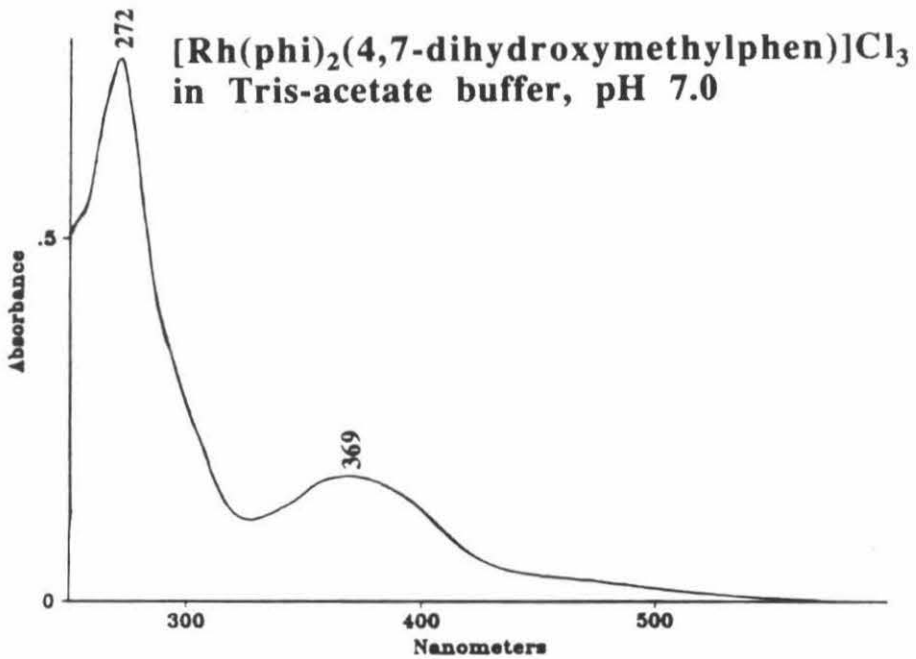
[Rh(phi)2(4,7-dihydroxymethylphen)]Cl3
in Tris-acetate buffer, pH 7.0
272
369
.5
0
Absorbance
300
400
500
Nanometers

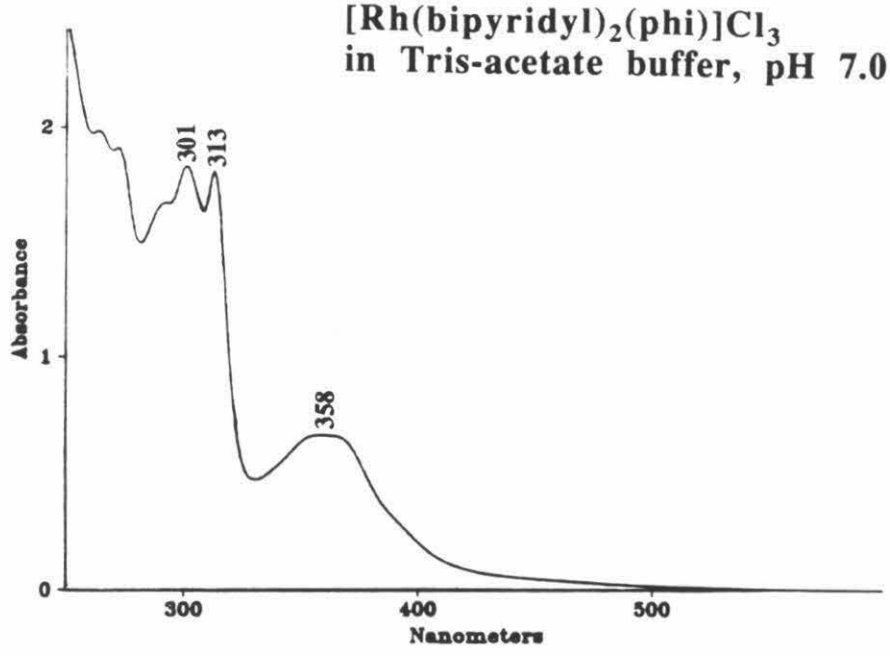
[Rh(bipyridyl)2(phi)]Cl3
in Tris-acetate buffer, pH 7.0
Absorbance
2
1
0
301
313
358
300
400
500
Nanometers

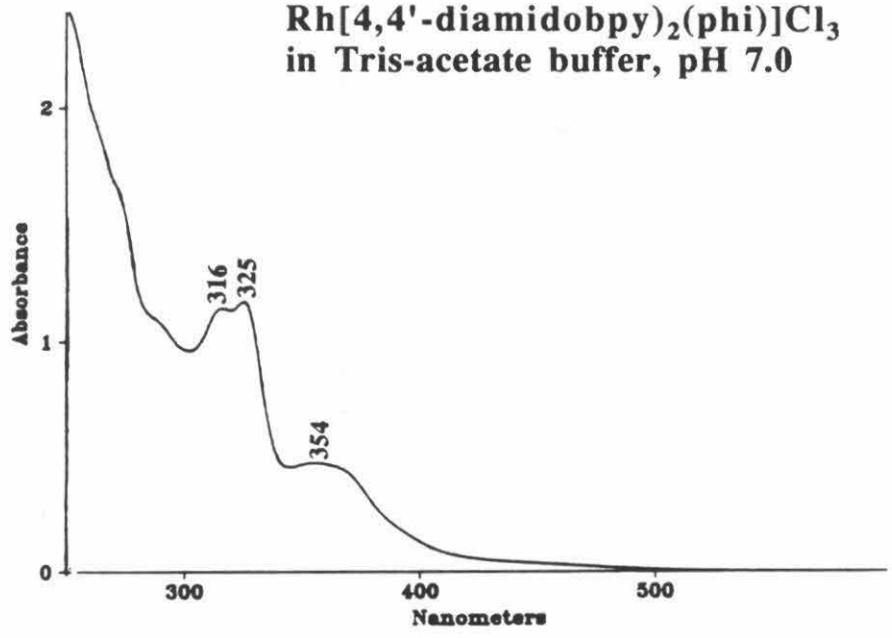
Rh[4,4'-diamidobpy)2(phi)]Cl3
in Tris-acetate buffer, pH 7.0
Absorbance
2
1
0
316
325
354
300
400
500
Nanometers

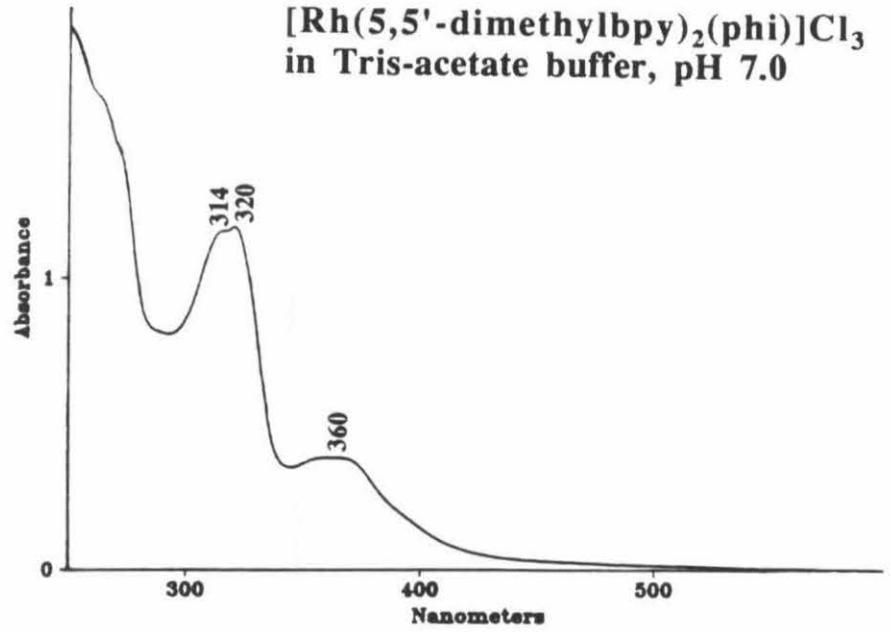
[Rh(5,5'-dimethylbpy)$_2$(phi)]Cl$_3$
in Tris-acetate buffer, pH 7.0
Absorbance
1
0
314
320
360
300
400
500
Nanometers

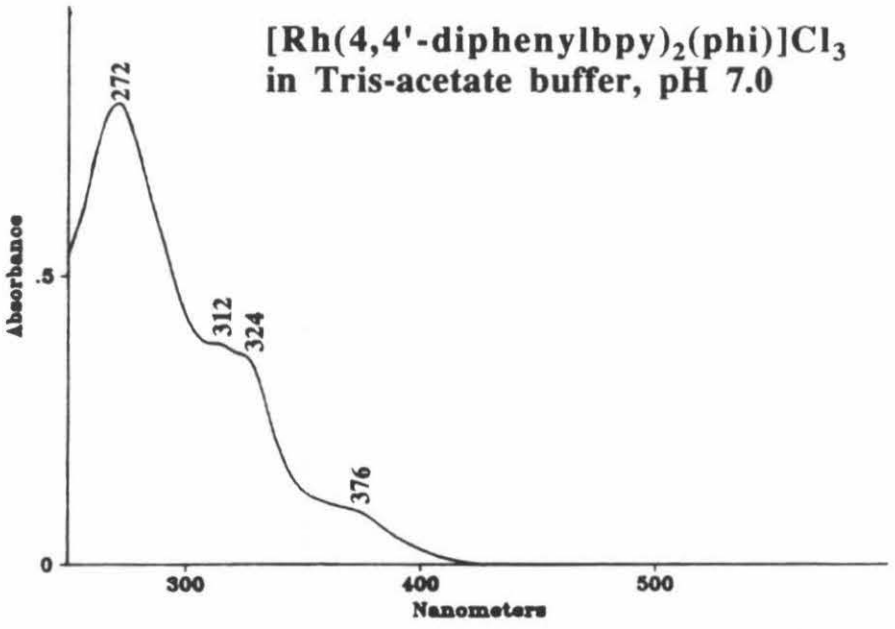
[Rh(4,4'-diphenylbpy)$_2$(phi)]Cl$_3$
in Tris-acetate buffer, pH 7.0
Absorbance
.5
0
272
312
324
376
300
400
500
Nanometers

Appendix II. NMR Spectra

$[Rh(phi)_2(4,7\text{-dimethylphen})]Cl_3$
CD_3OD, 400 MHz

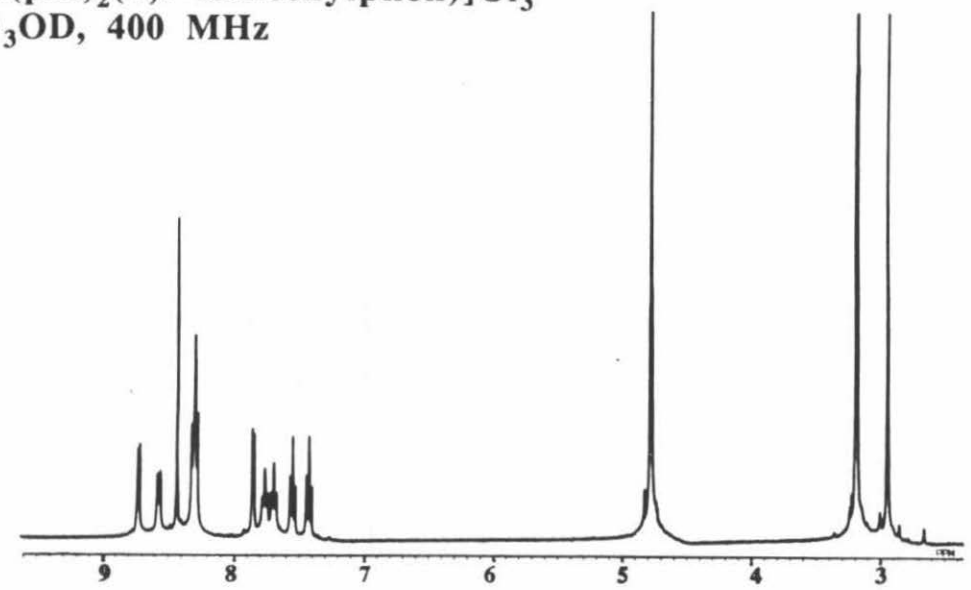

$[Rh(phi)_2(4\text{-hydroxymethylphen})]Cl_3$
CD_3OD, 400 MHz

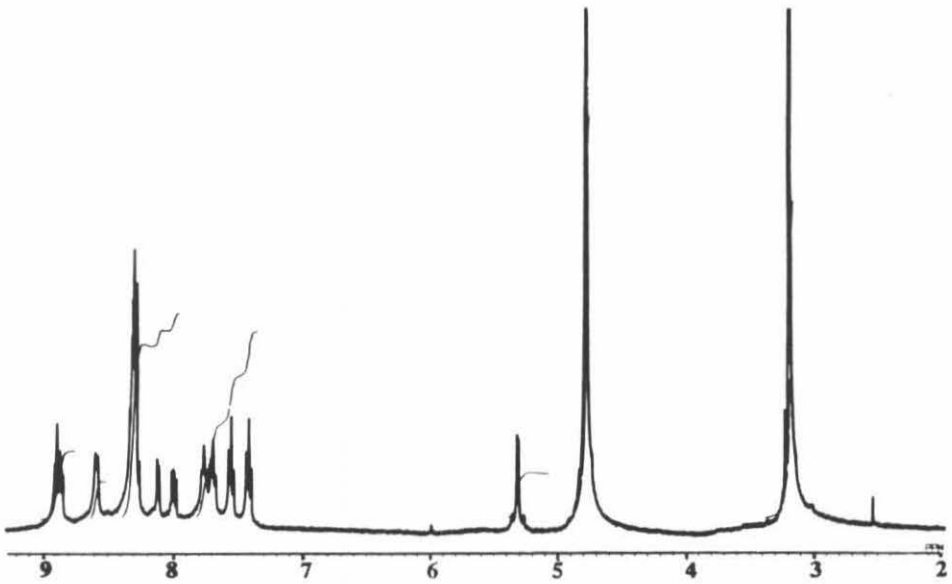

[Rh(phi)$_2$(4,7-dihydroxymethylphen)]Cl$_3$
CD$_3$OD, 400 MHz

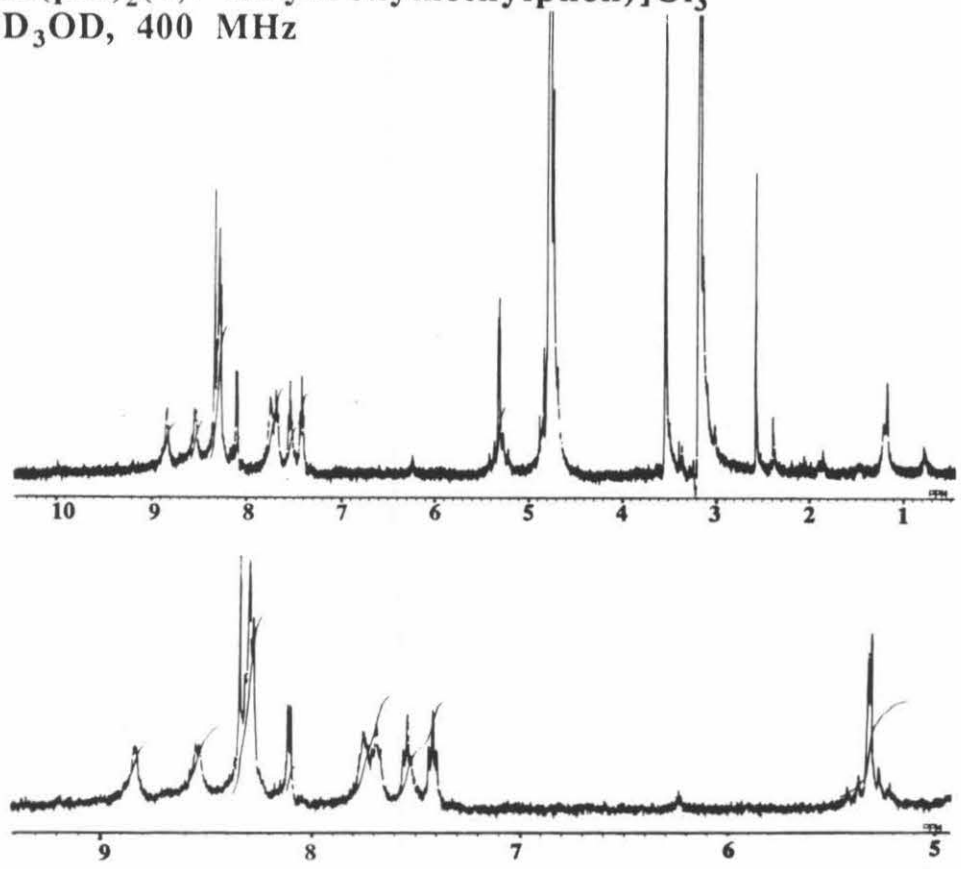

[Rh(phi)$_2$(4,7-dihydroxymethylphen)]Cl$_3$
D$_2$O, 400 MHz

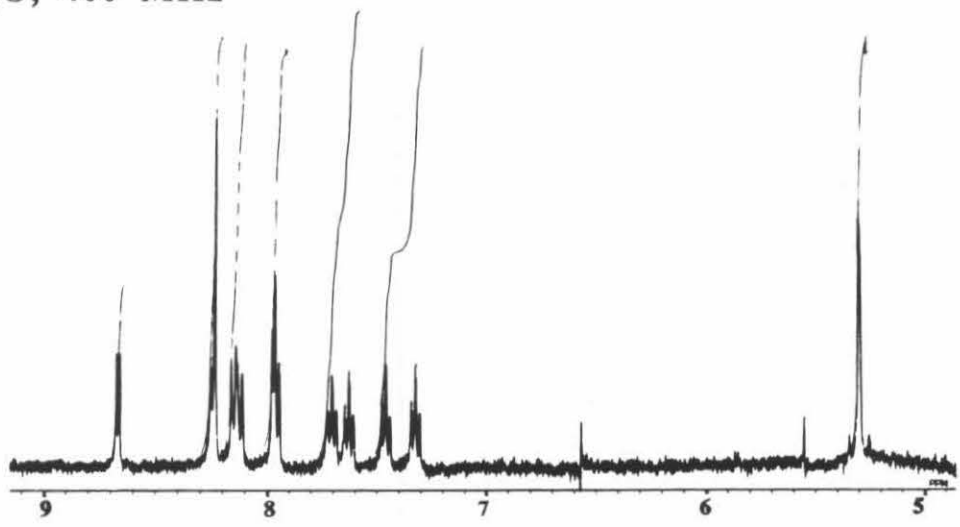

[Rh(5,5'-dimethylbpy)$_2$Cl$_2$]Cl
CD_3OD, 400 MHz

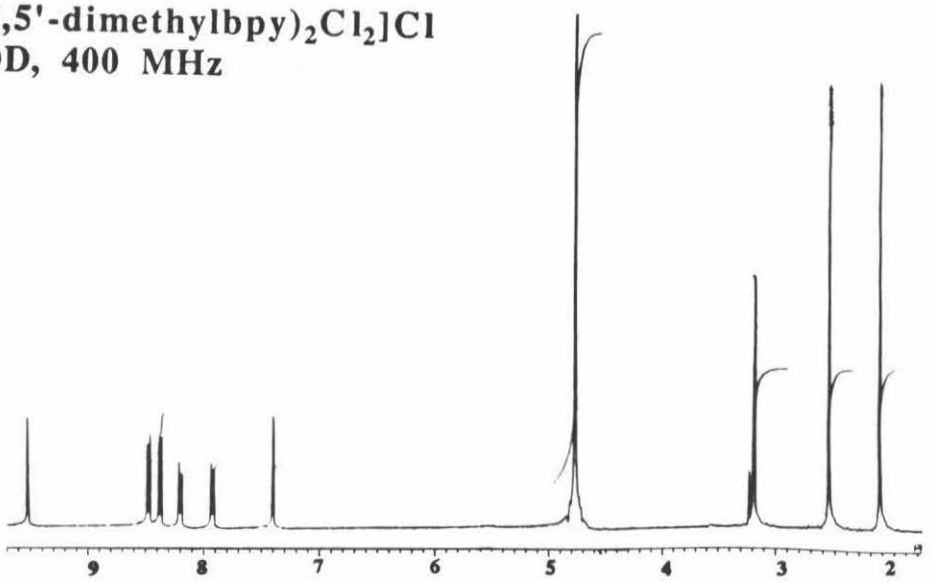

[Rh(5,5'-dimethylbpy)$_2$(H_2O)$_2$]Cl_3
CD_3OD, 400 MHz

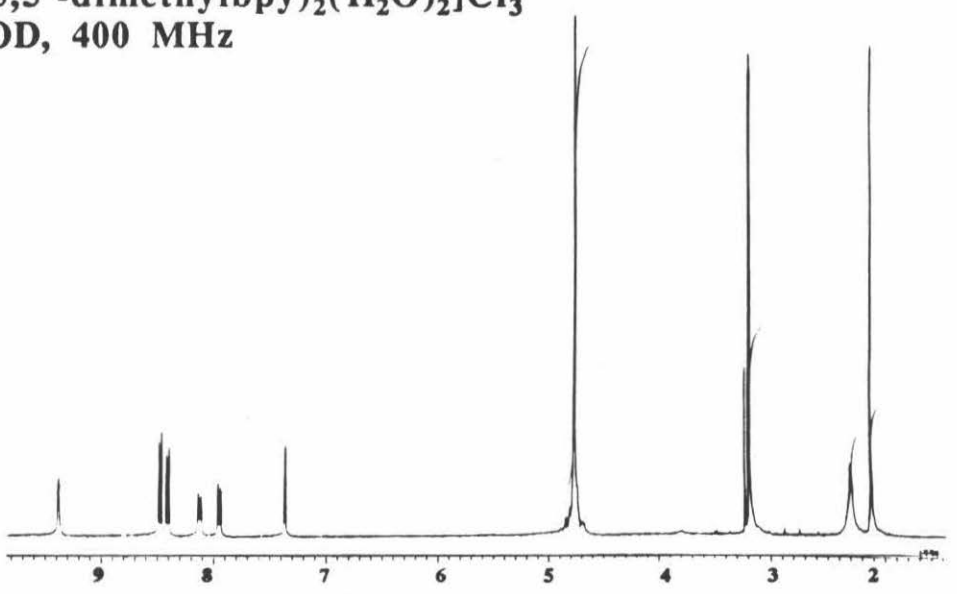

[Rh(5,5'-dimethylbpy)$_2$(phi)]Cl$_3$
D$_2$O, 400 MHz

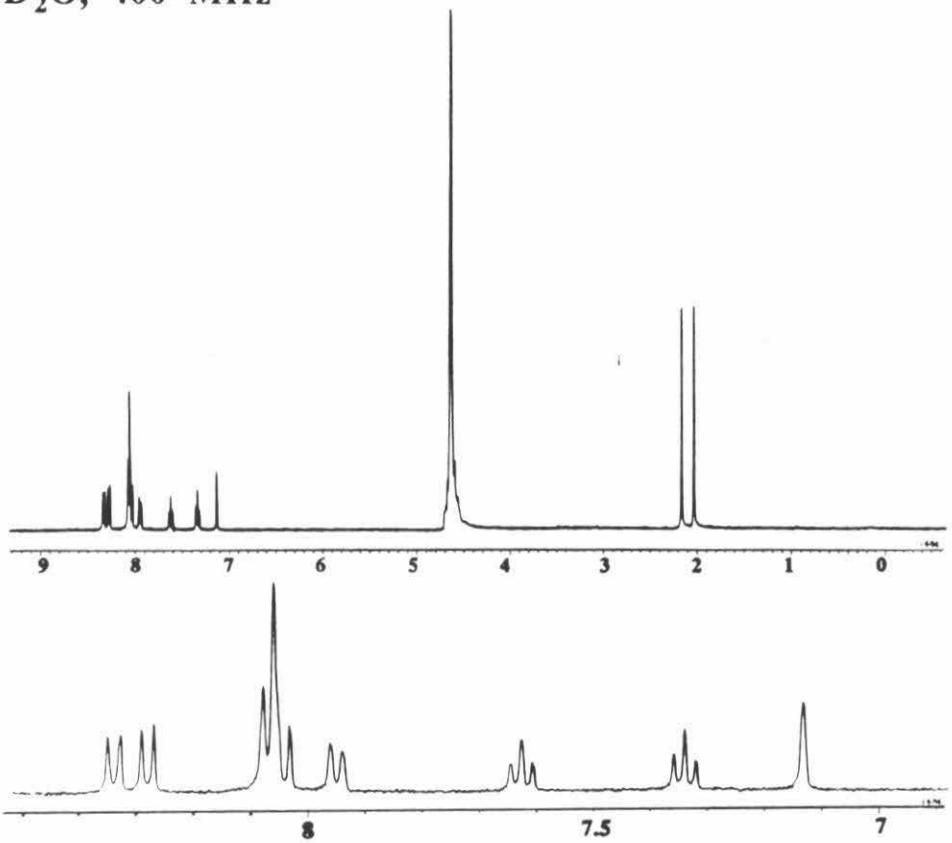

[Rh(bipyridyl)$_2$(phi)]Cl$_3$
D$_2$O, 300 MHz

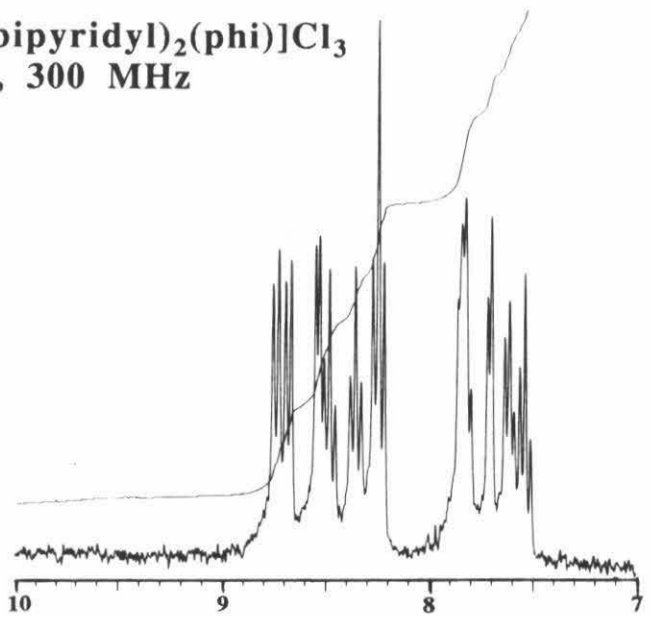

[Rh(4,4'-diamidobpy)$_2$Cl$_2$]Cl
D_2O, 400 MHz

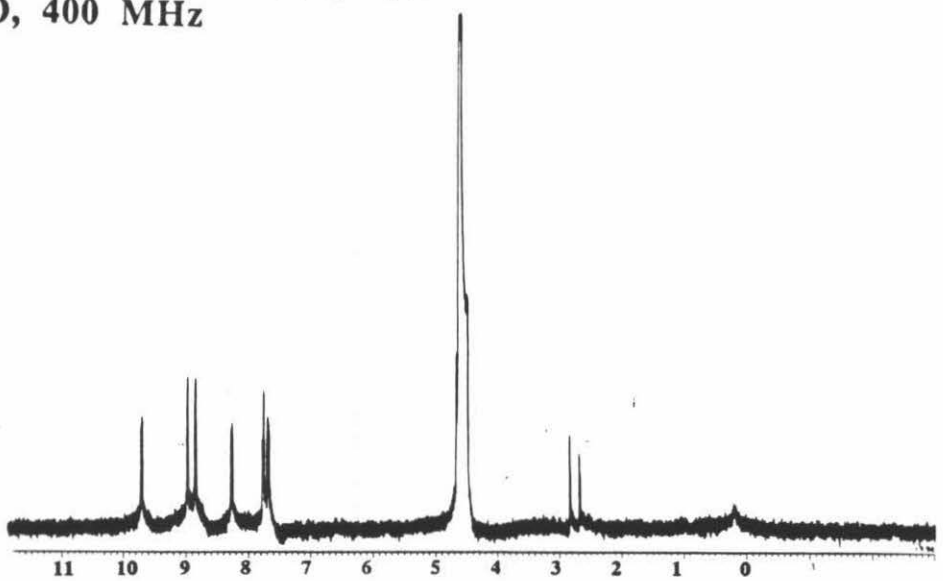

[Rh(4,4'-diamidobpy)$_2$(H_2O)$_2$]Cl$_3$
D_2O, 400 MHz

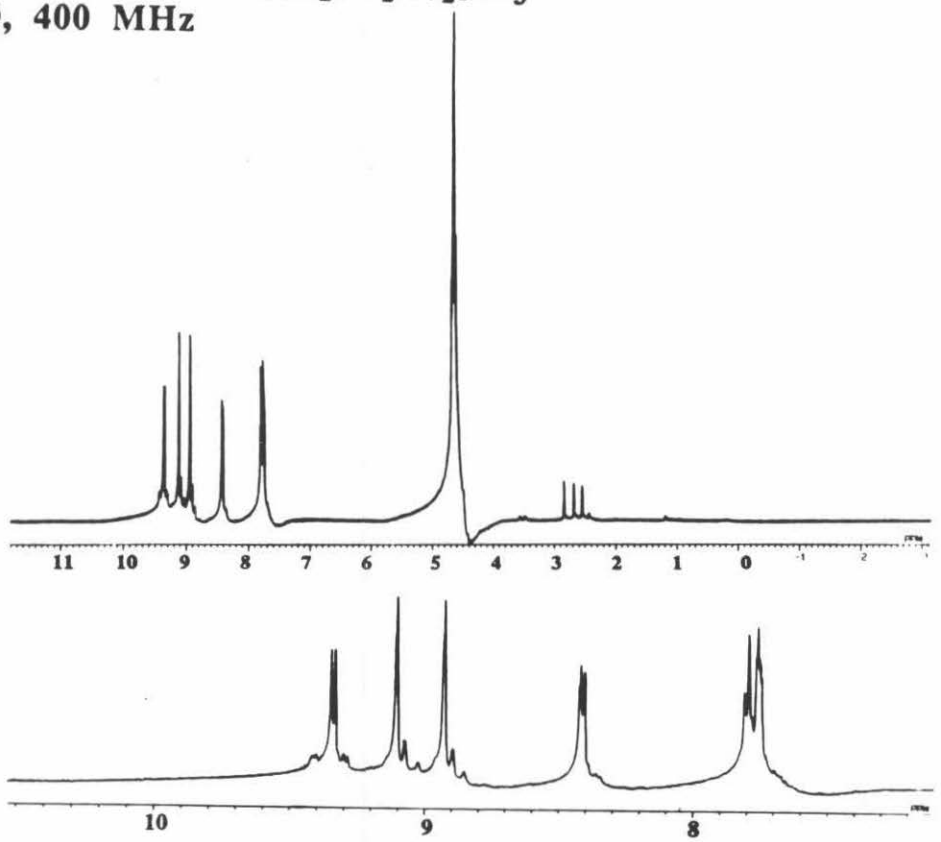

$[Rh(4,4'\text{-diamidobpy})_2(phi)]Cl_3$
D_2O, 400 MHz

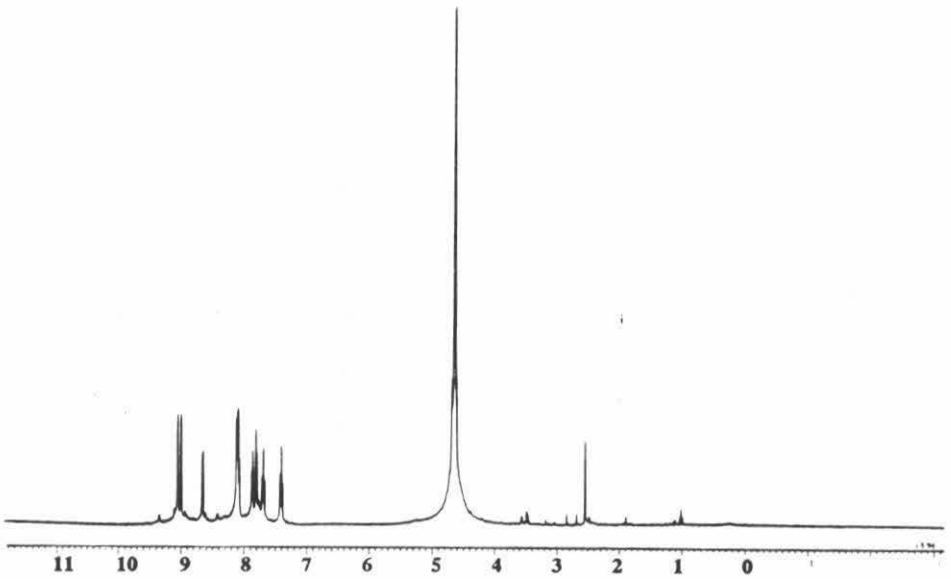

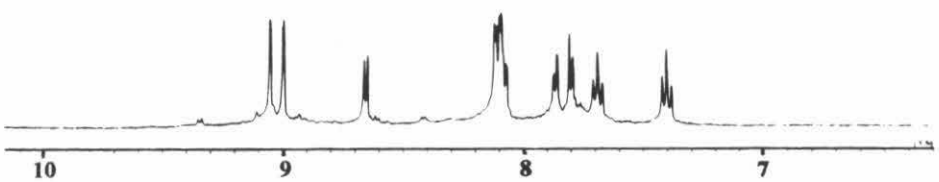

[Rh(4,4'-diphenylbpy)$_2$Cl$_2$]Cl
CD_3OD, 400 MHz

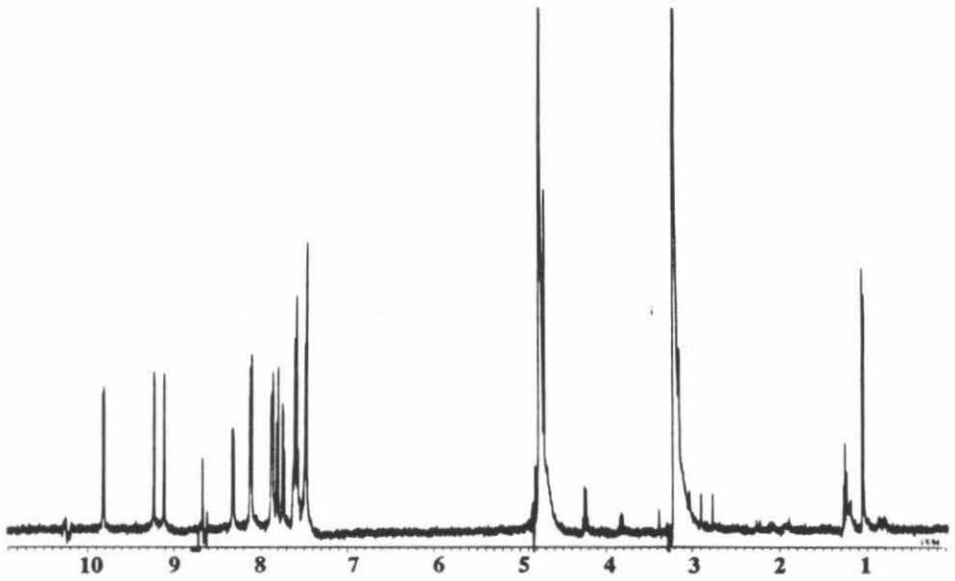

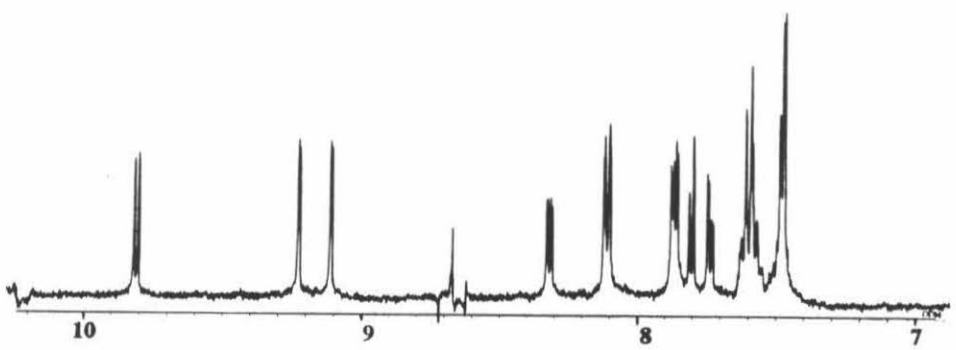

$[Rh(4,4'\text{-diphenylbpy})_2(H_2O)_2]Cl_3$
CD_3OD, 400 MHz

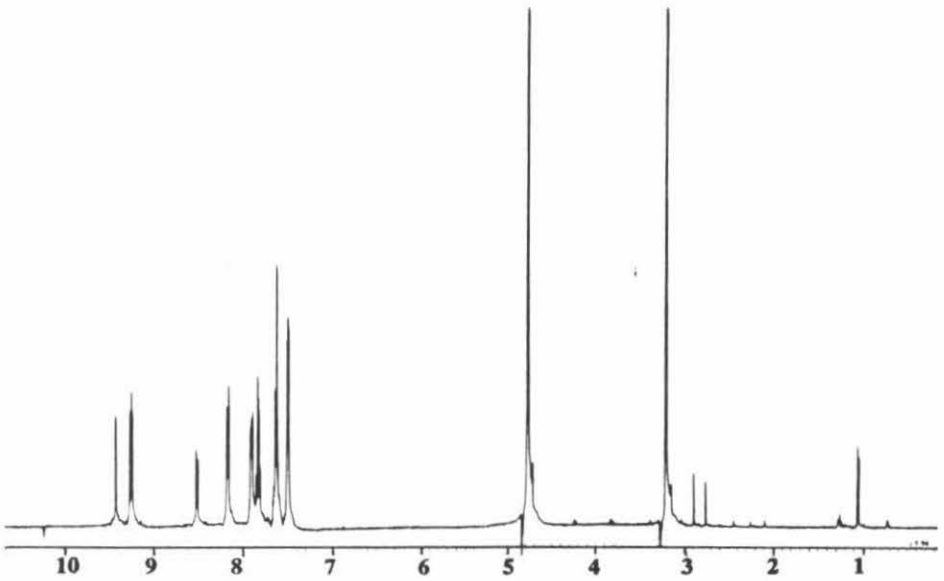

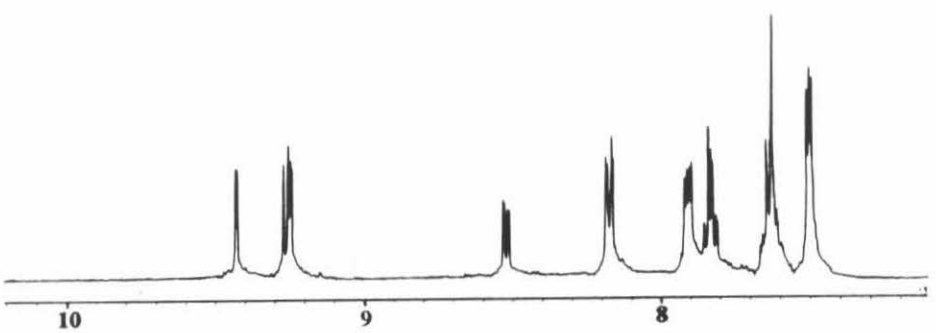

[Rh(4,4'-diphenylbpy)$_2$(phi)]Cl$_3$
D$_2$O, 400 MHz

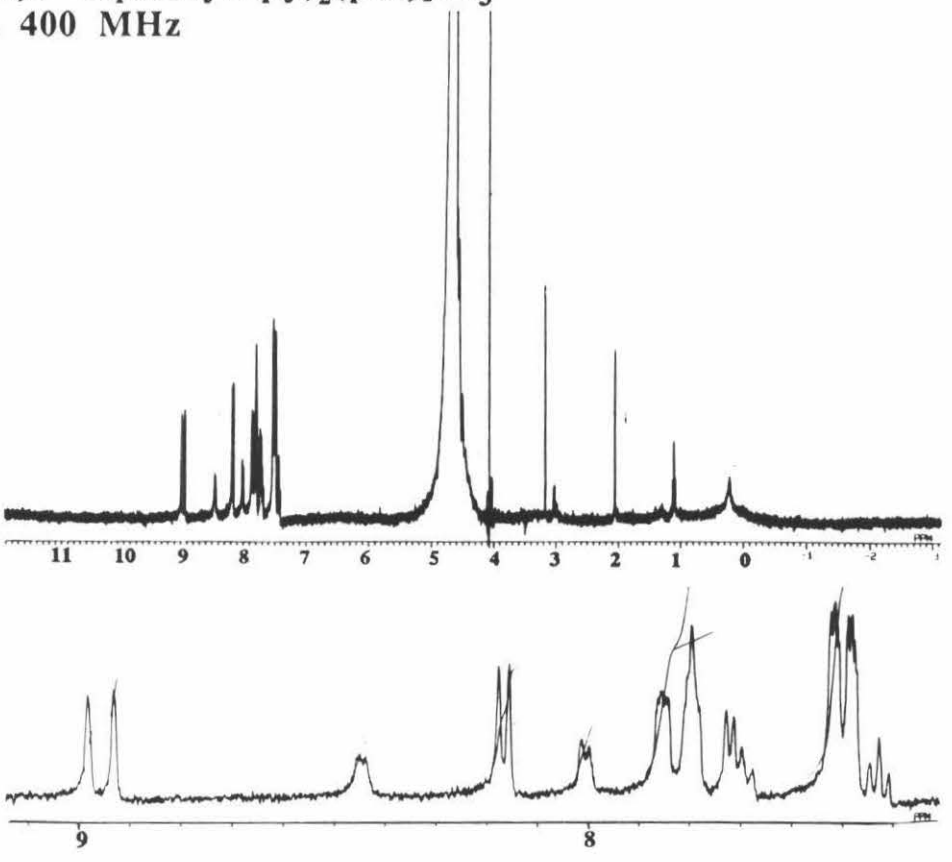

[Rh(4,4'-diphenylbpy)$_2$(phi)]Cl$_3$
CD$_3$OD, 300 MHz

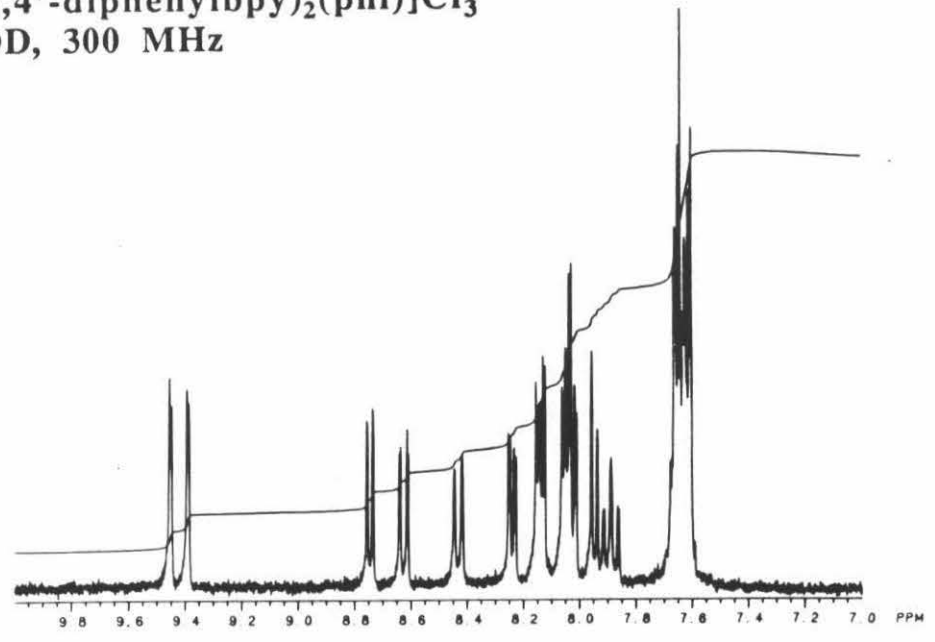

Chapter 4:

Sequence Specific Recognition of DNA by Phenanthrenequinone Diimine Complexes of Rhodium(III): Importance of Steric Interactions.§

4.1. Introduction

A central goal in understanding the recognition of nucleic acids by proteins (or small molecules) is to study the interactions that occur both in specific and non-specific protein-DNA complexes[1]. One approach to establishing the relative importance of particular contacts or groups in site-specific recognition of nucleic acids has been to build *de novo*, specific molecules from non-specific ones. Towards this goal, our laboratory has been interested in the design of transition metal complexes that bind site-specifically to nucleic acids. Unlike most small molecules and natural products which bind nucleic acids, transition metal complexes have well-defined shapes, as determined by their coordination geometries. Therefore, this provides us with a rigid scaffold on which to append moieties that may contribute to site-selective recognition of nucleic acids. A simple illustration of this strategy is the development[2-4] of nucleic acid binding octahedral metal complexes $[Ru(phen)_3]^{2+}$ and $[Ru(TMP)_3]^{2+}$ (phen = 1,10-phenanthroline; TMP = 3,4,7,8-tetramethylphenanthroline). The complementarity between B-form DNA and $[Ru(phen)_3]^{2+}$ is such that surface binding in the minor groove is favored by the Λ isomer and intercalative binding in the major groove is favored by the Δ isomer. In comparison, the TMP ligands of $[Ru(TMP)_3]^{2+}$ precludes both intercalation and surface binding of this complex to B-form DNA. Instead, the bulky and sterically hindered shape of $[Ru(TMP)_3]^{2+}$ allows a hydrophobic association between the Λ isomer of this complex and the shallow and wide minor groove of A-form helices. Thus, this

---

§ Adapted from Sitlani, A.; Pyle, A. M.; Barton, J. K. **1993,** manuscript to be submitted.

example illustrates that steric interactions can contribute significantly towards site-specific recognition of nucleic acids by metal complexes.

In addition to building metal complexes as probes that distinguish between *global* nucleic acid structures, it is also of interest to design transition metal complexes that recognize subtle variations in *local* sequence-dependent DNA structures. Towards this goal, our laboratory has recently reported[5] on the development of the complexes $[Rh(phen)_2phi]^{3+}$ and $[Rh(phi)_2bpy]^{3+}$ (phi = 9,10-phenanthrenequinone diimine), which recognize sequence-dependent DNA structure, also in a *shape-selective* manner. Both complexes bind in the DNA major groove[5d] through intercalation of their phi ligand[6], which allows them to associate intimately with the helix and sense the local structure at that site. However, these complexes display remarkably different DNA recognition characteristics from one another, based on subtle differences in their shapes[5a]. While $[Rh(phen)_2phi]^{3+}$ binds sequence-specifically to DNA, $[Rh(phi)_2bpy]^{3+}$ is relatively sequence-neutral in its recognition of DNA. Thus, to understand and explore the potential of $[Rh(phi)]^{3+}$ complexes as shape-selective probes of sequence-dependent DNA structure, we have attempted to alter their DNA recognition by introducing steric bulk at varying positions of their non-intercalating ligands.

This chapter describes in detail the DNA sequence-selectivities of a series of 9,10-phenanthrenequinone diimine (phi) complexes of rhodium(III) (Figure 4.1) to address the following questions. Firstly, can we alter the shape of a relatively sequence-neutral molecule like $[Rh(phi)_2bpy]^{3+}$ to make it more sequence-specific? Can the DNA photocleavage products produced by $[Rh(phi)_2]^{3+}$ complexes provide information about its DNA binding and recognition? Furthermore, by comparing the DNA recognition properties of both specific and non-specific metal complexes, can we learn more about sequence-specific recognition of DNA by small molecules and proteins? Here we illustrate that introducing hydrophobic groups in appropriate positions on the non-

intercalating bipyridyl ligands of the complexes $[Rh(bpy)_2phi]^{3+}$ and $[Rh(phi)_2bpy]^{3+}$ increases the steric requirements for phi intercalation and enhances the overall specificity of these complexes for local DNA structure. In comparison, hydrogen-bonding functionalities such as amido groups enhance the affinities, but not the specificities of $[Rh(phi)]^{3+}$ complexes for DNA. *Thus, the shapes of these complexes dominate their DNA recognition characteristics*. Furthermore, we describe here that an analysis of DNA photocleavage products provides supportive evidence for shape-selective recognition by $[Rh(phi)_2]^{3+}$ complexes. Importantly, this work also shows that steric and methyl-methyl van der Waals interactions may also be exploited on a more detailed level to significantly alter the chiral recognition of DNA by the Δ and Λ isomers of $[Rh(phi)]^{3+}$ complexes. Specifically, *negative* steric clashes can *increase* the overall DNA sequence-specificities of $[Rh(phi)]^{3+}$ complexes by allowing these complexes to bind to fewer number of DNA sequences. Furthermore, *positive* hydrophobic and van der Waals interactions can also *enhance* sequence recognition of $[Rh(phi)]^{3+}$ complexes by stabilizing their binding to specific sequences. Thus, these studies indicate that the shape-complementarity between metal complex and its cognate nucleic acid site is a crucial element in sequence-specific recognition of DNA, and it is likely that similar steric factors are significant in protein-nucleic acid recognition as well. Like most DNA-binding proteins, phi complexes of rhodium(III) also *bind in the major groove of DNA*; therefore, the study of sequence-specific recognition by these metal complexes may be viewed as a model to understand some aspects of protein-DNA interactions.

4.2. Experimental

Materials: Calf thymus DNA was purchased from Sigma, and plasmid pUC18 was purchased from Boeringer-Mannheim. Phosphoroamidites and solid supports for oligonucleotide synthesis were obtained from Pharmacia. All enzymes utilized were

Figure 4.1. Structures of $[Rh(bpy)_2phi]^{3+}$ (**1a**) and $[Rh(phi)_2bpy]^{3+}$ (**3a**). Bpy = 2,2'-bipyridine, phi = 9,10-phenanthrenequinone diimine. The complexes $[Rh(4,4'\text{-}R_2bpy)_2phi]^{3+}$ [R = phenyl (**1b**), amido(**1c**)], $[Rh(5,5'\text{-}Me_2bpy)_2phi]^{3+}$ (**1d**), $[Rh(phen)_2phi]^{3+}$ (**2**); and $[Rh(4,4'\text{-}R_2bpy)(phi)_2]^{3+}$ [R = phenyl (**3b**), amido (**3c**)], $[Rh(5,5'\text{-}Me_2bpy)(phi)_2]^{3+}$ (**3d**), and $[Rh(phen)(phi)_2]^{3+}$ (**4**) were used in this study.

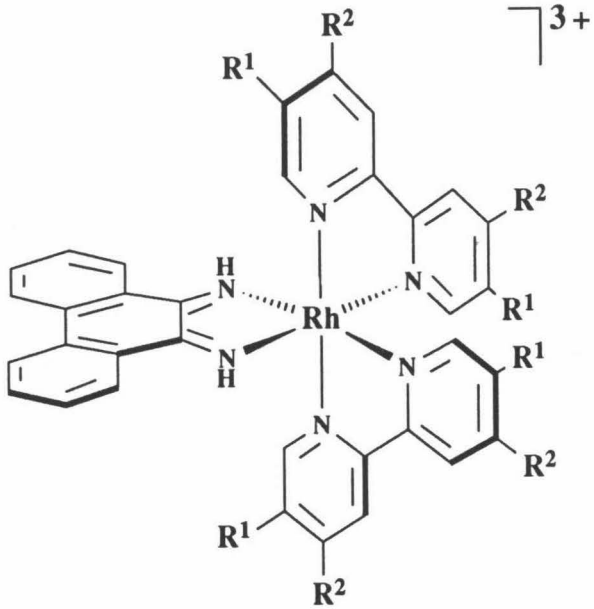

1a: R^1 = H, R^2 = H
1b: R^1 = H, R^2 = phenyl
1c: R^1 = H, R^2 = amido
1d: R^1 = methyl, R^2 = H
2: $[Rh(phen)_2phi]^{3+}$

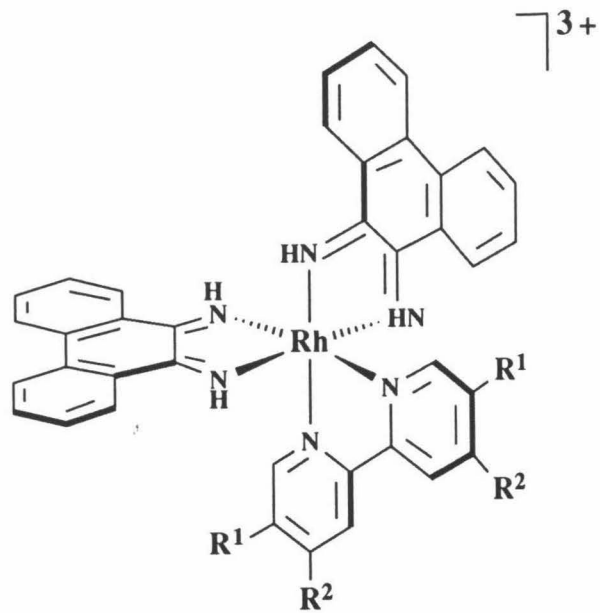

3a: R^1 = H, R^2 = H
3b: R^1 = H, R^2 = phenyl
3c: R^1 = H, R^2 = amido
3d: R^1 = methyl, R^2 = H
4: $[Rh(phi)_2phen]^{3+}$

from commercial sources. [α-^{32}P]dideoxy-ATP, [α-^{32}P]deoxy-ATP, [γ-^{32}P]deoxy-ATP were obtained from NEN-Dupont. The complexes [Rh(phi)$_2$(4,4'-R$_2$bpy)]Cl$_3$, [R = phenyl (**3b**), amido (**3c**)], [Rh(phi)$_2$(5,5'-Me$_2$bpy)]Cl$_3$ complexes (**3d**), and [Rh(phi)$_2$phen]Cl$_3$ (**4**) , as shown in Figure 4.1, were prepared as described in Chapter 3. The complexes [Rh(bpy)$_2$phi]Cl$_3$ (**1a**), and its derivatives [Rh(4,4'-R$_2$bpy)$_2$phi]Cl$_3$, [R = amido (**1c**)] and [Rh(5,5'-Me$_2$bpy)$_2$phi]Cl$_3$ complexes (**1d**), as shown in Figure 4.1, were prepared according to the reported synthesis[5c] of [Rh(phen)$_2$phi]Cl$_3$. The complex [Rh(4,4'-diphenyl 2,2'-bipyridyl)$_2$phi]Cl$_3$ (**1b**) was synthesized using an altered procedure as described in Chapter 3[7].

Instrumentation: ^{1}H-NMR spectra were obtained on a JEOL GX-400 spectrometer or on a General Electric QE-300 spectrometer in D$_2$O (referenced to 4.65 ppm), CD$_3$OD (referenced to 4.78 ppm), or d-DMSO (referenced to 2.49 ppm). UV-visible spectra and circular dichroism spectra were recorded on a Cary 2200 spectrophotometer and on a JASCO J-500A spectropolarimeter, respectively, in 50 mM Na-cacodylate buffer, pH 7.0. The light source utilized in all photocleavage experiments was an Oriel Model 6140 1000 W Hg/Xe lamp fitted with a monochromator and a 300 nm cut off filter to avoid light damage to DNA. High performance liquid chromatography (HPLC) was performed on a Waters 600E system equipped with a 484 tunable detector. Autoradiograms were scanned with a LKB 2202 Ultrascan Laser Densitometer.

Optical Resolution of [Rh(bpy)$_2$phi]Cl$_3$ [Rh(phen)$_2$phi]Cl$_3$ and [Rh(5,5'-dimethyl 2,2'-bipyridyl)$_2$phi]Cl$_3$: The Δ and Λ enantiomers of [Rh(phen)$_2$phi]Cl$_3$ were obtained as previously described[6]. A modified version of this published procedure was used to resolve [Rh(bpy)$_2$phi]Cl$_3$ and [Rh(5,5'-dimethyl 2,2'-bipyridyl)$_2$phi]Cl$_3$. An aqueous solution containing 30 mg of racemic complex was loaded onto a Sephadex CM C25 column. The enantiomers were resolved into two well-separated red bands using a 0.1 M

aqueous solution of tris(L-cysteinsulphinato)cobaltate(III) as the chiral eluent[8]. The column containing the two bands was then washed with 0.05 M NaCl to replace the [Co-(L-cysu)$_3$]$^{3-}$ anions with chlorides. The two bands were then eluted off the column using an aqueous solution of 0.3 M NaCl. CD spectra of the enantiomers were recorded in 50 mM Na-cacodylate buffer. The Δ isomers of [Rh(bpy)$_2$phi]Cl$_3$ at 318 nm (ΔE = - 72 l M^{-1}cm^{-1}) and of [Rh(5,5'-dimethyl 2,2'-bipyridyl)$_2$phi]Cl$_3$ at 329 nm (ΔE = - 79 l M^{-1}cm^{-1}) display negative circular dichroism. The absolute configurations were assigned on the basis of spectral similarity[8b] to [Rh(bpy)$_3$]Cl$_3$ and [Rh(4,4'-dimethylbpy)$_3$]Cl$_3$.

Photocleavage of DNA restriction fragments and oligonucleotides: A 140 base pair 5'-[γ-^{32}P]- or 3'-[α-^{32}P]- labeled EcoRI/PvuII fragment of pUC18 was prepared by standard methods[9]. The oligonucleotide 5'-CTGGCATGCCAG-3' was synthesized on a Pharmacia Gene Assembler using the phosphoramidite method, purified by reverse-phase HPLC, and labeled using established protocols. Cleavage reactions were carried out in 20 μl volumes contained in 0.65 ml siliconized eppendorf tubes. Unless otherwise specified, reaction mixtures contained 65 μM nucleotide DNA (calf thymus or oligonucleotide substrate), labeled DNA and 1 μM rhodium in 50 mM sodium cacodylate buffer, pH 7.0. Reaction mixtures containing [Rh(phi)$_2$]$^{3+}$ complexes (**3a-d, 4**) were irradiated for 20 min, while those containing [Rh(phi)]$^{3+}$ complexes (**1a-d, 2**) were irradiated for 8 min.

After irradiations, the reaction mixtures containing restriction fragment as the DNA substrate were ethanol precipitated with the addition of 10 μl of 7.5 M NH$_4$OAc and 60 μl EtOH. The DNA pellets were washed with 200 μl of 80% ethanol, dried and resuspended in 3 μl of loading buffer[9]. The samples were then heat denatured at 90° C and quick chilled on ice before loading onto an 8% denaturing polyacrylamide gel. Gels were electrophoresed at 1600 V for 2-3 hr, and dried at 70°C for 1 hr. Following

irradiations, 3 μl of the samples (25000 cpm ^{32}P) containing oligonucleotide substrate, were resuspended in loading dye, loaded onto a 20% denaturing polyacrylamide sequencing gel, and electrophoresed at 1200 V for 4 hr. The gels were transferred to a cassette and stored at -70° C with Kodak X-Omat film.

Quantitation of oligonucleotide photocleavage products: Quantitation of 3'-termini produced in the photocleavage of the oligonucleotide substrate 5'-CTGGCATGCCAG-3' by $[Rh(phi)_2]^{3+}$ complexes (**3a-d, 4**) was carried out using densitometry on autoradiograms produced from polyacrylamide gels. Specifically, the amounts of 3'-phosphate (dioxygen independent) and 3'-phosphoglycaldehyde (dioxygen dependent) termini formed were corrected for the total cleavage induced by each $[Rh(phi)_2]^{3+}$ complex and for the total counts loaded in each lane. Quantitation of nucleic acid base products was carried out on a Cosmosil 5μ, 15 cm C-18 column washed with 0.05 M ammonium formate at a flow rate of 1.5 ml min^{-1}. Following elution of the nucleic acid bases, the extent of oligonucleotide digested was quantitated using a 0-20% linear CH_3CN gradient. Products were detected by UV absorbance at 260 nm and quantitated by comparison of peak areas generated with commercial standards. Adenine, thymine, guanine and cytosine were eluted with retention times of 13.0, 5.7, 4.4, and 2.0 min, respectively.

4.3. Results

4.3.1. Sequence-Selectivities of $[Rh(phi)_2bpy]^{3+}$ and its Derivatives. The complex $[Rh(phi)_2bpy]^{3+}$ has been previously shown to cleave DNA upon photoactivation. All the derivatized $[Rh(phi)_2X]^{3+}$ complexes (**3b-d, 4**) also promote DNA strand scission and with comparable efficiencies[10]. Thus, a comparison of the sequence-selectivities of these complexes can be made by examining their photocleavage patterns on restriction

fragments. Previously, the parent complex $[Rh(phi)_2bpy]^{3+}$ was shown to cleave in a sequence-neutral manner at concentrations ≥ 5 μM; however, these studies show that at concentrations ≤ 1 μM, $[Rh(phi)_2X]^{3+}$ complexes cleave preferentially at some sites over others (Figure 4.2). In comparison, $[Rh(phi)_2(5,5'\text{-dimethylbpy})]^{3+}$ (**3d**) and particularly $[Rh(phi)_2(4,4'\text{-diphenylbpy})]^{3+}$ (**3b**) *cleave at a fewer number of sites,* due to the additional steric demands imposed by their respective 5,5-dimethyl and 4,4'-diphenyl moieties.

The hierarchy of sequence-selectivities of each $[Rh(phi)_2X]^{3+}$ complex studied, as deduced from their photocleavage patterns on the PvuII*-EcoR1 fragment (Figure 4.2) and other restriction fragments (data not shown), is presented in Table 4.1. The parent complex $[Rh(phi)_2bpy]^{3+}$ is selective for some 5'-pu-*py*-pu-py-3' sequences with cleavage occurring at the highlighted pyrimidine. The complexes $[Rh(phi)_2phen]^{3+}$ (**4**) and $[Rh(phi)_2(4,4'\text{-diamidobpy})]^{3+}$ (**3c**) have sequence-selectivities that are similar to $[Rh(phi)_2bpy]^{3+}$ but show slight enhancements in cleavage at a few preferred sites (Figure 4.2), such as the marked 5'-C*C*CA-3' and 5'-T*C*GT-3' sites. In comparison, the complexes, $[Rh(phi)_2(5,5'\text{-dimethylbpy})]^{3+}$ and $[Rh(phi)_2(4,4'\text{-diphenylbpy})]^{3+}$, generally cleave at a small subset of sites recognized by the parent complex; however, $[Rh(phi)_2(5,5'\text{-dimethylbpy})]^{3+}$ also cleaves at 5'-A*G*T sequences which are not cleaved by the parent $[Rh(phi)_2bpy]^{3+}$ complex.

4.3.2. Asymmetry in Cleavage by $[Rh(phi)_2bpy]^{3+}$ and its Derivatives: Evidence for Canting in Binding.

Previous studies have shown that the photoproducts formed in the DNA cleavage reaction by $[Rh(phi)_2bpy]^{3+}$ and $[Rh(phen)_2phi]^{3+}$ are consistent with the complexes binding in the major groove of DNA and promoting strand-scission via abstraction of the deoxyribose C3'-H atom[5d]. The formation of 3'-phosphoglycaldehyde and base-

Figure 4.2. Sequence-specific recognition of DNA by $[Rh(phi)_2bpy]^{3+}$ (**1a**) and its derivative complexes (**1b-d, 2**): importance of steric interactions. Autoradiogram of an 8% polyacrylamide gel after photocleavage of a [3'-^{32}P]-end-labeled PvuII/EcoR1 fragment of pUC18: Lane 1, Maxam-Gilbert A+G reaction; lane 2, untreated fragment; lane 3, fragment irradiated in the absence of rhodium complex; lane 4-8, [3'-^{32}P]-end-labeled fragment irradiated in the presence of 1 μM of $[Rh(phi)_2bpy]^{3+}$, $[Rh(phi)_2(5,5'\text{-dimethylbpy})]^{3+}$, $[Rh(phi)_2(4,4'\text{-diphenylbpy})]^{3+}$, $[Rh(phi)_2(4,4'\text{-diamidobpy})]^{3+}$, and $[Rh(phi)_2phen]^{3+}$, respectively. The complexes $[Rh(phi)_2bpy]^{3+}$ (lane 4), $[Rh(phi)_2(4,4'\text{-diamidobpy})]^{3+}$ (lane 7), and $[Rh(phi)_2phen]^{3+}$ (lane 8) cleave at most sites, but show a moderate preference for the 5'-A*T*GC-3', 5'-C*C*CA-3' and 5'-T*C*GT-3' sequences (marked with arrows), with cleavage occurring at the highlighted residues. The complexes $[Rh(phi)_2(5,5'\text{-dimethylbpy})]^{3+}$ (lane 4) and $[Rh(phi)_2(4,4'\text{-diphenylbpy})]^{3+}$ (lane 5) cleave preferentially only at the 5'-C*C*CA-3' sequence. This illustrates that additional steric interactions introduced by appropriately positioned methyl and phenyl groups make these complexes more selective towards sequence-dependent DNA structures.

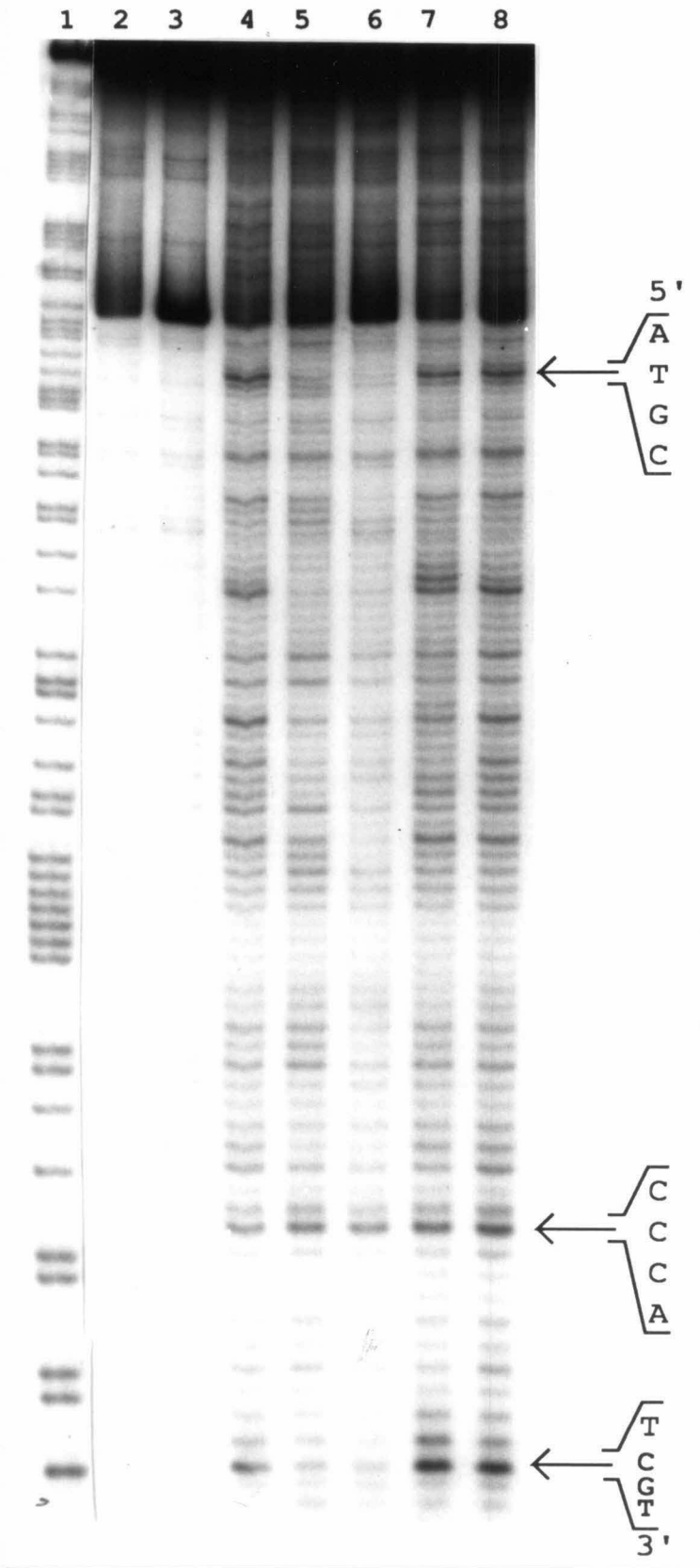
1 2 3 4 5 6 7 8
5'
A
T
G
C
C
C
C
A
T
C
G
T
3'

Table 4.1. DNA Sequence-Selectivities[a] of $[Rh(phi)_2bpy]^{3+}$ and its Derivatives.

Complex	Sequence-Selectivity (5'->3')[b]
$[Rh(phi)_2bpy]^{3+}$	A***T***GC (s), T***C***GT (s), A***C***GT (s), T***C***GC (s)
$[Rh(phi)_2phen]^{3+}$	A***T***GC (s), T***C***GT (s), T***C***GC (s), C***C***CA (s)
$[Rh(phi)_2(4,4'\text{-diamidobpy})]^{3+}$	A***T***GC (s), A***C***GG (s), T***C***AC (s), T***C***GT (s), T***C***GC (s)
$[Rh(phi)_2(4,4'\text{-diphenylbpy})]^{3+}$	C***C***CA (s), C***C***AG (s), A***C***GC (s)
$[Rh(phi)_2(5,5'\text{-dimethylbpy})]^{3+}$	C***C***CA (s), C***C***AG (s), A***G***TC (s), A***G***TG (s)

a: Sequence-selectivities were obtained from the photocleavage patterns of $[Rh(phi)_2X]^{3+}$ complexes observed on restriction fragments, derived from plasmid pUC18. Reaction mixtures containing 65 μM nucleotide and 1 μM Rh complex in 50 mM Na-cacodylate buffer, pH 7.0 were irradiated at 310 nm for 8 min.

b : Sequence preference in a 5'->3' direction with cleavage occurring at the highlighted residue; strong sites are labeled (s).

propenoic acid products were shown to be consistent with an *oxygen dependent* pathway of strand scission, while production of the 3'- and 5'-phosphates and free nucleic acid base products were shown to be consistent with an *oxygen independent* degradation pathway (Scheme 4.1). Interestingly, the partitioning between the oxygen dependent and independent pathways of DNA strand scission was found to correlate best with how the shape of the complex limits access of dioxygen to the C-3' position, suggesting that both the reaction and recognition of these complexes are shape-selective. Thus the shape of $[Rh(phi)_2bpy]^{3+}$ may lead to both its sequence-neutrality and its production of a higher percentage of oxygen-dependent cleavage products, as compared to $[Rh(phen)_2phi]^{3+}$. Based on these studies, an analysis of the distribution of cleavage products and their relation to the shapes and DNA recognition of the series of $[Rh(phi)_2X]^{3+}$ complexes studied here was explored.

Presently, as examined by gel-electrophoresis (Figure 4.3), all the $[Rh(phi)]^{3+}$ complexes produce termini which co-migrate with the previously characterized 3'-phosphate and 3'-phosphoglycaldehyde termini and, as analyzed by HPLC, produce free nucleic acid bases and base propenoic acids. Thus the photoproducts identified for each $[Rh(phi)_2X]^{3+}$ complex induced-DNA cleavage reaction are consistent with the previously proposed photocleavage mechanism[5d] that involves abstraction of the major groove C3'-H atom. Furthermore, as shown in Table 4.2, the amount of free nucleic acid bases produced by each complex, as expected, directly correlates with the extent of 3'-phosphate termini produced from cleavage of the 5'-CTGGCATGCCAG-3' oligonucleotide substrate. Interestingly, compared to the other complexes, the derivatives $[Rh(phi)_2$4,4'-diphenylbpy$]^{3+}$ and $[Rh(phi)_2$4,4'-diamidobpy$]^{3+}$ produce less 3'-phosphate and free nucleic acid base products, but more oxygen dependent cleavage products.

While the cleavage products identified are direct evidence in support of the model[5d] that $[Rh(phi)_2X]^{3+}$ complexes bind in the major groove of DNA and abstract the

Scheme 4.1. $[Rh(phi)]^{3+}$ Induced DNA Cleavage by C3'-H Atom Abstraction.

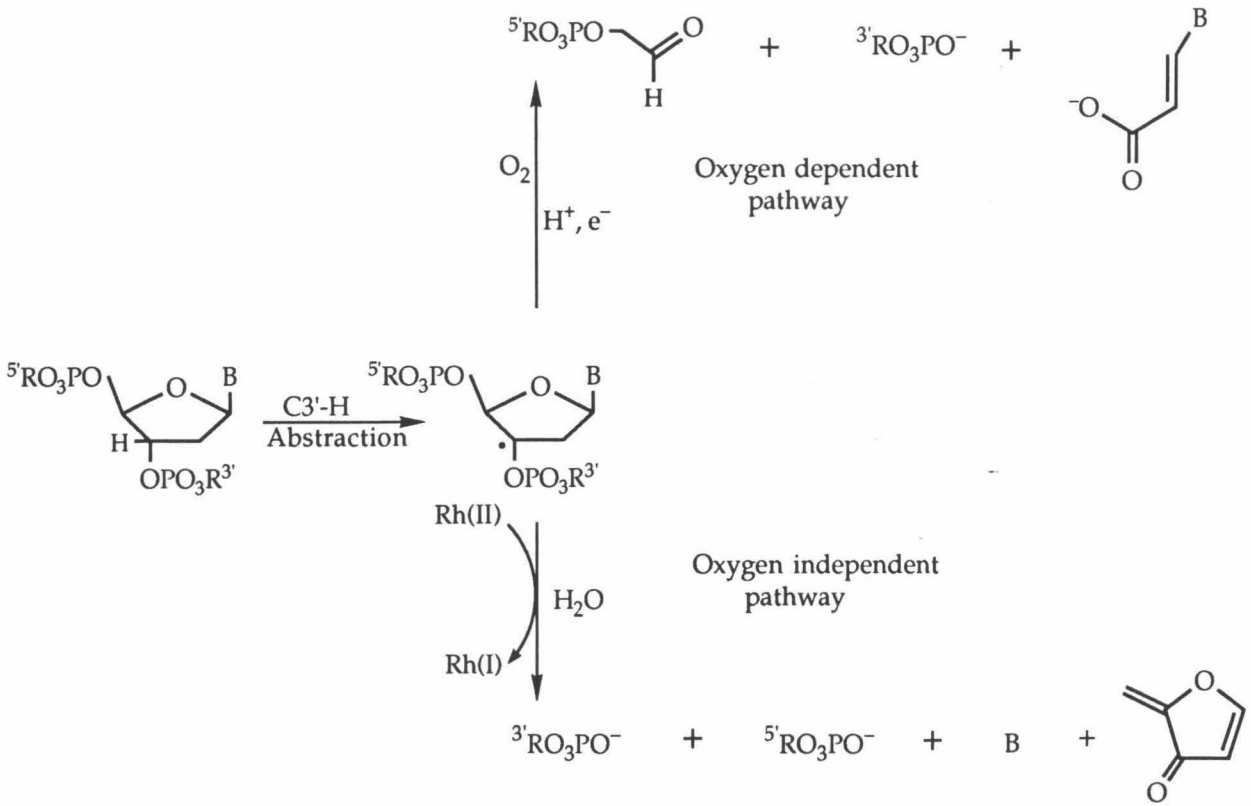

Figure 4.3. Comparison of photocleavage by $[Rh(phi)_2bpy]^{3+}$ (**1a**) and its derivative complexes (**1b-d, 2**) on the oligonucleotide 5'-CTGGCATGCCAG-3'. Autoradiogram of a 20% polyacrylamide gel of the [5'-^{32}P]-end-labeled oligonucleotide. Conditions for the cleavage reactions: 25 μM Rh^{3+}, 50 mM sodium cacodylate, 5 min irradiation at 310 nm; lanes 1 and 2, Maxam-Gilbert A+G and C+T reactions, respectively; lane 3, untreated oligonucleotide; lane 4, oligonucleotide irradiated in the absence of metal complex; lane 5-9, oligonucleotide irradiated in the presence of $[Rh(phi)_2bpy]^{3+}$, $[Rh(phi)_2(4,4'$-diamidobpy)$]^{3+}$, $[Rh(phi)_2(5,5'$-dimethylbpy)$]^{3+}$, $[Rh(phi)_2(4,4'$-diphenylbpy)$]^{3+}$ and $[Rh(phi)_2phen]^{3+}$. Note that each complex produces 3'-phosphate termini (which co-migrate with the 3'-phosphate markers in lanes 1 and 2) and the previously assigned[5d] slower moving 3'-phosphoglycaldehyde termini. The complexes cleave strongly at the T_7 of the 5'-A*T*GC-3' site on one strand, with some cleavage in a 5'-direction at the C_5 on the opposing strand. Note that the extent of C_5 glycaldehyde [(C_5-glyc/(C_5-phos)] produced by the complexes $[Rh(phi)_2(5,5'$-dimethylbpy)$]^{3+}$ (lane 7) and $[Rh(phi)_2(4,4'$-diphenylbpy)$]^{3+}$ (lane 8) is significantly lower than that produced by the other complexes. Shown below the gel is a schematic of the 12 mer double stranded oligonucleotide containing the 5'-A*T*GC-3' site. Arrows refer to cleavage by the complexes on both strands of the oligonucleotide, and the short bold line between the two strands represent the site of intercalation by the metal complex.

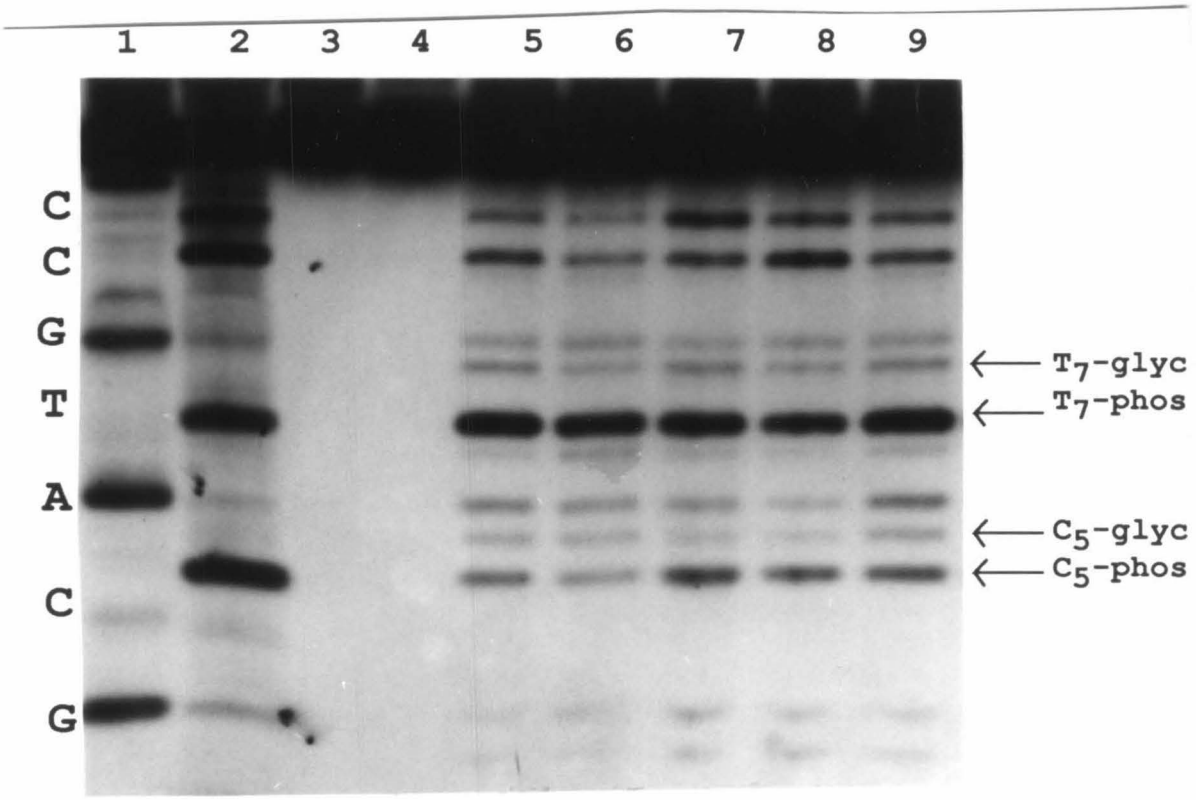
1
2
3
4
5
6
7
8
9
C
C
G
T
A
C
G
← T7-glyc
← T7-phos
← C5-glyc
← C5-phos


5'-CTGGCAT7 G8CCAG-3'
3'-GACCGTA6 C5GGTC-5'

Table 4.2. Quantitation of Products Formed in the Photocleavage of 5'-CTGGCATGCCAG-3' by $[Rh(phi)_2bpy]^{3+}$ and its Derivatives[a].

Rh complex	% phosphate[b]	Nucleic acid base (μM)[c]
$[Rh(phi)_2(bpy)]^{3+}$	85	8.2
$[Rh(phi)_2(phen)]^{3+}$	80.5	8.7
$[Rh(phi)_2(5,5'\text{-dimethylbpy})]^{3+}$	81.4	11.2
$[Rh(phi)_2(4,4'\text{-diphenylbpy})]^{3+}$	68.2	6.4
$[Rh(phi)_2(4,4'\text{-diamidobpy})]^{3+}$	68.6	4.6

a: Reaction mixtures containing 500 μM (in nucleotides) of oligonucleotide substrate and 25 μM metal complex in 50 mM sodium cacodylate buffer, pH 7.0 were irradiated at 310 nm for 7.5 min.

b: Percent 3'-phosphate termini of total cleavage of oligonucleotide substrate, determined by densitometric quantitation of two cleavage experiments. All numbers represent averages with deviations of $\pm$ 5%.

c: HPLC analyses of the amount of nucleic acid bases produced in the DNA cleavage reaction. The values are based on oligonucleotide digested and represent averages of two experiments with deviations < 5%.

C3'-H atom, the 5'-asymmetry in cleavage offers further support for the reaction occurring in the major groove[5,11]. The 5'-asymmetry in cleavage by $[Rh(phi)_2]^{3+}$ complexes was examined on the oligonucleotide 5'-CTGGCATGCCAG-3' substrate, by gel electrophoresis. As shown in Figure 4.3, all the $[Rh(phi)_2]^{3+}$ complexes cleave strongly at T_7 of the 5'-A*T*GC-3' site, but show relatively weak cleavage in a 5'-asymmetric direction on the C_5 of the opposing strand. Thus cleavage by these complexes occurs predominantly on the T-strand, suggesting that the complex is asymmetrically bound at that site by canting to one side of the helix. The ratio of total cleavage (3'-phosphate + 3'-phosphoglycaldehyde) produced at T_7 to the total cleavage at C_5 reflects the level of asymmetric cleavage and that site. As shown in Table 4.3, the complexes $[Rh(phi)_2bpy]^{3+}$, $[Rh(phi)_2phen]^{3+}$ and $[Rh(phi)_2$4,4'-diamidobpy$]^{3+}$ cleave preferentially at T_7 over C_5 by a factor of about 5, while the complexes $[Rh(phi)_2$4,4'-diphenylbpy$]^{3+}$ and $[Rh(phi)_2$5,5'-dimethylbpy$]^{3+}$ cleave only twice as strongly at T_7 as compared to C_5. Interestingly, the level of asymmetric cleavage induced by the $[Rh(phi)_2]^{3+}$ complexes may be further analyzed by examining the relative distribution of oxygen dependent and independent DNA photoproducts formed at T_7 and C_5. Specifically, *canting of the complex to the T_7 strand should increase accessibility of dioxygen to the complementary strand*; therefore, a greater percent of oxygen-dependent 3'-phosphoglycaldehyde product would be produced on the C_5 strand. For the complexes $[Rh(phi)_2bpy]^{3+}$, $[Rh(phi)_2phen]^{3+}$ and $[Rh(phi)_2$4,4'-diamidobpy$]^{3+}$, which cleave 5 fold more strongly at T_7 than at C_5, 10% of the total cleavage products at T_7 and a substantial 30-50% of the total cleavage products at C_5 includes the 3'-phosphoglycaldehdye product. In comparison, for the complexes $[Rh(phi)_2$4,4'-diphenylbpy$]^{3+}$ and $[Rh(phi)_2$5,5'-dimethylbpy$]^{3+}$ which cleave twice as strongly at T_7 than at C_5, the percentages of 3'-phosphoglycaldehyde product formed at both T_7 and C_5 are comparable (10-20%). Thus, as shown in Table 4.3, the formation of 3'-phosphoglycaldehyde at C_5 is

Table 4.3. Asymmetry in DNA Cleavage by $[Rh(phi)_2bpy]^{3+}$ and its Derivatives[a].

Oligonucleotide substrate 5'-CTGGCA**T**$_7$G$_8$CCAG-3'
3'-GACCGTA$_6$**C**$_5$GGTC-5'

Complex	T_7/C_5[b]	% glyc. at T_7[c]	% glyc. at C_5[d]
$[Rh(phi)_2bpy]^{3+}$	4.9	12	28
$[Rh(phi)_2phen]^{3+}$	4.0	11	29
$[Rh(phi)_2(4,4'\text{-diamidobpy})]^{3+}$	4.7	11	46
$[Rh(phi)_2(4,4'\text{-diphenylbpy})]^{3+}$	2.5	13	18
$[Rh(phi)_2(5,5'\text{-dimethylbpy})]^{3+}$	2.6	10	17

a: Reaction mixtures containing 500 μM (in nucleotides) of oligonucleotide substrate and 25 μM metal complex in 50 mM sodium cacodylate buffer, pH 7.0 were irradiated for 7.5 min at 310 nm.

b : Ratio of total cleavage at T_7 to total cleavage at C_5 (where total cleavage = 3'-phosphate + 3'-phosphoglycaldehyde termini produced). This value may reflect the level of canting by the complex to one strand of the oligonucleotide substrate over the other. All numbers represent averages with deviations of ±5% of the densitometric quantitation of two cleavage experiments, and are normalized to the amount of undigested oligonucleotide.

c : Percent 3'-phosphoglycaldehdye of total cleavage at T_7.

d : Percent 3'-phosphoglycaldehyde of total cleavage at C_5.

directly correlated to the level of asymmetric cleavage of the complex, which is represented by the ratio of total cleavage at T_7 to C_5. Therefore, the analyses of the distribution of the oxygen dependent and independent cleavage products supports the notion of the complex bound asymmetrically to one strand of the helix over the other, at this site.

4.3.3. Sequence-Selectivities of $[Rh(bpy)_2phi]^{3+}$ and its Derivatives. The sequence-selectivities and asymmetry in DNA cleavage by the $[Rh(phi)]^{3+}$ series of complexes (**1a-d, 2**) can be studied by examining their photocleavage patterns on [5'-^{32}P]- and [3'-^{32}P]-end-labeled restriction fragments. All the $[Rh(phi)]^{3+}$ complexes have comparable photocleavage efficiencies[12] to the previously studied $[Rh(phen)_2phi]^{3+}$ complex; however, under identical reaction conditions their sequence-selectivities differ markedly. Based on the previously estimated DNA binding affinity ($K_a \geq 10^6\ M^{-1}$) of $[Rh(phen)_2phi]^{3+}$, the photocleavage reactions were carried out at low concentrations ($\leq$ 1 μM) of each $[Rh(phi)]^{3+}$ metal complex to ascertain their sequence-selectivities. As shown in Figure 4.4, all the complexes cleave sequence-specifically on the restriction fragment. Compared to the $[Rh(phi)_2]^{3+}$ complexes (Figure 4.2), the $[Rh(phi)]^{3+}$ complexes show significantly greater specificity in DNA cleavage. As shown in Figure 4.4, the complexes $[Rh(bpy)_2phi]^{3+}$ and $[Rh(phen)_2phi]^{3+}$ have similar photocleavage patterns and are specific for 5'-*py*-py-3' and 5'-*py*-pu-3' base steps, with cleavage occurring at the highlighted pyrimidine. The complex $[Rh(4,4'\text{-diamidobpy})_2phi]^{3+}$ appears to prefer sequences that are also recognized by the parent complex; however, its affinity towards some sites is significantly increased, possibly from hydrogen bonding contacts between its amido groups and the phosphate backbone. In comparison, owing to the steric demands imposed by methyl and phenyl moieties, the complexes $[Rh(5,5'\text{-dimethylbpy})_2phi]^{3+}$ and $[Rh(4,4'\text{-diphenylbpy})_2phi]^{3+}$ show cleavage at only a small

subset of sites cleaved by the parent $[Rh(bpy)_2phi]^{3+}$. While [Rh(5,5'-dimethylbpy)$_2$phi]$^{3+}$ cleaves strongly at 5'-A***C***TG-3' and 5'-A***G***TC-3' sites, [Rh(4,4'-diphenylbpy)$_2$phi]$^{3+}$ is highly specific for the two 5'-CT***C***TAG-3' sites on opposing strands, contained in the palindromic 5'-CTCTAGAG-3' sequence. A summary of the sites targeted by the $[Rh(phi)X_2]^{3+}$ complexes is illustrated as histograms in Figure 4.5.

Owing to the high level of specific cleavage induced by $[Rh(phi)]^{3+}$ complexes, the 5'-asymmetry in their cleavage patterns, as would be expected from major groove binders, can be determined by comparing their cleavage patterns on the [5'-^{32}P]- and [3'-^{32}P]- end labeled EcoR1*-PvuII 144 bp fragment (Figure 4.4). In general, cleavage at sites containing a central 5'-*py*-py-3' base step occurs only on the pyrimidine strand, with no corresponding cleavage observed in a 5'-direction at the 5'-*pu*-pu-3' step of the opposing strand. However, as shown in the histograms in Figure 4.5, cleavage at some 5'-*py*-pu-3' base steps is associated with 5'-asymmetric cleavage at the complementary 5'-*py*-pu-3' base step on the opposing strand. These results suggests that the complex is more symmetrically bound in the helix at 5'-py-pu steps than at 5'-py-py-3' sites. For example, cleavage at 5'-T***T***GG is associated with 5'-cleavage at 5'-C***C***AA and cleavage at 5'-A***C***AA is associated with 5'-cleavage at T***T***GT. Thus in general, the complexes appear to strongly target sites containing central 5'-*py*-py steps with cleavage occurring on the pyrimidine strand; however, they also appear to moderately target sites containing 5'-*py*-pu-3' steps with cleavage occurring on both strands. Specifically, at low concentrations of complex ($\leq$ 1 μM), a preference for 5'-*py*-py-3' steps is observed (Figure 4.4 and 4.5); however, at concentrations of complex $\geq$ 5 μM (data not shown), additional cleavage at 5'-py-pu-3' steps are observed.

Figure 4.4. Sequence-specific recognition of DNA by $[Rh(bpy)_2phi]^{3+}$ (**3a**) and its derivative complexes (**3b-3d, 4**). Autoradiogram of an 8% polyacrylamide gel after photocleavage of a [5'-^{32}P]- (left) and [3'-^{32}P]- (right) end-labeled EcoR1/PvuII fragment of pUC18: Lanes 1 and 2, Maxam-Gilbert A+G and C+T reactions; lane 3, untreated fragment; lane 4, fragment irradiated in the absence of rhodium complex; lane 5-9, [5'-^{32}P]- or [3'-^{32}P]- end-labeled fragment irradiated in the presence of 1 μM of $[Rh(bpy)_2phi]^{3+}$, $[Rh(phen)_2phi]^{3+}$, $[Rh(4,4'\text{-diamidobpy})_2phi]^{3+}$, $[Rh(5,5'\text{-dimethylbpy})_2phi]^{3+}$ and $[Rh(4,4'\text{-diphenylbpy})_2phi]^{3+}$, respectively. Note that the complexes $[Rh(bpy)_2phi]^{3+}$ and $[Rh(phen)_2phi]^{3+}$ (lane 5 and 6, respectively) have similar cleavage patterns, with the former complex cleaving more strongly at most sites, showing a slightly less-selective pattern of cleavage. The complex $[Rh(4,4'\text{-diamidobpy})_2phi]^{3+}$ (lane 7) cleaves similarly to $[Rh(bpy)_2phi]^{3+}$ but shows a significant enhancement in cleavage at some sites, such as the marked 5'-T***C***TA-3' and 5'-T***T***GG-3' sequences viewed on the 5'-end labeled fragment (left), and the marked 5'-T***T***CG-3' sequence viewed on the 3'-end labeled fragment (right). The complex $[Rh(5,5'\text{-dimethylbpy})_2phi]^{3+}$ (lane 8) cleaves only at a small subset of sites, such as the marked 5'-A***C***TG-3' sequence viewed on the 5'-end labeled fragment. However, this complex also cleaves strongly at the 5'-A***G***TG-3' and 5'-A***G***TC-3' sequences, viewed on the 3'-end-labeled fragment, which are *not* cleaved by the parent $[Rh(bpy)_2phi]^{3+}$ complex. The complex $[Rh(4,4'\text{-diphenylbpy})_2phi]^{3+}$ cleaves very specifically at the 5'-CT***C***TAG-3' sequence located on both strands (lane 9). A comparison of the photocleavage patterns of complexes **3a-d** and **4**, illustrates the importance of steric interactions in their recognition of sequence-dependent DNA structure.

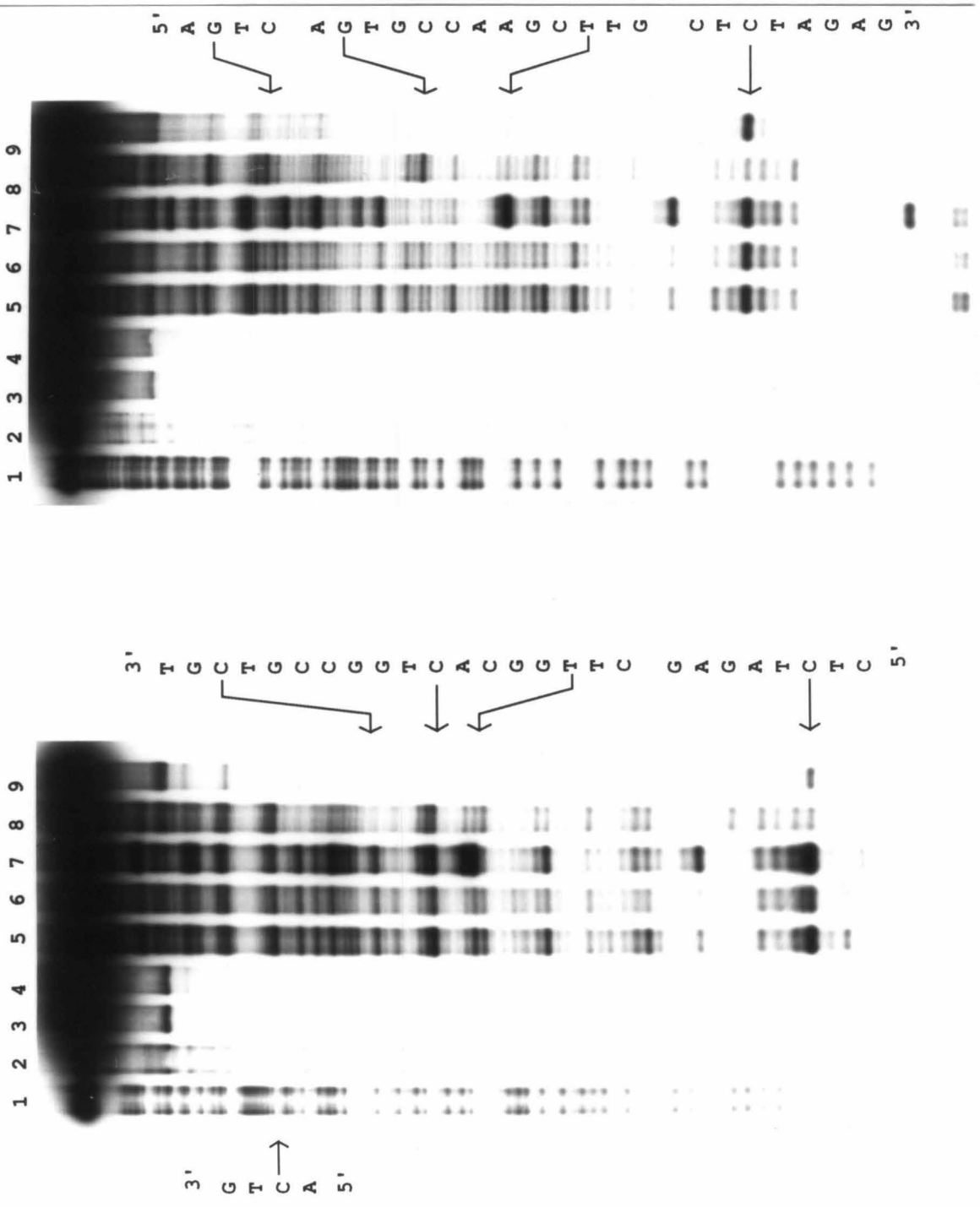
5' A G T C A G T G C C A A G C T T G C T C T A G A G 3'
1 2 3 4 5 6 7 8 9
3' T G C T G C C G G T C A C G G T T C G A G A T C T C 5'
1 2 3 4 5 6 7 8 9
3' G T C A 5'

Figure 4.5. Comparison of DNA photocleavage by $[Rh(phi)X_2]^{3+}$ complexes. Histogram illustrating the relative cleavage by the complexes $[Rh(bpy)_2phi]^{3+}$ (**1a**), $[Rh(phen)_2phi]^{3+}$ (**2**), [Rh(4,4'-diamidobpy)$_2$phi]$^{3+}$ (**1c**), [Rh(5,5'-dimethylbpy)$_2$phi]$^{3+}$ (**1d**) and [Rh(4,4'-diphenylbpy)$_2$phi]$^{3+}$ (**1b**) at sites along the 5'-labeled (top) and 3'-labeled (bottom) EcoR1/PvuII fragment of pUC18. Note that complexes **1a**, **2**, and **1c** target similar sequences and show a distinct 5'-asymmetry in cleavage at 5'-*py*-pu-3' sites, as represented by the boxed sequences. Complex **1c** shows significantly enhanced cleavage at some sites, likely due to hydrogen bonding between its amido functionalities and the phosphate backbone. Complexes **1d** and **1b** cleave at a fewer number of sites than the parent complex **1a** due to steric factors; interestingly, complex **1b** cleaves specifically only at the self-complementary 5'-CTCTAGAG-3' site.

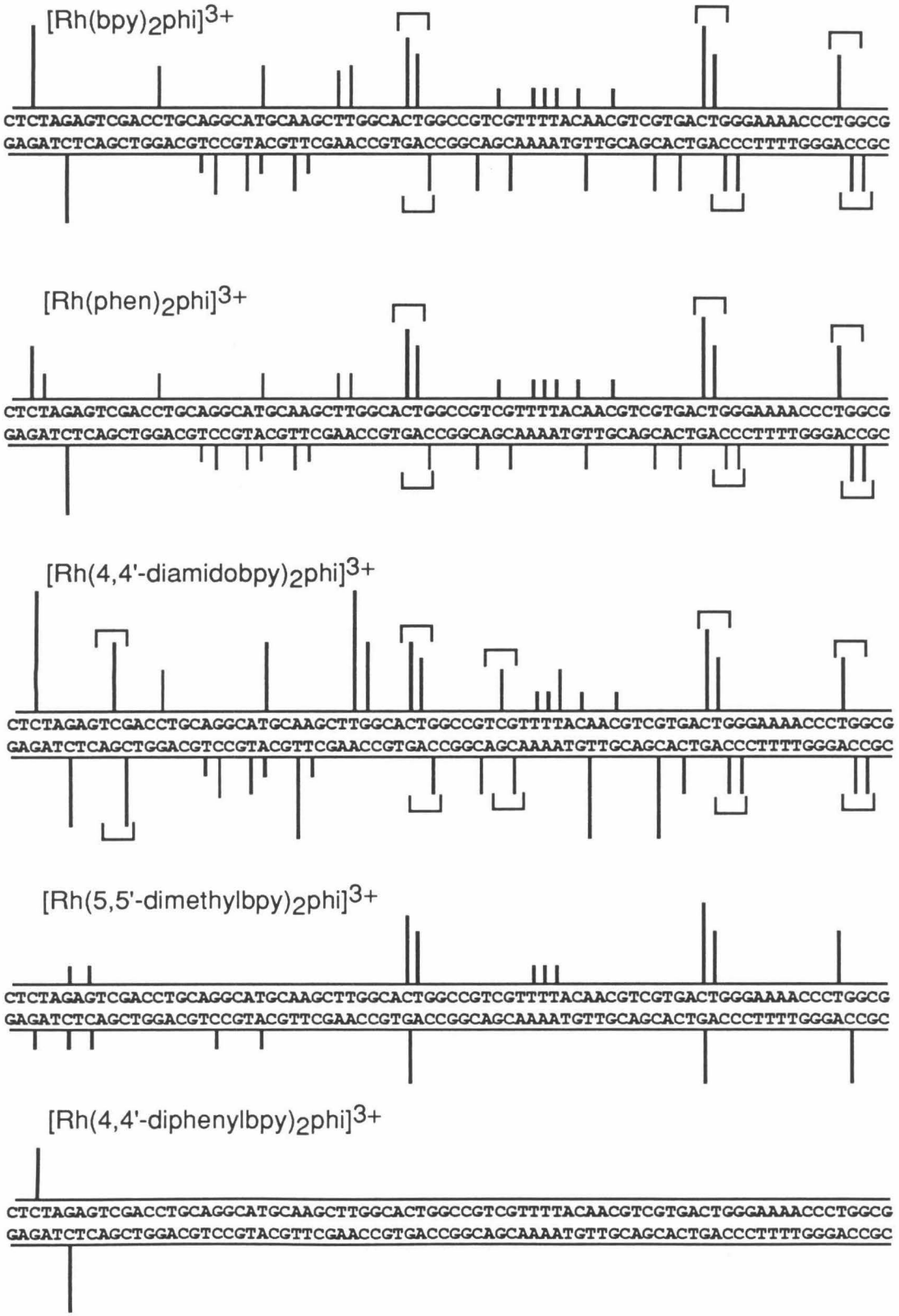
[Rh(bpy)2phi]3+
CTCTAGAGTCGACCTGCAGGCATGCAAGCTTGGCACTGGCCGTCGTTTTACAACGTCGTGACTGGGAAAACCCTGGCG
GAGATCTCAGCTGGACGTCCGTACGTTCGAACCGTGACCGGCAGCAAAATGTTGCAGCACTGACCCTTTTGGGACCGC
[Rh(phen)2phi]3+
CTCTAGAGTCGACCTGCAGGCATGCAAGCTTGGCACTGGCCGTCGTTTTACAACGTCGTGACTGGGAAAACCCTGGCG
GAGATCTCAGCTGGACGTCCGTACGTTCGAACCGTGACCGGCAGCAAAATGTTGCAGCACTGACCCTTTTGGGACCGC
[Rh(4,4'-diamidobpy)2phi]3+
CTCTAGAGTCGACCTGCAGGCATGCAAGCTTGGCACTGGCCGTCGTTTTACAACGTCGTGACTGGGAAAACCCTGGCG
GAGATCTCAGCTGGACGTCCGTACGTTCGAACCGTGACCGGCAGCAAAATGTTGCAGCACTGACCCTTTTGGGACCGC
[Rh(5,5'-dimethylbpy)2phi]3+
CTCTAGAGTCGACCTGCAGGCATGCAAGCTTGGCACTGGCCGTCGTTTTACAACGTCGTGACTGGGAAAACCCTGGCG
GAGATCTCAGCTGGACGTCCGTACGTTCGAACCGTGACCGGCAGCAAAATGTTGCAGCACTGACCCTTTTGGGACCGC
[Rh(4,4'-diphenylbpy)2phi]3+
CTCTAGAGTCGACCTGCAGGCATGCAAGCTTGGCACTGGCCGTCGTTTTACAACGTCGTGACTGGGAAAACCCTGGCG
GAGATCTCAGCTGGACGTCCGTACGTTCGAACCGTGACCGGCAGCAAAATGTTGCAGCACTGACCCTTTTGGGACCGC

4.3.4. Sequence-Selectivities of the Δ and Λ Enantiomers of $[Rh(bpy)_2phi]^{3+}$, $[Rh(phen)_2phi]^{3+}$ and $[Rh(5,5'\text{-dimethylbpy})_2phi]^{3+}$. To understand the sequence selectivities of the $[Rh(phi)]^{3+}$ complexes studied, it is essential to identify the individual sequence-preferences of their Δ and Λ isomers. Previous work has shown that the complex $[Rh(phen)_2phi]^{3+}$ binds enantioselectively at 5'-py-pu-3' base steps. While the Δ isomer of this complex cleaves specifically at the py of 5'-*py*-pu steps, the Λ isomer shows no corresponding cleavage at these steps[5b]. Presently, we compared the photocleavage patterns of the enantiomers of $[Rh(bpy)_2phi]^{3+}$, $[Rh(phen)_2phi]^{3+}$ and $[Rh(5,5'\text{-dimethylbpy})_2phi]^{3+}$ on the [5'-^{32}P]- and [3'-^{32}P]- end labeled EcoR1*-PvuII 144 base pair fragment from plasmid pUC18. The photocleavage experiment was carried out at low concentrations of each metal complex (0.2 μM) so as to differentiate clearly between strong sites recognized by their respective Δ and Λ isomers. As shown in Figure 4.5, isomers of $[Rh(bpy)_2phi]^{3+}$ and $[Rh(phen)_2phi]^{3+}$ show very similar recognition patterns. The Δ isomer of both complexes cleave strongly at both 5'-py-py and 5'-pu-pu base steps, while the Λ isomers have no strong sites. In comparison, the Δ and Λ isomers of $[Rh(5,5'\text{-dimethylbpy})_2phi]^{3+}$ each have distinctly different recognition sequences. While the Δ isomer cleaves strongly at 5'-C*T*TG-3' and 5'-C*A*TG-3' sites, the Λ isomer cleaves strongly at 5'-A*C*TG-3', 5'-A*G*TG-3' and 5'-A*G*TC-3' sites. This comparison points to the *importance of both steric clashes and methyl-methyl van der Waals interactions* in enhancing the sequence-specificity of $[Rh(phi)]^{3+}$ complexes. A summary of preferred sites of cleavage by the Δ and Λ isomers of the three complexes studied is presented in Table 4.4.

Figure 4.6. Enantioselectivity in DNA sequence-recognition by the Δ and Λ isomers of $[Rh(bpy)_2phi]^{3+}$, $[Rh(phen)_2phi]^{3+}$ and $[Rh(5,5'\text{-dimethylbpy})_2phi]^{3+}$. Autoradiogram of an 8% polyacrylamide gel after photocleavage of a [5'-^{32}P]- (left) and [3'-^{32}P]- (right) end-labeled EcoR1/PvuII fragment of pUC18: Lanes 1 and 2, Maxam Gilbert A+G and C+T reactions; lane 3, untreated fragment; lane 4, fragment irradiated in the absence of rhodium complex; lanes 5-10, [5'-^{32}P]- or [3'-^{32}P]- end-labeled fragment irradiated in the presence of 0.2 μM of Δ-$[Rh(bpy)_2phi]^{3+}$, Λ-$[Rh(bpy)_2phi]^{3+}$, Δ-$[Rh(phen)_2phi]^{3+}$, Λ-$[Rh(phen)_2phi]^{3+}$, Δ-$[Rh(5,5'\text{-dimethylbpy})_2phi]^{3+}$, and Λ- $[Rh(5,5'\text{-dimethylbpy})_2phi]^{3+}$. Not that the cleavage patterns by the Δ and Λ isomers of $[Rh(bpy)_2phi]^{3+}$ and $[Rh(phen)_2phi]^{3+}$ are very similar; the Δ isomers of both complexes cleave strongly at the 5'-T***C***TA-3' and 5'-A***C***TG-3' sequences while the corresponding Λ isomers have no strong sites of cleavage. In comparison, the Δ isomer of $[Rh(5,5'\text{-dimethylbpy})_2phi]^{3+}$ cleaves strongly at the 5'-C***T***TG-3' sequence while the Λ isomer cleaves strongly at the 5'-A***C***TG-3', 5'-A***G***TG-3', and 5'-A***G***TC-3' sequences.

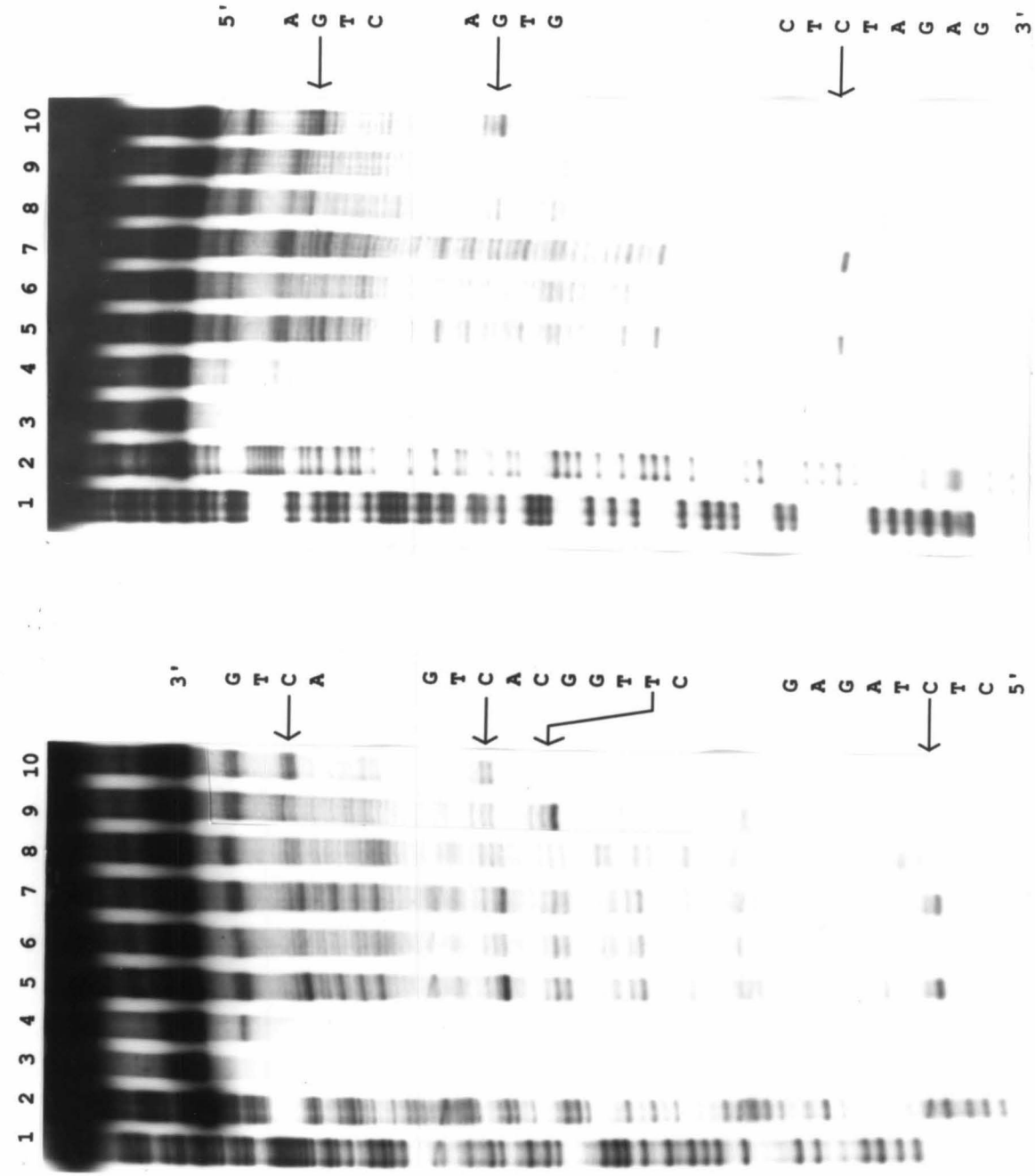
5' A G T C
A G T G
C T C T A G A G 3'
1 2 3 4 5 6 7 8 9 10
3' G T C A
G T C A C G G T T C
G A G A T C T C 5'
1 2 3 4 5 6 7 8 9 10

Table 4.4. Sequence-Selectivities[a] of the Δ and Λ Isomers of $[Rh(bpy)_2phi]^{3+}$, $[Rh(phen)_2phi]^{3+}$ and $[Rh(5,5'\text{-dimethylbpy})_2phi]^{3+}$.

Complex	Sequence selectivity[b] Δ enantiomer	Sequence selectivity Λ enantiomer
$[Rh(bpy)_2phi]^{3+}$	T***C***TA (s), C***T***TG (s), A***C***TG (s),	A***C***TG (w)
$[Rh(phen)_2phi]^{3+}$	T***C***TA (s), C***T***TG (s), A***C***TG (s),	A***C***TG (w)
$[Rh(5,5'\text{-dimethylbpy})_2phi]^{3+}$	C***T***TG (s), C***A***TG (s)	A***C***TG (s), A***G***TG (s), A***G***TC (s)
	Consensus sequence: C***N***TG	Consensus sequence: A***C***/***G***TC/G

a: The reaction mixtures containing 65 μM nucleotide and 0.2 μM Rh complex (Δ or Λ isomer) in 50 mM Na-cacodylate buffer, pH 7.0 were irradiated at 310 nm for 8 min.
b: All sequences are written in a 5'->3' direction. Cleavage is observed at the highlighted residue in the recognition sequences. The strong sites are labeled (s).

4.4. Discussion

Phenanthrenequinone diimine(phi) complexes of rhodium(III) have been shown to bind avidly ($K_a \geq 10^7$) in the major groove of DNA through intercalation of the phi ligand[5,6,13]. This mode of intercalative DNA binding allows $[Rh(phi)]^{3+}$ complexes to associate intimately with the helix and sense the local structure at their binding sites. The $[Rh(phi)]^{3+}$ complexes thus provide attractive frameworks for the design of sequence-specific DNA binding probes. The series of DNA-binding $[Rh(phi)]^{3+}$ complexes studied here (Figure 4.1) are derivatives of the previously studied[5a] metal complexes $[Rh(phen)_2phi]^{3+}$ (**2**) and $[Rh(phi)_2bpy]^{3+}$ (**3a**). As demonstrated by previous studies[5,13] and substantiated by this work, coordinatively saturated octahedral $[Rh(phi)]^{3+}$ complexes bind to DNA by phi intercalation and recognize variations in the sequence-dependent local structure of double-helical DNA by a *process of shape-selection.*

In this work we show that steric contributions dominate the sequence-specificities of $[Rh(phi)_2X]^{3+}$ complexes. Specifically, introducing hydrophobic residues such as methyl groups in the 5,5'-positions or phenyl groups in the 4,4'-positions of the ancillary bipyridyl ligand significantly restricts the DNA specificity of these complexes. The derivative complexes $[Rh(phi)_2(5,5'\text{-dimethylbpy})]^{3+}$ (**3d**) and $[Rh(phi)_2(4,4'\text{-diphenylbpy})]^{3+}$ (**3b**) *cleave at a significantly fewer number of sites* as compared to their parent complex $[Rh(phi)_2bpy]^{3+}$ (figure 4.2). Thus, the steric demands imposed by the bulky ancillary ligands of complexes **3d** and **3b** diminishes their binding affinity to most sequences and thereby enhances their overall sequence-specificities. Since these complexes bind very tightly to DNA ($K_a \geq 10^6\ M^{-1}$), their relative binding to different DNA sequences can be modulated by steric interactions. Therefore, by changing the overall shape of the sequence-neutral parent complex $[Rh(phi)_2bpy]^{3+}$, we have constructed a relatively sequence-specific molecule from a sequence-neutral one.

The shapes of $[Rh(phi)_2X]^{3+}$ complexes clearly determine their overall DNA recognition properties; however, the specific structural reasons for their individual sequence-selectivities is not so apparent. A comparison of the sequence-selectivities of the $[Rh(phi)_2X]^{3+}$ complexes (Table 4.1) indicates that there is no consensus sequence describing their selectivities. This is not surprising, since $[Rh(phi)_2X]^{3+}$ complexes lack a C_2 axis of symmetry about their intercalating phi ligand. Therefore, racemic mixtures of each $[Rh(phi)_2X]^{3+}$ complex should have four distinct intercalatively bound species (two derived from intercalation by each of the two phi ligands, and the other two from their Δ and Λ isomers), each of which would likely have their own distinct sequence-selectivities.

Interestingly, insight into some aspects of sequence-specific binding and recognition by $[Rh(phi)_2X]^{3+}$ complexes is derived from an analysis of their DNA photocleavage products. Specifically, the level of asymmetric cleavage may represent the extent of canting or asymmetric binding by the complexes. Consistent with a model proposed for major groove binders[15], these complexes cleave with 5'-asymmetry as observed in their cleavage patterns on the oligonucleotide 5'-CTGGCA*T*GCCAG-3'. Particularly, strong cleavage is observed at T_7 of the 5'-$A_6T_7G_8C_9$-3' site, with significantly less cleavage at C_5 on the opposing strand. This suggests that the complex is highly canted towards T_7; interestingly, this asymmetry in cleavage is reflected in the partitioning of the oxygen dependent and independent cleavage products formed at this site. A greater percentage of oxygen-dependent product is formed at C_5 than at T_7, consistent with the understanding that canting towards T_7 would increase accessibility of dioxygen to C_5 on the complementary strand.

In comparison to the $[Rh(phi)_2X]^{3+}$ complexes, the $[Rh(phi)X_2]^{3+}$ complexes cleave DNA at specific sites that may be defined by consensus sequences. The $[Rh(phi)X_2]^{3+}$ complexes are C_2-symmetric about their single intercalating phi ligand,

which contributes to their greater sequence-specificity than the $[Rh(phi)_2X]^{3+}$ complexes. Furthermore, the non-intercalating ligands in the $[Rh(phi)X_2]^{3+}$ complexes are in close proximity to the DNA helix, making them sensitive probes to variations in sequence-dependent structure. In general, the derivatized $[Rh(phi)X_2]^{3+}$ and $[Rh(phi)_2X]^{3+}$ complexes cleave strongly at a subset of sites recognized by their respective parent complexes $[Rh(bpy)_2phi]^{3+}$ and $[Rh(phi)_2bpy]^{3+}$, implying that the basic recognition characteristics of the modified complexes are derived from their parent complexes. Steric and van der Waals interactions dominate the overall DNA specificities of $[Rh(phi)X_2]^{3+}$ complexes and hydrogen-bonding contacts appear to enhance their overall DNA affinities. Thus, while the complex $[Rh(4,4'\text{-diamidobpy})_2phi]^{3+}$ cleaves more strongly at sites recognized by $[Rh(bpy)_2phi]^{3+}$, the complexes $[Rh(4,4'\text{-diphenylbpy})_2phi]^{3+}$ and $[Rh(5,5'\text{-dimethylbpy})_2phi]^{3+}$ *cleave at a small subset* of sites recognized by the parent complex. Remarkably, the complex $[Rh(4,4'\text{-diphenylbpy})_2phi]^{3+}$ is highly specific for the palindromic sequence 5'-CTCTAGAG-3' (Figure 4.4) which, as described in chapter 5, is derived from its bulky shape and its ability to dimerize on the DNA helix through hydrophobic interactions. Interestingly, the complex $[Rh(5,5'\text{-dimethylbpy})_2phi]^{3+}$, in addition to recognizing some parent recognition sequences, also cleaves specifically at the 5'-A*G*T-3' sequence, which is not recognized by the parent complex $[Rh(bpy)_2phi]^{3+}$. This example points to the importance of van der Waals contributions from methyl groups in altering the recognition characteristics of $[Rh(phi)]^{3+}$ complexes.

Most of the strong sites, or the sites preferentially recognized by the $[Rh(phi)X_2]^{3+}$ complexes, are 5'-*py*-py-3' base steps with cleavage occurring at the highlighted pyrimidine. Specifically, most of the strong cleavage sites contain 5'-*C*T-3' steps (Figures 4.5 and 4.6), implying that these complexes prefer to intercalate at this particular base step. Interestingly, energy calculations[16a,b] and thermal melting studies[16c] have shown that 5'-py-py-3' steps, particularly 5'-CT-3', 5'-TT-3' and 5'-CC-3'

steps, are less favorably stacked than 5'-TG, 5'-CG and 5'-CA py-pu steps. Since the primary driving force for metal complex intercalation into DNA is the free energy gained through stacking interactions between the intercalating ligand and the DNA base-pairs, it is likely that the complex prefers to intercalate at relatively destacked base steps such as 5'-CT and 5'-CC steps.

To understand the specific structural factors that contribute towards sequence-specific recognition, it is necessary to differentiate between the DNA recognition properties of the Δ and Λ enantiomers of $[Rh(phi)]^{3+}$ complexes. The importance of specific van der Waals methyl-methyl interactions in governing DNA recognition is apparent in the enantioselective cleavage by $[Rh(5,5'\text{-dimethylbpy})_2phi]^{3+}$. Both the Δ and Λ enantiomers of this complex have their own unique set of preferred cleavage sites. Specifically, the Δ isomer cleaves strongly at the 5'-C*T*TG-3' site, while the Λ isomer cleaves strongly at 5'-A*C*TG-3' sites and at 5'-A*G*T-3' sites. Molecular modeling studies predict that the Δ isomer would bind preferentially to 5'-$C_1T_2T_3G_4$-3' and 5'-$C_1T_2G_3G_4$-3' sites with the thymine methyl groups (at positions 2 and/or 3) located at 4 Å van der Waals distances from the 5,5'-methyl groups of the intercalated Δ-$[Rh(5,5'\text{-dimethylbpy})_2phi]^{3+}$. Furthermore, modeling studies have also indicated that this isomer cannot bind to sites with sequences of the type 5'-$T_1N_2N_3A_4$-3' (N = py/pu) due to strong steric clashes between the thymine methyl groups (at positions 1 and 4), and the 5,5'-methyl groups of the intercalated complex. Conversely, the thymine methyl groups at positions 1 and 4 of sequences 5'-$A_1N_2N_3T_4$-3' are far enough from the methyl groups of the intercalated complex such that they neither introduce steric clashes, nor afford positive van der Waals interactions. Therefore, consistent with molecular modeling predictions, the cleavage data shows that the Δ isomer cleaves strongly at 5'-C*T*TG-3' sequences and moderately at 5'-C*T*GG-3' sequences (Figure 4.6 and Table 4.4). Similarly, molecular modeling studies show that the Λ isomer would bind preferentially

to 5'-$A_1N_2T_3N_4$-3' sequences, with the thymine methyls in positions 1 and 3 located at van der Waals distances from the 5,5'-methyls of the Λ isomer. Consistent with these predictions, the Λ isomer cleaves at 5'-A*C*TG-3' and 5'-A*G*T-3' sequences on the fragment shown (Figure 4.6) and cleaves moderately at 5'-A*T*AA sequences of other fragments (data not shown). These studies of the sequence-recognition of the Δ and Λ isomers of $[Rh(5,5'\text{-dimethylbpy})_2phi]^{3+}$ have demonstrated that *each enantiomer targets a specific consensus recognition sequence. The Δ isomer cleaves specifically at 5'-CNNG-3' sequences and the Λ isomer cleaves specifically at 5'-ANT-3' sequences* (where N = py/pu).

A comparison of the DNA sequence-selectivities of the Δ isomers of $[Rh(bpy)_2phi]^{3+}$ (**1a**), $[Rh(phen)_2phi]^{3+}$ (**2**) and $[Rh(5,5'\text{-dimethylbpy})_2phi]^{3+}$ (**1d**) shows that the 5,5'-methyl groups of complex **1d** are enhancing both its binding affinity and chiral discrimination due to a combination of both steric and van der Waals interactions. For $[Rh(phen)_2phi]^{3+}$ and $[Rh(bpy)_2phi]^{3+}$, only their Δ enantiomers cleave at the preferred 5'-py-py-3' and 5'-py-pu-3' sites, with little cleavage induced by their corresponding Λ enantiomers (Figure 4.6). In comparison, *both* the Δ and Λ enantiomers of $[Rh(5,5'\text{-dimethylbpy})_2phi]^{3+}$ show strong sequence-selectivities for DNA with each enantiomer having its own set of preferred sites. Specifically, Δ-$[Rh(5,5'\text{-dimethylbpy})_2phi]^{3+}$ only binds at a subset of sites recognized by the Δ isomers of **1a** and **2**, owing to the additional steric demands imposed by its ancillary 5,5'-dimethyl groups. This example points to how *negative* steric clashes can increase the sequence-specificity of $[Rh(phi)]^{3+}$ complexes. In comparison, the Λ-$[Rh(5,5'\text{-dimethylbpy})_2phi]^{3+}$ is strongly enantioselective for 5'-AGT and 5'-ACT sites which are correspondingly not recognized by the Λ isomers of **1a** and **2.** This result shows that likely stabilizing interactions between the methyl groups on the complex and thymine-methyl groups in DNA has enhanced the binding affinity and therefore specificity of the Λ isomer for

certain DNA sequences. Similarly, the importance of van der Waals interactions have been recently reported for the DNA recognition by the Δ and Λ isomers of $[Rh(ethylenediamine)_2phi]^{3+}$. The Λ isomer of this complex was found to prefer 5'-TA steps, likely due to interactions between thymine methyl groups and the methylene groups on the complex, while analogous interactions for the Δ isomer were not available owing to the right-handed helicity of DNA[17].

4.4.4. Shape-selective recognition of DNA by $[Rh(phi)]^{3+}$ complexes: implications.

This work, in conjunction with previous studies[5], illustrates that steric interactions dominate sequence-selective binding and reaction of $[Rh(phi)]^{3+}$ complexes to DNA. Since all these complexes bind in the major groove of DNA via intercalation of their phi ligand, they are well poised to detect subtle variations in local DNA structure. These studies have shown that the complex $[Rh(bpy)_2phi]^{3+}$ (**1a**) and its derivatives (**1b-d, 2**) are significantly more discriminating of sequence-dependent DNA structure than the complex $[Rh(phi)_2bpy]^{3+}$ (**3a**) and its derivatives (**3b-d, 4**). Thus, the complementarity between the shapes of these rhodium intercalators and DNA *primarily* governs the ability of these complexes to detect sequence-dependent DNA structure. Consistent with this notion of shape-selective recognition, the more sterically bulky complexes with methyl or phenyl groups on their ancillary bipyridyl ligands show the strongest sequence-specificities. Most of the derivative complexes *bind selectively at a subset of sequences* recognized by their respective parent complexes, which shows that the DNA recognition properties of these derivatives are dominated by the recognition characteristics of their parent complexes. Interestingly, the derivative complexes $[Rh(5,5'\text{-dimethylbpy})_2phi]^{3+}$ and $[Rh(phi)_2(5,5'\text{-dimethylbpy})]^{3+}$ also bind specifically at 5'-AGT-3' sequences which are not selectively recognized by their respective parent complexes. This points to the importance of specific van der Waals interactions between methyl groups on the

intercalated metal complex and methyl groups on DNA in determining the sequence-specific recognition of these metal complexes. Analogous to these $[Rh(phi)]^{3+}$ complexes, it is likely that DNA major-groove binding proteins utilize steric and van der Waals interactions to discriminate between sequence-dependent structures. The role that steric interactions and specifically methyl-methyl van der Waals interactions play in sequence-specific recognition has significant implications in the rational design of drugs. These studies suggest that one should take advantage of shape-selection in designing highly sequence-specific probes of DNA structure. One may be able to design DNA binding agents, based entirely on steric factors, which bind specifically to DNA sequences previously characterized by NMR or X-ray methods.

References

1. (a) Pabo, C. O. *Annu. Rev. Biochem.* **1992,** 61, 1053. (b) Steitz, T. *Q. Rev. Bioph.* **1990,** 23, 205. (c) Luisi, B. F.; Xu, W. X.; Otwinowski, Z.; Freedman, L. P.; Yamamoto, K. P., Siglar, P. *Nature* **1991,** 352, 497.
2. (a) Barton, J. K.; Danishefsky, A. T.; and Goldberg, J. M. *J. Am. Chem. Soc.* **1984,** 106, 2172. (b) Kumar, C. V.; Barton, J. K.; Turro, N. J. *J. Am. Chem. Soc.* **1985,** 107, 5518. (c) Fleisher, M. B.; Waterman, K. C.; Turro, N. J.; Barton, J. K. *Inorg. Chem.* **1986,** 25, 3549.
3. (a) Rehmann, J. P. and Barton, J. K. *Biochemistry* **1990,** 29, 1701. (b) Rehmann, J. P. and Barton, J. K. *Biochemistry* **1990,** 29, 1710.
4. (a) Mei, H.-Y. and Barton, J. K. *J. Am. Chem. Soc.* **1986,** 108, 7414. (b) Mei, H.-Y.; Barton, J. K. *Proc. Natl. Acad. Sci. U.S.A.* **1988,** 85, 1339.
5. (a) Pyle, A. M.; Long, E. C.; Barton, J. K. *J. Am. Chem. Soc.* **1989,** 111, 4520. (b) Pyle, A. M.; Morii, T.; Barton, J. K. *J. Am. Chem. Soc.* **1990,** 112, 9432. (c) Pyle, A. M.; Chiang, M. Y.; Barton, J. K. *Inorg. Chem.* **1990,** 29, 4487. (d) Sitlani, A.; Long, E. C.; Pyle, A. M.; Barton, J. K. *J. Am. Chem. Soc.* **1992,** 114, 2303.
6. David, S. and Barton, J. K. *J. Am. Chem. Soc.* **1993,** 115, 2984.
7. Chapter 3, this work.
8. (a) Gideney, P. M.; Gillard, R. D.; Heaton, B. T. *J. C. S. Dalton*, **1972**, 2621. (b) Dollimore, L. S. and Gillard, R. D. *Polyhedron* **1989,** 8, 1163. (c) Cartwright, P.

S.; Gillard, R. D.; Sillanpaa, E. R. J. *Polyhedron* **1987,** 6, 105.

9. Maniatis, T.; Fritsch, E. F.; Sambrook, J. *Molecular Cloning;* Cold Spring Harbor Laboratory: 1982.
10. All the $[Rh(phi)_2]^{3+}$ complexes studied were found to nick plasmid pUC18 DNA with comparable photoefficiencies. Furthermore, HPLC and gel-electrophoretic

analyses showed comparable extents of photocleavage of the oligonucleotide 5'-CTGGCATGCCAG-3' by these complexes.

11. Sluka, J. P.; Horvath, S. J.; Bruist, M. F.; Simon, M. I.; Dervan, P. B. *Science* **1987,** 238, 1129.

12. All the mono-phi $[Rh(phi)]^{3+}$ complexes studied were found to nick plasmid pUC18 DNA with comparable photoefficiencies.

13. Pyle, A. M.; Rehmann, J. P.; Meshoyrer, R.; Kumar, C. V; Turro, N. J.; Barton, J. K. *J. Am. Chem. Soc.* **1989,** 111, 3051.

14. Neidle, S. and Abraham, Z. *CRC Crit. Rev. Biochem.* **1984,** 17, 73.

15. Rhodium polypyridyl complexes are known to be potent photooxidants; we have shown[5d] that irradiation into a phi transition promotes preferential reactions of the phi ligand, likely through formation of a phi-cation radical.

16. (a) Crothers, D. M. and Ratner, D. I. *Biochemistry* **1968,** 7, 1823. (b) Ornstein, R. L.; Rein, R.; Breen, D. L.; MacElroy, R. D. *Biopolymers* **1978,** 17, 2341. (c) Gotoh, O. and Takashira, Y. *Biopolymers* **1981,** 20, 1033.

17. Krotz, A. H.; Kuo, L. Y.; Shields, T. P.; Barton, J. K. *J. Am. Chem. Soc.* **1993,** in press.

Chapter 5:

Eight Base-Pair Sequence-Specific Recognition by [Rh(4,4'-diphenylbpy)$_2$phi]$^{3+}$: Importance of Dimerization.

5.1. Introduction

Exploring the structural basis for sequence-specific recognition of DNA is central in understanding the molecular mechanisms involved in the repression and activation of gene expression[1]. For example, how do proteins that regulate the expression of genetic information bind to and discriminate among DNA sites with a high level of affinity and fidelity? While most small molecules and natural products bind in the minor groove of DNA, most proteins prefer to bind in the DNA major groove. It is not surprising that the major groove is more important for site-specific recognition by proteins, since the major groove of B-DNA is larger, more accessible, and importantly has more potential for hydrogen-bonding and hydrophobic contacts. This laboratory has attempted to understand protein-DNA recognition through the development of novel 9,10-phenanthrenequinonediimine(phi) complexes of rhodium(III) which bind sequence-selectively in the major groove of DNA[2]. Recent studies have shown that these complexes bind in the DNA major groove via intercalation of their phi ligand, and upon photoactivation cleave DNA through abstraction of the C3'-H atom[2d]. In this chapter we report on the DNA-binding properties of the metal complex [Rh(4,4'-diphenylbpy)$_2$phi]$^{3+}$ that specifically recognizes the palindromic sequence 5'-CTCTAGAG-3' both due to its shape and hydrophobicity and its ability to associate cooperatively through non-covalent dimerization on the DNA helix.

Previously, a comparison of the DNA-binding and recognition properties of the two complexes [Rh(phen)$_2$phi]$^{3+}$ and [Rh(phi)$_2$bpy]$^{3+}$ led us to understand that DNA recognition by [Rh(phi)]$^{3+}$ complexes is dominated by their *shapes*[2]. While

$[Rh(phen)_2phi]^{3+}$ is specific for sites that are more "open" in the DNA major groove, owing to potential steric clashes between its non-intercalated phenanthroline ligands and the DNA base-pairs, $[Rh(phi)_2bpy]^{3+}$ is sequence-neutral in its recognition, in spite of the possibility for hydrogen-bonding between its ancillary phi ligand and the DNA helix. Similarly, previous studies had suggested that the *shape and hydrophobicity* of the diphenylphenanthroline ligand is responsible for the specificity of $[Rh(diphenylphenanthroline)_3]^{3+}$ for unusual non B-DNA tertiary structures such as cruciforms[3a], Holliday junctions[3b], and introns[3c]. These studies prompted us to design and prepare the complex $[Rh(4,4'\text{-diphenylbpy})_2phi]^{3+}$ (Figure 5.1), that has both a phi ligand which can avidly intercalate into B-form DNA and has ancillary 4,4'-diphenylbpy ligands which could, owing to its hydrophobicity and bulky shape, be sensitive to sequence-dependent local structure along the DNA helix.

In Chapter 4 we showed that the complex $[Rh(4,4'\text{-diphenylbpy})_2phi]^{3+}$ cleaves DNA specifically at the eight base-pair palindromic sequence 5'-CTCTAGAG-3'. This remarkable sequence-specificity is comparable to DNA-binding proteins; therefore, we decided to explore the basis for this high level of DNA recognition. In this chapter we demonstrate, that like some DNA binding proteins, this metal complex achieves eight base-pair recognition by dimerizing on the DNA helix through hydrophobic interactions. Owing to its high level of specificity, the complex can compete with the restriction enzyme Xba1 for specific binding to 5'-CTCTAGAG-3' and thus inhibit enzymatic cleavage at this site.

5.2. Experimental

Materials: Calf thymus DNA was purchased from Sigma, and plasmid pUC18 was purchased from Boeringer-Mannheim. Phosphoroamidites and solid supports for oligonucleotide synthesis were obtained from Pharmacia. All enzymes utilized were

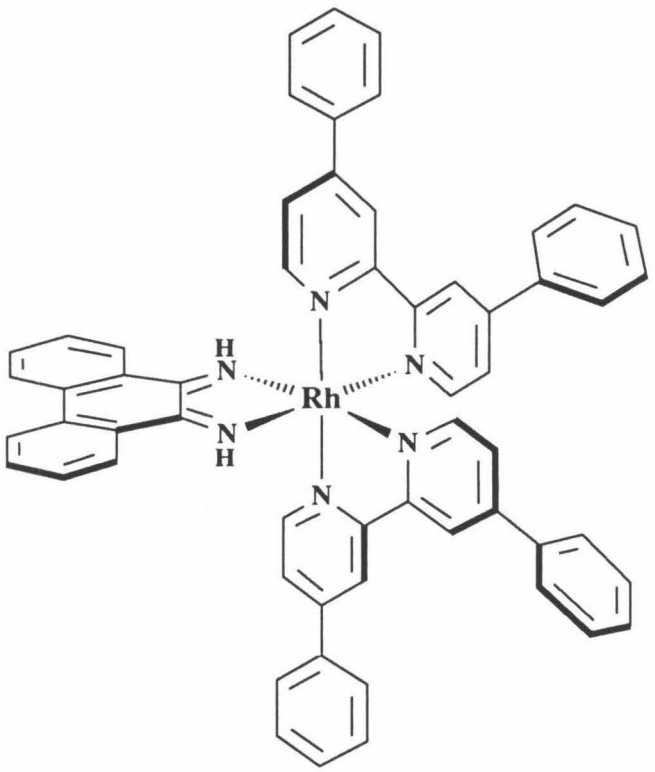

Figure 5.1. Structure of $[Rh(4,4'\text{-diphenylbpy } 2,2'\text{-bipyridyl})_2phi]^{3+}$; phi = 9,10-phenanthrenequinone diimine.

from commercial sources. The complex $[Rh(4,4'\text{-diphenylbpy})_2phi]^{3+}$ was synthesized as described in Chapter 3. MPE (methidium propyl EDTA) was a gift from the Dervan group.

Photocleavage of DNA restriction fragments and oligonucleotides: A 140 base-pair [5'-^{32}P]- and [3'-^{32}P]- end labeled EcoR1/PvuII fragment of pUC18 was prepared by standard methods[4]. The oligonucleotides 5'-GTGACTCTAGAGTCTATGACTCTAGTCT-3' and 5'-AGACTAGAGTCATAGACTCTAGAGTCAC-3' were synthesized on an ABI DNA synthesizer using phosphoramidite chemistry, labeled, and isolated using established protocols[4]. Cleavage reactions were carried out in 20 μl volumes using an Oriel Model 6140 1000 W Hg/Xe lamp fitted with a monochromater and a 300 nm cut off filter to avoid light damage to DNA. As described in Chapter 4, the irradiated reaction mixtures were analyzed by electrophoresis on polyacrylamide gels. The gels were exposed to a Molecular Dynamics phosphorimager screen and quantitation of cleavage was carried out using Molecular Dynamics ImageQuant software.

Footprinting assays: $[Rh(4,4'\text{-diphenylbpy})_2phi]^{3+}$ bound to DNA was footprinted using MPE-Fe^{2+} in the following way. Reaction mixtures containing 50 μM (in nucleotides) of linearized pUC18 plasmid in 50 mM Na-cacodylate buffer were incubated in the presence of rhodium complex (0.1 μM -> 2.0 μM) for 1 hr at RT, followed by 1 hr at 4°C. Subsequently, MPE-Fe^{2+} (final conc = 0.5 μM) and reducing agent sodium-ascorbate (final conc = 0.5 mM) were added to the reaction mixtures at 4°C. The reactions were allowed to proceed for 1 hr and quenched by ethanol precipitation.

Enzyme inhibition assays: Inhibition of restriction enzyme Xba1 hydrolytic cleavage by $[Rh(4,4'\text{-diphenylbpy})_2phi]^{3+}$ was carried out in the following way. Plasmid pUC18 was linearized with AlwN1 and purified by phenol/chloroform extractions and

ethanol precipitation. Linearized plasmid (LP) was incubated with rhodium complex in NE2 buffer (NE2 buffer = 10 mM Tris HCl, 10 mM $MgCl_2$, 50 mM NaCl, pH 7.9), keeping the ratio of nucleotide/Rh constant at 13:1. Specifically, a 200 μl reaction containing 6.5 μM nucleotide LP and 0.5 μM rhodium complex, and a 1000 μl reaction containing 1.3 μM nucleotide LP and 0.1 μM rhodium complex, were incubated in NE2 buffer at room temperature for 2 hr. Restriction enzyme Xba1 (~ 60 units) was added to the reaction mixtures, which were then incubated for 1 hr. The enzyme reaction was quenched by ethanol precipitation.

5.3. Results and Discussion

5.3.1. Sequence-Specificity of [Rh(4,4'-diphenylbpy)$_2$phi]$^{3+}$: Photocleavage and Footprinting Studies.

The DNA recognition properties of [Rh(4,4'-diphenylbpy)$_2$phi]$^{3+}$ were ascertained from its photocleavage patterns on a [3'-^{32}P]-end labeled EcoRI*-PvuII fragment from pUC18. At rhodium metal concentrations of 2 μM and below, specific photocleavage is observed at the highlighted cytosine in the self-complementary sequence 5'-CT*C*TAGAG-3', as shown in figure 5.2. Furthermore, specific cleavage is also observed at the corresponding cytosine on the complementary strand of this sequence (data shown in Chapter 4, Figure 4.4). Thus the overall cleavage pattern at this site is:

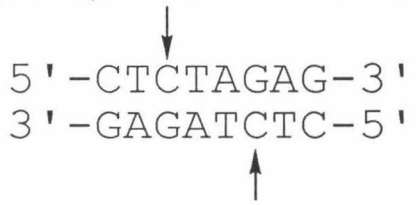

DNA photocleavage induced by [Rh(4,4'-diphenylbpy)$_2$phi]$^{3+}$ was also examined on other restriction fragments from pUC18 (data not shown); these studies revealed no strong cleavage sites. Importantly, the complex showed no cleavage at the sequences

Figure 5.2. Sequence-specific recognition of DNA by [Rh(4,4'-diphenylbpy)$_2$phi]$^{3+}$ (**1b**) as a function of rhodium concentration and irradiation time. Autoradiogram of an 8% polyacrylamide gel after photocleavage of a [3'-^{32}P]-end-labeled EcoR1/PvuII fragment from plasmid pUC18: Lane 1, Maxam-Gilbert C+T reaction; lane 2, untreated fragment; lane 3, fragment irradiated for 2 min in the absence of rhodium complex; lanes 4-8, [3'-^{32}P]-end-labeled fragment irradiated for 2 min in the presence of 1 μM, 2 μM, 3 μM, 4 μM and 5 μM rhodium complex, respectively; lanes 9-11, fragment irradiated in the presence of 5 μM rhodium complex for 30 sec, 1 min and 2 min, respectively; lanes 12-14, fragment irradiated in the presence of 1 μM rhodium complex for 2 min, 4 min and 8 min, respectively; lanes 15 and 16, fragment irradiated for 4 and 8 min in the absence of rhodium complex. Note that at 1 μM rhodium complex, specific cleavage at the highlighted cytosine in the 5'-CTCTAGAG-3' sequence is observed. Cleavage at this site is enhanced by increasing the irradiation time from 2 min to 8 min.

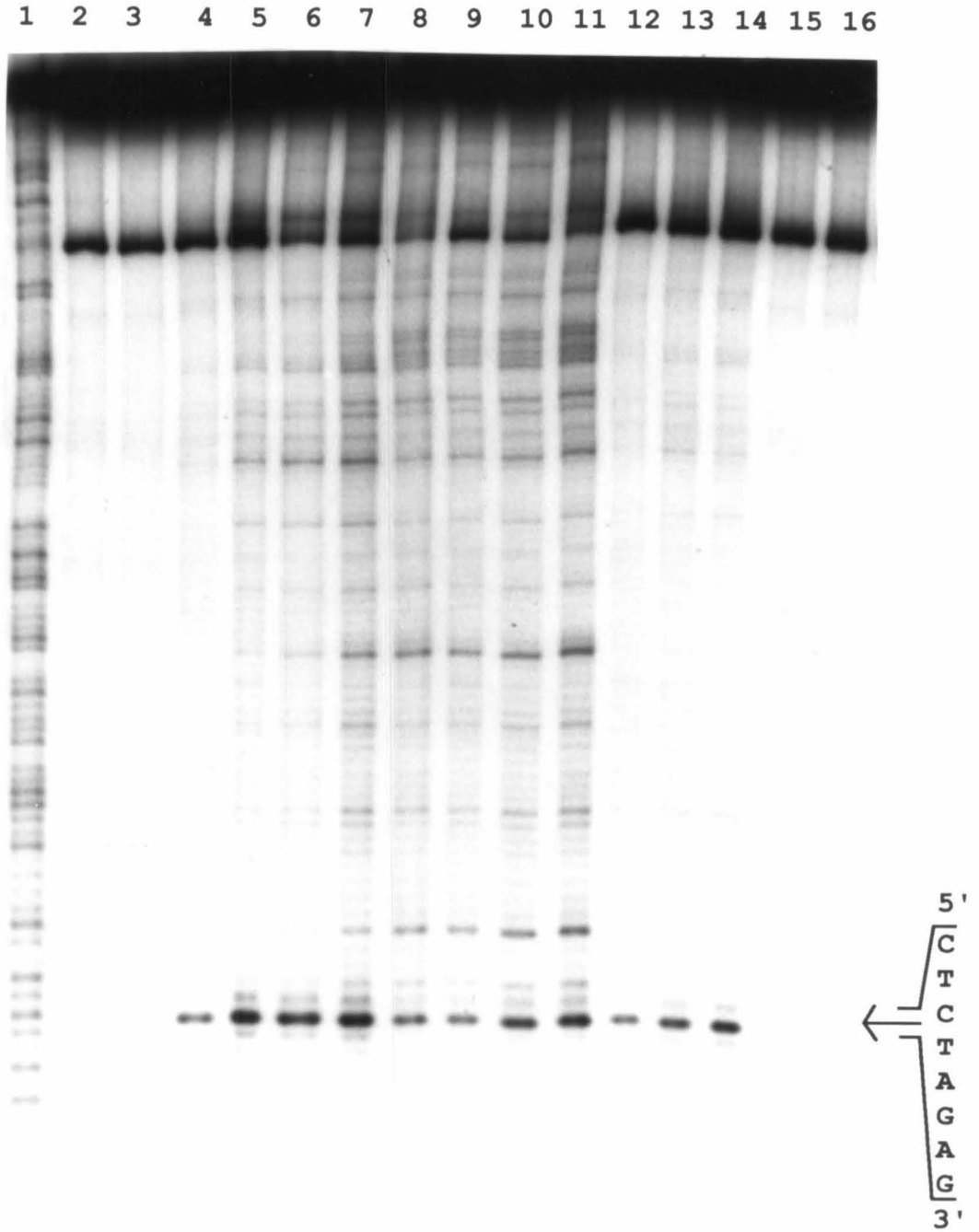
1 2 3 4 5 6 7 8 9 10 11 12 13 14 15 16
5'
C
T
C
T
A
G
A
G
3'

5'-CCCCAGGG-3' and 5'-TTCCGGAG-3', indicating that its recognition is not defined by the general 5'-py-py-*py*-py-pu-pu-pu-pu-3' consensus sequence.
Instead, the consensus recognition sequence for the complex *is* the specific eight base-pair 5'-CTCTAGAG-3' sequence.

This high level of sequence-specific photocleavage induced by the metal complex is reflected in its sequence-specific binding, as demonstrated by footprinting experiments. Footprinting is one of the most powerful assays used to visualize site-specific binding of proteins or small molecules to DNA. In this method, DNA is incubated with a sequence-specific DNA binding molecule of interest, followed by addition of a sequence-neutral cleaving agent. The presence of a bound molecule to DNA blocks the normal cleavage by the agent and one sees a blank spot or "footprint" in the position of DNA protected by the bound molecule. One of the most widely used footprinting agents is MPE-Fe^{2+} which contains methidium (which intercalates into the DNA minor groove in a relatively non-specific manner), tethered onto the reactive $[Fe(EDTA)]^{2-}$ species, which releases diffusible DNA cleaving hydroxyl radical species[5]. MPE-Fe^{2+} has been previously shown to determine accurately the binding locations and site sizes of both small molecules such as netropsin and distamycin, and of large proteins. Here we used the minor groove intercalator MPE-Fe^{2+} to footprint the DNA-bound rhodium complex, and the results are shown in Figure 5.3A.

As shown in Figure 5.3A and B, specific photocleavage by $[Rh(4,4'\text{-diphenylbpy})_2phi]^{3+}$ at the 5'-CTCTAGAG-3' site is associated with a distinct 3'-shifted footprint in the MPE-Fe^{2+} cleavage reaction. The schematic shown in Figure 5.3B is a composite of the footprint obtained on the [5'-^{32}P]-end labeled (Figure 5.3A) and on the [3'-^{32}P]-end labeled EcoR1/PvuII fragment (data not shown). According to a model (illustrated in Figure 5.3C) proposed by Dervan and coworkers, a 3'- or 5'- asymmetry in

Figure 5.3. Footprinting [Rh(4,4'-diphenylbpy)$_2$phi]$^{3+}$ (**1b**) bound to DNA using MPE-Fe^{2+}, (MPE = methidium propyl EDTA): correlation between DNA binding and photocleavage by the rhodium complex. **A.** Autoradiogram of an 8% polyacrylamide gel after photocleavage and footprinting reactions done on a [5'-^{32}P]-end-labeled EcoR1/PvuII fragment from pUC18: Lanes 1 and 2, Maxam-Gilbert A+G reaction and C+T reactions; lane 3, untreated fragment; lane 4, fragment irradiated for 8 min in the absence of rhodium complex; lane 5, fragment irradiated for 8 min in the presence of
1 μM [Rh(4,4'-diphenylbpy)$_2$phi]$^{3+}$; lanes 6-10, fragment incubated for 2 hr with 0 μM, 0.1 μM, 0.5 μM, 1.0 μM, and 0 μM rhodium complex, respectively, and subsequently reacted with 0.5 μM MPE-Fe^{2+}, 0.5 mM Na-ascorbate at 4°C for 60 min. Note that cleavage by the rhodium complex at the 5'-CTCTAGAG-3' site corresponds to a 3'-shifted footprint. **B.** Schematic representing the 3'-shifted footprinted region at the
5'-CTCTAGAG-3' site. The figure is a composite of the footprinted regions obtained on the [3'-^{32}P]- and [5'-^{32}P]- end-labeled EcoR1/PvuII fragment from pUC18. **C.** Model describing the cleavage patterns produced by a diffusible oxidant generated by a cleaving agent localized in the minor and major grooves of DNA. **D.** Schematic (adapted from reference 5) demonstrating that the footprinting agent MPE-Fe^{2+} generates diffusible hydroxyl radicals in the minor groove of DNA to produce 3'-shifted fooprints.

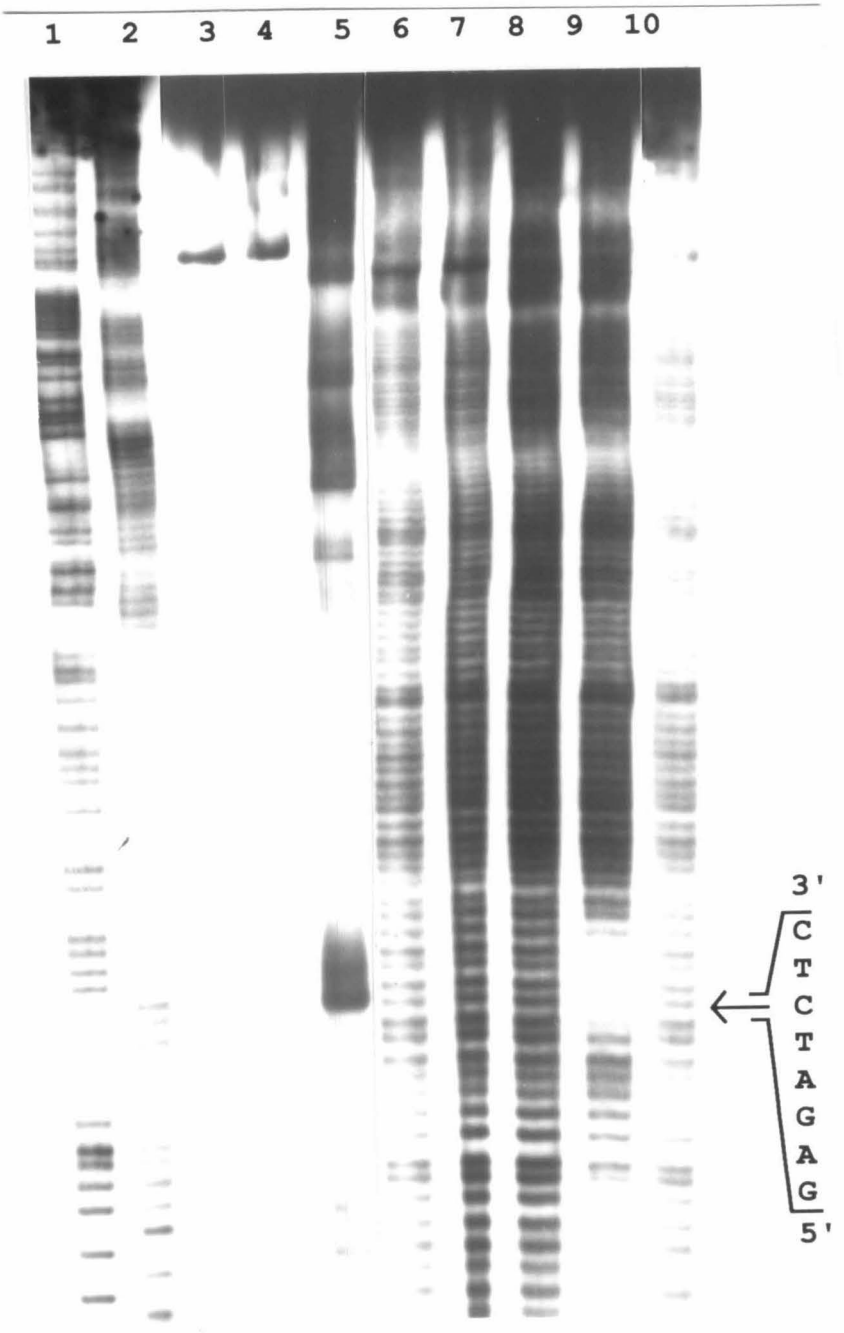
1
2
3
4
5
6
7
8
9
10
3'
C
T
C
T
A
G
A
G
5'

B

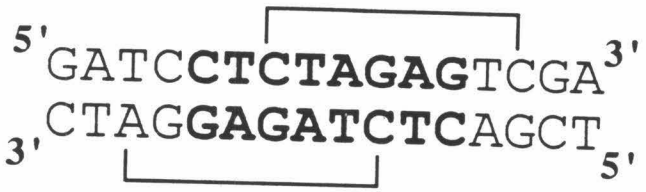
5' GATCCTCTAGAGTCGA 3'
3' CTAGGAGATCTCAGCT 5'

C

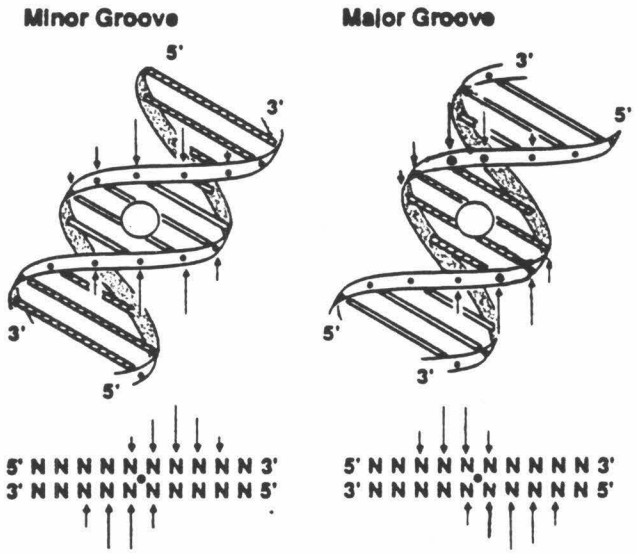
Minor Groove
Major Groove
5' NNNNNNNNNN 3'
3' NNNNNNNNNN 5'

D

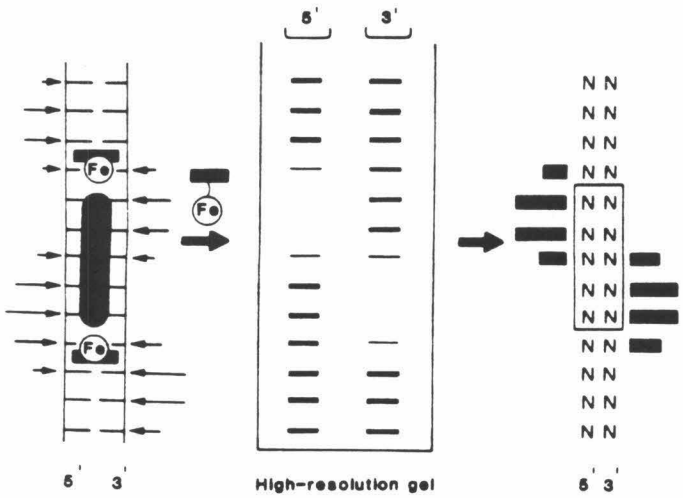
Fe
5'
3'
High-resolution gel
N N

the cleavage pattern by a diffusible species indicates that the DNA cleaving agent is bound in the minor or major groove, respectively. Thus, in the case of the minor groove footprinting agent MPE-Fe^{2+}, asymmetric cleavage protection shifted typically by two to three base-pairs towards the 3'-side of each strand is observed (as represented in Figure 5.3D). Similarly, as shown in Figure 5.3B, the footprint produced by the minor groove intercalator MPE-Fe^{2+} for the DNA-bound rhodium complex is also 3'-shifted by approximately two base-pairs on both strands. In this case, the efficacy in using the *minor groove* binding reagent MPE-Fe^{2+} to footprint the *major groove* binding rhodium complex also comes from the fact that both drugs are DNA *intercalators*, although they intercalate from opposite sides of the DNA helix. This is a clear illustration that specific DNA cleavage by the complex at the 5'-CTCTAGAG-3' sequence is associated with specific DNA *binding* at this site.

5.3.2. Recognition of the Eight Base-Pair Site 5'-CTCTAGAG-3' Sequence by $[Rh(4,4'\text{-diphenylbpy})_2phi]^{3+}$.

It is remarkable that this complex, based entirely on its sterically bulky shape, is able to recognize specifically the sequence-dependent structure associated with the 5'-CTCTAGAG-3' site. Interestingly, the 8 mer 5'-CTCTAGAG-3' site is a composite of two overlapping 6 mer 5'-CTCTAG-3' sequences located on opposing strands, which introduces the possibility that two rhodium complexes are *simultaneously* and *cooperatively* binding at the overlapping 5'-CTCTAG-3' sites of the composite 8 mer 5'-CTCTAGAG-3' site. This raises the question of whether the complex can discriminate the eight base-pair palindrome from an isolated six base-pair 5'-CTCTAG-3' site through dimerization on the DNA helix. Furthermore, if the complex is intercalating between the CT base step, it is also of interest to understand if it can distinguish the central four base-pair 5'-TCTA-3' sequence from the six base-pair 5'-CTCTAG-3' site.

To understand the sequence-specificity of $[Rh(4,4'\text{-diphenylbpy})_2phi]^{3+}$, photocleavage by the complex was examined on a 28 mer double-stranded oligonucleotide designed to contain the isolated 5'-CTCTAG-3' 6 bp site, the dimeric 5'-CTCTAGAG-3' eight base-pair site, and the 5'-TCTA-3' four base-pair site. The experiments reported here are carried out on racemic mixtures of the complex because initial attempts to resolve the enantiomers of $[Rh(4,4'\text{-diphenylbpy})_2phi]^{3+}$ using previously described (Chapter 4) ion-exchange chromatography with a chiral eluent were not successful. This complex is highly hydrophobic in nature and binds tightly to sephadex and dowex ion-exchange columns. However, it is likely that intercalation in the major groove of DNA is strongly preferred by the Δ isomer of this complex. Molecular modeling studies have indicated that intercalation by the Λ isomer of this complex in the major groove of DNA is sterically not feasible. Furthermore, as presented in Chapter 4, the Δ isomer of the parent complex $[Rh(bpy)_2phi]^{3+}$ cleaves strongly at this 5'-CTCTAGAG-3' site while no apparent cleavage is observed by the Λ isomer of $[Rh(bpy)_2phi]^{3+}$. More recently, separation of this complex into its enantiomers has been shown to occur on a DNA-cellulose column, where one enantiomer (the Δ isomer) is retained tightly to the DNA-column, while the Λ enantiomer elutes off the column. Interestingly, these preliminary observations are consistent with the complex binding to DNA in a strongly enantioselective manner where this sterically bulky complex may well be able to sense the right-handed helicity of B-form DNA. Thus, it is likely that specific intercalation of $[Rh(4,4'\text{-diphenylbpy})_2phi]^{3+}$ at the 5'-CTCTAGAG-3' site is favored by the Δ isomer of this complex.

The photocleavage patterns of $[Rh(4,4'\text{-diphenylbpy})_2phi]^{3+}$ on both strands of a [5'-^{32}P]-end labeled 28 mer oligonucleotide substrate containing the eight-mer, six-mer and four-mer sites is shown in figure 5.4. Cleavage at these sites was examined as a function of the absolute concentrations of rhodium and DNA, at a constant DNA to

rhodium ratio. This binding titration experiment shows that the complex cleaves specifically at both the isolated 5'-CT*C*TAG-3' six base-pair site, and the overlapping dimeric eight base-pair 5'-CT*C*TAGAG-3' sequence containing two overlapping six bp sites. Little cleavage is apparent at the four base-pair 5'-TCTA-3' site. Importantly, at low concentrations (≤ 0.5 μM) of rhodium and DNA, preferential cleavage is observed at each of the two dimeric 5'-CTCTAG-3' half-sites on strand I and II of the palindromic eight base-pair site over the isolated six base-pair site.

The photocleavages at the eight-mer half-sites, six-mer and four-mer sites may be quantitated precisely using the phosphoroimager to examine the extent of cooperativity in binding at the eight-mer half-site over the six-mer site. The results are quantitated and represented as a semilogarithmic plot of the photocleavage values (normalized for the counts loaded per lane) at each site as a function of total rhodium concentration (Figure 5.5A). At rhodium concentrations ≥ 0.5 μM, saturation of photocleavage at the six-mer and eight-mer sites occurs, indicating that at these concentrations all the rhodium complex is bound. Furthermore, HPLC experiments have shown that under the irradiation conditions (1 hr at 310 nm) of the experiment, complete photoanation of the complex is observed at these concentrations. This shows that at each condition in the experiment, we are not limited by the photons emitted for the total irradation time, nor are we limited by the rate of photon absorption by the rhodium complex at each concentration used. Therefore, below saturation of binding, we assume a constant photoefficiency of reaction at the rhodium concentrations used in the experiment. Thus, based upon relative photocleavage values, the concentrations of *bound rhodium complex* can be ascertained at each site and for every condition used in the experiment.

A comparison of the fraction of rhodium bound at each site (θ), based upon these photocleavage experiments, as a function of total rhodium concentration, is represented in the semilogarithmic plots in Figure 5.5b and c. The titration data for the 8 mer half-sites

and the isolated 6 mer site represent binding curves, from which the dissociation constants (K_d) can be estimated by locating the point of inflection. Similar derivations of free energy for oligonucleotide directed triplex formation have been made using a quantitative affinity cleavage titration[6,7]. The data were fit to the binding expression,

$$\theta = K_d(Rh)_t / [1 + K_d(Rh)t]$$

where K_d = dissociation constant; $(Rh)_t$ = total Rhodium concentration; θ = fraction of bound rhodium concentration at site, to obtain binding affinities for the 8 mer half sites and the 6 mer site as:

$$K_a(\text{eight-mer half-site}) = 5 \pm 0.6 \times 10^6\ M^{-1} \text{ and}$$

$$K_a(\text{six-mer site}) = 2 \pm 0.5 \times 10^6\ M^{-1}.$$

This enhancement in binding affinity of the metal complex for the 5'-CTCTAG-3' sites contained in the 8 mer 5'-CTCTAGAG-3' site as compared to the isolated 5'-CTCTAG-3' site, suggests that two bound rhodium complex molecules are cooperatively interacting with one another to afford added stabilization energy by binding as a dimer to the 8 mer 5'-CTCTAGAG-3' site. Dimerization between two bound rhodium complexes intercalated at the 5'-CTCTAGAG-3' site may be derived from π stacking and/or van der Waals interactions between the diphenyl and bipyridyl rings of adjacent complexes. These results show that the metal complex is able to recognize the local structure associated with the six base-pair site 5'-CTCTAG-3' with high affinity and fidelity. Furthermore, the two overlapping six base-pair sites that generate the eight base-pair palindrome 5'-CTCTAGAG-3' are recognized preferentially through dimerization between 2 complexes on the DNA helix.

Figure 5.4. Sequence-specific recognition of the eight base-pair 5'-CTCTAGAG-3' site by [Rh(4,4'-diphenylbpy)$_2$phi]$^{3+}$ (**1b**). Autoradiogram of an 8% polyacrylamide gel after photocleavage of a [5'-^{32}P]-end-labeled 28 mer double-stranded oligonucleotide containing the eight base-pair 5'-CTCTAGAG-3', six base-pair 5'-CTCTAG-3' and four base-pair 5'-TCTA-3' sites shown where,
Strand I of 28 mer oligo: 5'-GTGACTCTAGAGTCTATGACTCTAGTCT-3'
Strand II of 28 mer oligo: 5'-AGACTAGAGTCATAGACTCTAGAGTCAC-3'.
Lanes 1-9 and lanes 10-18 represent photocleavage reactions on the 28 mer double-stranded oligonucleotide containing 5'-[^{32}P]-end-labeled strand I and 5'-[^{32}P]-end-labeled strand II, respectively. Lanes 1 and 10, Maxam-Gilbert A+G reaction; lanes 2 and 11, Maxam-Gilbert C+T reaction; lanes 3 and 12, 28-mer oligonucleotide irradiated for 30 min in the absence of rhodium complex; lanes 4-9 and lanes 13-18, 28-mer oligonucleotide irradiated in the presence of 5.0 μM, 1.0 μM, 0.5 μM, 0.3 μM, 0.1 μM and 0.05 μM rhodium complex, respectively, where the DNA-duplex to Rh ratio is kept constant at 2, for each condition. Note that at Rh concentrations of 0.1 μM and 0.05 μM, cleavage at both 5'-CTCTAG-3' sites on strand I and II, contained in the palindromic 5'-CTCTAGAG-3' sequence, is stronger than cleavage at the isolated 5'-CTCTAG-3' site contained on strand I. Furthermore, only weak cleavage is observed at the four base-pair 5'-TCTA-3' site.

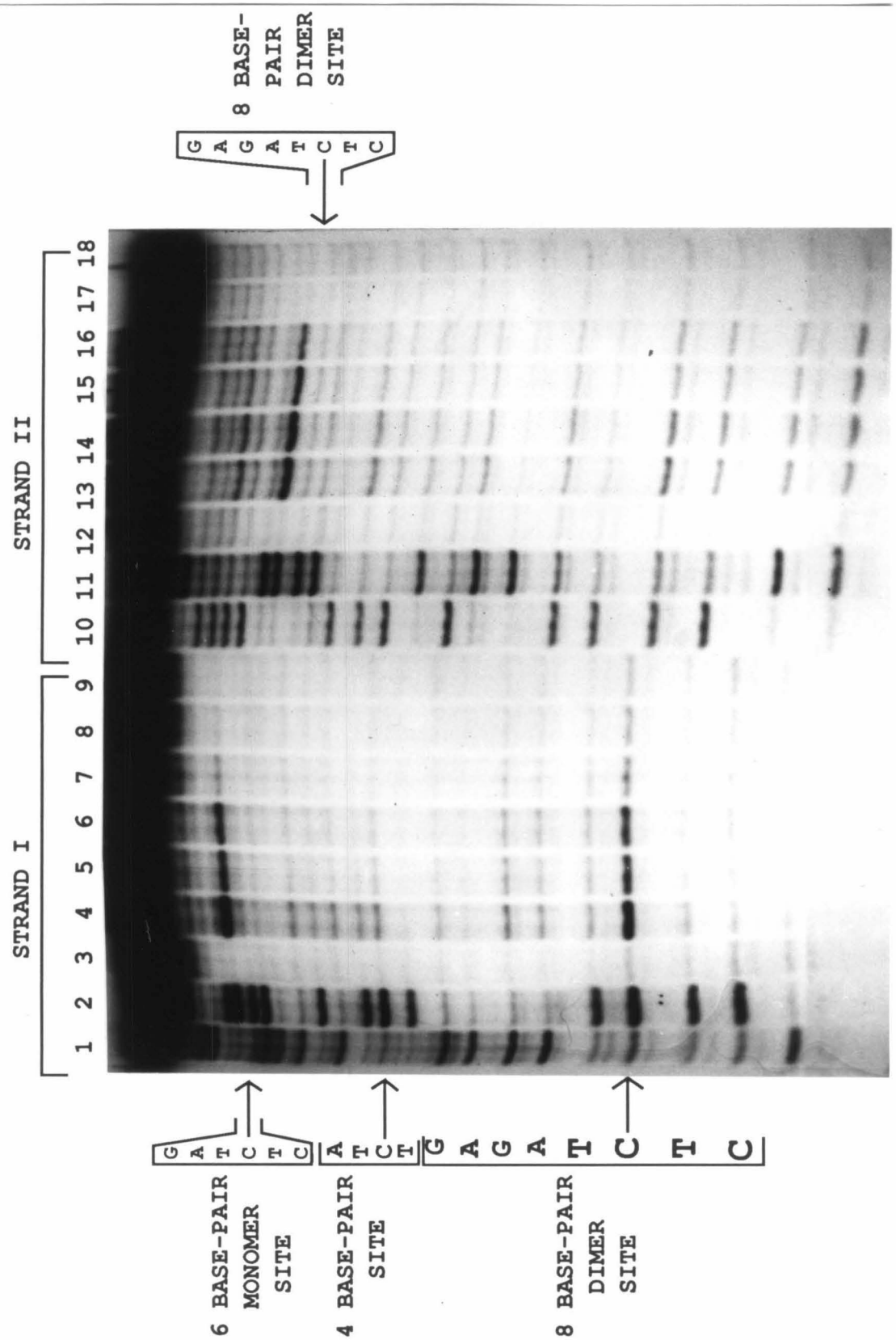
STRAND I
STRAND II
1 2 3 4 5 6 7 8 9 10 11 12 13 14 15 16 17 18
G A G A T C T C
8 BASE-PAIR DIMER SITE
G A T C T C
6 BASE-PAIR MONOMER SITE
A T C T
4 BASE-PAIR SITE
G A G A T C T C
8 BASE-PAIR DIMER SITE

Figure 5.5. Comparison of the binding affinity of $[Rh(4,4'\text{-diphenylbpy})_2phi]^{3+}$ for the eight-mer 5'-CTCTAGAG-3', six-mer 5'-CTCTAG-3' and four-mer 5'-TCTA-3' sequences. **A.** Schematic of the oligonucleotide substrate containing the eight-mer, six-mer and four-mer sites. **B.** A semilogarithmic plot of the percent photocleavage as a function of total rhodium concentration (Rh_t). Note that at low concentrations, cleavage at the eight-mer half-site is preferred over the six-mer site. At concentrations ≥ 5 μM, saturation of cleavage at the eight-mer half-site and six-mer sites is observed. **C.** A semilogarithmic plot of θ (θ = fraction of total rhodium bound at each site) as a function of total rhodium concentration (Rh_t). The concentration of bound rhodium complex at each site is determined from the cleavage data (shown in Figure 5.4), as described in the text. The K_d (dissociation constant) can be estimated by locating the inflection point in the semilog plot.

A

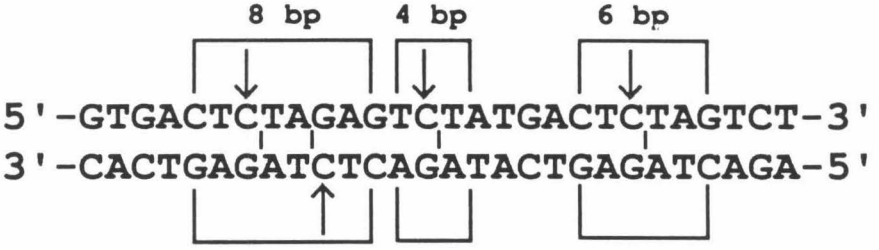
8 bp
4 bp
6 bp
5'-GTGACTCTAGAGTCTATGACTCTAGTCT-3'
3'-CACTGAGATCTCAGATACTGAGATCAGA-5'

B

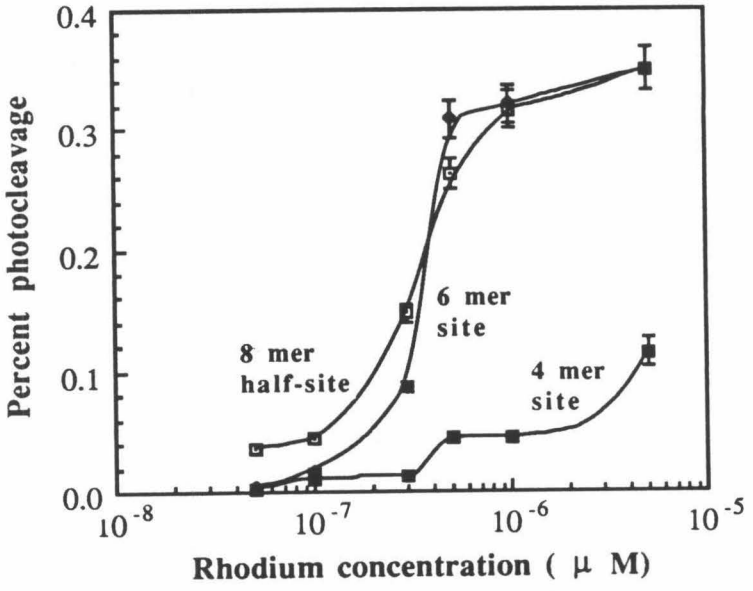
Percent photocleavage
0.4
0.3
0.2
0.1
0.0
8 mer
half-site
6 mer
site
4 mer
site
10^-8
10^-7
10^-6
10^-5
Rhodium concentration (μ M)

C

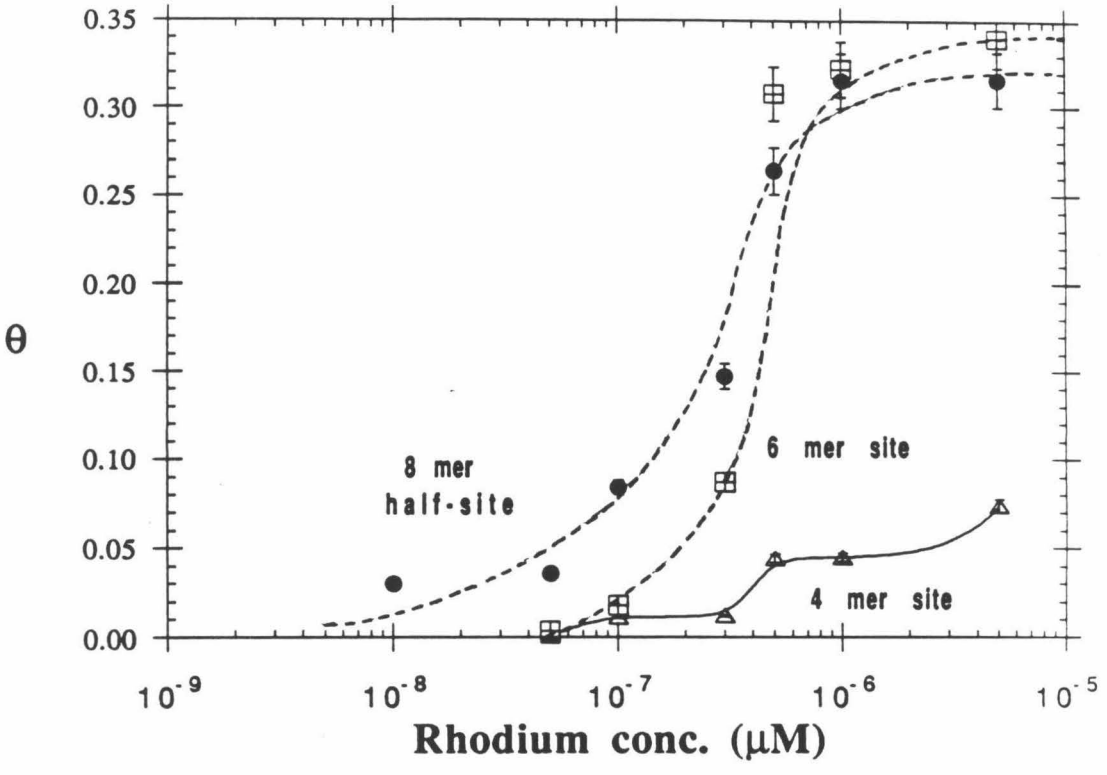

Ka (8 mer half-site)= 5.0 ± 0.6 x 10^6 M^{-1}
Ka (6 mer site) = 2.0 ± 0.3 x 10^6 M^{-1}

5.3.3. Enzyme Inhibition by $[Rh(4,4'\text{-diphenylbpy})_2phi]^{3+}$.

Owing to the high level of specificity of the complex for the 5'-CTCTAGAG-3' site, experiments to compare the specificity and affinity of $[Rh(4,4'\text{-diphenylbpy})_2phi]^{3+}$ with that of restriction enzymes were conducted. The restriction endonuclease Xba1 is specific for the sequence 5'-TCTAGA-3', contained in the eight base-pair palindromic site 5'-CTCTAGAG-3'. Therefore, experiments to probe inhibition of Xba1 cleavage by the rhodium complex were conducted. These experiments were carried out on linearized pUC18 plasmid, which contains one copy of the 5'-CTCTAGAG-3' site. Linearized pUC18 was first incubated with the rhodium complex (at a ratio of DNA nucleotides to rhodium = 13:1), followed by incubation with the enzyme Xba1. Hydrolytic cleavage of the linearized 2687 mer by Xba1 into a 1890 mer and 797 mer was viewed on agarose gels, as shown in Figure 5.6. Importantly, the extent of enzyme inhibition depended on both the ratio of DNA nucleotides to rhodium complex, and the absolute concentration of rhodium complex. Complete inhibition of Xba1 cleavage is observed at 0.5 μM rhodium (concentration above its K_d), while partial inhibition is observed at 0.1 μM rhodium (concentration in the range of its K_d). Furthermore, the DNA to rhodium ratio was also important, since all the 5'-CTCTAGAG-3' sites in solution need to be occupied with bound rhodium complex, for inhibition of enzyme induced cleavage to occur.

Inhibition of enzyme cleavage by the rhodium complex does not necessarily imply that the complex is competing with the enzyme for binding to DNA. The complex may instead be binding to or inducing a conformational change in the enzyme, which may cause this loss of enzyme activity. To confirm that inhibition of enzymatic cleavage is induced by the rhodium complex, two controls experiments were carried out. Firstly, as shown in Figure 5.6, the complex $[Rh(4,4'\text{-diphenylbpy})_2phi]^{3+}$ shows no significant inhibitory effect on the hydrolytic cleavage induced by the restriction enzymes Sca1 (lanes 9 and 10) and Ssp1 (data not shown), which cleave at sites not recognized by the

rhodium complex. This suggests that the complex is not binding to the enzyme Xba1 to induce inhibition but, instead, is actually competing with Xba1 for binding to DNA. Furthermore, the *sequence-neutral* complex $[Rh(phi)_2bpy]^{3+}$ has no inhibitory effect on Xba1 enzyme cleavage; this further confirms the finding that the *sequence-specific* complex $[Rh(4,4'\text{-diphenylbpy})_2phi]^{3+}$ is able to induce enzyme inhibition by competing with the enzyme for binding to the 5'-CTCTAGAG-3' site. Thus, the experiments described here show that the *complex* $[Rh(4,4'\text{-diphenylbpy})_2phi]^{3+}$ *sequence-specifically competes with the enzyme for binding to DNA, and thereby inhibits enzyme cleavage*. Importantly, this result also indicates that the rate at which the complex $[Rh(4,4'\text{-diphenylbpy})_2phi]^{3+}$ dissociates from the 5'-CTCTAGAG-3' site is slow enough to prevent competitive displacement of the complex by the restriction enzyme Xba1. The ability of the complex to compete with proteins for binding to DNA has important implications in that it underscores its potential usage as a highly sequence-specific drug. Thus, this experiment shows that a synthetic and hydrophobic metal complex is able to bind to DNA with a level of specificity that rivals DNA-binding proteins. The complex derives its unusual specificity from its bulky shape, which precludes binding at most sequences, and its ability to dimerize cooperatively on the DNA helix through hydrophobic interactions.

5.3.4. Modeling Studies.

Modeling two Δ isomers of $[Rh(4,4'\text{-diphenylbpy})_2phi]^{3+}$ at the 5'-CTCTAGAG site suggests the possibility for hydrophobic interactions between the non-intercalated 4,4'-diphenylbpy ligands on each of the two bound complexes. We propose that two molecules of Δ-$[Rh(4,4'\text{-diphenylbpy})_2phi]^{3+}$ are able to dimerize on the DNA through non-covalent hydrophobic interactions, and thereby preferentially bind to the eight base pair site over the six base-pair site. The results reported here indicate that like

Figure 5.6. $[Rh(4,4'\text{-diphenylbpy})_2phi]^{3+}$ as an inhibitor of restriction enzyme Xba1 induced DNA cleavage at the 5'-CTCTAGAG-3' site of plasmid pUC18. Lane 1, 123 bp markers; lane 2, plasmid pUC18 that has been linearized with restriction enzyme AlwN1; lanes 3 and 4, Xba1 induced cleavage of linearized pUC18 in the absence and presence of 0.5 μM $[Rh(4,4'\text{-diphenylbpy})_2phi]^{3+}$, respectively; lanes 5 and 6, Xba1 induced cleavage of linearized pUC18 in the absence and presence of 0.1 μM $[Rh(4,4'\text{-diphenylbpy})_2phi]^{3+}$, respectively; lanes 7 and 8, Xba1 induced cleavage of linearized pUC18 in the absence and presence of 0.1 μM $[Rh(phi)_2bpy]^{3+}$, respectively; lanes 9 and 10, restriction enzyme Sca1 induced cleavage of linearized pUC18 in the absence and presence of 0.1 μM $[Rh(4,4'\text{-diphenylbpy})_2phi]^{3+}$. Note that cleavage of the linear DNA (2687 mer) by Xba1 into smaller fragments (1890 and 797 mers) is inhibited in the presence of $[Rh(4,4'\text{-diphenylbpy})_2phi]^{3+}$ (lanes 4 and 6), but not in the presence of the metal complex $[Rh(phi)_2bpy]^{3+}$ (lanes 7 and 8). Furthermore, the complex $[Rh(4,4'\text{-diphenylbpy})_2phi]^{3+}$ does not inhibit Sca1 cleavage.

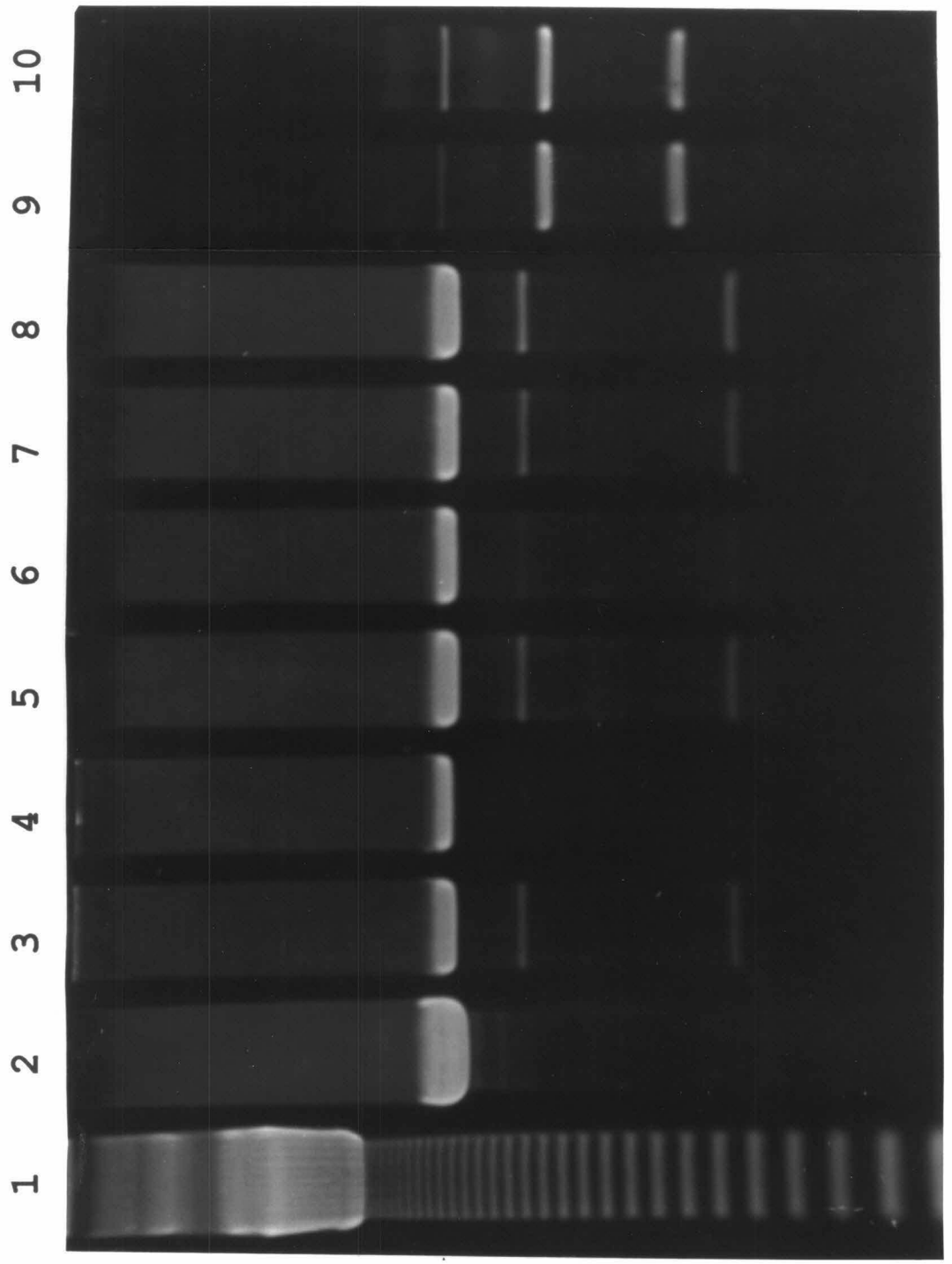
1
2
3
4
5
6
7
8
9
10

DNA-binding proteins, the metal complex $[Rh(4,4'\text{-diphenylbpy})_2phi]^{3+}$ uses dimerization as a tool to enhance its specificity and binding affinity to DNA. Figure 5.7 is a model which describes the binding of two rhodium complex molecules to the 5'-CTCTAGAG-3' site. We propose that each rhodium complex intercalates between the central CT step of the 5'-CTCTAG-3' site by canting to the C-strand of the helix. This canting model is supported by the observation that the complex induces specific photocleavage at the C of this CT base step with no corresponding cleavage in a 5'-direction at the complementary A. Canting positions the two complexes at a relative distance from one another so as to promote positive hydrophobic interactions between the phenyl groups of one complex and the bipyridyl rings of the adjacent complex. This double stacking interaction between the phenyl and bipyridyl rings of adjacent complexes could occur across the central CTAG site,which is the overlapping region for the two monomeric CTCTAG sites located on complementary strands. Interestingly, this central CTAG site is contained in the recognition sequences of several DNA-binding transcription factors and nucleases. There is increasing evidence in the literature that suggests that the conformationally distorted backbone at the CTAG site provides a recognition signal for several DNA-binding proteins[8,9,10]. Therefore, we propose that a similar structural distortion at the CTAG site is recognized by the *shape selective* metal complex $[Rh(4,4'\text{-diphenylbpy})_2phi]^{3+}$ and that this unusual backbone conformation may promote simultaneous and cooperative binding of two metal complexes at this site.

5.3.5. Comparisons to DNA-Binding Proteins.

The crystal structures of the *E.coli trp* repressor- and *E.coli met* repressor-operator complexes[9,10] support the notion that the distorted phosphate backbone at the CTAG site is providing the structural motif for recognition by proteins. Important *trp*

Figure 5.7. CPK model illustrating the intercalation of two molecules of Δ-[Rh(4,4'-diphenylbpy)$_2$phi]$^{3+}$ at an unwound eight base-pair 5'-CTCTAGAG-3' site. The figure shows that phenyl groups (marked in purple) attached to the non-intercalated bipyridyls provide a hydrophobic surface for potential van der Waals interactions between the adjacently bound rhodium complexes. Note that while one molecule of the metal complex is canted to the DNA strand marked in white, the other molecule is in closer contact with the DNA strand marked in aqua.

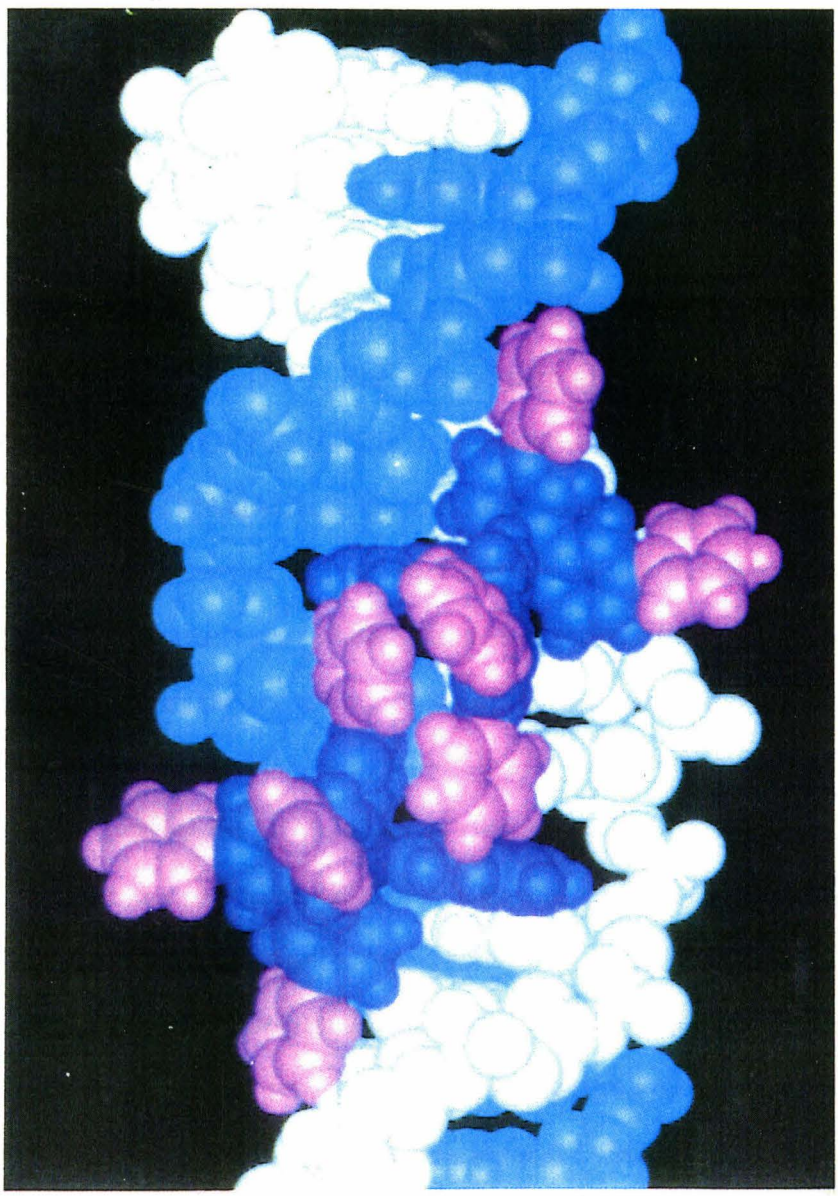

repressor-phosphate interactions involve the two CTAG segments of the operator sequence TGTACTAGTTAACTAGTAC. No direct hydrogen-bonding or nonpolar interactions to the bases are observed in the *trp* repressor/operator complex; therefore, it has been proposed that the locally stable conformation of the CTAG site represents a *specific shape* that the *trp* repressor is best able to recognize and bind. Similarly, the recently solved crystal structure[10] of the *E. coli met* repressor-operator complex provides further evidence for recognition of sequence-dependent distortions or flexibility of the phosphodiester backbone at the 5'-CTAG-3' site. Sequence specificity by the *met* repressor is achieved by insertion of double-stranded antiparallel protein β-ribbons into the major groove of B-form DNA. The 19 base-pair oligonucleotide 5'-TT[AGACGTCT][AGACGTCT]A-3' in the *met*-operator crystal structure contains two copies of the "met box" (AGACGTCT) with a central 5'-CTAG site. While each *met* box is recognized by direct interactions between amino acid side chains and base-pairs, there is evidence of indirect readout or *shape selection* of the displaced G10' phosphate of the CTAG sequence, across the central boundary of the *met* boxes. Furthermore, the central bases of the *met* box, C4 and G5 make no direct contacts to the protein, but form the center of the 25º bend in the DNA, which allows it to wrap tightly round the repressor. Therefore, like the *met* repressor, $[Rh(4,4'\text{-diphenylbpy})_2phi]^{3+}$ may also be recognizing the overall structure associated with, possibly, an inherently bent 5'-CTCTAGAG site. Importantly, *like the metal complex* $[Rh(4,4'\text{-diphenylbpy})_2phi]^{3+}$ *described here, both the trp and the met repressor proteins are also recognizing the unusual shape associated with the 5'-CTAG-3' sequence.* Furthermore, the *met*-DNA crystal structure shows that the *met* dimerization domain contains β-sheets which lie across the central CTAG site. Similarly, we propose that binding two $[Rh(4,4'\text{-diphenylbpy})_2phi]^{3+}$ complexes to DNA involves dimerization through their non-intercalating diphenylbpy ligands across the central CTAG site. Based on these observations it is tempting to conclude that the

distorted conformation at the CTAG site provides a flexible pocket that is able to accommodate dimerization domains.

The results described here point to the importance of hydrophobic interactions in sequence-specific recognition of DNA. The metal complex $[Rh(4,4'\text{-diphenylbpy})_2phi]^{3+}$ (phi = phenanthrenequinone diimine), which binds in the major groove of DNA via intercalation of its phi ligand, specifically recognizes the eight base-pair sequence 5'-CTCTAGAG-3'. Owing to its shape and hydrophobicity, the complex has a high level of specificity and affinity that allows it to inhibit hydrolytic cleavage by the restriction endonuclease XbaI. We propose that two molecules of the rhodium complex bind cooperatively by dimerizing, through hyrophobic interactions, on the DNA, to recognize the self-complementary eight base-pair site. This study underscores the importance of *shape-selection* and non-covalent dimerization in the development of highly sequence-specific DNA binding drugs.

References and Footnotes

1. (a) Pabo, C. O. and Sauer, R. T. *Annu. Rev. Biochem* **1992,** 61, 1053. (b) Steitz, T. Q. *Q. Rev. Bioph.* **1990,** 23, 205.
2. (a) Pyle, A. M.; Long, E. C.; Barton, J. K. *J. Am. Chem. Soc.* **1989,** 111, 4520. (b) Pyle, A. M.; Morii, T.; Barton, J. K. *J. Am. Chem. Soc.* **1990,** 112, 9432. (c) Pyle, A. M.; Rehmann, J. P.; Meshoyrer, R.; Kumar, C. V.; Turro, N. J.; Barton, J. K. *J. Am. Chem. Soc.* **1989,** 111, 3051. (d) Sitlani, A.; Long, E. C.; Pyle, A. M.; Barton, J. K. *J. Am. Chem. Soc.* **1992,** 114, 2303.
3. (a) Kirshenbaum, M. R.; Tribolet, R.; Barton, J. K. *Nuc. Acids Res.*, **1988**, 16, 7948. (b) Waldron, K.; Voulgaris, J.; Barton, J. K., unpublished results. (c) Lee, I. and Barton, J. K. *Biochemistry* **1993,** in press.
4. Maniatis, T.; Fritsch, E. F.; Sambrook, J. *Molecular Cloning;* Cold Spring Harbor Laboratory: 1982.
5. (a) Hertzberg, R. P. and Dervan, P. B. *Biochemistry* **1984,** 23, 3934 (b) Dervan, P. B. *Science* **232,** 464.
6. Singleton, S. and Dervan, P. B. *J. Am. Chem. Soc.***1992,** 114, 6957.
7. Binding Constants: The Measurement of Molecular Complex Stability. Connors, K. A. **1987**, John Wiley and Sons, Inc.
8. Fairall, L.; Martin, S.; Rhodes, D. *EMBO J.* **1989**, 8, 1809.
9. Otwinowski, Z.; Schevitz, R. W.; Zhang, R.-G.; Lawson, C. L.; Joachimiak, A.; Marmorstein, R. Q.; Luisi, B. F. and Siglar, P. B. *Nature* **1988,** 335, 321.
10. Somers, W. S. and Phillips, S. E. V. *Nature* **1992,** 359, 387-393.

Chapter 6:

Conclusions and Perspectives.

Understanding the mechanism by which proteins recognize DNA and RNA through a variety of non-covalent interactions, is a central goal in biochemical research today. Several processes central to a living cell, such as the expression and translation of genetic material and DNA repair, occur as a result of site-specific protein-nucleic acid interactions. Site-specific recognition of DNA is clearly not a simple feat, given the rich local structure of linear DNA and the various folded tertiary forms in which DNA has been shown to exist. Nature has thus fulfilled a herculean task by constructing a plethora of proteins which recognize specific nucleic acid sites. In the work described here, we have used simple DNA-binding rhodium(III) complexes as model systems to unravel some of the basic principles governing protein-DNA recognition.

Like most DNA binding proteins, the octahedral $[Rh(phi)]^{3+}$ complexes (phi = 9,10 - phenanthrenequinone diimine) studied here also bind in the *major* groove of DNA and recognize variations in sequence-dependent structure along the DNA helix. These metal complexes bind very tightly to DNA by intercalation of the phi ligand, which brings their non-intercalating ligands interact in close contact with DNA base-pairs above and below the intercalation site; thus, these complexes are well poised to detect subtle variations in local DNA structure. The studies presented here highlight the importance of steric and van der Waals interactions in achieving high levels of sequence-specificity. Specifically, the complementarity in shape between the metal complex and the nucleic acid binding site is crucial in achieving site-specific binding.

Interestingly, one $[Rh(phi)]^{3+}$ analog described in this work is specific for the local structure associated with the eight base-pair 5'-CTCTAGAG-3' site. The complex achieves this level of specificity based primarily on its shape, and also due to its ability to dimerize on the DNA helix. Similarly, several DNA-binding transcription factors also

achieve significant levels of specificity through dimerization. Thus, remarkably, this complex has used one of nature's tricks to achieve eight base-pair recognition through non-covalent dimerization. Thus, we have shown that the specificity of a simple and small inorganic metal complex, based entirely on steric and van der Waals interactions, can rival that of large DNA binding proteins.

The octahedral and coordinatively saturated $[Rh(phi)]^{3+}$ complexes studied here are unique in that they bind in the *major* groove of DNA, unlike most other small molecules and natural products which bind in the *minor* groove of DNA (Table 6.1). Furthermore, these metal complexes, unlike minor groove binding small molecules, are extremely sensitive to sequence-dependent structure. Indeed, the major groove of DNA has more potential for hydrogen bonding and hydrophobic contacts; therefore, it is not surprising that major groove binders can achieve a high levels of sequence-specificity. However, importantly, $[Rh(phi)]^{3+}$ complexes bind in the major groove of DNA via *intercalation*, unlike proteins which generally bind in the DNA major groove through surface interactions. Clearly, intercalation is a more intimate interaction than surface binding;therefore, the small metal complex $[Rh(4,4'\text{-diphenylbpy})_2phi]^{3+}$ can achieve similar levels of DNA sequence-specificity as large restriction enzymes (Table 6.1).

Analogous to some DNA-binding proteins, $[Rh(phi)]^{3+}$ complexes use *shape-selection* to achieve high levels of sequence-specificity. These findings have important implications in the design of sequence-specific DNA binding agents. Shape-selection is a powerful tool that dominates the sequence-specificities of $[Rh(phi)]^{3+}$ complexes; however, we still need to understand the predictability of shape-selection, in order to exploit its usage in the rational design of chemotherapeutic agents. This work has shown that specific van der Waals interactions, particularly between methyl groups on the metal complex and thymine methyl groups in the DNA major groove, can contribute significantly to sequence-specificity. Such specific interactions should be incorporated in

Table 6.1. DNA Sequence-Recognition by Major Groove- and Minor Groove- Binding agents.

DNA-BINDING DRUG/ PROTEIN	MAJOR/ MINOR GROOVE	SURFACE/ INTERCALATION	RECOGNITION SEQUENCE	DNA CLEAVAGE TARGET
Distamycin A	minor	surface	AT-rich sequences	-
Actinomycin D	minor	intercalation	GC base steps	-
Luzopeptin	minor	bis-intercalation	5'-CATG-3'	-
Bleomycin-Fe^{2+}	minor	surface	5'-GC and 5'-GT	sugar (4'-H)
Calicheamicin	minor	surface	5'-TCCT-3' and 5'-CTCT-3'	sugar (5'-H)
M-porphyrin	minor	surface	AT-rich sequences	sugars
EcoRV	major	surface	5'-GATATC-3'	phosphate
Xba1	major	surface	5'-TCTAGA-3'	phosphate
Not1	major	surface	5'-GCGGCCGC	phosphate
$[Rh(DPB)_2phi]^{3+}$	major	intercalation	5'-CTCTAGAG	sugar (3'-H)

the design of sequence-specific DNA binding agents. However, given a particular structurally characterized DNA sequence, can we design a shape-selective probe to bind specifically at the desired sequence? Before we attempt to build molecules to address this issue, we need to understand the importance of sequence-dependent deformability in a quantitative and predictive manner. Importantly, we need to carefully assess the effect of altering sequences flanking the recognition site, on the sequence-specificities of different $[Rh(phi)]^{3+}$ complexes, before we can use shape-selection in a more predictive fashion.